



UNIVERSITY OF
LEICESTER

Deep eutectic solvent-water mixtures

Thesis submitted for the degree of
Doctor of Philosophy
at the University of Leicester

By

Azhar Yaseen Muhi Al-Murshedi
Department of Chemistry
University of Leicester

March 2018

Abstract
Deep eutectic solvent-water mixtures
Azhar Yaseen Muhi Al-Murshedi
University of Leicester 2018

Salt forms homogeneous solutions with water; most studies to date have assumed that deep eutectic solvents (DES) and water form similar homogeneous systems. Several studies have used quantum mechanical and molecular dynamic simulations to prove that this is indeed the case. Study of physical properties of ionic liquid-water/ systems have revealed some anomalous observations without considering the fact that there may be micro- or nano-heterogeneities with in these systems. The key aim of this project is to demonstrate the heterogeneity of DES-water mixtures by careful measurement of physical properties such as viscosity, conductivity, surface tension and density.

The first stage of the study involved the investigation of the above physical properties for pure DESs and DESs mixed with different amounts water to investigate if these were homogeneous or heterogeneous in nature. Analysis of these data showed some characteristics of heterogeneity, the extent of which depends on the number of hydrogen bond donors in the pure DES. Dynamic light scattering was used to determine the extent of the heterogeneity in the three DESs under investigation, namely Ethaline, Glyceline and Reline.

Pulsed Field Gradient NMR (PFG-NMR) and electrochemical techniques have been used to study diffusion coefficients in DES-water mixtures. The results of PFG-NMR showed that the behaviour of DES-water mixtures was non-Stokesian, hence DES-water mixtures have water-dominant and some ion-dominant domains. Electrochemical studies also showed the same trends due to the electroactive species partitioning between the different phases. It is thought that Reline-water mixtures are more heterogeneous than the corresponding Ethaline and Glyceline systems.

Electroplating in DES-water mixtures has previously been shown to improve the quality of deposited films. The electrodeposition of copper from Ethaline was studied as a function of water content. It was found that water affected the speciation of copper in solution.

Publications

A) Papers:

- 1) C. D'Agostino, L. F. Gladden, M. D. Mantle, A. P. Abbott, E. I. Ahmed, A. Y.M. Al-Murshedi and R. C. Harris, *Physical Chemistry Chemical Physics*, 2015, **17**, 15297-15304.
- 2) Andrew P. Abbott, Azhar Y. M. Al-Murshedi, Odeh A.O. Alshammari, Robert C. Harris, Jalil H. Kareem and Idrees B. Qader, Karl S Ryder, *Fluid-Phase-Equilibria*, 2017, **488**, 1-6.
- 3) Andrew P. Abbott, Sahar S. M. Alabdullah, Azhar Y. M. Al-Murshedi and Karl S. Ryder, *Faraday Discussions*, 2018, **206**, 365-377.

B) Conferences:

Talks:

- 1) Azhar Al-Murshedi, Andrew P. Abbott and Karl S Ryder, Mass transport and phase behaviour in Deep Eutectic Solvents, *Leicester University for the 21st meeting of the ELECTROCHEM conference series*, 17th-19th August 2016, Leicester.
- 2) Azhar Al-Murshedi, Andrew P. Abbott and Karl S Ryder, Novel solvent deep eutectic solvents with water mixtures, *Department of Chemistry Postgraduate Research Day*, 4th July 2017, University of Leicester, Leicester.

Posters:

- 1) Azhar Y. Al-Murshedi, Andrew P. Abbott and Karl S. Ryder, Diffusion in deep eutectic solvent-water mixtures, *Department of Chemistry Postgraduate Research Day*, 14th April 2015, University of Leicester, Leicester.
- 2) A. Y. Al-Murshedi, A. P. Abbott and K. S. Ryder, Influence of water on the electrodeposition of copper from deep eutectic solvents. *Midlands Electrochemistry Group (MEG)*, 25th May 2016, University of Leicester, Leicester.
- 3) Azhar Y. Al-Murshedi, Andrew P. Abbott and Carmine D'Agostino, Microemulsions formed from ionic liquid-water mixtures, *Faraday Discussions*, 11th-13th September 2017, University of Cambridge, Cambridge.

Statement

The accompanying thesis submitted for the degree of Ph. D entitled "*Deep eutectic solvent-water mixtures*" is based upon work conducted by the author in the Department of Chemistry at the University of Leicester during the period between July 2014 and March 2018.

All the work recorded in this thesis is original unless otherwise acknowledged in the text or by references. None of the work has been submitted for another degree in this or any other university.

Signed:

Date:

Acknowledgments

I would like to show my very great appreciation to my supervisor, Professor Andrew Abbott. I really appreciate his patience and encouragement, not just a supervisor but like a father who made me think differently and deeply. He has been a great source of support and motivation during the research and preparation of this thesis. I appreciate having this opportunity to work as one of his Ph.D. students and for his flexible guidance with my work and development as a researcher.

My thanks also to my second supervisor, Professor Karl Ryder, for his support, suggestions, ideas and for allowing me the opportunity to work with him to learn more.

A big thanks to all members in the Materials Group for their help and support and for making the last four years very enjoyable. A special thank you to Dr Robert Harris, Dr Andrew Ballantyne, Dr Christopher Zaleski and Dr Alex Goddard for their unforgettable help during my study. A great thanks to Dr Carmine D'Agostino (Cambridge University) for measuring the PFG-NMR. My acknowledgements to Professor Rachel O'Reilly and Maria Inam (Warwick University) for help while measuring the zeta potentials.

I would like to thank my close friends Dr Hani Ismail, Rokaya Azaga, Dr Huda Ismail, Rajaa Al-Hadrawi and Heyam Alkhayyat for lots of support and help during my study. I am thankful to all the Materials Centre Group members, both past and present, and all my colleagues Dr Essa Ismail, Dr Hassan Al-Esary, Dr Mohammed G. Mohammed, Dr Jalil Kareem, Dr Jamil Juma, Idrees Qadir, Sahar Alabdullah and Ahmed Al-Bassam. I would also like to extend my thanks to Dr Azeez Al-Barzinjy for his help in the first year of my study.

I would also like to thank the Iraqi Ministry of Higher Education and Scientific Research and University of Kufa, Iraq, for the financial support required for me to complete my study.

Finally, and most importantly, I give my warmest thanks and deepest appreciation to my mother and father and my sister and brothers for all their prayers, support and unconditional love throughout this journey.

Thesis contents

Abstract.....	i
Publications.....	ii
Statement	iii
Acknowledgments	iv

Chapter 1: Introduction.

1 Introduction.....	2
1.1 Ionic liquids.	2
1.2 Synthesis of ionic liquids.	3
1.3 Physical properties of ionic liquids.....	4
1.4 Applications of ionic liquids.	5
1.5 Deep eutectic solvents.	6
1.6 Structure of ionic liquids.	10
1.7 Structure of deep eutectic solvents	13
1.8 Ionic liquid and DESs -water mixtures.	15
1.9 Application of ionic liquid and DESs- water mixtures.	23
1.10 Aim of project.	25
1.11 References.....	27

Chapter 2: Experimental and methods.

2 Experimental and Methods.	38
2.1 Materials.	38
2.1.1 Chemicals.	38
2.2 Humidity measurement.....	39
2.3 Preparation of deep eutectic solvents.....	39
2.4 Measurement of amount of water in pure DESs.....	40
2.5 Measurement of thermophysical properties.	40
2.5.1 Viscosity.	40
2.5.2 Conductivity.	42
2.5.3 Surface tension and density.	42
2.5.4 Reflective index.	43

2.6	Dynamic light scattering.	43
2.7	Measurement of acidity of liquids.	44
2.8	Measurement of fluidity characteristics.....	44
2.9	Thermodynamic properties	45
2.10	Thermal properties.	45
2.10.1	Heat capacity.	45
2.11	Measurement the diffusion coefficient.	45
2.11.1	PFG-NMR measurements.	45
2.12	Electrochemical measurements.	46
2.12.1	Cyclic voltammetry measurement.....	46
2.12.2	Capacity double layer measurements.....	47
2.13	UV-Vis spectroscopy measurements.	48
2.14	Microchemical and microstructural analyses.	48
2.14.1	Scanning electron microscopy.	48
2.14.2	X-ray diffraction (XRD).	48
2.15	References	50

Chapter 3: Thermophysical properties of pure DESs and their mixtures with water.

3	Thermophysical properties of pure DESs and their mixtures with water.	52
3.1	Introduction.....	52
3.2	Objective.....	52
3.3	Results and discussion.	52
3.3.1	Viscosity of DESs using a rotational viscometer.	52
3.3.2	Viscosity measurements using QCM.	60
3.4	Rheological study.	62
3.4.1	Influence of temperature on fluidity of DESs.	65
3.5	Surface tension.	66
3.6	Ionic conductivity.	69
3.7	Density.	73
3.8	Reflective index.	75
3.9	Dynamic light scattering.	75

3.10	Enthalpy of mixing DES with water.	84
3.11	Extraction using DES-water mixtures.	86
3.12	Conclusions.....	90
3.13	References.	91

Chapter 4: Diffusion in DES/ water mixtures.

4	Diffusion in DES/ water mixtures.	99
4.1	Overview.....	99
4.2	Objective.....	100
4.3	Results and discussion.	100
4.3.1	Diffusion coefficient by PFG-NMR.....	100
4.4	Study of diffusion coefficients by electrochemical methods.	109
4.5	Cyclic voltammetry of iron chloride in deep eutectic solvents.	109
4.6	UV-Vis spectroscopy.	116
4.7	Electrical double layer.	119
4.8	Double layer capacitance.	126
4.8.1	Iodine speciation with in DES-water mixtures.	127
4.9	Conclusion.	128
4.10	References.....	129

Chapter 5: Effect of water on copper electrodeposition in Ethaline.

5	Effect of water on copper electrodeposition in Ethaline.....	134
5.1	Introduction.....	134
5.2	Objective.....	136
5.3	Electrochemistry study.....	137
5.3.1	Effect of water on the electrochemical window of Ethaline.....	137
5.3.2	Effect of water on the bulk electrolysis of copper.....	138
5.4	X-Ray diffraction analysis (XRD).....	142
5.5	Cyclic voltammetry.....	144
5.6	Diffusion coefficient in copper-water system.....	152
5.7	Chronoamperometry.....	156

5.8	Effect of the anode.	160
5.9	Conclusion.....	167
5.10	References.....	168

Chapter 6: Conclusions and future work.

6	Conclusions and future work.	173
6.1	Conclusion.	173
6.2	Future work.	176

Chapter 7: Appendices.

7	Appendices	180
7.1	Appendix A	180
7.1.1	Thermophysical properties of pure DESs raw data.	180
7.1.2	Thermophysical properties of DESs with water raw data.	182
7.1.3	Dynamic light scattering.	183
7.2	Appendix B.	188
7.2.1	Electrochemistry study.....	188

Chapter 1: Introduction

1	Introduction.	2
1.1	Ionic liquids.	2
1.2	Synthesis of ionic liquids.	3
1.3	Physical properties of ionic liquids.	4
1.4	Applications of ionic liquids.	5
1.5	Deep eutectic solvents.	6
1.6	Structure of ionic liquids.	10
1.7	Structure of deep eutectic solvents	13
1.8	Ionic liquid and DESs -water mixtures.	15
1.9	Application of ionic liquid and DESs- water mixtures.	23
1.10	Aim of project.	25
1.11	References.	27

1 Introduction.

1.1 Ionic liquids.

Ionic liquids are a large class of materials made up of an organic cation and an organic or inorganic anion. They remain liquid at low temperatures due to bulky, asymmetric ions which resist crystalline packing. ILs have properties including extremely low vapour pressure, high ionic conductivity and very good chemical and thermal stability. Ionic liquids have been used for a variety of applications such as electrodeposition, catalysis and biomass dissolution, and for these applications it is useful to use their wide thermal stability range. In most cases ionic liquids are used in their pure form but in some cases it has been found that the addition of co-solvents produces enhanced properties.¹⁻³

Figure 1.1 shows a wide variety of the cations and anions that are used in the preparation of ionic liquids. One of their most important properties is that they were considered to be “designer solvents”, so their ultimate purpose has an effect on the preparation of different kinds of ILs. This depends on whether the researcher wants, for example, an IL which is miscible, partially miscible or totally immiscible with water.⁴

The first generation of ILs were prepared from metal halides and chloroaluminate as anions, and alkyl pyridinium and dialkylimidazolium as cations.⁵ These liquids, while extensively investigated, were water and air sensitive and required an inert gas atmosphere during preparation and use.⁶ The second generation of ILs were prepared from anions such as Cl^- , Br^- , I^- , BF_4^- , PF_6^- and $\text{C}_6\text{H}_5\text{CO}_2^-$, and cations such as dialkylimidazolium or alkylpyridinium. These liquids are more stable in water and air although they are expensive and are relatively toxic.⁷

As mentioned previously, ILs are designer solvents that are used to create a vast range of ionic liquids with different properties e.g., for enhanced stability the $[(\text{CF}_3\text{SO}_2)_2\text{N}]^-$ ion is used, while if more environmental compatibility is required then amino or organic acids, alkylsulphates, or alkylphosphates, and choline are used.⁸ In general, in ILs the type of anion chosen controls the chemistry, while the selected cation controls the physical properties.⁹

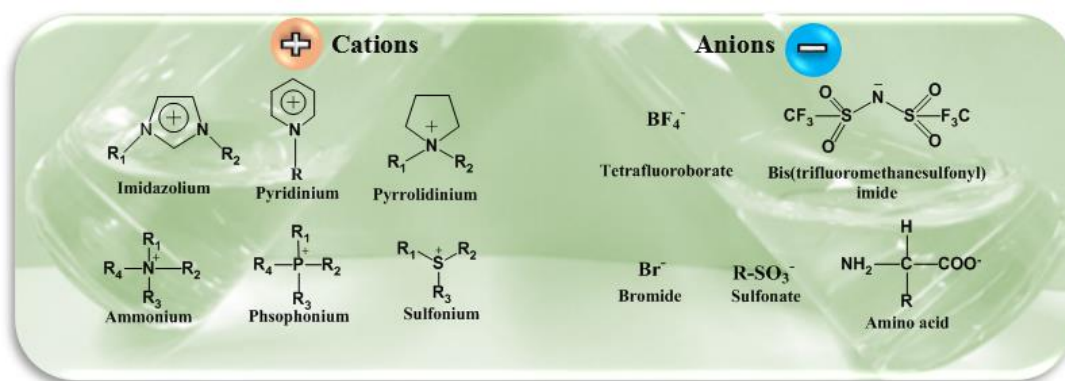


Figure 1.1: The most commonly used cations and anions in forming ionic liquids.

1.2 Synthesis of ionic liquids.

Previous studies have shown that there are many ways to prepare ionic liquids; however, the most common method is the quaternisation of an imidazole or amine to form a cation. The quaternisation is executed by using an alkylating agent such as halogenoalkane.^{10, 11} The common method to prepare ionic liquids is by direct quaternisation, for example [C₄C₁im][Cl] and [C₂C₁im][CF₃SO₃].¹¹ However, sometimes it is impossible to form the desired anion directly by this procedure, in which case the process can be carried out in two steps, as per **Figure 1.2**. Step one starts from an ammonium halide species, [R'R₃N]⁺X⁻, the ammonium halide can be treated with a Lewis acid, MX_y, to form an ionic liquid [R'R₃N]⁺[MX_{y+1}], as per step IIa. Step II can be completed in three ways: first, mixing with a metal salt M⁺[A]⁻; secondly, treating with a strong acid, H⁺A⁻; and finally, anion exchange, which can be completed by treatment of halide salts with a Lewis acid to produce a Lewis acid-based ionic liquid; as shown in **Figure 1.2**. Unfortunately, it can be difficult to remove the last traces of halide ions from the finished liquid which can affect the physical and chemical properties of the fluid.¹¹

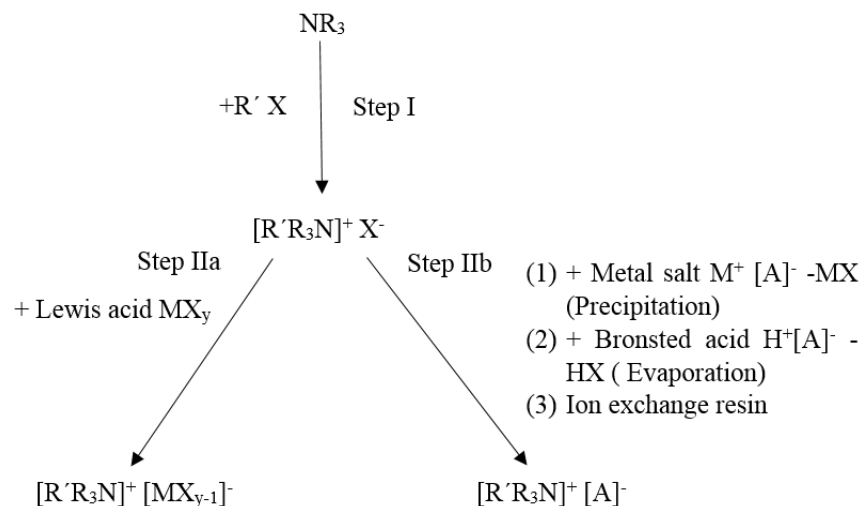
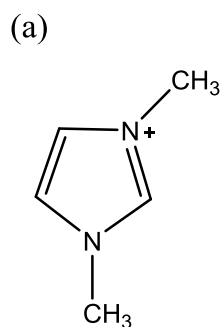


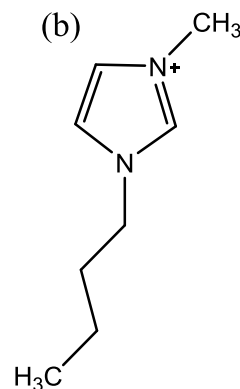
Figure 1.2: Steps in the preparation of ionic liquids

1.3 Physical properties of ionic liquids.

The melting point of an ionic compound is affected by both the size and symmetry of the cation, species with lower symmetry have lower melting points. For instance, 1,3-dimethylimidazolium and 1,3-diethylimidazolium salts show higher melting points than 1-butyl-3-methylimidazolium; **Figure 1.3 (a) and (b)** illustrate this behaviour.⁹



1,3- dimethyl imidazolium



1-butyl-3-methylimidazolium

Figure 1.3: influence of symmetry on melting point of ionic liquids; $[\text{C}_1\text{C}_1\text{im}]^+$ (a) mp = 124.5°C, $[\text{C}_4\text{C}_1\text{im}]^+$ (b) mp = 65°C .

In addition, the molecular structure and symmetry and the length of the alkyl chain of cations has a strong influence on the melting point; for instance, the melting point of $[\text{C}_1\text{C}_1\text{im}][\text{Cl}]$ has been shown to be 124.5°C, whilst that of $[\text{C}_4\text{C}_1\text{im}][\text{Cl}]$ is 65°C. This is

due to the difference in alkyl chain length of the two species; for a chain C_n , when n is greater than 10 the salts generally show very complex phase behavior.¹²

1.4 Applications of ionic liquids.

Most of the successful applications of ionic liquids to date have been in niche areas, generally with small volumes of liquid. It is the designer properties which have made them useful such as the design of a specific melting point or the ability to dissolve a specific solute such as cellulose.¹³ There are almost no examples where ionic liquids have been used as replacement solvents for a molecular solvent. This is probably due the increased viscosity and cost of the liquids compared to molecular solvents making their use undesirable except where an alternative does not exist. Ionic liquids have mostly been studied for use in the areas of organic synthesis, analytical science and electrochemistry.¹⁴

Figure 1.4 illustrates some of the most important applications for ionic liquids.

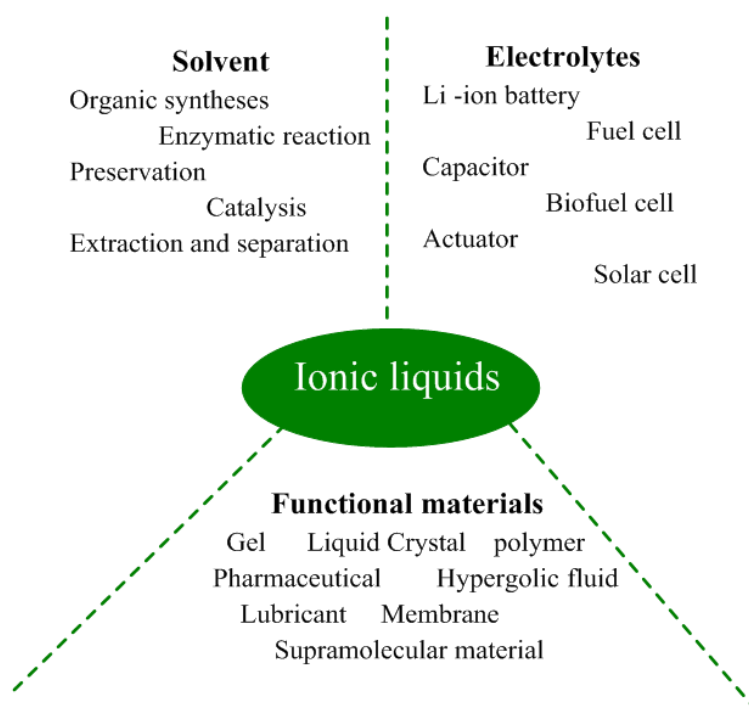


Figure 1.4: Applications of ionic liquids.²

Ionic liquids have been lauded as green solvents due to their non-flammability, low volatility and rapid biodegradability. It should, however be noted that it is dangerous to make general statements about such a large class of materials.^{15, 16,17} In general, some ionic liquids have significant toxicity, most currently have a high cost, as purification is difficult compared to molecular solvents, and some have low moisture tolerance and some have poor biodegradability. Their green credentials can also be questioned given the low

E-factors associated with their manufacture.^{9, 10, 18, 19} A variety of alternative liquids have been proposed where cations or anions have been prepared using natural products such as proteins, amino acids, chitosan and lignin amongst others.²⁰⁻²³ To overcome the high price and toxicity of ILs, a new generation of solvent, termed deep eutectic solvents (DESs), has been proposed.⁸ The aim of this thesis is to investigate what happens when an ionic liquid (IL), or more specifically a deep eutectic solvent, becomes mixed with water. **The hypothesis of this thesis is that water and DESs do not mix homogeneously and it is this heterogeneous emulsion which gives rise to the unusual physical properties.**

1.5 Deep eutectic solvents.

One issue with ionic liquids is that each new combination of a cation and an anion is, in effect, a new compound which needs to be registered and its toxicological properties characterised. Registration and testing can be expensive and labour intensive. An alternative approach is to make a complex anion in the same way that the original ionic liquid did with a quaternary ammonium halide and aluminium chloride. In this case a series of haloaluminate anions were produced. Abbott *et al.* extended this idea, initially to other metal halides and then to compounds which were able to complex the chloride anion of the quaternary ammonium salt with a hydrogen bond donor. These so-called deep eutectic solvents (DESs) have been widely used as they are simple to prepare, relatively inexpensive and many have low toxicity and are biodegradable.²⁴ DES are produced by mixing a quaternary ammonium salt (usually a halide) and molecular hydrogen bond donor. The interaction of a hydrogen bond acceptor (HBA) and a hydrogen bond donor (HBD) decrease the freezing point of the non-ideal mixture forming a single liquid phase with a melting point below 100°C. The mixture is a “eutectic” as it has a lower lattice energy and hence a lower melting point than its individual components due to the strong interactions between the components.^{25, 26} The initial definition of an ionic liquid was “a fluid composed only of ions” and so DESs were not generally considered as ILs. It has been realised that all ionic systems have some molecular component so the original ethylammonium nitrate is composed of ethylamine and nitric acid and so the definition of ionic liquids has been broadened to include DESs as they are liquids in which the ionic character dominates.²⁷ **Figure 1.5** shows a typical phase behaviour of a two component mixture.²⁸

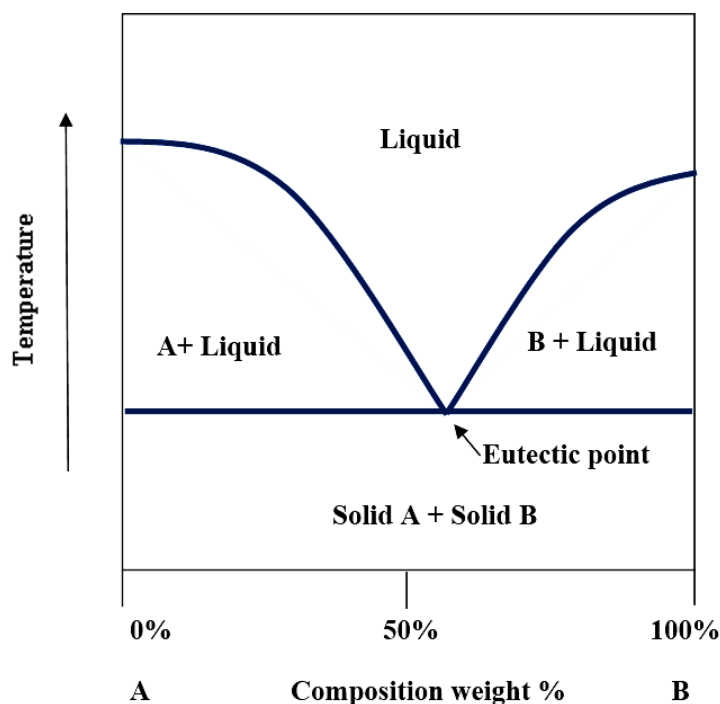


Figure 1.5: Schematic diagram of a two-component phase diagram displaying a eutectic point.²⁸

The most common salts used are the quaternary ammonium halides with hydrogen bond donors (HBDs) such as amines, amides, alcohols and carboxylic acids.²⁹ In general, there are many hydrogen bond donor and hydrogen bond acceptor species used in forming DESs³⁰, as shown in **Figure 1.6**. It is important to point out here that DESs are more green than other types of ionic liquids due to there being no waste in the process of preparation and the fact that no purification is required.²⁷ In addition, DESs encompass a variety of amides and polyols such as urea, glycerol, ethylene glycol and fructose, which have low inherent toxicity. Furthermore, both choline chloride and hydrogen bond donor such as ethylene glycol are non-harmful to the environment, and both are readily biodegradable, with the resultant DES also readily biodegradable.²⁶

Much of the work to date has focussed on DESs containing urea, ethylene glycol, glycerol and oxalic acid. They are relatively benign and low cost ingredients and they display a range of viscosities, pH and solvent properties. Relatively few groups have studied ternary or quaternary mixtures which enable the solvent and transport properties of the

fluid to be tuned to an application. Most of the large-scale studies using DESs for electroplating, electropolishing or metal oxide dissolution have used ternary mixtures for this purpose.²⁵

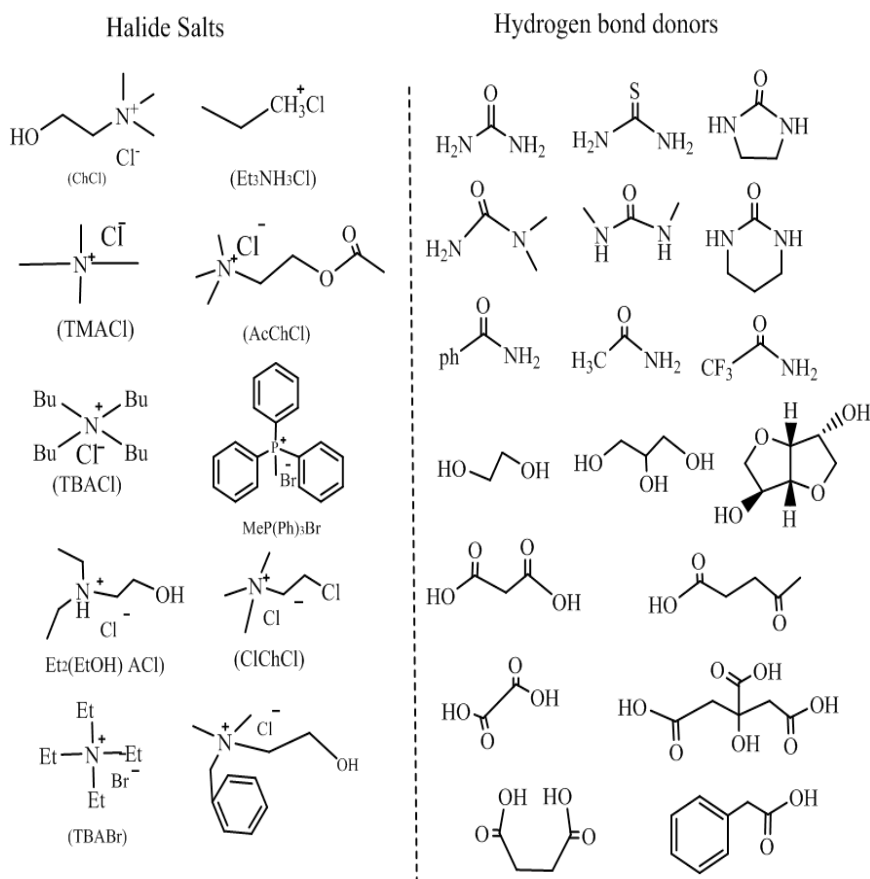


Figure 1.6: Typical structures of halide salts with hydrogen bond donors used in the formation of DESs.¹⁹

Abbott *et al.* classified DESs into four types depending on the nature of the complexing agent used. **Table 1.1** illustrates the general formula used.³⁰

Table 1.1: Types of deep eutectic solvent.

Type 1	• Quaternary ammonium salt+ metal chloride
Type 2	• Quaternary ammonium salt +metal chloride hydrate
Type 3	• Quaternary ammonium salt+ hydrogen bond donor
Type 4	• Metal chloride(hydrate)+ hydrogen bond donor

Type 1 eutectics are formed from metal halides, MCl_x , where M is a metal such as Zn, Sn, Fe, Al and Ga with chloroaluminate and imidazolium salts. However, this type is limited because of the limited number of non-hydrated metal salts that can be used in their preparation. Generally, the eutectic temperature depends on the melting point of the metal halide. Those listed above have the lowest melting points of the commonly available metals.

Type 2 eutectics can be prepared from choline chloride with any of various hydrated metal salts and this is just an extension of the idea used for Type 1 eutectics. Metal hydrate salts have significantly lower melting points than the corresponding anhydrous salt. Anhydrous $CrCl_3$ has a melting point of $1152^\circ C$ whereas $CrCl_3 \cdot 6H_2O$ melts at $83^\circ C$.

Type 3 eutectics are probably the most widely studied as they are very versatile. The sheer number of alcohols, amides and carboxylic acids makes the type 3 eutectics very tuneable. They can include simple sugars and benign weak acids such as citric acid or ascorbic acid. They can solvate a wide range of compounds including metal oxides, amino acids, polar organic molecules and surfactants. Type 3 DESs can be formed from a wide variety of hydrogen bond donors and quaternary ammonium salts which makes them easy to prepare, most have low cost, and many are biodegradable.²⁶

The most recently developed DESs are the type 4 eutectics. These use a metal halide and a hydrogen bond donor. The unusual aspect of these formulations is that the metal salt disproportionates to give both a metal containing cation and anion. e.g.,



These have been studied for the electrodeposition of metals.³¹

DESs have found application in different areas. One of the most common is as an electrolyte in the electrodeposition of different metals, e.g., Cr,³² Al,³³ Ni,³⁴ Cu,³⁵ Ag,³⁶ Co,³⁷ Zn^{38, 39} and Sn.³⁷ There are many advantages to the use of DESs in the field of electrodeposition, for example the high solubility of metal salts in DESs, relatively large potential windows, and the ability to deposit on water-sensitive substrates such as aluminium.²⁵ In addition, many alloys can be deposited using DESs. In addition to electrochemistry, deep eutectic solvents have also been used in synthesis, biochemistry, nanomaterial and separation.⁴⁰ The large increase in the interest in DESs can be seen from the papers published on the topic as shown in **Figure 1.7**.⁴¹

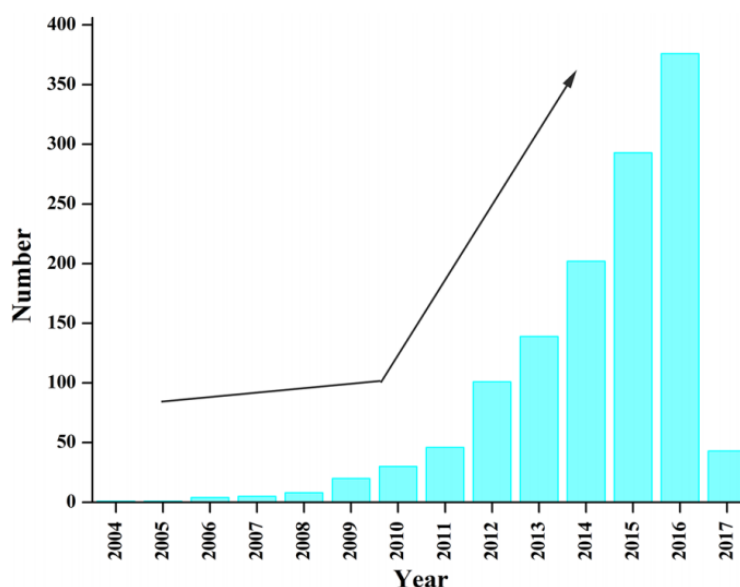


Figure 1.7: The number of papers published on DESs over the last ten years.⁴¹

1.6 Structure of ionic liquids.

Understanding the structure of ionic liquids is key to studying the physical, chemical and dynamic properties for these liquids. Previous studies of the bulk structure of ionic liquids have dealt with ionic liquids as being similar to molecular liquids, that is, homogenous, coherent, and essentially irregular systems.⁴² Other studies have shown that the bulk ionic liquid structure is similar to that of a highly concentrated salt solution or a molten salt. Nowadays, the models that have been used to study the structure of ionic liquids suggests

they are structured solvents such as ion pairs, ion clusters, hydrogen bond networks, micelle-like, and bicontinuous morphologies, as per **Figure 1.8**.⁴³⁻⁴⁶

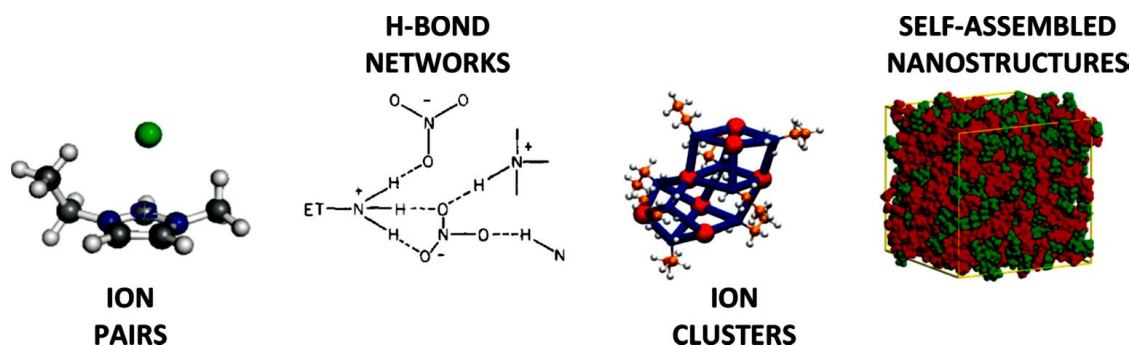


Figure 1.8: Various models for bulk structures of ionic liquids.⁴⁷

As discussed earlier, the study of physiochemical properties and behaviour of ILs requires an understanding of the microstructure of ionic liquids. The clustering or micro-heterogeneous structure is key to understanding the intermolecular interactions in ionic liquids. **Figure 1.9** illustrates ionic liquid clusters and their applications.⁴⁸

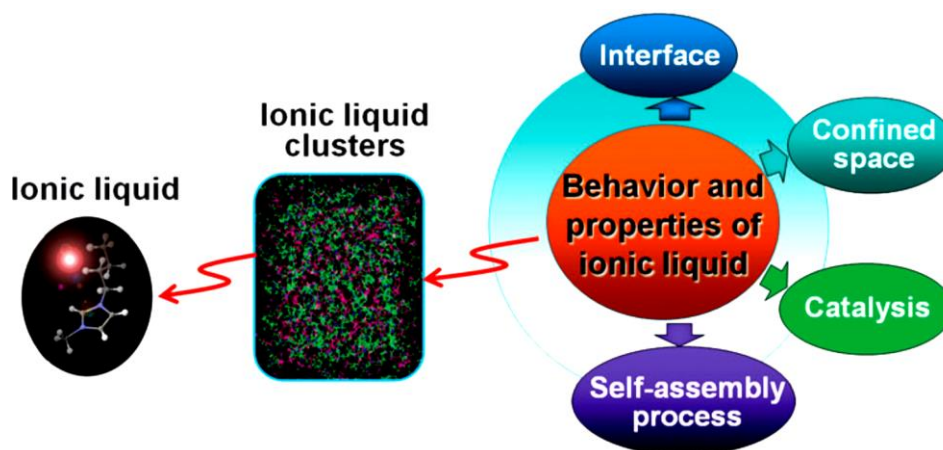


Figure 1.9: Clusters of ionic liquids and common applications.⁴⁹

It should be noted that in some literature, there are different terms that have been used to describe ionic liquid clusters; for example, aggregates, nanostructures, local structure, heterogeneity, etc. In ionic liquids an aggregate of more than three ions can form into clusters although there are some claims that clusters do not really exist in pure ionic liquids.⁴⁸ Previous studies have reported the experimental and theoretical micro-heterogeneity of pure ILs.⁴⁹ This micro-heterogeneity is one of the crucial factors in

explaining the unforeseen physical properties of ionic liquids such as heterogeneous, self-diffusion, surfactant-like micelles and surface layering that forms in ionic liquid-water mixtures. The first serious discussions and analysis of clusters in pure ionic liquids was published by Voth *et al.* in 2005 who applied a coarse-grained model to study the segregated domains in ILs.⁵⁰ Lopes and Padua used theoretical simulations to argue that the ILs are not homogeneous. In addition, they suggested that in $[C_n\text{mim}][\text{PF}_6]$ ($n = 2$ to 12), ILs with alkyl side chains $> C_4$, polar-nonpolar domains can appear.⁴⁶

Pure ionic liquids are only composed of cations and anions; ion pairs are the basic unit of the structure of ionic liquids although the importance of pair-wise interactions is disputed. The structure and interaction of an ion pair have been used to understand the formation of the clusters. Various methods have been used to study ion pairs in ionic liquids. The findings of this study suggest that the relaxation profile of ion pairs show that in ILs free ions exist. In addition, the study suggested approximately 8% of ions were in contact ion pairs and 92% were free ions. The ion pairs' lifetime was measured to be 10^{-10} s at 298 K, where this lifetime is extremely close to that for anion-cation coupling in front of the C_2 carbon. The anion-cation interaction occurred via hydrogen bonds which were not linear ($< 165^\circ$) and relatively long ($> 2.5 \text{ \AA}$) compared with 'ideal' hydrogen bond arrangements.⁵¹

Intermolecular interactions are the key to studying the behaviour of ionic liquids. There are many spectroscopic methods that have been used to study and characterise the interactions between cations and anions in ionic liquids.⁵²⁻⁵⁴ Early studies by Seddon *et al.* suggested that hydrogen bonds (H-bonds) exist in ion pairs of $[C_4\text{C}_{1\text{im}}][\text{I}]$ ion pairs, which are noncovalent interactions and influence the properties of ILs.⁵⁵ Hydrogen bonding in imidazolium-based ILs has been investigated. The presence of H-bonds can be studied by substituting a $-\text{CH}_3$ group for a proton on the imidazolium ring, which results in the complete disappearance of bands associated with H-bonds. Ludwig *et al.* explained this behaviour via various techniques, for instance, far-IR and X-ray diffraction, and argued that the disappearance occurs due to the removal of the relatively acidic protons on the imidazolium ring.⁵⁶

However, these studies are not sufficient to fully understand hydrogen bonding on a molecular level. Theoretical calculations can provide more information to understand the interactions between species in an IL. There are many methods that have been used to

study ionic arrangements and thermodynamic properties in the pure bulk IL, such as molecular dynamics simulations (MD). MD simulations are a computer simulation method for studying the velocities and atomic position of atoms and molecules using Newton's Second Law.⁵⁷

Dong *et al.* used density functional theory (DFT) calculations to investigate the interactions in [C₂C₁im][BF₄] and [C₄C₁im][PF₆]. They found that C-H...F H-bonds existed between the cations and anions.⁵⁸ There are several studies in the literature characterizing H-bonds in ILs by low-frequency spectroscopy combined with DFT calculations and MD simulations. The results of this investigation showed that the hydrogen bonds in imidazolium-based ILs perturb the Coulombic forces and this has the effect of deviating from charge symmetry. As a result, this has the influence of decreasing the viscosity and raising the fluidity of ILs.^{56,59} All of these studies give indirect evidence of the formation clusters in ionic liquids. Triolo *et al.* used X-ray scattering to determine the existence of clusters in bulk ILs. Their investigation showed that the use of this technique allows the probing of electron density fluctuations on a scale ranging from angstroms to several nanometres. As a result, this technique represents an ideal tool to determine the complex morphology of ILs.⁶⁰

1.7 Structure of deep eutectic solvents

Previous studies have illustrated how the nanostructure of DESs has an effect on the physical properties of DESs; for example, viscosity, density and melting point. The melting point for pure DESs such as Reline, at 12°C, is lower than that of the pure constituent components (choline chloride 302°C and urea 133°C).^{8,61}

Previous research has established that the melting point depression in DESs is due to complexation of the anion via hydrogen bonding which produces a delocalization of the negative charge, therefore decreasing the Coulombic interactions between the cation and the anion.^{61,62} In the Reline system, there is a decrease in melting point due to urea molecules interacting with Cl⁻ anions through N-H...Cl hydrogen bonds in mixtures of choline chloride with urea, decreasing the hydrogen-bonding interactions between the choline cations and Cl⁻ anions.⁶¹

Ab initio molecular dynamics simulation studies suggest a different mechanism may also occur. *Ab initio* methods are quantum mechanical method used to distinguish the behaviour of molecules, and which assign electron density by applying Schrödinger's wave equations.⁵⁷

These *ab initio* molecular dynamics simulations suggest there is negligible charge spread from the chloride to the urea.⁶³ Atkin *et al.* showed that there is a strong connection between the melting point and the strength and nature of the hydrogen-bonded network in Reline, Glyceline and Ethaline. Their results suggested that there are three important interactions in Ethaline system: the choline and chloride charge centres (N^+-Cl^-), choline and ethylene glycol OH groups ($H_{OH}-O_{EG}$) and the ethylene glycol OH group and the chloride anion ($H_{EGOH}-Cl^-$). The radial distribution functions (RDF) simulation shows that the choline and chloride charge centres are more strongly associated in choline chloride: ethylene glycol (ChCl:EG) compared with choline chloride: urea (ChCl:U). As a result, the ethylene glycol is therefore less able to disrupt the electrostatic cation-anion interactions than urea.⁶⁴

The ethylene glycol OH group and the chloride anion ($H_{EGOH}-Cl^-$) correlation function ChCl:EG shows a strong peak, indicating that the HBD- anion interaction is key in the formation of this DESs. The hydrogen bond structure in both Ethaline and Reline is essentially different; in the Ethaline ChCl:EG exhibits mostly linear hydrogen bonds, while in Reline ChCl:U shows nonlinear hydrogen bonds. Moreover, there is no additional long range correlations are observed for ChCl:EG unlike ChCl:U. As a results, the extent of interaction between the HBD and anion in ChCl:EG is reduced. This is consistent with the calculated coordination number of Cl^- anions around H_{EGOH} , which is lower than the total coordination between hydrogen bond Cl^- -H in ChCl:U.⁶⁴

The choline-ethylene glycol hydroxyl interaction in the ChCl:EG DES is also noteworthy, with ($H_{OH}-O_{EG}$) RDF results being dominated by a single strong peak for both ChCl:EG and ChCl:U. However, in ChCl:EG system the ($H_{OH}-O_{EG}$) RDF also observed two weak interaction, which are missing completely in the (O_U-H_{OH}). This indicates that the urea HBD show a discriminatory interaction with the Cl^- anion in ChCl:U; however, the ethylene glycol HBD interacts with both the cation and anion. As a results, this will reduce its ability to disrupt the cation- anion interaction resulting in a smaller temperature depression compared to ChCl:U. Perkins *et al.* used RDF simulations to study the

interaction between three DESs namely, Ethaline, Glyceline and Maline. Their results showed that there are multiple types of hydrogen bonds formed, including $\text{OH}_{(\text{malonic})}\cdots\text{Cl}^-$, $\text{OH}_{(\text{choline})}\cdots\text{Cl}^-$ and malonic acid \cdots malonic acid interactions.⁶⁵ Hammond *et al.* argue that there is a strong and complex hydrogen-bonding network between choline chloride and urea in the Reline system. Their results exhibit that choline interacts very strongly with the chloride ion by hydrogen bonding. This has influence on the formation of a complex ion as a most possibly 3D configuration, including one choline, one chloride and two urea molecules.^{64, 66}

1.8 Ionic liquid and DESs -water mixtures.

Molecular dynamics (MD) simulations of ionic liquid-water mixtures were studied for the first time in 2002 by Lynden-Bell and co-workers. MD simulations have been used to study the changes in the structure of ionic liquids and their mixtures. In their study, $[\text{C}_n\text{C}_1\text{im Cl}][\text{Cl}]$ was mixed with a variety of molecules with properties ranging from polar such as H_2O and MeOH , non-polar like Me_2CH_2 . Polar molecules such as water and methanol show strong interactions in which hydrogen bonding occurs between the chloride ion and hydroxyl group of water and methanol. However, other molecules which have less polarity than water, including dimethyl ether and propane, interact with the cation.⁶⁷

Zhou *et al.* used MD simulations to study the change of dynamics properties and microstructure of a series of IL-water systems. Their study found that the viscosities of $[\text{C}_4\text{C}_1\text{im}][\text{BF}_4]$ and $[\text{C}_4\text{C}_1\text{im}][\text{Tf}_2\text{N}]$ decrease rapidly in the first instance, and then decrease more slowly with an increasing amount of water. However, for $[\text{C}_4\text{C}_1\text{im}][\text{Ac}]$, the viscosity rises in the first instance, and then decreases. The odd behaviour of $[\text{C}_2\text{C}_1\text{im}][\text{Ac}]$ is due to the formation of chain-like anion \cdots water \cdots anion structures. On the other hand, their results showed that the presence of a small amount of water influences the structure of ionic liquids. The results show that the water has an effect on the formation of hydrogen bonds between water and the anions, which help to aggregate water in ionic liquids and the clusters formed.⁶⁸

Lynden-Bell *et al.* used radial distribution functions (RDF) to investigate the structure and dynamic properties of a variety of ILs such as 1,3-dimethylimidazolium chloride and 1,3-dimethylimidazolium hexafluorophosphate when mixed with water. Their results

showed that with low concentrations, the water molecules are either isolated or exist in small independent clusters. However, increased water concentrations change the properties of the mixture, and IL-water mixtures become a continuous water network.⁶⁹

Feng and Voth studied the effects of alkyl side chain length and anion on the structure and dynamics of different ionic liquid-water mixtures, including 1-butyl-3-methylimidazolium [C₄C₁im][BF₄], 1-octyl-3-methylimidazolium [C₈C₁im][BF₄], and [C₈C₁im][Cl] using MD simulations. Their results showed that changing the alkyl side chain length does not affect the distribution of water. In contrast, when changing the anion from [BF₄]⁻ to [Cl]⁻, the water coordination number was decreased. As a result, they concluded that interactions between the anions and water molecules has a strong effect on the structure of water.⁷⁰

Moreno *et al.* used MD simulations of water-[C₄C₁im][BF₄] mixtures changing x_{H_2O} from 0 to 0.5. Their investigation focussed on an extensive analysis of structural parameters; for example, pair correlation functions, nearest-neighbour analysis and the size distribution of the water clusters formed at higher concentrations of water. They found the clusters are formed by hydrogen-bonding molecules and take a linear chain shape. Moreover, they found that there is a nanoscale structuring of the mixtures; however, there is no macroscopic phase separation among the components. This is attributed to two reasons: firstly, there is a selective coordination by individual water molecules at low mole fractions of water; secondly, at high mole fractions of water, the ionic network is disrupted or swollen in a nonspecific manner by the water clusters. **Figure 1.10** illustrates the behaviour of [C₄C₁im][BF₄] with different amounts of water; it is clear that there is difference between a small and a large amount of water.⁷¹

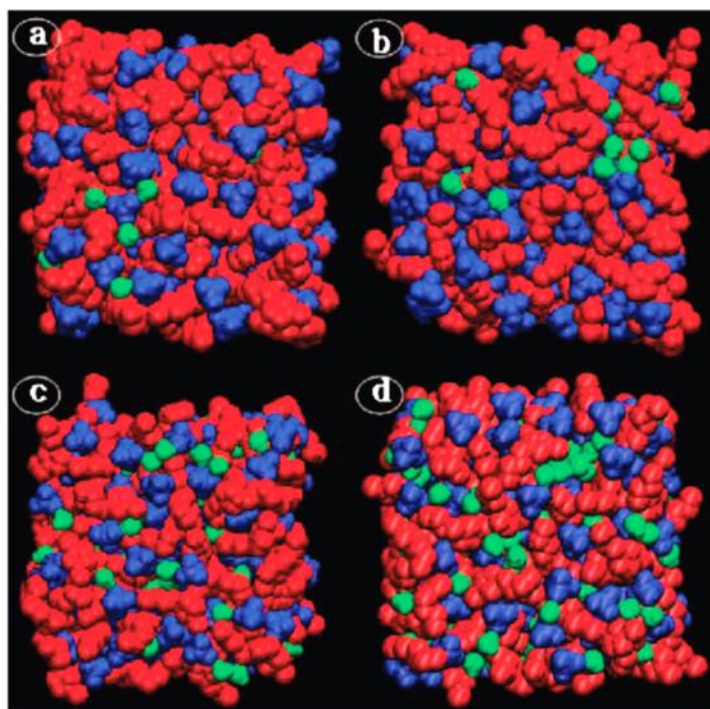


Figure 1.10: Snapshots for MD simulations of $[\text{C}_4\text{C}_1\text{im}][\text{BF}_4]$ with different amounts of water including: (a) 1:8 mixture, (b) 1:4 mixture, (c) 1:2 mixture and (d) 1:1 mixture. Colour code: water in green, cations in red, anions in blue. The hydrogen bonds are not shown.⁷³

As mentioned above, MD simulations have been used to study the changes in structure of ionic liquids and their mixtures for example, tetramethylguanidinium salts, either benzoate or salicylate, were mixed with water. MD simulation results reveal that there are more discrete ion pairs in the salicylate than benzoate; however, there is stronger participation of the ions in the hydrogen-bonding network in benzoate. Differences in the link sites for these ionic liquids have a significant influence on the transport properties, even though the viscosity decreases and conductivity increases.¹ Previous studies have shown that the water aggregated in $[\text{C}_4\text{C}_1\text{im}][\text{Tf}_2\text{N}]$ to form clusters more than in $[\text{C}_4\text{C}_1\text{im}][\text{BF}_4]$ or $[\text{C}_2\text{C}_1\text{im}][\text{Ac}]$, whereas RDF results indicated that water interacts with anions in the order $[\text{BF}_4]^- > [\text{Ac}]^- > [\text{Tf}_2\text{N}]^-$.⁶⁸

The presence of water in chemical systems is important and affects particularly the extent of hydrogen bonding.⁷² Ionic liquids are generally hygroscopic solvents, and will tend to absorb moisture from the atmosphere. Water will change the microstructure and dynamic properties of ionic liquids; i.e., viscosity, density, refractive index, conductivity and surface tension, self-aggregation and melting temperature.^{19, 73-79} In general, water

influences the physical properties chemical properties, and the structure and nanostructure of ionic liquids.

Considering the influence of water on the physical properties of ionic liquids, there is a direct effect of the nanostructure on properties such as molar conductivity. The molecular species can decrease the electrostatic friction between the ions which move in an electric field; however, the molar conductivity is still below that observed for a dilute salt. In addition, the high dielectric constant of water ($\epsilon = 80.1$ at 20°C), can result in dielectric screening between the ions which has the influence of increasing the molar conductivity. Solvents with low dielectric constants such as dichloromethane ($\epsilon = 9$) mixed with $[\text{C}_4\text{C}_1\text{im}][\text{BF}_4]$, causes a drop in molar conductivity due to the effects of ion pairing. Recent evidence suggests that there is an influence of adding salt to the conductivity of ionic liquid, e.g., mixing NaBr with ionic liquids caused an increase in conductivity despite an increase in viscosity. The molar conductivity of some partially miscible salts in water, for instance nalidixate and hydroxycinnamate, is very low. As a result, the molar conductivity of ions depends on the medium in which the ion moves.¹

In addition, water has a significant effect on the diffusion coefficients of ionic liquids. Menjoge *et al.* used pulsed field gradient NMR to demonstrate the influence of mixing water with ionic liquids using $[\text{C}_2\text{C}_1\text{im}]^+$ as a cation and $[\text{EtSO}_4]^-$ and $[\text{TfO}]^-$ as anions. They observed that there is a shift in the proton signal of the water due to a decrease in the extent of the hydrogen bonding between water and the ions with an increasing amount of water. MD simulations suggested that the self-diffusivities for the cationic and anionic species of $[\text{C}_2\text{C}_1\text{im}][\text{EtSO}_4]$ are lower than those found via PFG NMR. This due to deficiencies in the force fields used to model the interactions between the ions.⁸⁰

While molecular modelling is a common method of looking at clustering it must be viewed in terms of its limitations to bulk observations. The size of the ensemble used for the calculation is usually about 1000 molecules, so it is only a 1 nm cubic box and it does not give a realistic picture of macroscopic clustering. It does not consider bulk thermodynamic information or bulk physical properties such as density.

Sharma and Ghorai studied the formation clusters of water at different mole fractions, x_{H_2O} between 0 and 0.886 in $[C_4C_1im][PF_6]$. Their results illustrated that at a low mole fraction of water, $x_{H_2O} = 0.2$, almost 40% of the water molecules were in a totally free state, hence water molecules do not form clusters at this concentration.⁸¹ However, Cammarata *et al.* showed that at low water mole fractions, $x_{H_2O} = 0.2, 0.4$ and 0.6 , there are many clusters that have been observed. At a high mole fraction of water, less than 1% of the water molecules remain free, and this indicates that the water molecules have become part of an extended hydrogen bonding network. Hence the water forms a separate phase.⁸²

The miscibility of ionic liquids with non-aqueous liquids is dependent largely on the dielectric constant; ionic liquids are miscible with liquids that have high dielectric constants, but tend to be immiscible with liquids that have low dielectric constants. It is well known that mixing organic solvents with water can produce either a homogeneous solution, two immiscible layers, or an emulsion with water droplets in an organic phase (or vice versa). In the last case, the dispersed phase is generally nanostructured or microstructured. **Figure 1.11** shows this behaviour schematically.⁸³ As mentioned above, dielectric constants play an important role in the miscibility of ILs. Bonhôte *et al.* argued that ILs based on certain anions, for instance, perfluorocarboxylate, bistriflimide and triflate, were miscible with liquids having high dielectric constants. However, for liquids with low dielectric constants, for example diethyl ether, dioxane, toluene, and alkanes, miscibility was dependent on the polarity of the ILs under investigation; for instance, ethyl acetate is miscible in bistriflimide and triflate ILs.^{84, 85} In addition, in polar ILs the solubility of complex organic molecules, for instance cyclodextrins, glycolipids and antibiotics, was found to be increased.^{86, 87}

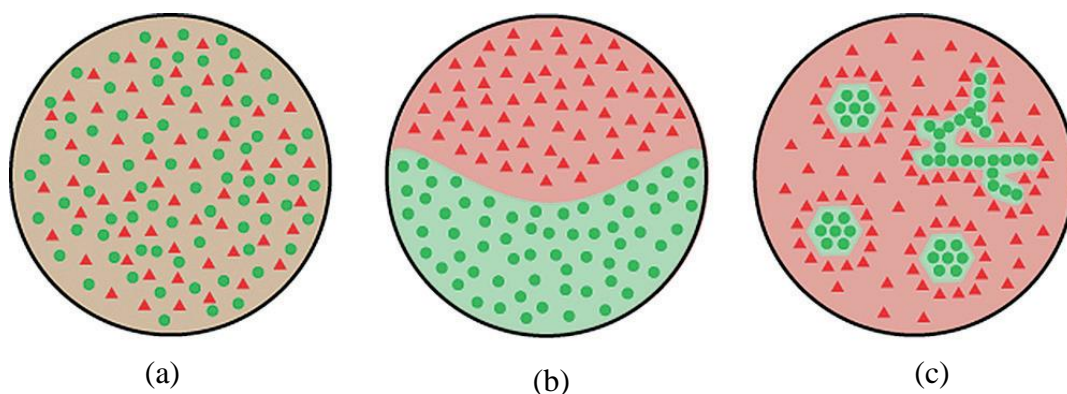


Figure 1.11: Water-organic solvent mixtures: (a) homogeneous solution, (b) heterogeneous solution and (c) nanostructured and micro-structured mixture.⁸³

In terms of the bulk miscibility of ionic liquids in water, there are two general observations. The first is that the effect of any anions depend on whether they are hydrophilic or hydrophobic. It is well known that some common anions are hydrophobic, such as $[\text{Tf}_2\text{N}]^-$ and $[\text{PF}_6]^-$, and that these anions will tend to form two layers when mixed with water. However, hydrophilic anions, such as halides like Cl^- , Br^- , phosphates $[\text{R}_2\text{PO}_4]^-$, carboxylates $[\text{RCOO}]^-$ and $[\text{BF}_4]^-$, show high miscibilities with water. The second observation is the influence of cations on miscibility of ionic liquids in water. In general, as one might expect, an increase in alkyl chain length decreases the miscibility of ionic liquids with water.⁸⁸ Moreover, $[\text{C}_4\text{C}_1\text{im}][\text{PF}_6]$, $[\text{C}_6\text{C}_1\text{im}][\text{PF}_6]$ and $[\text{C}_8\text{C}_1\text{im}][\text{PF}_6]$ have been found to be immiscible with alcohols. However, miscibility will be increased when adding water to these ionic liquids. This mixture as it is can help to remove ionic liquids from the product as well as it being useful, more generally, in extraction systems.^{89,90} It should, however, be noted that no one to date has noted that the miscibility can also be affected by density and this may explain some of the observations.

In addition to the effect of water on anion-cation interactions there are whole classes of ionic liquids which are acidic, and the presence of water will clearly influence the dissociation of protonic groups. Ionic liquids can be aprotic ionic liquids (AILs) and protic (PILs) in nature. PILs show the distinguishing features of proton-donor and proton-acceptor sites, which can be useful in the formation of hydrogen-bonding networks. As a result, the macrostructure of PILs look like the three-dimensional hydrogen-bonding network of water. Far-IR spectroscopy can be used to demonstrate the associated characteristic intermolecular bonding, which appears above 250 cm^{-1} , as well as bending and intermolecular stretching vibrations in the range $50\text{-}250\text{ cm}^{-1}$.⁹¹

The question arises as to which of the two types more strongly interacts with water, PILs or AILs? In order to answer this question, the comparison between two different ionic liquids, for example [Ch][NTf₂] and [DMEtA][NTf₂], was investigated. At lower water concentrations, the AIL [Ch][NTf₂] interacts more with water than [DMEtA][NTf₂], even though both of these ILs have hydroxyl functional groups on the cation which has the ability to form hydrogen bond donors with water. PILs form strong hydrogen bonds with water due to the charge transfer of ions, which suggests that at lower water concentrations it is difficult to form hydrogen bonds purely due to the limited availability of the OH groups in the cations; however, this difficulty is negated with AILs due to their ability to form ion-ion interactions, or in other words that their interaction is dependent on diffuse electrostatic effects.⁹²

Recent evidence suggests that there can be a strong interaction between water and PILs; Reid *et al.* argue that PILs such as [DMEtA][Pr] form strong hydrogen bonds with water due to the N-H site of the protic cation having the ability to form a stronger hydrogen bond with water than the C-H site in AILs such as [Ch][NTf₂], in which the latter shows only weak hydrogen bonds.^{92, 93} Additionally, however, different AILs or PILs can show a difference in their interactions with water; for example, [EIm][OTf] and [EIm][NTf₂] are both PILs, but [EIm][OTf] shows a more favourable interaction with water than [EIm][NTf₂] due to the influence of pK_{a(aq)} of the conjugated acid.⁹²

Huddleston *et al.* studied the miscibility of a series of ionic liquids with water. Their study examined the influence of water on hydrophilic and hydrophobic ionic liquids [C_nC₁im] with [Tf₂N⁻], [PF₆⁻], [BF₄⁻], [Cl⁻] and [I⁻]. Their results illustrated that [C_nC₁im][PF₆] formed two layers when n = 4, 6 or 8; however, [C_nC₁im][Cl] when n = 4, 6 or 8 was a homogeneous mixture. Furthermore, the miscibility of [C_nC₁im][PF₄] was dependent on both the length of the alkyl chain as well as the temperature of the system; in terms of alkyl chain length, if n = 2 – 6, [C₄C₁im][PF₄] was fully soluble in water, but when n = 6 – 10 [C_nC₁im][PF₄] was biphasic.^{94, 95}

In addition, for the anions [Br]⁻, [Cl]⁻ and [OTf]⁻ with [C₄C₁im]⁺, the IL-water mixtures favoured the formation of a seemingly homogeneous phase.⁹⁵ In fact, the hydrophobic anions salts showed different properties compared with the corresponding hydrophobic anions salts. For example, [BF₄]⁻ exhibits a lower viscosity, lower density and higher water solubility compared to [BF₆]⁻.⁹⁶ Moreover, highly diluted mixtures of

[C₁₀C₁im][Cl]-water, i.e., above 85 mole %, will be mostly composed of anionic species, [O(HCl)₂]²⁻, due to water's preference to form stronger hydrogen bonds with chloride ions rather than other water molecules.⁶⁹ In the same manner, other studies have argued that the structure of ionic liquids at higher dilutions of water, e.g., in [C₄C₁im][BF₄], illustrate that the self-association of water was not favoured, and rather that anion-water-water-anion chains were observed.⁹⁷⁻¹⁰⁰ **Figure 1.12** illustrates water hydrogen bonding networks with ionic liquids.

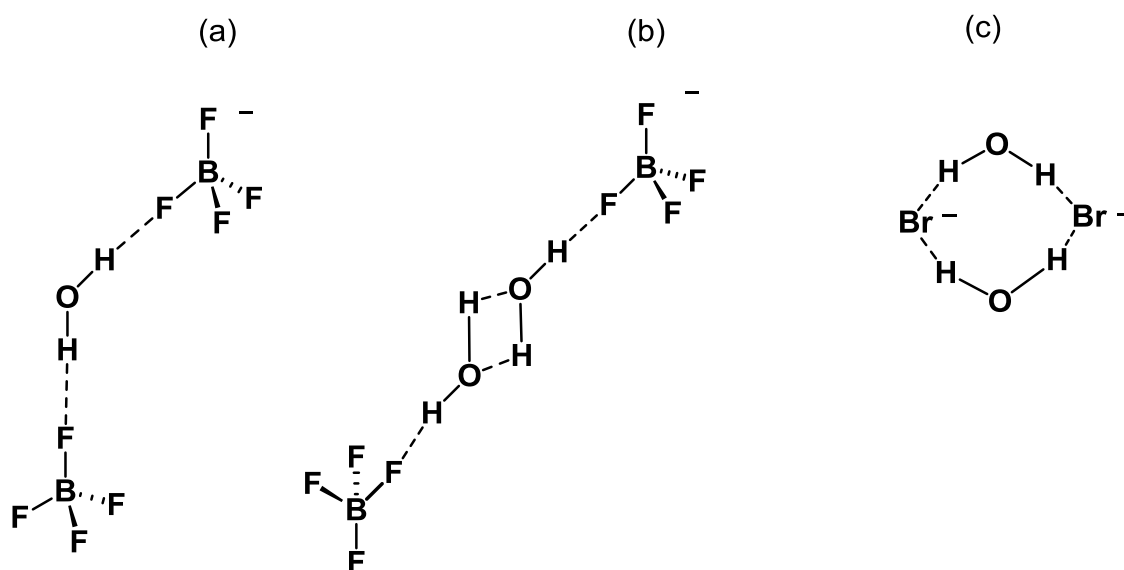


Figure 1.12: Hydrogen bonding networks of water with ILs: (a) symmetric 2:1 anion-water, (b) anion-water-water-anion and (c) anion-water-anion-water cyclic dimer.¹⁰⁰

In addition, the dynamic phase transition of IL-water mixtures is important, especially in the field of biopolymers. It is important to understand that the phase transition of IL-water mixtures arises from a change in the temperature of a system. In liquid-liquid binary mixtures, there are two types of temperature-driven phase transition. The first is the upper critical solution temperature (UCST), and second is the lower critical solution temperature (LCST). In general, the miscibility of one liquid in another increases with increasing temperature. As an example of the effect of temperature on phase transitions, the results of mixing 50 wt% water with tetrabutylphosphonium *N*-trifluoromethanesulfonyl-leucine [P₄₄₄₄][Tf-Leu] demonstrated that at 25°C, the mixture formed two layers. However, upon cooling to 22°C, there were two observations: the first that the volume of the IL phase increased, and the second that the mixture became a homogenised, miscible mixture. Moreover, upon further heating to 22.8°C, the

homogenised phases start to separate again. It can thus be seen that temperature plays an important role in the phase separation of IL-water mixtures, especially of the LCST type.⁸⁸ This is due in part to differences in interactions but also to differences in density with temperature between the two components.

The following is a brief description of studies that have been carried out on DESs- water mixtures. Meng *et al.* examined the influence of water on the melting temperature of a Reline-water mixture, with the melting point giving an indication as to the strength of the hydrogen bonding between a donor and acceptor. They found that there is a linear decrease in melting temperature below room temperature with increasing amounts of water. This study was undertaken both optically and using a differential scanning calorimeter.⁷⁹ Hammond *et al.* showed that adding different amounts of water to Reline leads to weaker interactions between all the components, i.e. Ch-Cl, Ch-urea, urea-Cl and urea-urea. Their investigation showed that the DES interactions changed with the amount of water added. At low water concentrations the DES clusters still exist, but are separated by water molecules. At low water mole fractions, the anion preferentially undergoes hydrogen bonding with the water molecules than the urea molecules. When water was the dominant phase a decrease in the hydrogen bonding between urea-urea molecules and between urea and the chloride was observed. This is important because it gives us useful information about the potential nanostructure of DES/water mixtures.^{101, 102} Several studies have used MD simulations to understand the formation and structure of both pure DESs, and their mixtures with water. Their results showed that mixing DESs with a small amount of water, typically less than 30%, does not affect the diffusion of ions. Furthermore, the thermophysical properties of these DESs also remain the same. However, on increasing the amount of water to a 50%, the water changes the intermolecular and intramolecular interaction in the DESs, and hence changes the properties of these liquids significantly.¹⁰³

1.9 Application of ionic liquid and DESs- water mixtures.

In general the applications of water mixtures with ILs and DES depends on the advantages that comes from the chemical and physical properties, i.e., less viscous liquids, a hybrid environment between ionic and molecular and processes where the presence of water is essential, e.g., for biological systems.⁸⁸ In some applications just the ability to reduce the

cost is seen as a major advantage of adding water. One of the most commonly studied areas is for the dissolution and modification of cellulose.¹⁰⁴⁻¹¹⁰

IL-water mixtures are of importance in biochemical applications due to the ability of the mixture to dissolve a wide range of salts and stabilise enzymes. From this perspective, it is important to understand the interactions in the IL-water mixtures. Various approaches have been proposed to gain further evidence about the nature of these interactions which have focussed on the use of ¹H-NMR, IR spectroscopy and X-ray scattering.⁸⁸ Several reports have shown the increased stability of proteins and DNA in IL-water mixtures. Fujita *et al.* studied the solubility and stability of cytochrome c and lysozyme in ILs and in IL-water mixtures and showed that water significantly increase the stability of both enzymes.¹¹¹ The water allows a hydration layer to form between the enzyme and bio-macromolecules which increases stability. Moreover, it is responsible for the stability of lectins, a type of protein that is used to bind to cell membranes. Lectins are soluble in a hydrated IL composed of cholinium cations [Ch] and dihydrogen phosphate anions [dhp]. The resultant mixture is a very stable solution, even after thermal treatment and long-term storage.¹¹² The same behaviour was observed for DNA, which can be dissolved in hydrated choline-based ionic liquids, where DNA shows high stability due to mild H-bonding environment which has low water activity. Hence, this will help to slow the rate of hydrolytic reactions, which will have the effect of slow depolymerization or degradation of the macromolecule.¹¹³ MD studies and spectroscopic measurements have shown that the IL cations in the mixture interact in the groove of the helix via hydrophobic and polar interactions and that provide for the increased stability of DNA.¹¹⁴

Extensive literature has been published on the control of pH in IL-water mixtures due to the associated importance in separation processes. For instance, [C₄C₁im][PF₆] is water immiscible and forms two layers; this is useful in extraction systems, for example, the extraction of thymol blue from its aqueous phase to the ionic phase by use of [C₄C₁im][PF₆] under pH control.¹¹⁵ Wei *et al.* extracted metal-dithizone complexes by mixing with [C₄C₁im][PF₄]. Their work employed UV-Vis spectroscopy to observe the resultant absorption spectra, which illustrated the strong correlation between pH and the extraction of heavy metals. At low pH, there was a limited amount of deprotonated dithizone for the formation of metal-dithizonate.¹¹⁶

The influence of water on DESs has been shown to improve the growth rate of conductive polymers. Ismail compared the growth rate of polyaniline (PANI) films in pure DESs and a 10 wt% H₂O admixture with DESs. The results showed that the polymerisation rate of solutions of 10 wt% H₂O in various DESs tends to be higher than for the pure DESs. The water decreases the viscosity, which is one of the most important factor in the growth of such polymer systems.¹¹⁷ In addition, the solubility of the polymers in water is generally very low; recent research has suggested that polymer solubility increases when mixing ionic liquids with water. As an example, the solubility of poly(*N*-vinylimidazole) (L-PVI) in water has been found as $9.6 \pm 0.4 \text{ g L}^{-1}$ at 25°C, However, when mixing ionic liquids with water, the polymer's solubility increases significantly to $42 \pm 5 \text{ g L}^{-1}$.¹¹⁸

1.10 Aim of project.

The literature described above shows that water-DESs systems have been frequently studied but little is known about transport in such systems or the structural properties beyond quantum mechanical and molecular dynamic simulations. Even less is known about deep eutectic solvents. The studies to date have focussed on collecting physical data without explaining the causes of the observed trends. Most studies have assumed that water-IL and water-DES mixtures are homogeneous, and few have considered whether the micro- or nanostructure will affect mass transport.

The aim of this study is to go beyond the simple viscosity, conductivity and density measurement to understand the size of the heterogeneity using dynamic light scattering and to probe the data in alternative methods to investigate the structure breaking and making effects of water. Calorimetry will be used for the first time to determine the enthalpy of mixing to see whether the two components are thermodynamically more stable in separate phases and whether they only form an emulsion due to similarities in density.

In addition to probing the phase behaviour, diffusional studies will be made using both Pulsed Field Gradient (PFG) NMR and electrochemical techniques. This will show the self-diffusion of the different components and provide an insight into how they diffuse, which can highlight differences in local structure. By using bulk viscosity data, the diffusional data can be compared with the values predicted from the Stokes-Einstein equation to see if the local viscosity is different to the bulk viscosity. This is also a good

probe for local structure. Electrochemical techniques will reveal the diffusion coefficient of simple, electroactive molecular probes. This will be particularly useful for metal containing species where speciation can change when water is added, and it may explain whether the metal partitions from a mainly ionic phase to a mainly water-based phase as the composition of the mixture changes. Visible-spectroscopy will be used to probe speciation in solution and these will be correlated with the diffusion coefficient data.

In the final part of this study, the effect of water on copper electroplating will be studied. It has empirically been observed that small concentrations of water change the morphology of the copper deposit. The study will aim to determine whether this is due to changes in mass transport, speciation or double-layer structure.

1.11 References.

1. D. R. MacFarlane, A. L. Chong, M. Forsyth, M. Kar, R. Vijayaraghavan, A. Somers and J. M. Pringle, *Faraday Discussions*, 2018, **206**, 9-28.
2. R. Hayes, G. G. Warr and R. Atkin, *Physical Chemistry Chemical Physics*, 2010, **12**, 1709-1723.
3. J.-P. Belieres and C. A. Angell, *The Journal of Physical Chemistry B*, 2007, **111**, 4926-4937.
4. A. Schmid, A. Kollmer, R. G. Mathys and B. Witholt, *Extremophiles* 1998, **2**, 249–256.
5. A. S. Wells and V. T. Coomb, *Organic Process Research and Development*, 2006, **10**, 794-798.
6. F. Endres and S. Z. El Abedin, *Physical Chemistry Chemical Physics*, 2006, **8**, 2101-2116.
7. K. M. Docherty and J. Charles F. Kulpa, *Green Chemistry*, 2005, **7**, 185.
8. A. P. Abbott, G. Capper, D. L. Davies, R. K. Rasheed and V. Tambyrajah, *Chemical Communications*, 2003, 70-71.
9. N. V. Plechkova and K. R. Seddon, *Chemical Society Reviews*, 2008, **37**, 123-150.
10. T. Welton, *Chemical Reviews*, 1999, **99**, 2071-2084.
11. P. Wasserscheid and W. Keim, *Angewandte Chemie International Edition*, 2000, **39**, 3772-3789.
12. S. Zhang, J. Wang, X. Lu and Q. Zhou, *Structures and Interactions of Ionic Liquids*, Springer 2014.
13. M. Isik, H. Sardon and D. Mecerreyes, *International Journal of Molecular Sciences*, 2014, **15**, 11922-11940.

14. O. Fontaine, C. Lagrost, J. Ghilane, P. Martin, G. Trippé, C. Fave, J. C. Lacroix, P. Hapiot and H. N. Randriamahazaka, *Journal of Electroanalytical Chemistry*, 2009, **632**, 88-96.
15. C. Capello, U. Fischer and K. Hungerbühler, *Green Chemistry*, 2007, **9**, 927-934.
16. P. T. Anastas and J. C. Warner, *Green Chemistry: Theory and Practice*, Oxford university press, 2000.
17. J. S. Wilkes, *Green Chemistry*, 2002, **4**, 73-80.
18. A. Romero, A. Santos, J. Tojo and A. Rodriguez, *Journal of Hazardous Materials*, 2008, **151**, 268-273.
19. K. R. Seddon, A. Stark and M.-J. Torres, *Pure and Applied Chemistry*, 2000, **72**, 2275-2287.
20. Y. Dai, J. van Spronsen, G.-J. Witkamp, R. Verpoorte and Y. H. Choi, *Journal of Natural Products*, 2013, **76**, 2162-2173.
21. B. Tang, H. Zhang and K. H. Row, *Journal of Separation Science*, 2015, **38**, 1053-1064.
22. L. Duan, L.-L. Dou, L. Guo, P. Li and E.-H. Liu, *ACS Sustainable Chemistry & Engineering*, 2016, **4**, 2405-2411.
23. A. P. Abbott, A. Y. Al-Murshedi, O. A. Alshammari, R. C. Harris, J. H. Kareem, I. B. Qader and K. Ryder, *Fluid Phase Equilibria*, 2017, **448**, 99-104.
24. R. C. Harris, PhD Thesis, University of Leicester, 2009.
25. A. P. Abbott, G. Frisch and K. S. Ryder, *Annual Review of Materials Research*, 2013, **43**, 335-358.
26. E. L. Smith, A. P. Abbott and K. S. Ryder, *Chemical Reviews*, 2014, **114**, 11060-11082.

27. D. V. Wagle, H. Zhao and G. A. Baker, *Accounts of Chemical Research*, 2014, **47**, 2299-2308.
28. F. Endres, D. MacFarlane and A. Abbott, *Electrodeposition from Ionic Liquids*, 2008.
29. Z. Maugeri and P. D. d. María, *Royal Society of Chemistry*, 2012, **2**, 421.
30. Q. Zhang, K. D. O. Vigier, S. Royer and F. Jerome, *Chemical Society Reviews*, 2012, **41**, 7108-7146.
31. H. M. Abood, A. P. Abbott, A. D. Ballantyne and K. S. Ryder, *Chemical Communications*, 2011, **47**, 3523-3525.
32. A. P. Abbott, A. A. Al-Barzinjy, P. D. Abbott, G. Frisch, R. C. Harris, J. Hartley and K. S. Ryder, *Physical Chemistry Chemical Physics*, 2014, **16**, 9047-9055.
33. H. M. Abood, A. P. Abbott, A. D. Ballantyne and K. S. Ryder, *Chemical Communications*, 2011, **47**, 3523-3525.
34. A. P. Abbott, K. E. Ttaib, K. S. Ryder and E. L. Smith, *The International Journal of Surface Engineering and Coatings*, 2008, **86**, 234-240.
35. A. P. Abbott, K. E. Ttaib, G. Frisch, K. J. McKenzie and K. S. Ryder, *Physical Chemistry Chemical Physics*, 2009, **11**, 4269-4277.
36. A. P. Abbott, K. E. Ttaib, G. Frisch, K. S. Ryder and D. Weston, *Physical Chemistry Chemical Physics*, 2012, **14**, 2443-2449.
37. E. Gómez, P. Cojocar, L. Magagnin and E. Valles, *Journal of Electroanalytical Chemistry*, 2011, **658**, 18-24.
38. A. P. Abbott, J. C. Barron, G. Frisch, K. S. Ryder and A. F. Silva, *Electrochimica Acta*, 2011, **56**, 5272-5279.
39. A. P. Abbott and K. J. McKenzie, *Physical Chemistry Chemical Physics*, 2006, **8**, 4265-4279.

40. B. Tang and K. Row, *Monatshefte für Chemie - Chemical Monthly*, 2013, **144**, 1427-1454.
41. P. Xu, G.-W. Zheng, M.-H. Zong, N. Li and W.-Y. Lou, *Bioresources and Bioprocessing*, 2017, **4**, 34.
42. J. D. Bernal, *Proceedings of the Royal Society of London. Series A, Mathematical and Physical Sciences*, 1964, **280**, 299-322.
43. E. I. Izgorodina and D. R. MacFarlane, *The Journal of Physical Chemistry B*, 2011, **115**, 14659-14667.
44. D. F. Evans, S.-H. Chen, G. W. Schriver and E. M. Arnett, *Journal of the American Chemical Society*, 1981, **103**, 481-482.
45. R. Ludwig, *The Journal of Physical Chemistry B*, 2009, **113**, 15419-15422.
46. J. N. Canongia Lopes and A. A. Padua, *The Journal of Physical Chemistry B*, 2006, **110**, 3330-3335.
47. R. Hayes, G. G. Warr and R. Atkin, *Chemical Reviews*, 2015, **115**, 6357-6426.
48. S. Chen, S. Zhang, X. Liu, J. Wang, J. Wang, K. Dong, J. Sun and B. Xu, *Physical Chemistry Chemical Physics*, 2014, **16**, 5893-5906.
49. Y. Wang, W. Jiang, T. Yan and G. A. Voth, *Accounts of Chemical Research*, 2007, **40**, 1193-1199.
50. Y. Wang and G. A. Voth, *Journal of the American Chemical Society*, 2005, **127**, 12192-12193.
51. H. Weingärtner, A. Knocks, W. Schrader and U. Kaatze, *The Journal of Physical Chemistry A*, 2001, **105**, 8646-8650.
52. J. D. Holbrey, W. M. Reichert, M. Nieuwenhuyzen, S. Johnson, K. R. Seddon and R. D. Rogers, *Chemical Communications*, 2003, 1636-1637.

53. J. D. Holbrey, W. M. Reichert, M. Nieuwenhuyzen, O. Sheppard, C. Hardacre and R. D. Rogers, *Chemical Communications*, 2003, 476-477.
54. A. Yokozeki, D. J. Kasprzak and M. B. Shiflett, *Physical Chemistry Chemical Physics*, 2007, **9**, 5018-5026.
55. K. Ala'a, A. M. Greenway, P. B. Hitchcock, T. J. Mohammed, K. R. Seddon and J. A. Zora, *Chemical Communications*, 1986, 1753-1754.
56. K. Fumino, A. Wulf and R. Ludwig, *Angewandte Chemie International Edition*, 2008, **47**, 8731-8734.
57. A. R. Leach, *Molecular Modelling: Principles and Applications*, Pearson Education, 2001.
58. K. Dong, S. Zhang and J. Wang, *Chemical Communications*, 2016, **52**, 6744-6764.
59. K. Fumino, A. Wulf and R. Ludwig, *Angewandte Chemie International Edition*, 2008, **47**, 3830-3834.
60. A. Triolo, O. Russina, H.-J. Bleif and E. Di Cola, *The Journal of Physical Chemistry B*, 2007, **111**, 4641-4644.
61. H. Sun, Y. Li, X. Wu and G. Li, *Journal of Molecular Modeling*, 2013, **19**, 2433-2441.
62. A. P. Abbott, D. Boothby, G. Capper, D. L. Davies and R. K. Rasheed, *Journal of the American Chemical Society*, 2004, **126**, 9142-9147.
63. S. Zahn, B. Kirchner and D. Mollenhauer, *ChemPhysChem*, 2016, **17**, 3354-3358.
64. R. Stefanovic, M. Ludwig, G. B. Webber, R. Atkin and A. J. Page, *Physical Chemistry Chemical Physics*, 2017, **19**, 3297-3306.

65. S. L. Perkins, P. Painter and C. M. Colina, *Journal of Chemical & Engineering Data*, 2014, **59**, 3652-3662.
66. O. S. Hammond, D. T. Bowron and K. J. Edler, *Green Chemistry*, 2016, **18**, 2736-2744.
67. C. Hanke, N. Atamas and R. Lynden-Bell, *Green Chemistry*, 2002, **4**, 107-111.
68. J. Zhou, X. Liu, S. Zhang, X. Zhang and G. Yu, *American Institute of Chemical Engineers Journal*, 2017, **63**, 2248-2256.
69. C. G. Hanke and R. M. Lynden-Bell, *The Journal of Physical Chemistry B*, 2003, **107**, 10873-10878.
70. S. Feng and G. A. Voth, *Fluid Phase Equilibria*, 2010, **294**, 148-156.
71. M. Moreno, F. Castiglione, A. Mele, C. Pasqui and G. Raos, *The Journal of Physical Chemistry B*, 2008, **112**, 7826-7836.
72. Y. Kohno and H. Ohno, *Chemical Communications*, 2012, **48**, 7119-7130.
73. W. Liu, T. Zhao, Y. Zhang, H. Wang and M. Yu, *Journal of Solution Chemistry*, 2006, **35**, 1337-1346.
74. T. Singh and A. Kumar, *Colloids and Surfaces A: Physicochemical and Engineering Aspects*, 2008, **318**, 263-268.
75. N. A. Smirnova, A. A. Vanin, E. A. Safonova, I. B. Pukinsky, Y. A. Anufrikov and A. L. Makarov, *Journal of Colloid and Interface Science*, 2009, **336**, 793-802.
76. M. Brehm, H. Weber, A. S. Pensado, A. Stark and B. Kirchner, *Physical Chemistry Chemical Physics*, 2012, **14**, 5030-5044.
77. M. S. Kelkar and E. J. Maginn, *The Journal of Physical Chemistry B*, 2007, **111**, 4867-4876.

78. J. Wang, H. Wang, S. Zhang, H. Zhang and Y. Zhao, *The Journal of Physical Chemistry B*, 2007, **111**, 6181-6188.
79. X. Meng, K. Ballerat-Busserolles, P. Husson and J.-M. Andanson, *New Journal of Chemistry*, 2016, **40**, 4492-4499.
80. M. S. Kelkar, W. Shi and E. J. Maginn, *Industrial & Engineering Chemistry Research*, 2008, **47**, 9115-9126.
81. A. Sharma and P. K. Ghorai, *The Journal of Chemical Physics*, 2016, **144**, 114505.
82. L. Cammarata, S. Kazarian, P. Salter and T. Welton, *Physical Chemistry Chemical Physics*, 2001, **3**, 5192-5200.
83. A. S. Kashin, K. I. Galkin, E. A. Khokhlova and V. P. Ananikov, *Angewandte Chemie International Edition*, 2016, **55**, 2161-2166.
84. P. Bonhôte, A.-P. Dias, N. Papageorgiou, K. Kalyanasundaram and M. Graätzel, *Inorganic Chemistry*, 1996 **35**, 1168-1178.
85. P. Wasserscheid and T. Welton, *Ionic Liquids in Synthesis*, Wiley, 2007.
86. S. G. Cull, J. D. Holbrey, V. Vargas-Mora, K. R. Seddon and G. J. Lye, *Biotechnology and Bioengineering* 2000, **69**, 227-233.
87. D. W. Armstrong, L. He and Y.-S. Liu, *Analytical Chemistry*, 1999, **71**, 3873-3876.
88. Y. Kohno and H. Ohno, *Chemical Communications*, 2012 **48**, 7119–7130.
89. R. P. Swatloski, A. E. Visser, W. M. Reichert, G. A. Broker, L. M. Farina, J. D. Holbrey and R. D. Rogers, *Green Chemistry*, 2002, **4**, 81-87.
90. R. P. Swatloski, A. E. Visser, W. M. Reichert, G. A. Broker, L. M. Farina, J. D. Holbrey and R. D. Rogers, *Chemical Communications*, 2001, 2070-2071.

91. K. Fumino, A. Wulf and R. Ludwig, *Angewandte Chemie International Edition*, 2009, **48**, 3184-3186.
92. J. E. Reid, R. J. Gammons, J. M. Slattery, A. J. Walker and S. Shimizu, *Journal of Physical Chemistry B*, 2017, **121**, 599-609.
93. N. Yaghini, L. Nordstierna and A. Martinelli, *Physical Chemistry Chemical Physics*, 2014, **16**, 9266-9275.
94. J. D. Holbrey and R. Seddon, *Journal of the Chemical Society, Dalton Transactions*, 1999, 2133–2139.
95. J. G. Huddleston, A. E. Visser, W. M. Reichert, H. D. Willauer, G. A. Broker and R. D. Rogers, *Green Chemistry*, 2001, **3**, 156-164.
96. Sandra T. M. Vidal, M. Joana Neiva Correia, M. Matilde Marques, M. Rosinda Ismael and M. T. A. Reis, *Separation Science and Technology* 2004, **39**, 2155–2169.
97. M. López-Pastor, M. J. Ayora-Cañada, M. Valcárcel and B. Lendl, *Journal of Physical Chemistry B*, 2006, **110**, 10896-10902.
98. Y. Jeon, J. Sung, D. Kim, C. Seo, H. Cheong, Y. Ouchi, R. Ozawa and H. Hamaguchi, *Journal of Physical Chemistry B*, 2008, **112**, 923-928.
99. B. Fazio, A. Triolo and G. Di Marco, *Journal of Raman Spectroscopy*, 2008, **39**, 233-237.
100. J. P. Hallett and T. Welton, *Chemical Reviews*, 2011, **111**, 3508-3576.
101. O. S. Hammond, D. T. Bowron and K. J. Edler, *Angewandte Chemie*, 2017.
102. D. Shahi and F. S. Mjalli, *Physical Chemistry Chemical Physics*, 2014, **16**, 23900-23907.
103. T. Zhekenov, N. Toksanbayev, Z. Kazakbayeva, D. Shah and F. S. Mjalli, *Fluid Phase Equilibria*, 2017, **441**, 43-48.

104. L. Crowhurst, P. R. Mawdsley, J. M. Perez-Arlandis, P. A. Salter and T. Welton, *Physical Chemistry Chemical Physics*, 2003, **5**, 2790-2794.
105. M. J. Muldoon, C. M. Gordon and I. R. Dunkin, *Journal of the Chemical Society, Perkin Transactions*, 2001, **2**, 433-435.
106. A. J. Carmichael and K. R. Seddon, *Journal of Phasical Organic Chemistry*, 2000, **13**, 591-595.
107. Y. Fukaya, A. Sugimoto and H. Ohno, *Biomacromolecules*, 2006, **7**, 3295-3297.
108. Y. Fukaya, K. Hayashi, M. Wada and H. Ohno, *Green Chemistry*, 2008, **10**, 44-46.
109. M. Abe, Y. Fukaya and H. Ohno, *Green Chemistry*, 2010, **12**, 1274.
110. H. Kobayashi and A. Fukuoka, *New and Future Developments in Catalysis*, Elsevier Science, 2013.
111. K. Fujita, D. R. MacFarlane, M. Forsyth, M. Yoshizawa-Fujita, K. Murata, N. Nakamura and H. Ohno, *Biomacromolecules*, 2007, **8**, 2080-2086.
112. K. Fujita, M. Sanada and H. Ohno, *Chemical Communications*, 2015, **51**, 10883-10886.
113. R. Vijayaraghavan, A. Izgorodin, V. Ganesh, M. Surianarayanan and D. R. MacFarlane, *Angewandte Chemie International Edition*, 2010, **49**, 1631-1633.
114. A. Chandran, D. Ghoshdastidar and S. Senapati, *Journal of the American Chemical Society*, 2012, **134**, 20330-20339.
115. A. E. Visser, R. P. Swatloski and R. D. Rogers, *Green Chemistry*, 2000, 1-4.
116. W. Guor-Tzo, Y. Zusing and C. Chao-Jung, *Analytica Chimica Acta*, 2003, **488**, 183-192.
117. H. K. Ismail, PhD Thesis, University of Leicester, 2017.

118. C. S. Renamayor, A. Pastoriza, C. L. Usma and I. F. Pierola, *Colloid and Polymer Science*, 2013, **291**, 2439-2446.

Chapter 2: Experimental and Methods.

2	Experimental and Methods.....	38
2.1	Materials.....	38
2.1.1	Chemicals.....	38
2.2	Humidity measurement.....	39
2.3	Preparation of deep eutectic solvents.....	39
2.4	Measurement of amount of water in pure DESs.....	40
2.5	Measurement of thermophysical properties.....	40
2.5.1	Viscosity.....	40
2.5.2	Conductivity.....	42
2.5.3	Surface tension and density.....	42
2.5.4	Reflective index.....	43
2.6	Dynamic light scattering.....	43
2.7	Measurement of acidity of liquids.....	44
2.8	Measurement of fluidity characteristics.....	44
2.9	Thermodynamic properties.....	45
2.10	Thermal properties.....	45
2.10.1	Heat capacity.....	45
2.11	Measurement the diffusion coefficient.....	45
2.11.1	PFG-NMR measurements.....	45
2.12	Electrochemical measurements.....	46
2.12.1	Cyclic voltammetry measurement.....	46
2.12.2	Capacity double layer measurements.....	47
2.13	UV-Vis spectroscopy measurements.....	48
2.14	Microchemical and microstructural analyses.....	48
2.14.1	Scanning electron microscopy.....	48
2.14.2	X-ray diffraction (XRD).....	48
2.15	References.....	50

2 Experimental and Methods.

2.1 Materials.

2.1.1 Chemicals.

All the experiments carried out in an ambient atmosphere at the same temperature as the laboratory (typically between 20-25°C) and were completed without using dry air or nitrogen gas. Each experiment was repeated at least three times, from which the average value was taken. Finally, the standard deviation was calculated for each sample. All materials used in this work are shown in **Table 2.1**, including source and purity. No additional purification was carried out prior to the experiments.

Table 2.1: List of chemicals used in this thesis and their source and purity.

Chemicals	Source	Purity%
Choline chloride	Sigma-Aldrich	≥98
Glycerol	Fischer	98
Urea	Sigma-Aldrich	99.9
Ethylene glycol	Sigma-Aldrich	≥99
Oxalic acid dihydrate	Fischer	99
Iron (III) chloride	Sigma-Aldrich	≥97
Sodium iodide	Sigma-Aldrich	> 99
Potassium perchlorate	Sigma-Aldrich	>99
Iodine	Fischer	>98
Sodium chloride	Fischer	≥97
Potassium ferrocyanide	BDH	99
Copper(II) chloride dihydrate	Sigma-Aldrich	≥99
1-Butyl-3-methylimidazolium tetrafluoroborate	Sigma-Aldrich	≥98
1-Butyl-3-methylimidazolium chloride	Merck	98
1-Ethyl-3-methylimidazolium acetate	Sigma-Aldrich	≥98
1-Butyl-3-methylimidazolium bis(trifluoromethanesulfonyl)imide	Sigma-Aldrich	≥98
1-Butyl-3-methylimidazolium trifluoromethanesulfonate	Sigma-Aldrich	≥98

2.2 Humidity measurement.

Humidity of laboratory was measured by humidity and temperature recorder RH520 EXTECH instruments, the humidity within the laboratory was measured to be between 45 - 65%. It is important to note here the humidity will change depending on the weather and season.

2.3 Preparation of deep eutectic solvents.

Type 3 deep eutectic solvents were prepared by mixing the quaternary ammonium salt choline chloride with a hydrogen bond donor (HBD). The molar composition of the eutectic point was recorded from previous studies¹ and it was based on a 1:2 composition ratio for choline chloride: ethylene glycol, choline chloride: glycerol and choline chloride: urea. However, a 1:1 composition ratio for oxalic acid: choline chloride was used. The solutions were made up by mixing 250 g choline chloride with 215.11 g, 215.08 g and 329.78 g of ethylene glycol, urea and glycerol, respectively. The mixture was continuously stirred by using magnetic bar stirrer under ambient laboratory conditions and heated at 60°C for 5 hours until a clear liquid was formed.^{2,3}

Oxaline was prepared by mixing choline chloride 250 gm and oxalic acid 161.20 gm in a 1:1 molar ratio. The mixture was stirred and placed in an oven at 50°C. The mixture was stirred every 30 minutes until a clear liquid was formed. **Table 2.2** shows the quaternary ammonium salt and hydrogen-bond donor forming each DES with the appropriate molar ratios.

Table 2.2: The specifications of the deep eutectic solvents used in this study.

DES	Components		Molar ratio Ch Cl: HBD
	Quaternary ammonium salt	Hydrogen bond donor (HBD)	
Ethaline 200	Choline Chloride	Ethylene glycol	1:2
Glyceline 200	Choline Chloride	Glycerol	1:2
Reline 200	Choline Chloride	urea	1:2
Oxaline 100	Choline Chloride	Oxalic acid dehydrate	1:1

2.4 Measurement of amount of water in pure DESs.

The water content of each of the pure liquids were measured using volumetric Karl-Fischer (KF) titrator SNR B727340076 and were found to be 1.50 wt% \pm 0.04%, 0.8 wt% \pm 0.02, 0.72 wt% \pm 0.01 and 2.40 wt% \pm 0.03 for Ethaline, Glyceline, Reline and Oxaline, respectively. After running the experiments re-measured the amount of water for all liquids were found to have increased by about 0.5 wt% , 0.4 wt% , 0.3 wt% and 0.8 for Ethaline, Glyceline, Reline and Oxaline, respectively. It is worth noting here that all measurements were carried out using fresh liquids to reduce the absorption of water.

2.5 Measurement of thermophysical properties.

2.5.1 Viscosity.

The viscosity of the pure DESs were measured using two methods. The viscosity of DESs (pure and as admixtures with water) were measured using a rotational viscometer (Brookfield DV-E+ Pro) instrument. The spindle was rotated in a given liquid at specific speed which varied according to the viscosity of liquids (5-200 revolution per minute having acceptable ranges of torque (10-100) and at a temperature of 25°C -75°C). **Figure 2.1** shows a schematic of the rotational viscometer. The calibration procedure was performed by measuring the viscosity of a standard fluid such as mineral oil at 25°C. The viscosity was recorded at least three times at each temperature, and an average taken for each sample.

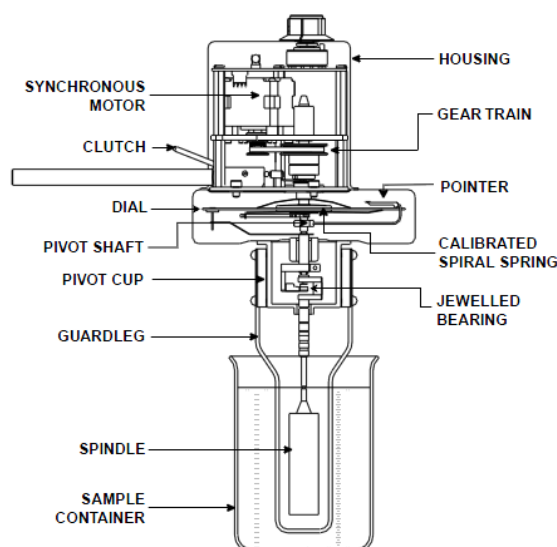


Figure 2.1: A schematic of the rotational viscometer

The viscosities of pure DESs were also measured using a Quartz Crystal Microbalance (Agilent Technologies E5061A 300 kHz ENA Series Network Analyzer) at different temperatures (40, 50, 60 and 70°C) using a polished crystal. The frequency of the crystal was necessary as a measurement of the viscosity by QCM required calibration using the frequency for the dry quartz crystal before performing any liquid measurements. The frequency of the dry crystal was thus recorded. The cell used in this work, which was built in-house, as shown in **Figure 2.2**, was a quartz crystal wafer in a glass tube and was connected with electrical wires. The cell was then immersed in the liquid under investigation. **Figure 2.2** illustrates a schematic of the cell. Each sample was scanned 20 times by machine then the average value was taken for each and the standard deviation (SD) evaluated. To ensure the device was accurate, the viscosity of glycerol liquids was measured via QCM at 25°C. Each sample was mixed at least 10 min before each measurement was taken.

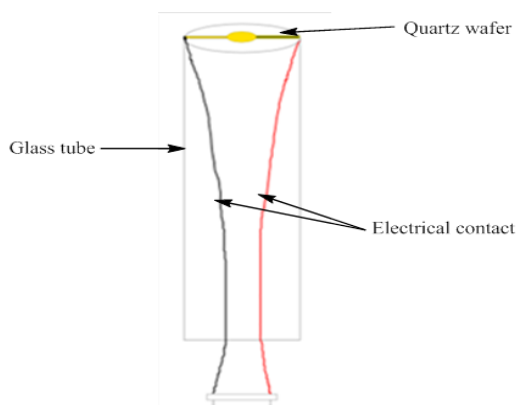


Figure 2.2: A schematic of the QCM cell used in this study.

2.5.2 Conductivity.

The conductivities of the DESs used in this study were measured using a Jenway 4510 conductivity meter as follows: the conductivity meter probe was immersed in a liquid over a range of temperatures (25°C- 70°C), with the conductivity recorded at least three times at each temperature, from which the average was determined for each sample. The calibration of the conductivity probe was done by dissolving 0.746 g of KCl in 1 litre of deionized water to prepare a 0.01 M solution at 25°C.

2.5.3 Surface tension and density.

A KRÜSS Tensiometer K9 model K9MK1 was used to measure the density and surface tension of the DESs. The temperature was controlled through the use of a thermostat connected to the jacket that contained a glass dish in which to place the liquid sample. The density of the liquid sample was measured when its temperature had reached the specified temperatures (25, 30, 35, 40, 45, 50, 55 and 60°C) of interest, and this procedure was repeated at least three times. A silicon log of known density (2.03 g cm⁻³) was placed on a Pt-Ir cradle and submerged in the liquid, and the density values recorded. Surface tension measurements were taken using a Pt-Ir alloy plate (KRUSS, part number PL01). The surface tension and the density were recorded at least three times at each temperature, the average of which was determined for each sample. The calibration of machine was done by measurement of the surface tension of glycerol at 25°C. Each sample was mixed at least 10 min before each measurement was taken.

2.5.4 Reflective index.

The refractive indices of the pure DESs and those with different water mixtures varied from 5 – 95 wt% were performed using a REFRACTOMETR, RFM 732 automatic digital at room temperature. The calibration of machine was done by measurement of the reflective index of deionized water at 25°C.

2.6 Dynamic light scattering.

Dynamic light scattering (DLS) was used to study the aggregation size of particles or droplets, their size distributions, and the shapes of the nanoparticles in the liquids. **Figure 2.3** shows a schematic diagram of the DLS apparatus.⁴ The DLS can measure light scattering on a microsecond time scale, and the size of droplets was found by analysing the scattered light intensity through time autocorrelation, $g_2(\tau)$, which can be defined as per **Equation (2.1)**.

$$g_2 = [I(t)I(t + \tau)]/[I(t)]^2 \quad \text{Equation (2.1)}$$

where $I(t)$ and $I(t+\tau)$ are the scattered intensities at some initial time t and some later time $(t+\tau)$, τ is the delay time, and averaging was done over the observation time, t . The relationship between fitting the time autocorrelation function with an exponential decay function integrated over the relaxation rate distribution, $G(\Gamma)$, allows the calculation of the relaxation times of the particles.

$$g_2(\tau) = 1 + \beta' g_1^2(\tau) \quad \text{Equation (2.2)}$$

$$g_1(\tau) = \int G(\Gamma) \exp(-\Gamma\tau) d\Gamma \quad \text{Equation (2.3)}$$

$$\Gamma = q^2 \quad \text{Equation (2.4)}$$

$$q^2 = \left(4\pi \frac{n_o}{\lambda}\right) \sin\left(\frac{\theta}{2}\right) \quad \text{Equation (2.5)}$$

where n_o is the refractive index of the solvent, λ is the laser wavelength in vacuum, θ is the scattering angle, and β' is an instrument alignment-dependent coherence factor. In addition, at infinite dilution the hydrodynamic radii (R_h) can be obtained from the Stokes–Einstein equation.

$$D = k_B T / 6\pi\eta R_h \quad \text{Equation (2.6)}$$

where T is the solution temperature, k_B is the Boltzmann constant, and η is the solution viscosity.⁵

The size of droplets formed when water was mixed in the ionic liquids was determined using a Malvern instrument, Zetasizer Nano dynamic light scattering apparatus. To each ionic liquid, 5 wt% water was added, and each mixture was stirred for 10 minutes before filtration through a 0.22 μm Nylon filter to remove any solid particles from the liquids under investigation. Each sample was scanned seven times with the DLS machine and the average value was taken for each. The standard deviation (SD) was then determined, which is presented in the form of error bars.

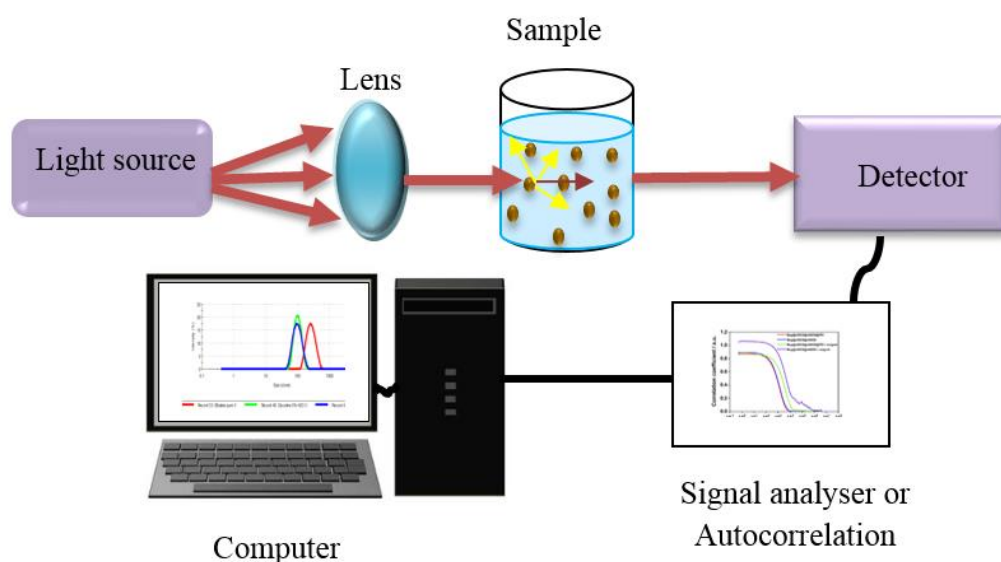


Figure 2.3: A schematic diagram of dynamic light scattering. Adapted from Ref.6.

2.7 Measurement of acidity of liquids.

The acidities of Ethaline, Glyceline and Reline with 20 wt% water were measured individually using a JENWAY ST150SA, 3510 pH meter at 20°C.

2.8 Measurement of fluidity characteristics.

To determine whether the DESs behaved in a Newtonian or non-Newtonian manner, their viscosities were measured at different temperatures (30°C and 50°C) using a rotational

viscometer (Brookfield DV-E+ Pro). A variety of spindles (LV1, LV2 and LV3) were used with rotational speeds of 5 - 200 rpm to obtain appropriate viscosity data.

2.9 Thermodynamic properties

For the iodine extraction experiments, a hexane solution was prepared (1.19×10^{-3} mol kg⁻¹ of iodine in 7.0 g hexane) and this was extracted at two different temperatures (25°C and 35°C) with 1.0 g of DES, at a stirring rate of 500 rpm for 5 min. The hexane layer was analysed by UV-Vis spectroscopy using a Shimadzu model UV-1601 spectrophotometer and the amount extracted was determined using a calibration plot. The same method was used with mixtures of hexane and water. The UV-Vis spectrum was recorded at least three times for each sample at 25°C and 35°C, then the average absorption was taken for each sample.

2.10 Thermal properties.

2.10.1 Heat capacity.

A Mettler Toledo Differential Scanning Calorimeter (DSC) was used to carry out a study of heat capacity and enthalpy of formation for all DESs under investigation. It is important to mention here that the empty crucible, which was made from aluminium, was used to obtain a baseline due to use of these data for heat transfer calculations. The pans, with and without liquids, were heated until a fixed heating rate of 5-10 K min⁻¹ was obtained under an inert atmosphere of nitrogen (75 cm³ min⁻¹). The STAR^e system software was used to analyse the data. Each experiment was repeated at least three times, then the average value was taken. Finally, the standard deviation was calculated for each sample.

2.11 Measurement the diffusion coefficient.

2.11.1 PFG-NMR measurements.

PFG-NMR diffusion measurements were conducted on a Bruker DMX 300 spectrometer, equipped with a diffusion probe capable of producing magnetic field gradient pulses up to 11.76 T/m in the *z*-direction and using a pulsed gradient stimulated echo (PGSTE) sequence with a homospoil gradient, which is usually preferred to the standard pulsed gradient spin echo or PGSE sequence, resulting in a better signal-to-noise ratio. The NMR signal attenuation, $E_{(g)}/E_0$, is related to the experimental variables and the diffusion coefficient *D* according to:

$$\frac{E(g)}{E_0} = \exp\left[-D\gamma_H^2 g^2 \delta^2 \left(\Delta - \frac{\delta}{3}\right)\right] \quad \text{Equation (2.7)}$$

In **Equation (2.7)**, $E(g)$ and E_0 are the NMR signal in the presence and absence of the gradient pulse, respectively; γ_H is the gyromagnetic ratio of the nuclei being studied (i.e., ^1H in our case), g is the strength of the gradient pulse of duration δ , and Δ is the observation time. The measurements were performed by holding Δ (equal to 50 ms) and δ (values in the range 1 – 4 ms) constant and varying g in sixteen increments. In order to achieve full signal attenuation, maximum values of g of up to 11.50 T/m were necessary. The diffusion coefficients D can be calculated by fitting **Equation (2.7)** to the experimental data. More details on the experimental set-up can be found elsewhere.⁷

2.12 Electrochemical measurements.

2.12.1 Cyclic voltammetry measurement.

Electrochemical measurements were performed using cyclic voltammetry with an Autolab PGSTAT20 software-controlled potentiostat using three electrodes; a 0.5 mm platinum wire as the working electrode, a silver wire as the reference electrode and a platinum sheet as the counter electrode. **Figure 2.4** shows the cyclic voltammetry setup.

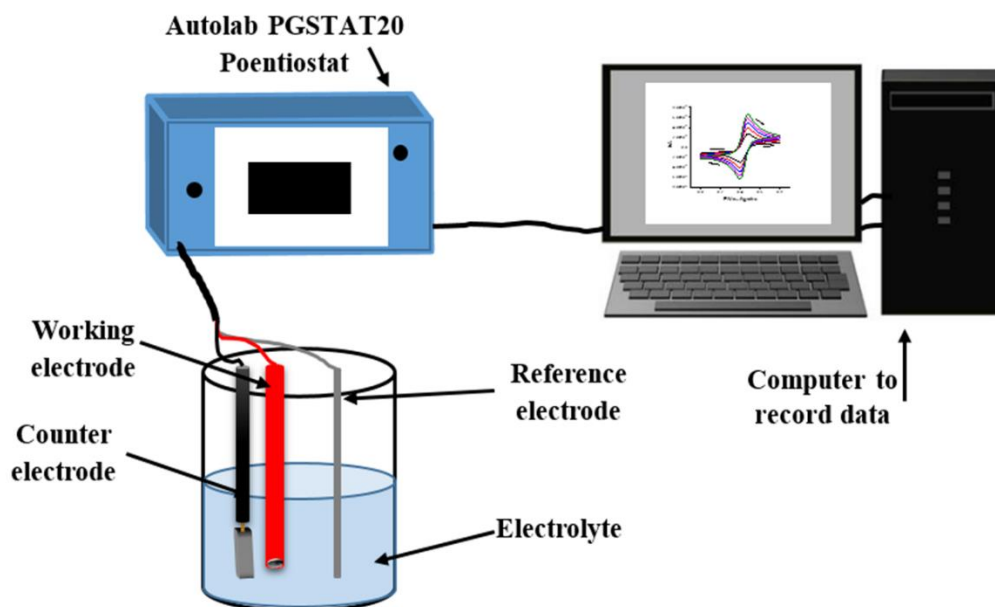


Figure 2.4: A schematic of the cyclic voltammetry experiment.

Cyclic voltammetry was performed for iron chloride dissolved in pure Ethaline, Glyceline and Reline, and repeated for each with different water content (5 wt% -100 wt% H₂O). Iron chloride was used as a probe to study mass transport properties. Solutions of this probe were made by adding iron chloride to the respective liquids, followed by stirring at 50°C until they were completely dissolved. All solutions were made up to a concentration of 0.02 mol dm⁻³ iron chloride. Moreover, sodium iodide, iodine and potassium ferrocyanide were dissolved in Ethaline and Ethaline with different water contents. All these solutions were made up to concentrations of 0.1 mol dm⁻³, 0.02 mol dm⁻³ and 0.002 mol dm⁻³, respectively, for each of these chemical probes. In addition, the solutions of FeCl₃, NaI and K₄Fe(CN)₆·3H₂O in water were also made up to 0.1 mol dm⁻³ KClO₄, 0.1 mol dm⁻³ NaCl and 0.1 mol dm⁻³ KCl, respectively, which were used as supporting electrolytes to minimise any migratory effects. Cyclic voltammetry of FeCl₃ and K₄Fe(CN)₆·3H₂O was carried out at different scan rates of 5, 10, 15, 20 and 25 mVs⁻¹. In addition, NaI and I₂ were measured at scan rates of 4, 5, 8 and 10 mVs⁻¹. The Randles-Sevcik equation, **Equation (2. 8)**, used the peak current for the reversible couple at room temperature to determine diffusion coefficient:

$$i_p = (2.69 \times 10^5) n^{3/2} ACD^{1/2}v^{1/2} \quad \text{Equation (2. 8)}$$

where n is the number of electrons, A is the electrode area (in cm²), C is the concentration of the electroactive species (in mol cm⁻³), D is the diffusion coefficient (in cm² s⁻¹) and v is the scan rate (in V s⁻¹). A plot of current vs. the square of the scan rate gives a linear relationship.⁸ In addition, the diffusion coefficient of the various species in Ethaline and Ethaline–water mixtures could be found by appropriate rearrangement of **Equation (2.8)**.

2.12.2 Capacity double layer measurements.

The capacity double layer was examined using cyclic voltammetry with the same modelling as given above in section 2.10.1 and with the same electrodes. These measurements were conducted for three systems, Ethaline, Glyceline and Reline, with different amounts of water ranging from 0 wt% - 70 wt%. A plot of total charge vs. water content can then be used to find the capacity double layer.

2.13 UV-Vis spectroscopy measurements.

UV-Vis spectroscopy was performed using A Shimadzu Model UV-1601 Spectrophotometer. UV-Vis spectroscopy was used to find whether potential changes in the speciation of all systems were iron in iron chloride and iodide in iodine in three systems: pure Ethaline, Glycine, and Reline, and then subsequently the same species with water. Liquids of these solutions were prepared by serial dilution from original solution. Well-resolved peaks were observed once the solutions had been diluted to different concentrations of $5 \times 10^{-4} \text{ mol dm}^{-3} \text{ FeCl}_3$, $1 \times 10^{-4} \text{ mol dm}^{-3} \text{ I}_2$ in Ethaline, $5 \times 10^{-4} \text{ mol dm}^{-3} \text{ I}_2$ in Glycine and $5 \times 10^{-3} \text{ mol dm}^{-3} \text{ I}_2$ in Reline. A quartz cuvette was used in this study.

2.14 Microchemical and microstructural analyses.

2.14.1 Scanning electron microscopy.

The surface analysis of the copper deposits was undertaken in this work using an FEI SIRION SEM scanning electron microscope, which were carried out under vacuum (10^{-5} Pa).

2.14.2 X-ray diffraction (XRD).

X-ray diffraction is useful technique that is used for qualitative and quantitative atomic characterisation. X-ray diffraction has been used for both solid and powder samples. X-ray diffraction was undertaken using a Phillips model PW 1730 X-ray generator. Bragg's Law demonstrates the relationship between the wavelength, λ , of the X-ray and the reflection angle of the X-ray, θ , via **Equation (2.9)**:

$$2d \sin \theta = n\lambda \qquad \text{Equation (2.9)}$$

where d is the distance between the crystal planes on the grating, θ and is the reflection angle of the X-ray, n is an integer number, and λ is the wavelength of X-ray⁹. X-rays scan the sample over a range of 2θ angles; it should be noted that the X-rays will penetrate deep inside the material, so observations are not just indicative of the surface of the sample. **Figure 2.5** illustrates Bragg's Law.

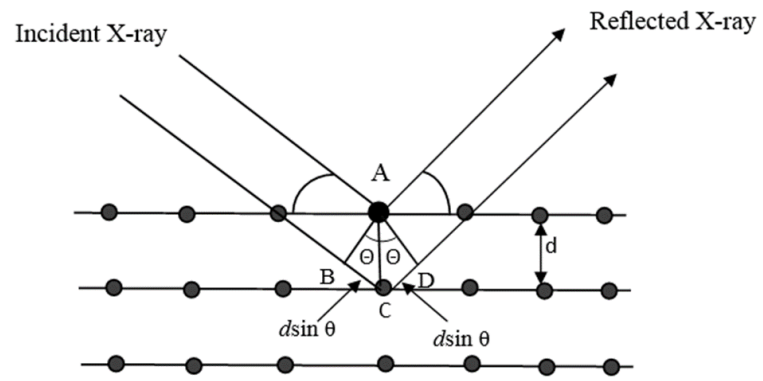


Figure 2.5: Schematic diagram of X-ray diffraction at a plane.

2.15 References

1. E. I. Ahmed, PhD Thesis, University of Leicester, 2015.
2. A. P. Abbott, G. Capper, K. J. McKenzie and K. S. Ryder, *Journal of Electroanalytical Chemistry*, 2007, **599**, 288-294.
3. A. P. Abbott, J. C. Barron, K. S. Ryder and D. Wilson, *Chemistry-A European Journal*, 2007, **13**, 6495-6501.
4. R. Pecora, *Journal of Nanoparticle Research*, 2000, **2**, 123–131.
5. R. J. Murphy, D. Pristinski, K. Migler, J. F. Douglas and V. M. Prabhu, *The Journal of Chemical Physics*, 2010, **132**, 194903.
6. R. Pecora, *Dynamic Light Scattering: Applications of Photon Correlation Spectroscopy*, Springer Science & Business Media, 2013.
7. C. D'Agostino, R. C. Harris, A. P. Abbott, L. F. Gladden and M. D. Mantle, *Physical Chemistry Chemical Physics*, 2011, **13**, 21383-21391.
8. J. Wany, *Analytical Electrochemistry*, Wiley-VCH, 2000.
9. G. Attard and C. Barnes, *Surfaces. Edition en Anglais*, Oxford University Press, 1998.

Chapter 3: Thermophysical properties of pure DESs and their mixtures with water.

3	Thermophysical properties of pure DESs and their mixtures with water.	52
3.1	Introduction.....	52
3.2	Objective.....	52
3.3	Results and discussion.	52
3.3.1	Viscosity of DESs using a rotational viscometer.....	52
3.3.2	Viscosity measurements using QCM.....	60
3.4	Rheological study.	62
3.4.1	Influence of temperature on fluidity of DESs.....	65
3.5	Surface tension.....	66
3.6	Ionic conductivity.	69
3.7	Density.....	73
3.8	Reflective index.....	75
3.9	Dynamic light scattering.....	75
3.10	Enthalpy of mixing DES with water.....	84
3.11	Extraction using DES-water mixtures.	85
3.12	Conclusions.....	89
3.13	References.....	91

3 Thermophysical properties of pure DESs and their mixtures with water.

3.1 Introduction.

Ionic liquids have found application in areas such as catalysis, separation, nanotechnology, and manufacturing, but the purity of the liquid and its effect on the process chemistry is a topic for much discussion.^{1, 2} Several studies have shown that the physical and chemical properties of ionic liquids can be tuned with an appropriate choice of cation and anion.^{3, 4} The physical properties of ionic liquids including viscosity,^{5, 6} density,⁷ surface tension⁸ and conductivity⁹ have been studied in great detail; however, a topic which has been studied in particular detail is the role of water in ionic liquids and at what composition an ionic liquid starts to behave like an aqueous solution.

3.2 Objective.

Recently, several groups have reported the physical properties of pure DESs and their mixtures with water. However, prior studies have all assumed the behaviour of these mixtures are homogenous. An initial objective of this project was to identify whether this assumption was in fact the case, and evidence was sought in terms of changes in physical properties. The analysis will take a different approach to any previous work reported in the literature, and will ultimately show that the physical data are not consistent with a homogeneous mixture.

3.3 Results and discussion.

3.3.1 Viscosity of DESs using a rotational viscometer.

A simple definition of viscosity is that of a measure of “resistance to flow or shear”. Viscosity is one of the most essential properties of all liquids.¹⁰ The viscosities of ionic liquids tend to be greater than those of organic solvents, and increased viscosity is known to be useful in certain applications, for instance in chromatography where they have been utilized as a stationary phase.¹¹ However, lower viscosity is required in this application order to increase mass transfer rates and ease pumping and filtering.¹² In 1984, the first known work to determine the viscosities of 1,3-dialkylimidazolium chloride-aluminium chloride ionic liquids via a rotational viscometer was undertaken.⁶ The viscosity of an ionic liquid depends on the temperature, type of cation and anion, the impurities present, and hydrogen bond donor.^{11, 13} Previous studies have demonstrated the influence of the cations, such as imidazolium, pyridium, pyrrolidinium or ammonium, and anions, for

example, $[\text{Tf}_2\text{N}]^-$, $[\text{TfO}]^-$ and sulphates, used on physicochemical properties of ILs. Rotrekl *et al.* prepared three ILs, imidazolium bis[(trifluoromethyl)sulfonyl imide] ionic liquids with different alkyl chains. The first contained a linear alkyl chain (1-pentyl-3-butylimidazolium) bis[(trifluoromethyl)sulfonyl imide], $[\text{C}_4\text{C}_5\text{Im}][\text{Tf}_2\text{N}]$; the second contained a branching alkyl chain (1-isopentyl-3-butylimidazolium) bis[(trifluoromethyl)sulfonyl imide], $[\text{C}_4\text{iC}_5\text{Im}][\text{Tf}_2\text{N}]$; whilst the third contained a cyclic group (1-cyclopentyl-3-butylimidazolium bis(trifluoromethyl)sulfonyl imide, $[\text{C}_4\text{cC}_5\text{Im}][\text{Tf}_2\text{N}]$. This work has focussed on the determination of various physical properties of these liquids, namely viscosity, density, conductivity and diffusion coefficient at different temperatures in the range 298.15 to 353.15 K. Perhaps unsurprisingly, the viscosity of $[\text{C}_4\text{iC}_5\text{Im}][\text{Tf}_2\text{N}]$ and $[\text{C}_4\text{cC}_5\text{Im}][\text{Tf}_2\text{N}]$ were found to be greater than that of $[\text{C}_4\text{C}_5\text{Im}][\text{Tf}_2\text{N}]$ due to the influence of the branched alkyl chain and cyclic group on intermolecular bonding.¹⁴ Recently work by the same research group has shown that physical properties can be used as a benchmark of the quality of recycled ILs, such as their densities.¹⁵ In the same way, molecular symmetry has an effect on the viscosity of these liquids, which increases with increasing asymmetry.¹⁶

Yu *et al.* observed that the viscosity of $[\text{C}_4\text{C}_1\text{im}][\text{OAc}]^-$ was 139.7 cP with 746 ppm of water. This viscosity increased to 440 cP when the water content was 11,003 ppm. It has been suggested that this is because of the strong interaction between water and the -COO group of $[\text{OAc}]^-$.¹¹ Ghaedi *et al.* introduced the viscosity of allyltriphenyl phosphonium bromide (ATPPB) with diethylene glycol (DEG) and triethylene glycol (TEG) as hydrogen bond donors (HBD). Their results demonstrated that the hydrogen bonding between the -Br of the salt and -H of the hydroxyl group of HBD (Br...H) had a significant effect on the viscosity; a higher viscosity was observed on formation of the strong hydrogen bonding between these species.¹² In the latter case, when the alkyl chain length increases, the van der Waals forces “including hydrogen bonding and London forces” between molecules increases, and as a consequence increases the liquid’s viscosity.

Qiao and co-workers investigated the influence of pressure and temperature on viscosity for $[\text{C}_4\text{C}_1\text{im}][\text{PF}_6]$, $[\text{C}_4\text{C}_1\text{im}][\text{PF}_6]$ with ethanol, and $[\text{C}_4\text{C}_1\text{im}][\text{PF}_6]$ with benzene. Their results showed that viscosity *increased* with increasing pressure; however, generally

speaking, it would be expected that viscosity *decreases* with increasing temperature,¹⁷ as the interactions between molecules become weaker with the effects of thermal motion.¹⁸

Abbott investigated the fundamental cause of the viscosity of ionic liquids using hole theory. Ionic liquids are not fundamentally viscous because they are ionic. Comparison with high-temperature molten salts such as NaCl above their melting point shows that they are less viscous than water. The difference between high temperature and low temperature molten salts comes in the differences in their ionic sizes. One method of viewing motion in a liquid is to say that an ion can only move if there is a hole next to it which is sufficiently large for it to move into. The viscosity can therefore be modelled from a probability perspective. In hole theory, there are empty spaces in the ionic material that increase due to thermally generated fluctuations in local density. These holes have random locations and sizes and undergo constant flux. Hole size is controlled mostly by the temperature of the system and the surface tension of the liquid. The average size of holes in a molten salt at *ca.* 1000 K are between 1.5 - 2.5 Å, whilst the size of ions that pass into these holes is 1.0 - 1.6 Å. As a result, most ions have a high probability of finding holes next to them.¹⁹ With ambient temperature molten salts, holes are much smaller, at around 1.3 Å, and ions are much larger, at around 3 - 5 Å, so the probability of finding a hole suitable for the moving ions is very limited (10^{-6} - 10^{-7}) and thus these voids are effectively at infinite dilution. This is the reason that the viscosity of ionic liquids can be as high as 10^1 - 10^3 Pa.s at room temperature. Consequently, the high viscosity of ionic liquids can be ascribed to having large ions and small void volumes. To make an ionic liquid less viscous it is necessary to decrease the size of the ions or increase the void volume by decreasing the surface tension. This is the reason why most of the ionic liquids with lower viscosity will have fluorinated anions. For the topic of this thesis, hole theory is important as water will tend to increase the surface tension, but water molecules are small compared to the ions of an ionic liquid and should move more easily and so should decrease the viscosity of the mixture.

The viscosity of fluids can be modelled by determining the probability of ion motion. The probability, P , of finding a hole of radius r is given by **Equation (3.1)**.

$$Pdr = \frac{16}{15\sqrt{\pi}} a^{7/2} r^6 e^{-ar^2} d \quad \text{Equation (3.1)}$$

where a is given by **Equation (3.2)**.

$$a = 4\pi\gamma/kT \quad \text{Equation (3.2)}$$

where γ is the surface tension, k is the Boltzmann constant and T the absolute temperature. Integration of **Equation (3.1)** gives the probability of finding a hole of sufficient dimensions to accommodate an ion over the limits $r = R_{+/-}$ “ionic radii” to $r = \infty$, as per **Equation (3.3)**.

$$P = 0.602 a^{\frac{7}{2}} - \frac{r^5 e^{-ar^2}}{2a} + 2.5 \left[\left[-\frac{r^3 e^{-ar^2}}{2a} + \frac{1.5 \left(\frac{r e^{-ar^2}}{2a} + \frac{0.443 r e f \sqrt{ar}}{a^{\frac{3}{2}}} \right)}{a} \right] \right] / a \quad \text{Equation (3.3)}$$

Equation (3.3) was tested using NaCl at 1000 K and the [C₄C₁im][PF₆] at 298 K. The results indicated that the temperature has a significant influence on the probability of finding a void of appropriate dimensions $P(r > R_{+/-})$. For the two systems above, $P(r > R_{+/-})$ was 0.773 and 3.06×10^{-5} , respectively.²⁰

Various methods have been used to determine viscosity such as U-tube viscometers, oscillating piston viscometer, rotational viscometers, Stabinger viscometers, and bubble viscometers. Here, we used two apparatus to study viscosity. The first was a rotational viscometer, which are used to study rheological behaviour. The principle use of a rotational cylinder is to measure the torque required to turn a motor-driven spindle that is immersed in a fluid. The accuracy of a rotational viscometer is dependent on percentage torque, spindle size and temperature.²¹

The viscosities of Ethaline, Glyceline, Reline and Oxaline have been measured as a function of temperature, as shown in **Figure 3.1**. The viscosities of these four systems were found to decrease with increasing temperature. The results show that the viscosity of Reline is greater than for any of the other DESs considered in this study, whilst Ethaline displays the lowest viscosity. The salt is the same in all these systems and the extent of hydrogen bonding is the most significant difference between the liquids. Ethylene glycol is the weakest of the hydrogen bond donors and so it is of little surprise that it has the lowest viscosity of the DESs examined.

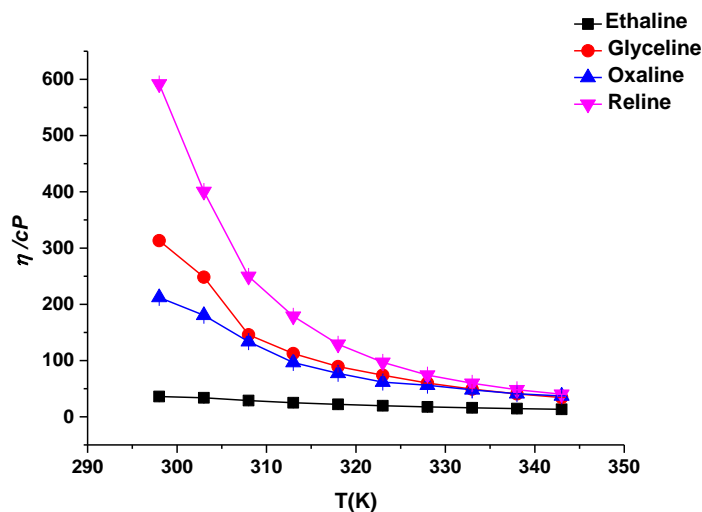


Figure 3.1: Viscosity of four different DESs versus temperature. Error bars indicate one standard deviation.

Recently, Stefanovic *et al.* suggested that Reline has highest hydrogen bond density (13.8 bonds nm^{-3}) followed by Glyceline (10.8 bonds nm^{-3}) and finally Ethaline (9.4 bonds nm^{-3}). This is due to the urea in Reline, which can form four hydrogen bonds compared with glycerol, which can form three, and ethylene glycol, which can form two. It was argued that this is the reason that Reline solidifies at about room temperature, compared with Ethaline and Glyceline whose freezing points are significantly below.²²

Recent evidence suggests that there are other phenomena that can have an effect on the viscosity of DESs; for example, sample preparation procedures, and impurities.²³ According to Yadav *et al.* and Yujiao *et al.*, the viscosity of DESs decreases with increased water content.^{24, 25}

Figure 3.2 illustrates the effect of water on viscosity for three types of DES: Ethaline, Glyceline and Reline; it is clear that water has a significant impact on all three systems. However, there is only a limited effect for water between 1 - 2.5 wt% which is equal to a 0.1 - 0.3 molar equivalent. Recently, Hammond *et al.* have argued that all interactions, including choline-choline, choline-chloride, urea-urea and urea-chloride, in DESs are weakened upon addition of a 1 molar equivalent of water. These results are consistent with the earlier observations of Shah and Mjalli who, with their studies on the radial distribution functions (RDF), indicate that with increasing water fraction the urea-urea

and urea-anion hydrogen bonding decreases. This is due, at lower water fraction, to the anion preferably hydrogen bonding to water than urea.²⁶ Moreover, in the Reline-water mixture, there is a lower Coulombic attractive interaction compared with pure Reline; both of these factors have the effect of decreasing the viscosity of the Reline-water mixture.²⁴ A noteworthy exception to this is the choline-urea hydrogen-bonding interaction (OH-NH₂), which shows a high coordination number compared to other interactions. This unexpected increase in intermolecular interaction strength was proposed to be the reason why the viscosity does not change for lower water contents.²⁷

A previous study showed a linear correlation between viscosity and water²⁵ leading to the clear conclusion that the mixture is homogeneous; however, this study shows that the relationship between viscosity and water content is not linear, thus implying that this might not, in fact, be the case.

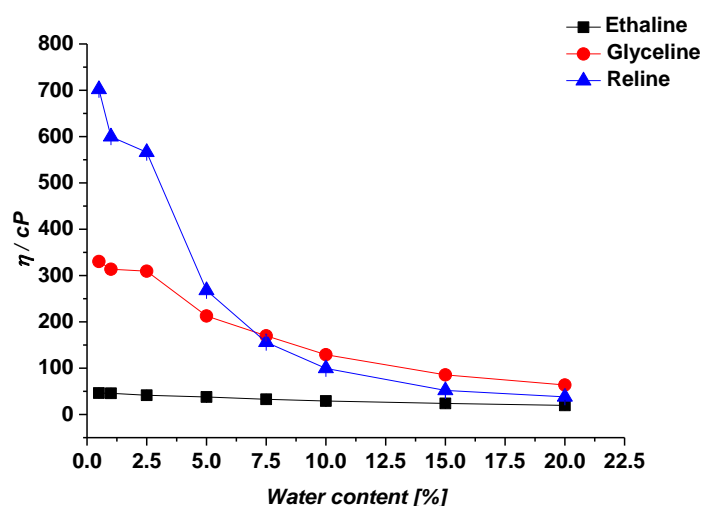


Figure 3.2: Viscosity of three DESs versus wt% water content. Error bars indicate one standard deviation.

An alternative approach that could be used to analyse the effect of water on the viscosity of DESs is to use the method employed for aqueous electrolyte solution. Changes in solvent viscosity due to addition of salts have been shown to follow an Arrhenius model, **Equation (3.4)** where A is the salt constant at a given temperature and c is the salt concentration.²⁸

$$\eta = A^c \quad \text{Equation (3.4)}$$

Dole-Jones improved the Arrhenius model and illustrated that the viscosity of a salt solution is dependent on ion concentration, as per **Equation (3.5)**.

$$\eta_r = \frac{\eta}{\eta_0} = 1 + A\sqrt{c} + Bc \quad \text{Equation (3.5)}$$

Where η_r is relative viscosity which is an expression of the relationship between both the viscosity of the solution η and the viscosity of the pure solvent η_0 . A and B are system-specific constants and c is the concentration of the salt. Dole-Jones found that A is a constant that describes the ion-ion interaction, is independent of concentration and can be calculated from Debye-Hückel theory;²⁹ however, the B constant is related to the solute effect on the solvent, as well as the size and shape of the solute molecules. Rearranging **Equation (3.5)** gives **Equation (3.6)** and should lead to a linear correlation between $(\eta_r - 1)/\sqrt{c}$ versus \sqrt{c} , where A is the y-intercept and B is the slope of the plot.²⁸

$$\frac{\eta_r - 1}{\sqrt{c}} = A + B\sqrt{c} \quad \text{Equation (3.6)}$$

Figure 3.3 shows the Dole-Jones plots for a series of ChCl: HBD mixtures as a function of the square root of salt concentration. Increasing the choline chloride concentration increases the $(\eta_r - 1)/\sqrt{c}$ term, resulting in a positive B constant in all systems. The choline salts investigated all demonstrated negative A values. The A and B values determined for all the systems investigated have been listed in **Table 3.1**.

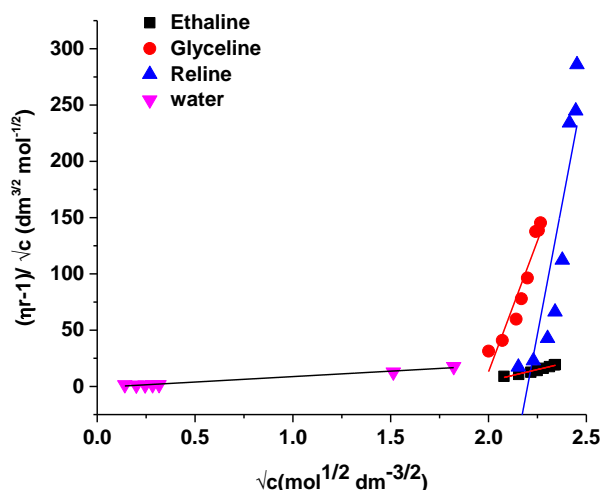


Figure 3.3: Dole-Jones plot for a series of ChCl:HBD mixtures as a function of ChCl concentration.

Table 3.1: Dole-Jones A and B parameters for the DESs and water systems investigated in Figure 3.3.

ChCl in	A ($\text{dm}^{3/2} \text{mol}^{-1/2}$)	B ($\text{dm}^3 \text{mol}^{-1}$)
Ethaline	-77 ± 7.07	41 ± 3.14
Glyceline	-917 ± 126.0	465 ± 58.1
Reline	-2019 ± 447.7	918 ± 191.2
water	-0.930 ± 0.42	9.67 ± 0.46

According to Dole-Jones, if the salt solution of interest has a lower viscosity than water, these electrolytes break down the structure of water. However, solutions that have a higher viscosity than water were assumed to increase the net structure of the solvent, which is due to the ion-solvent bonds that are formed being stronger than the solvent-solvent bonds.³⁰ **Table 3.1** provides a summary of Dole-Jones parameters, from which the B parameters suggest the ChCl salts investigated are acting as kosmotropes, reinforcing the structure of the HBD.

In general, the A **parameter** describes how **charge-charge** interactions effect viscosity and the B **parameter** describes the **solvent-solute** interactions affect viscosity. In these concentrated systems it is difficult to define which of the components is the solvent and which is the solute, but the charge-charge interactions should always be the same.

The magnitude of the A and B parameters are clearly related. A recent study by Davis showed that mixtures of inorganic salts with glycerol gave small negative A parameters.³¹ The study also showed that the B parameters were mostly positive although much smaller than those in **Table 3.1**. The Dole -Jones plot is also non-linear which is almost certainly due to the high concentration used, i.e., the charge-charge interactions increase exponentially as the concentration increases towards 5 mol dm^{-3} .²⁸ The B -coefficients become increasingly positive in the solvent order water, Ethaline, Glyceline and Reline, suggesting that the extent of association should be least in water and most pronounced in Reline.³² Moreover, the positive value of the B parameter was due to the shielding of polar terminal groups of hydrogen-bonding donor in DESs. The shielding of polar groups is the result of increased interaction between these polar ends and ions in the electrolytes. As a result, the contraction of water around the positively charged group is caused by an electrostatic ion-solvent interaction.^{33,28}

3.3.2 Viscosity measurements using QCM.

The second method used to study the viscosity of DESs in this study used a Quartz Crystal Microbalance (QCM). Research into QCM has a long history, starting in 1880 with Jacques and Pierre Curie.^{34, 35} QCM uses a thin quartz crystal sandwiched between two metal electrodes, which with a fixed electric field across the crystal, gives rise to vibrational motion of the crystal at its resonant frequency, i.e., the quartz crystal is piezoelectric.³⁶ Raleigh was the first to report the theoretical foundation for the use of piezoelectricity in 1885. A piezoelectric quartz crystal resonator is a slice cut from a crystal of quartz (whether natural or synthetic). The cutting angle is very important when producing the quartz crystals, as different piezoids (modes of oscillation) can be prepared depending on the cutting angle; for example, AT-cut crystals, as shown in **Figure 3.4 (a), (b) and (c)**.³⁵ The AT-cut crystal is commonly used due to its high stability, low cost and zero temperature coefficient.³⁶ Application of a charge to a crystal when a mechanical stress is applied leads to a shift of dipoles as a consequence of the displacement of atoms.³⁶ This interpretation differs from that when an electrical potential is applied to one of the faces of the crystal which creates a corresponding mechanical distortion, this known as the “converse piezoelectric effect”.³⁷

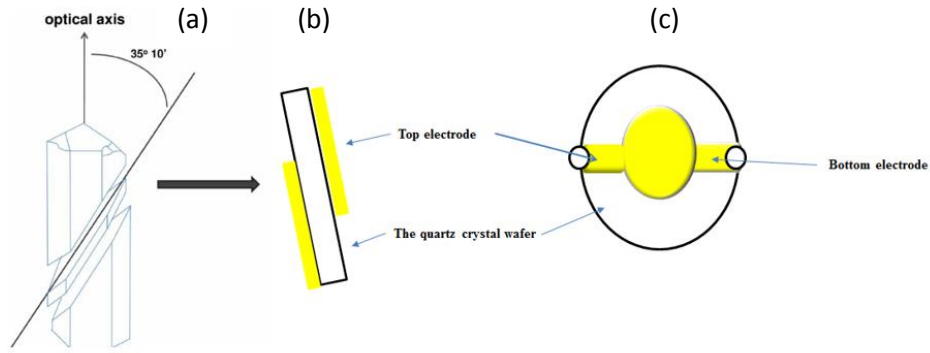


Figure 3.4: (a) and (b) AT cut crystal; (c) the quartz thickness-shear mode resonator consists of a gold electrode on the both side of the quartz crystal.³⁸

Accordingly, QCM can be used to measure the density and viscosity of fluids. When the crystal is exposed to a liquid, the frequency will be changed because there is physical coupling between the quartz crystal and the liquid. Kanazawa and Gordon suggested that the relationship between the frequency change and the viscosity-density product is as shown in **Equation (3.7)**.³⁹

$$\Delta f = -f_0^{3/2} (\rho_{liq} \eta_{liq} / \pi \rho_q \mu_q)^{1/2} \quad \text{Equation (3.7)}$$

where Δf is the change in the frequency of the crystal, f_0 is the [fundamental] frequency of the dry crystal, ρ_{Liq} is the density of the liquid, η_{Liq} is the viscosity of the liquid, ρ_q is the density of the crystal (2.648 g cm^{-3}) and μ_q is the sheer modulus of the quartz ($2.927 \times 10^{11} \text{ g cm}^{-1} \text{ s}^{-2}$). Rearranging **Equation (3.7)** allows the liquid viscosity to be calculated:

$$\eta_{Liq} = \left(\frac{(\Delta f)^2}{f_0^3 \rho_{Liq}} \right) \pi \rho_q \mu_q \quad \text{Equation (3.8)}$$

The advantage of using QCM to study viscosity is that only a very small sample is required, *ca.* 10 ml, compared with 600 ml for the rotational viscometer. The result shows that the viscosity of all four systems is similar for both the rotational viscometer and QCM. For example, the viscosity of Ethaline at 40°C was found as $29.67 \pm 0.46 \text{ cP}$ via

QCM, compared with a viscosity of 27.35 ± 0.03 cP found by rotational viscometer. **Figure 3.5** shows comparable data for all four liquids, which show a good correlation between both techniques. As a result, QCM was used here to study the viscosity because this technique allows the use of small liquid volumes; this was the first time that QCM was used to measure the viscosity of this class of liquids.

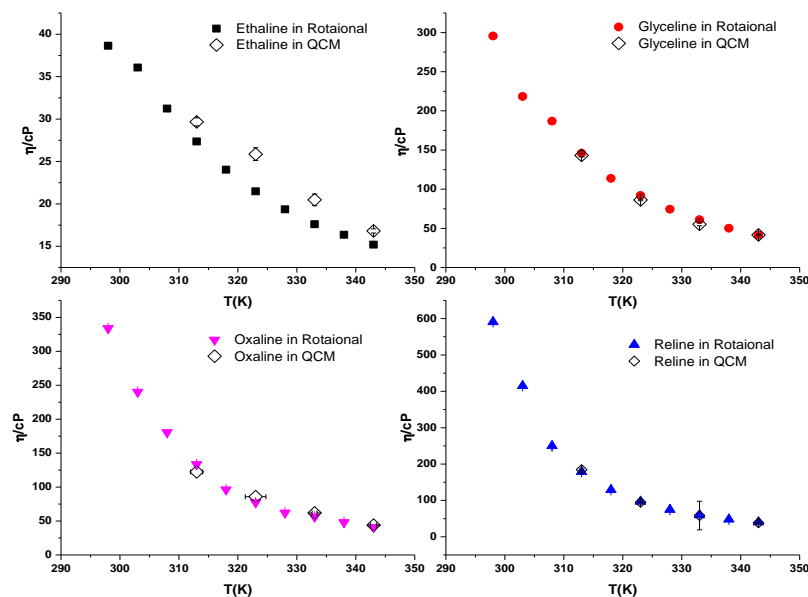


Figure 3.5: Viscosity of type III DESs as recorded by QCM and rotational viscometer. Error bars indicate one standard deviation for both rotational and QCM measurements.

3.4 Rheological study.

Previous studies have considered the rheology of ionic liquids. Smith *et al.* showed the behaviour of a series of protonic ionic liquids (PILs) including ethylammonium nitrate (EAN), propyl ammonium nitrate (PAN), ethanol ammonium nitrate (EtAN), ethyl ammonium formate (EAF), and dimethylethyl ammonium formate (DMEAF). This study focussed on the behaviour of ionic liquids through an understanding of the effects of both the H-bond network and the solvophobic nanostructure. The results showed that both EtAN and DMEAF have Newtonian behaviour; however, the other three ILs, which are solvophobic nanostructured liquids, show non-Newtonian behaviour.⁴⁰

Generally, most ionic liquids can be described as having Newtonian flow.⁴⁰ Viscosity is one of the most important factors to consider when studying the rheological behaviour of liquids, which can be subdivided into two types.

1. Absolute or dynamic viscosity.
2. Kinematic viscosity.

Newton's model characterizes the absolute viscosity, as per **Figure 3.6**. It was suggested that if there are two layers *A* and *B*, and these layers are separated by a distance *dx* and moving in the same direction at different velocities, *V₁* and *V₂* respectively, under a force *F*.¹⁰

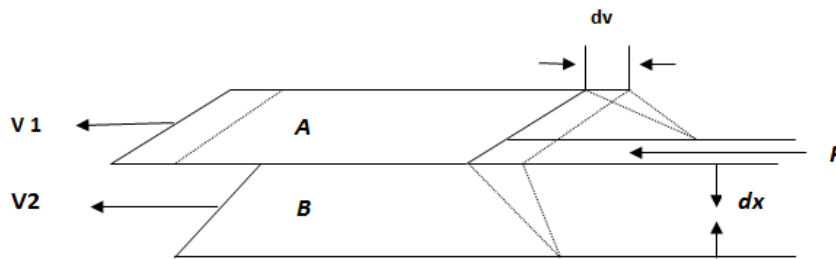


Figure 3.6: Newton's model for viscosity.¹⁰

Figure 3.6 shows Newton's explanation of fluid behaviour; however, it can also be explained mathematically, as follows:¹⁰

$$\sigma = \eta \dot{\epsilon} \quad \text{Equation (3.9)}$$

Where σ is the shear stress, which means the "resistance to flow"⁴¹, η is the viscosity and $\dot{\epsilon}$ is strain rate or shear rate, which means "the rate of motion of the fluid".⁴¹ The strain rate is equal to:

$$\dot{\epsilon} = \frac{1}{x} \frac{dx}{dt} \quad \text{Equation (3.10)}$$

where x is length, t is time and dx/dt is the velocity, v . As a result, the dynamic viscosity becomes:

$$\eta = \dot{\epsilon} \frac{x}{v} \quad \text{Equation (3.11)}$$

In addition, the kinematic viscosity can be defined using the liquid density (ρ):

$$v = \frac{\eta}{\rho} \quad \text{Equation (3.12)}$$

where v is the kinematic viscosity, η is the dynamic viscosity and ρ is the density of the liquid.¹⁰ If there is a linear relationship between shear rate and shear stress, the fluids are said to demonstrate Newtonian behaviour, as per **Figure 3.7**.¹⁰

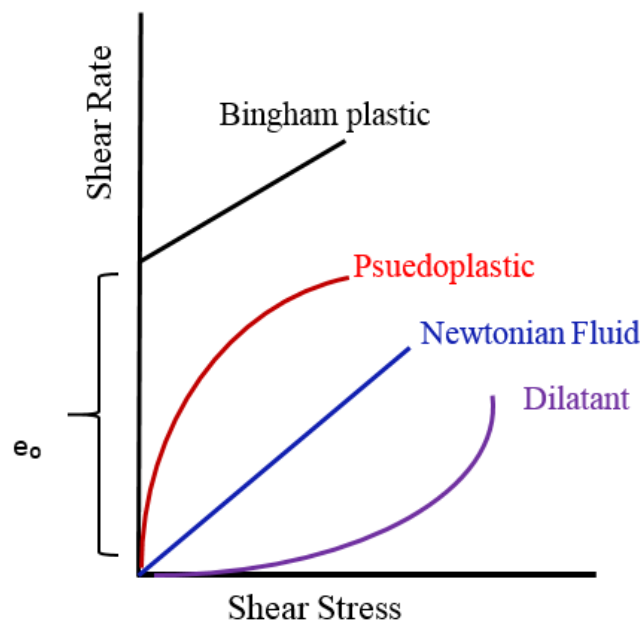


Figure 3.7: Various types of fluid behaviour.¹⁰

Kulkarni and co-workers prepared ionic liquids and studied their behaviour using **Equation (3.9)**, the results of which indicated that the relationship between sheer stress and sheer rate is linear. This shows that viscosity is not dependent on the sheer stress for $[C_4C_1im][SAC]$ at $20^\circ C$.⁴² If the viscosity depends on the sheer rate and time, these liquids show non-Newtonian behaviour.¹⁰ In other words, with non-Newtonian behaviour the viscosity will be constant when sheer stress is low ($< 100 Pa.s$). However, if the viscosity decreases significantly with increased sheer stress, this is referred to as sheer thinning behaviour.⁴²

Generally, when the fluids have a significant amount hydrogen bonding, this leads to increased sheer thinning; for example, as seen in paints, motor oil and liquid polymers.⁴¹ Non-Newtonian behaviour of liquids has different types, the first of which is when the

viscosity decreases with increasing shear rate, which is called “pseudoplastic” or shear thinning behaviour; the second is where the viscosity increases with increasing shear rate, which is called dilatant or shear thickening behaviour. In addition, if the shear rate is zero and shear stress is less than or equal to a yield stress e_0 this type is referred to as a Bingham plastic.¹⁰ **Figure 3.7** illustrates these different non-Newtonian behaviours. Furthermore, time is an important factor in defining non-Newtonian fluids. If the shear rate remains constant and the viscosity decreases with time, such a fluid would be referred to as being thixotropic **Figure 3.8(a)**; however, if the viscosity increases with time, the fluid is referred to as being rheopectic **Figure 3.8(b)**.

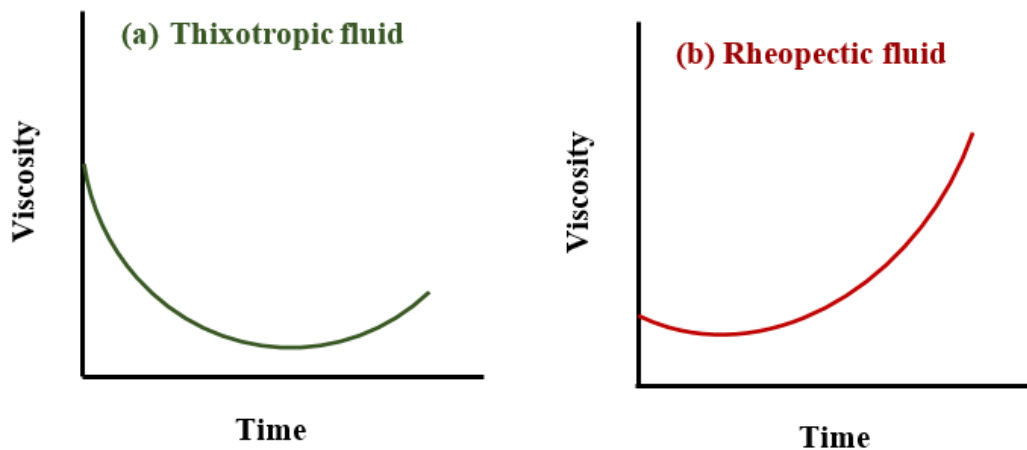


Figure 3.8: Viscosity-time behaviour for (a) Thixotropic and (b) Rheopectic fluids.

3.4.1 Influence of temperature on fluidity of DESs.

In this part the influence of rotational rate was determined at temperatures (30°C and 50°C). **Figure 3.9** shows the relationship between viscosity and shear rates at 30°C. Ethaline and Glyceline can be seen to exhibit Newtonian behaviour. This due to the hydrogen bonding between ethylene glycol, glycerol and chloride anions being weaker than the hydrogen bonding in urea and oxalic acid. Both Oxaline and Reline show a gradual decreases in viscosity with increasing shear rate, i.e., they exhibit Non-Newtonian behaviour. As previously mentioned, non-Newtonian behaviour was observed in fluids with extensive hydrogen bonding, and Reline and Oxaline both have the potential for a large number of hydrogen bonds compared with other liquids.⁴¹

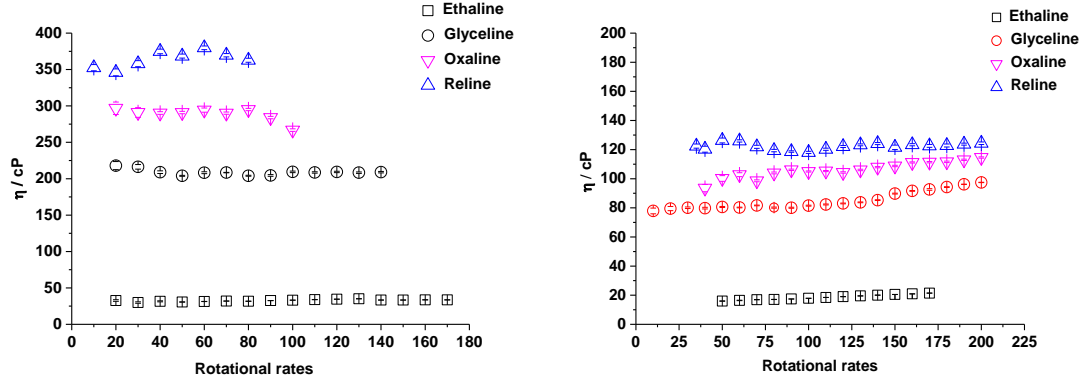


Figure 3.9: Plot of the behaviour of type III DESs in different rotational rates at 30°C (left) and 50°C (right). Error bars indicate one standard deviation.

Increasing the temperature to 50°C makes Oxaline and Reline behave in a more Newtonian manner, which would be expected as the hydrogen bonds are broken up at higher temperatures. Previous studies have argued that at lower shear rates there are surfactant-like sponge phases which led to the onset of layering of polar and a polar regions in the shear gradient direction.⁴⁰

3.5 Surface tension.

There are many forces between molecules in liquids. The cohesive force between liquid molecules is called surface tension which, put simply, is the force per unit length. Surface tension is highly sensitive to temperature, and when temperature is increased the surface tension (γ) will decrease according to the Eötvös Equation.⁴³

$$(V_{ML})^{2/3} \gamma = \check{k} (T_c - T) \quad \text{Equation (3.13)}$$

$$V_{ML} = M_W / \rho_L \quad \text{Equation (3.14)}$$

where V_{ML} is the molar volume of the liquid, M_W is the molar mass, ρ_L is the density of the liquid, T_c is the critical temperature of the liquid, and \check{k} is a constant ($2.2 \times 10^{-7} \text{ J mol}^{-2/3} \text{ K}^{-1}$).

There are many factors that can influence an IL's surface tension. Previous researchers have studied the influence of the constituent cations and anions on surface tension.²⁰

Kolbeck and co-workers showed that surface tension will decrease with increasing alkyl chain length for $[C_nC_1Im][Tf_2N]$ species, where $n = 1, 2, 4, 6, 8, 10$, due to the Coulomb interaction becoming weaker with the increasing length of the alkyl chain.⁴⁴ In contrast, when n is greater than 8 and the alkyl chains interact with the ethylene glycol groups, this results in an increase in surface tension.⁴⁵

In addition, functional groups can also affect surface tension, if they are hydrophobic or hydrophilic. Several reports have shown that both groups help to increase the surface tension of ILs such as $[Me(EG)_2C_1Im][Tf_2N]$ and $[C_6C_1Im][Tf_2N]$, for which the surface tensions were found as 36.5 and 30.2 $mN\ m^{-1}$, respectively. On the other hand, non-functionalised ILs can contribute to surface tension, with this contribution arising from either group. These groups can form intermolecular and intramolecular hydrogen-bonding interactions in the imidazolium ring due to hydrogen bond formation with surface molecules without preferential orientation of the cations due to this hydrogen bonding, which leads to a surface with no preferential orientation of the imidazolium.⁴⁴

Surface tension data for the pure liquids DESs studied in this work are shown in **Figure 3.10**. In each case the viscosity decreases with increasing temperature which will result in an increased free volume and an associated decrease in viscosity. Surface tension is dependent on the intermolecular forces among liquid molecules.^{43,46,47} The results showed that Reline displayed a higher surface tension than any of the other DESs considered in this study, whilst Ethaline displays the lowest surface tension. This is in accordance with the viscosity data presented above.

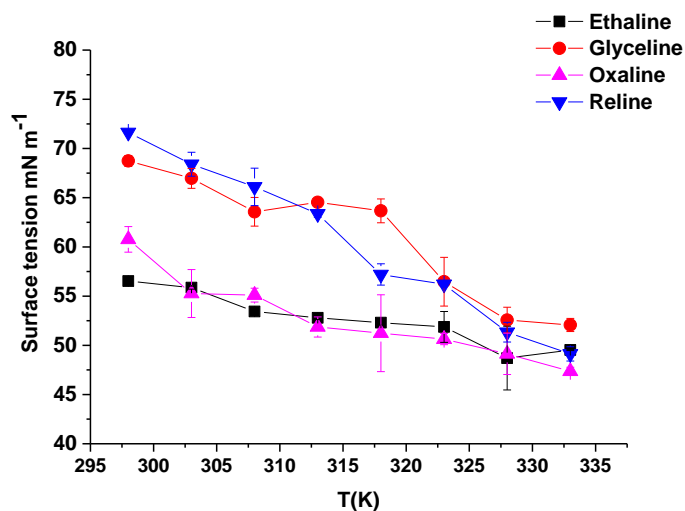


Figure 3.10: Surface tensions of four DESs as a function of temperature. Error bars indicate one standard deviation.

Figure 3.11 shows the surface tensions for three liquids (Ethaline, Glyceline and Reline) with different amounts of water. In principle, the surface tension should change from the value for bulk DES to that for bulk water (72 mN m^{-1}) in a linear manner if the systems were homogeneously mixed. It can be seen that the value for Ethaline starts at 57 mN m^{-1} and rises slowly towards that of bulk water. The value for Glyceline is similar to that for water so does not change significantly with increasing water content. The value for Reline starts at about 50 mN m^{-1} and changes rapidly to the value for bulk water with the addition of only 2.5 wt% water. This suggests that water is not homogeneously mixed with Reline, and instead is preferentially located at the air-liquid interface. In contrast, with Ethaline the surface tension does not change much when water is added showing that water does not preferentially partition to the interface. As a result, the behaviour of Reline-water mixtures is considerably more heterogeneous from that of Ethaline-water mixtures. This agrees with the results of the diffusion observed for these liquids reported in chapter four. The increased water content allows the formation of new hydrogen bonds between water and these liquids.⁴⁷

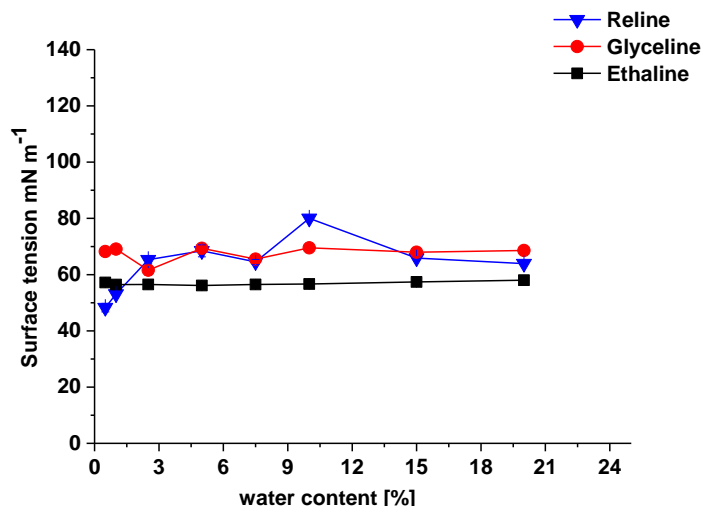


Figure 3.11: Surface tension of Ethaline, Glyceline and Reline with different water contents at 25°C. Error bars indicate one standard deviation.

3.6 Ionic conductivity.

Most ionic liquids and DESs have low ionic conductivities compared to aqueous electrolyte solutions, often $< 1 \text{ mS cm}^{-1}$ at room temperature. They generally display high viscosities usually $> 50 \text{ cP}$. Temperature plays a significant role in their conductivities. Low conductivity is a difficult problem in electrochemical applications as it leads to high cell resistances which can result in Ohmic heating during bulk electrolysis.^{23, 48} Abbott *et al.* have shown that there are different charge transfer mechanisms in ionic liquids to those observed in ionic solution or high temperature molten salts.⁴⁹

Previous studies have attempted to correlate molar conductivity with the reciprocal of viscosity. It is wrongly claimed that this should be valid from the Walden relationship, **Equation (3.15)**.

$$\Lambda_m \eta = \text{constant} \quad \text{Equation (3.15)}$$

where Λ_m is the molar conductivity and η is the viscosity.^{50, 51} The Walden relationship was actually developed to be able to calculate limiting molar conductivities, Λ_m° of electrolytes in non-aqueous solvents and should be expressed for a given salt, as per **Equation (3.16)**.

$$\Lambda_m^\circ \eta^\circ = \text{constant} \quad \text{Equation (3.16)}$$

where η° is the viscosity of the pure solvent.⁴⁰ The Walden rule stems from the Nernst-Einstein **Equation (3.17)**, which shows that the molar conductivity at infinite dilution, Λ_m° of an electrolyte is dependent on the diffusion coefficient, D° , of the ions.

$$\Lambda_m^\circ = \frac{z^2 F}{6\pi\eta} \left(\frac{1}{R_+} + \frac{1}{R_-} \right) \quad \text{Equation (3.17)}$$

where z is the charge of the ions, F is the Faraday constant, R is ionic radii of species.

In an electrolyte solution the conductivity increases with increasing ionic concentration is described in **Equation (3.18)**.

$$\sigma = (u_+ z_+ + u_- |z_-|) c F \quad \text{Equation (3.18)}$$

where u_+ and u_- are mobilities of the ions and c is the concentration of the charge carriers. It is clear that ionic atmosphere and formation of ion pairs have the effect of decreasing molar conductivity with increasing electrolyte concentration.⁵²

Figure 3.12 shows the conductivity of four pure DESs as a function of temperature. The conductivity increases with increasing temperature which is consistent with previous results.^{53,54} The highest conductivity is observed for Ethaline while both Reline and Glyceline have much lower conductivities due to their higher viscosities. The conductivity increases with increased temperature due to a lower density and lower viscosity which enable higher ionic mobility.⁵⁵

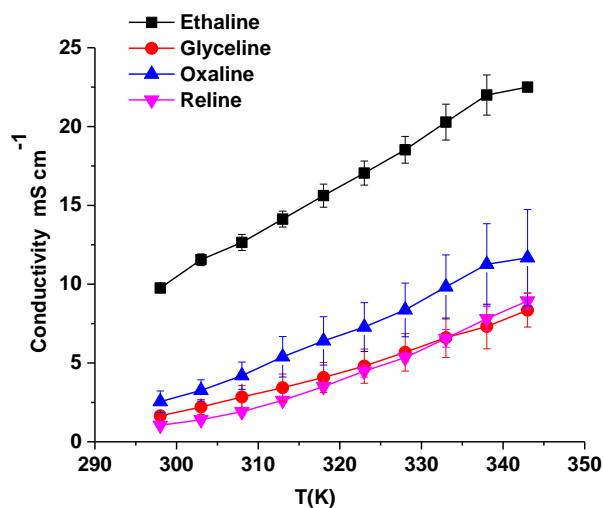


Figure 3.12: Conductivity as a function of temperature for four DESs. Error bars indicate one standard deviation.

In addition, water has a strong effect on the conductivity of ILs. Widegren *et al.* examined the increased conductivity of $[\text{C}_4\text{C}_{1\text{im}}][\text{Tf}_2\text{N}]$ with increased water mole fraction.⁵⁶ However, the kind of anion used can also have a significant influence on conductivity, for example in $[\text{C}_4\text{C}_{1\text{im}}]^+$, where the conductivity decreases according to the series $[\text{C}_4\text{C}_{1\text{im}}][\text{DCA}] > [\text{C}_4\text{C}_{1\text{im}}][\text{TA}] > [\text{C}_4\text{C}_{1\text{im}}][\text{TfO}] > [\text{C}_4\text{C}_{1\text{im}}][\text{PF}_6]$.⁵⁷ Several reports have shown that an increased amount of water leads to the increased conductivity of the mixture due the hydrophilicity of the anion.⁵⁸

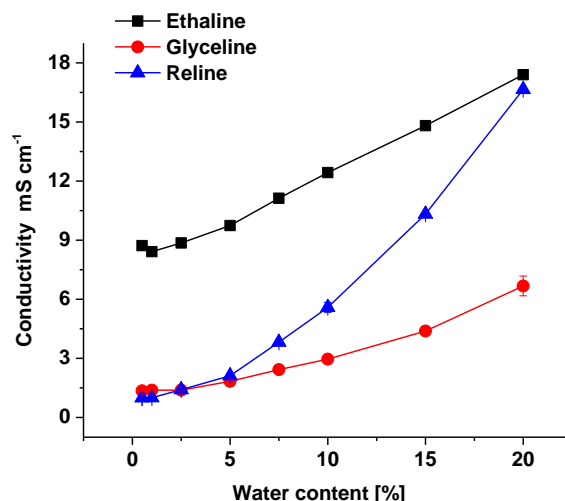


Figure 3.13: Conductivity Ethaline, Glyceline and Reline with different water contents at 25°C. Error bars indicate one standard deviation.

The influence of water content on conductivity is presented in **Figure 3.13**. The results indicate an increase in conductivity for all systems with an increased amount of water. Ethaline shows the highest conductivity of the three liquids due to the fact that Ethaline has a lower viscosity, as indicated in section 3.3.1. It can be seen that the conductivity for Ethaline and Glyceline-water mixtures increases gradually with water content in contrast to Reline where the conductivity increases more rapidly when water is added. **Figure 3.2** shows that the viscosity for Reline decreases more rapidly when water is added than to Ethaline or Glyceline. In all cases, the charge carriers should be the same, *viz.* Ch^+ and Cl^- . The data in **Figure 3.13** can only be really compared if the molar conductivities are analysed. **Figure 3.14** shows the molar conductivity as a function of fluidity (inverse viscosity) of DESs with different amounts of water added to them. These so-called Walden plots are used in ionic liquids, however, **Equation (3.15)** shown that they are not really valid as the Walden rule is only valid at infinite dilution for a given electrolyte. The reason that linear trends are observed is because the charge carriers are holes which are at low concentration.

Deviations from the Walden plot will occur if ionic carriers become more important than holes in governing charge mobility. There is some evidence regarding the dissociation of the ionic structure due to the number of charge carrier species present, and which are responsible for the increased conductivity of system. This behaviour is known, and has

been observed previously by Ries *et al.*⁵⁹ **Figure 3.14** shows a less linear behaviour for Reline compared to Ethaline and Glyceline. This could be because Reline-water mixtures are less homogeneous than the other two systems. Partitioning of ChCl in a water phase would result in more free charge carriers which would increase the conductivity.

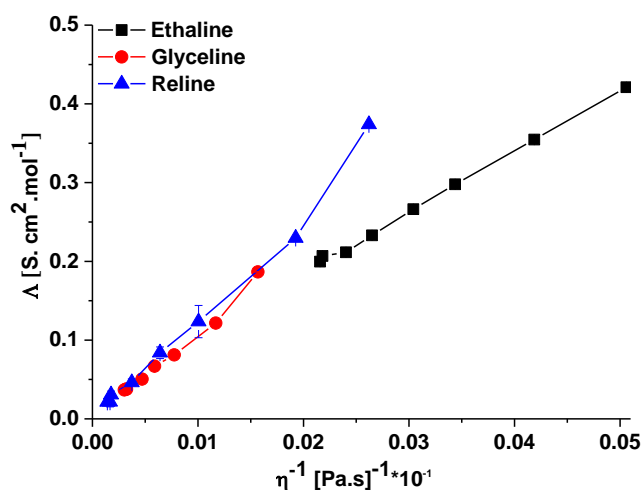


Figure 3.14: Plot of molar conductivity versus fluidity for three DESs. Error bars indicate one standard deviation.

3.7 Density.

Generally, most ILs have densities between 1.0 and 1.6 g cm⁻³ due to the influence of the ion structure of ILs.⁶⁰ Dzyuba and Bartsch studied the influence of alkyl chain length on the density of a series of ionic liquids. Their study focussed on using [C_nmim][PF₆] (n = 4 – 9), [C_nC₁im][NTf₂] (n = 2 -10), [Ph(CH₂)₃mim][PF₆], and [Ph(CH₂)_nmim][NTf₂] (n = 1-3). For [PF₆] and [NTf₂] liquids increasing the length of the alkyl decreased the density.⁶¹

The density data for the pure DESs are shown in **Figure 3.15**. The density increases with decreasing temperature.²⁵ The figure shows that the density of Reline seems to be greater than for any other DES in this study, whilst Ethaline shows the lowest density. Usually, when the temperature increases the free volume also increases which leads to a decrease in density.⁶²

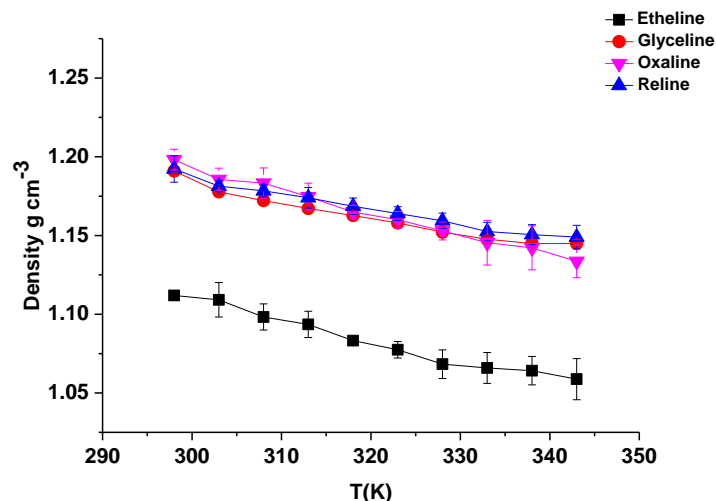


Figure 3.15: Density of four DESs as a function of temperature. Error bars indicate one standard deviation.

Figure 3.16 shows the density of three types of DESs as a function of water content. The density of all liquids decreased with increasing amounts of water towards the value for pure water. The change in density with water content is not linear, which supports the main hypothesis of the thesis that DES-water mixtures heterogeneous. Reline exhibited a higher density than Glyceline and Ethaline due to the decreased in the free volume arising from the higher hydrogen bonding and increased surface tension.

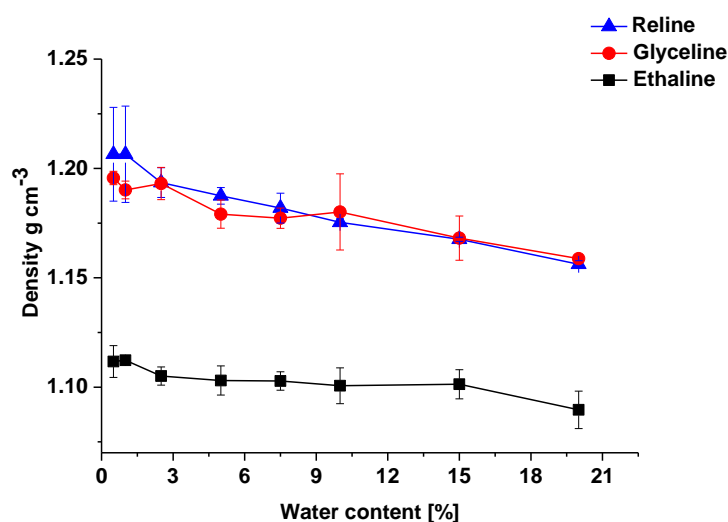


Figure 3.16: Density of Ethaline, Glyceline and Reline as a function of water content. Error bars indicate one standard deviation.

3.8 Reflective index.

To be able to determine whether different phases are forming in DES-water mixtures dynamic light scattering can be used. This technique requires knowledge of the viscosity and refractive indices of the fluids. Reflective index measures the bending of light when it passes through different media.⁶³ In ionic liquids, the cation and anion can significantly influence the reflective index. For example, for the imidazolium cation, the reflective index was found to increase with increasing alkyl chain length. In addition, the influence of the anion on the refractive index of ILs has also been studied. A high reflective index was found for larger anions such as $[\text{Tf}_2\text{N}]^-$ compared to smaller anions such as acetate and the halides.⁶⁴

The refractive indices of pure Ethaline, Glyceline and Reline and their aqueous binary mixtures were measured at room temperature. The experimental values are tabulated in **Table 3.2**. For lower water content, the results indicate that there is a high refractive index because of the increased ion arrangement and the efficient packing of the ions.^{65, 66}

Table 3.2: Reflective index for three DESs with different water content.

Water wt%	Ethaline	Glyceline	Reline
0	1.4590 ± 0.004	1.4876 ± 0.051	1.5077 ± 0.005
5	1.4526 ± 0.006	1.4792 ± 0.002	1.4927 ± 0.040
10	1.4465 ± 0.012	1.4707 ± 0.073	1.4872 ± 0.063
20	1.4336 ± 0.023	1.4543 ± 0.005	1.4675 ± 0.057
50	1.3939 ± 0.007	1.4051 ± 0.063	1.4124 ± 0.039
70	1.3690 ± 0.031	1.3754 ± 0.030	1.3789 ± 0.007
90	1.3447 ± 0.009	1.3467 ± 0.004	1.3477 ± 0.046
95	1.3390 ± 0.005	1.3399 ± 0.011	1.3404 ± 0.074
100	1.3330 ± 0.022	1.3330 ± 0.022	1.3330 ± 0.022

3.9 Dynamic light scattering.

Dynamic light scattering (DLS) has been used to study the size distribution profile of colloidal dispersions in solution on the microsecond time scale.^{67, 68} In addition, DLS is a useful technique to study scattering intensities, which is indicative of particle

concentration. Here, DLS was used to detect aggregates in DESs and ionic liquids mixtures with water. Previous studies have suggested that ILs form aggregates in aqueous solution. Wang *et al.* found that for the same cationic species, [C₈C₁im], there is a pronounced effect of the anion used on the critical aggregation concentration (CAC) value. It was found that the capability of these anions to cause the aggregation of ILs follows the order [CF₃COO]⁻ > [NO₃]⁻ > [Br]⁻ > [Cl]⁻ > [CH₃COO]⁻.⁶⁹ On the other hand, Blesic and co-workers illustrated that when the anion [Cl]⁻ in [C₁₀C₁im][Cl] was replaced by the [NTf₂] or [PF₆] anion, no micelle formation was detected due to both of the [NTf₂] and [PF₆] having low solubilities in water.

Recently, it has been suggested that nanodomains of water exist, rather than the water being homogeneously mixed with the ionic liquid⁷⁰ or DES.⁷¹ To demonstrate that this is indeed the case, dynamic light scattering was carried out with ionic liquids and DESs containing 5 wt% water. **Table 3.3** shows the average droplet size and distribution for [C₄C₁im][BF₄], [C₂C₁im][OAc], 2 glycerol : 1 ChCl and 2 EG : 1 ChCl. Clearly, far from creating homogeneous solutions, the water forms nanodomains. These are largest in 2 EG: 1 ChCl with an average diameter of 311 nm. This is effectively a microemulsion with a droplet containing approximately 4 × 10⁸ molecules. It is unlikely that this will be a pure water droplet, and thus there will be an equilibrium between water monomers in the DES and the constituent parts of the DES in the water phase. In chapter four, the self-diffusion coefficients of the constituent species in 2 EG: 1 ChCl-water mixtures were measured. At low water content (< 2.5 wt%) the OH protons on Ch⁺ and EG were found to diffuse at a rate controlled by the bulk viscosity of the liquid. At higher water content, the OH diffused at a rate more characteristic of bulk water, showing that a biphasic system existed.

Table 3.3: Average aqueous dispersed phase size for 5 wt% water in two ILs and two DESs at 25°C. Uncertainty is stated to one standard deviation.

Bulk phase	Dispersed phase size (nm)
2 EG: 1 ChCl	311 ± 18
2 glycerol: 1 ChCl	105 ± 12
[C ₄ C ₁ im] [BF ₄]	96.0 ± 4.0
[C ₂ C ₁ im] [OAc]	72.0 ± 8.0

The observation that microemulsions form must mean that ionisation occurs at the interface between the two phases, such that a zeta potential is set up stabilising these large droplets. It is interesting to note that the droplet size distribution is relatively narrow. The 2 glycerol: 1 ChCl liquid has a slightly smaller droplet with an average diameter of 105 nm. [C₄C₁im][BF₄] and [C₂C₁im][OAc] are slightly smaller but still show that the domains are significant in size. There are two consequences of this observation: firstly, the acid is more likely to partition into the aqueous phase, which could lead to regions of different micro-pH; and, secondly, these nanodomains may explain several unusual phenomena such as the stability of proteins in aqueous–ionic liquid mixtures.⁷²⁻⁷⁴ The light scattering experiment with 5 wt% water in 2 EG: 1 ChCl was repeated with 0.01 mol kg⁻¹ triflic acid, where it was found that the particle size was 239 ± 20.8 nm, which is similar to that without acid, suggesting that the acid does not significantly affect the zeta potential and hence the size of the droplet.

On the other hand, the mechanism aggregation formed in ionic liquids- water mixture are two steps. firstly, the electrostatic interactions between the cationic groups which decreases the aggregate; and, secondly, attractive hydrophobic interactions involving the alkyl chains which increase aggregation.⁷⁵ To further understand the effect of water on the aggregation behaviour of DESs with different water content, the dynamic light scattering technique was used to determine the size of the DES aggregates with different amounts of water (5 wt% to 95 wt%). **Figure 3.17** illustrates the droplet sizes in three DESs with different amounts of water amount. The results for Ethaline are different from the other two liquids in the case that larger droplets are formed with high and low water content. The dispersed phases are typically in the range 20 to 350 nm and therefore contain 10⁴ - 10⁷ molecular or ionic species showing that they are relatively large on a molecular scale. The differences in sizes could be related to the differences in surface tension and mutual solubility of the components. Hence, these results confirm that DESs and water form phases which are heterogeneous on a nanometre scale. It should however be noted that both water in DES and DES in water emulsions form over almost the complete compositional range.

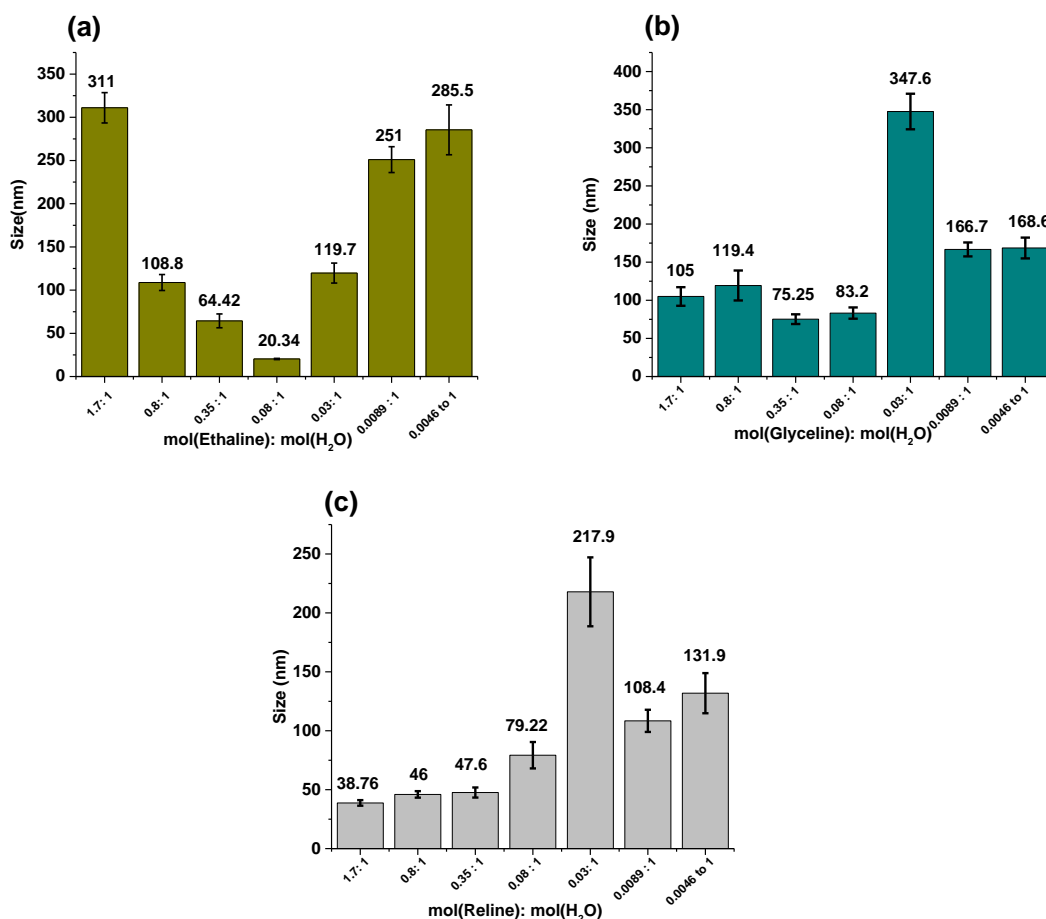


Figure 3.17: Size of dispersed phase in water mixtures with (a) Ethaline, (b) Glyceline and (c) Reline. Error bars indicate one standard deviation.

As a result, it is clear that the behaviour of the Reline-water mixture is different from the other two liquids. To clarify this difference, through the simple expedient of mixing Reline with 20 wt% water. **Figure 3.18(a)** and **(b)** compares the behaviour of a mixture of Reline with 20 wt% water with that of pure Reline, from which it is clear that the Reline water mixture it is not homogeneous due to its separation into two layers. These two layers can be easily remixed and that is why the behaviour has probably not been reported previously.

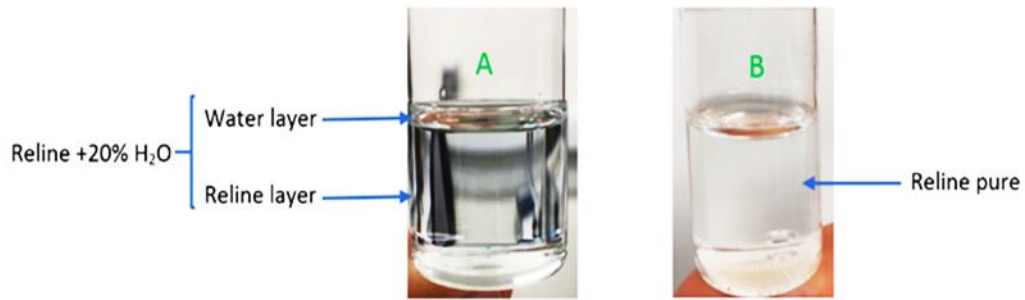


Figure 3.18: (a) Reline-20 wt% water and (b) pure Reline.

For a colloidal dispersion to be stable it needs to have a charge on the surface of the dispersed phase. The zeta potential, or “ ζ potential”, is an important parameter through which to understand the stability of a colloidal dispersion. The particles in colloidal systems have electric charges; if this charge is negative, there is a thin layer of positive charge that forms around the particle (the Stern Layer). After the Stern Layer, there is a wide layer that carries the opposite charge to Stern Layer, known as the Diffuse Layer. The distance, and thus difference in electrostatic potential, between surface of the particle to the Diffuse Layer known as the Nernst potential; however, the distance between the surface of the Stern Layer and Diffuse Layer is known as the ζ potential.^{76,77} **Figure 3.19** illustrates the zeta potential of a particle.

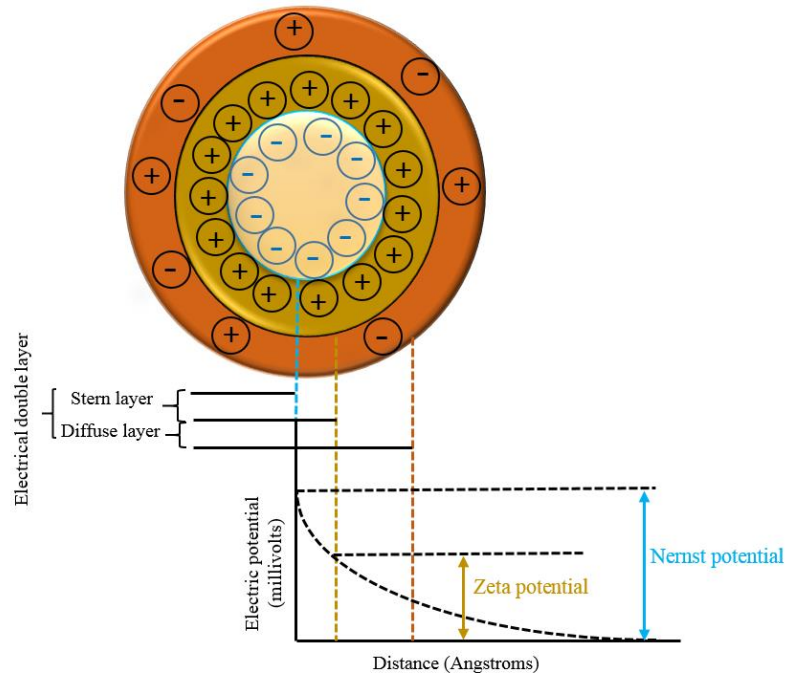


Figure 3.19: Schematic diagram showing the ζ potential, Stern layer and diffuse layer.⁷⁸

Both the Stern layer and diffuse layer together are known as the electrical double layer. It is important to note that the thickness of the double layer gives the Debye length or “screening length”, which is a necessary parameter to understand the ζ potential. The Debye screening length for a 1:1 electrolyte is given in **Equation (3.19)**.

$$L_D = \kappa^{-1} = \left[\frac{\epsilon_r \epsilon_0 K T}{2 N_A e^2 I} \right]^{1/2} \quad \text{Equation (3.19)}$$

where L_D is the Debye screening length, ϵ_r , which is the dielectric constant of the solution, ϵ_0 is the permittivity of vacuum ($8.854 \times 10^{-12} \text{ C}^2 \text{ J}^{-1} \text{ m}^{-1}$), I is the ionic strength in mol dm^{-3} , k is the Boltzmann constant, T is the temperature in Kelvins, e is the elementary charge, and N_A is Avogadro’s constant. Placing the dispersed phase in an external electrical field has the influence of moving the particle with a certain speed and direction depending on the potential of the electric field as well as the size of the particles. The particle causes light scattering, which can be calculated using the electrophoretic mobility (u_E). The Henry equation has been used to find the ζ potential from the measured electrophoretic mobility, as shown in **Equation (3.20)**.⁷⁸

$$u_E = \frac{2 \times \varepsilon \times ZP \times f(k \times a)}{3 \times \eta} \quad \text{Equation (3.20)}$$

Where ZP is the ζ potential (mV), ε is the dielectric constant, $f(\kappa \cdot a)$ is the Henry function, where κ is the inverse screening length of electrostatics (m^{-1}) and a is the particle radius (nm) and η the viscosity ($\text{kg s}^{-1} \text{m}^{-1}$). Generally, the Debye screening length will decrease with increasing ion concentration; for example, at room temperature, the Debye length was $L_D = 9.6 \text{ nm}$ for a solution of $1 \times 10^{-3} \text{ mol dm}^{-3}$ NaCl in water; however, when the concentration was set to 0.1 mol dm^{-3} , the Debye length become $L_D = 0.96 \text{ nm}$ because of the effective screening of charges over short distances.⁷⁹ **Table 3.4** shows the ζ potential for Ethaline with different amounts of water. The data indicates that the ζ potential for Ethaline–water mixture was positive for all water concentrations under investigation.

Table 3.4: ζ potential of Ethaline with different amounts of water.

Water content (wt%)	Water:ChCl mol eq	Zeta potential (mV)
0	0	+26 ± 9
5	0.76	+142 ± 13.5
10	1.6	+237 ± 2.51
20	3.6	+414 ± 15.8
50	14.6	+271 ± 7.77
70	35.2	+21 ± 1
90	131.9	+4 ± 3
95	279.2	+5 ± 0.2

In general, for pure systems there is no ζ potential; however, for our system, pure Ethaline shows a small ζ potential due to Ethaline being hygroscopic and thus having absorbed a negligible amount of water, though enough to have sufficient effect to observe a ζ potential for the ‘pure’ liquid. For other water concentrations, our data implied that an increased ζ potential could be associated with an increased water content until the water was 20 wt%; at higher water contents the ζ potential decreased with increasing amounts of water. This could be related to the change in Debye screening length with increasing amounts of water. It is generally considered that a ζ potential $> \pm 10 \text{ mV}$ produces a highly stable colloidal dispersion. The data in **Table 3.4** show that the colloidal dispersion of DES in water is stable over most of the compositional range studied here.

The high ionic charge and the large ζ potential will ensure that any dispersed phase will be relatively stable. In a DES-water mixture, choline chloride concentration plays an important role; however, adding water to the DES changes the concentration of choline chloride. **Figure 3.20** shows the concentration of choline chloride in different amounts of water versus ζ -potential. It is clear that one obtains an increased ζ potential with increasing amounts of water, which equates to a decreased choline chloride concentration. However, a 20 wt% mix with water, where the choline chloride concentration is 3.3 mol dm^{-3} , shows the highest ζ potential, which could be that due to water being the dispersed phase as it is still the minor phase by volume. At higher water content the water becomes the continuous phase and the ionic phase becomes the dispersed phase so the ζ potential decreases.

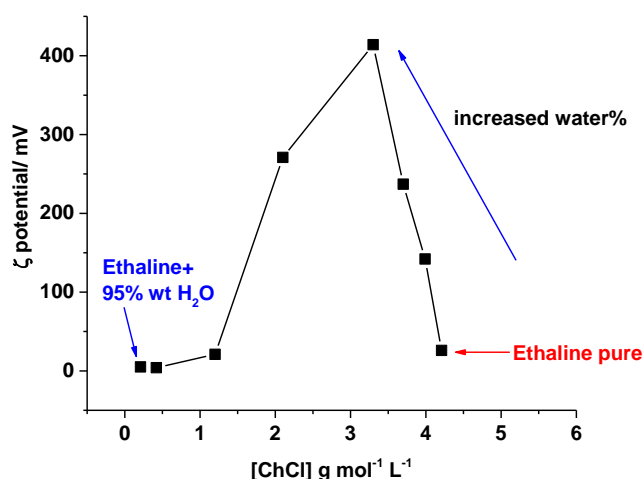


Figure 3.20: ζ potential of Ethaline at different concentrations of choline chloride.

It is useful at this point to discuss the possible structures of the dispersed and continuous phases in DES water mixtures. Analysing first a DES major phase with water as the minor component by mass (and volume). Taking a 10 wt% water-DES mixture for example. Although water is in slight molar excess the components of the DES will form the major phase by volume. However, there will be mutual solubility of some water in the continuous DES phase and some DES components in the dispersed phase. If this was not the case then the liquids would not exhibit a ζ potential. The presence of a ζ potential suggests the separation of charges at the interface between the dispersed and continuous phases.

There are a variety of scenarios which could fit with the data presented above;

- 1) The two phases could form a bicontinuous emulsion in the same way that some oil/water/surfactant systems do. This would, however, tend to produce a wide spread of sizes for the dispersed phase in the dynamic light scattering experiments. This has been observed within the group when studying micelles in DESs but is not the case for DES-water mixtures.
- 2) Regions of water dominated composition could partition chloride preferentially at the interface where they meet regions where there is less water. Having networks of water molecules in a water rich phase would explain the conductivity and density data shown above and also the diffusion data shown in Chapter 4. This would also explain the narrow size distribution observed by DLS.
- 3) The third model could be that water forms a semi-pure phase which is driven by the thermodynamic barrier to mixing. Coalescence of the water phases is precluded by the ζ potential caused by charge separation at the interface between the phases. This is less likely since ChCl is as soluble in water as it is in EG. These three potential models are shown schematically in **Figure 3.21**.

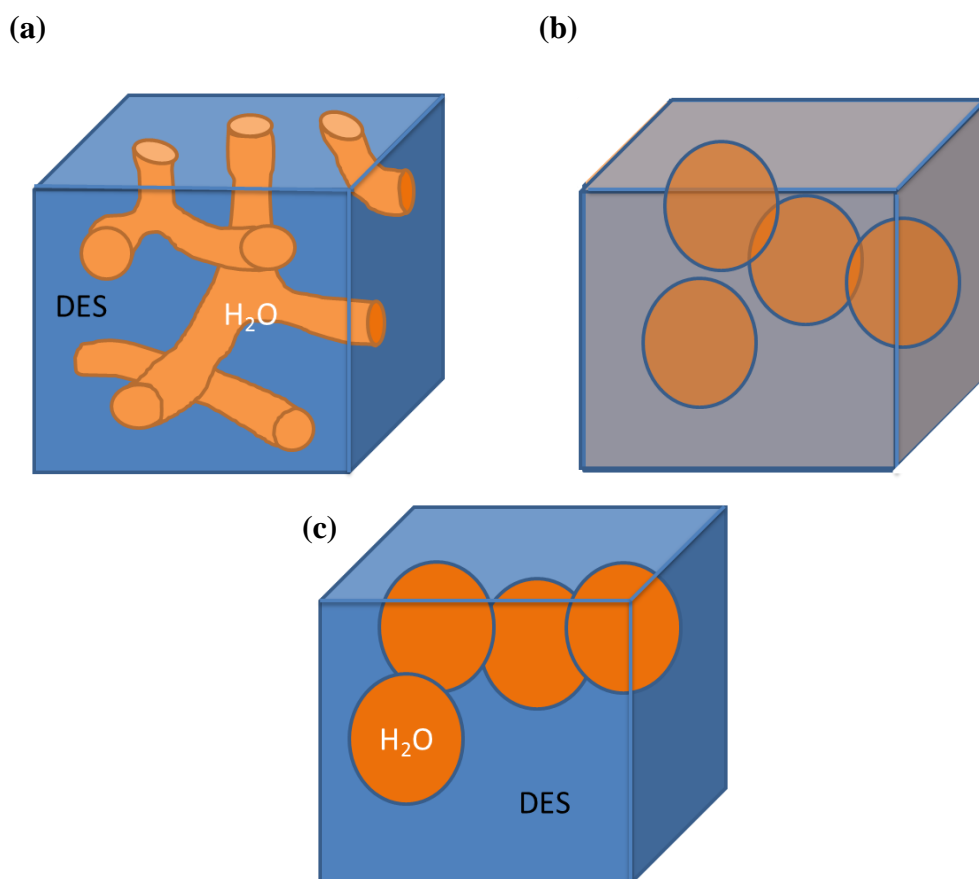


Figure 3.21: Three potential models for DES-water mixtures (a) bicontinuous emulsion, (b) semi-heterogeneous phases (partial mutual solubility) and (c) heterogeneous phases.

It would be difficult to determine the exact composition of both phases as exchange is rapid between the two phases. Some spectroscopic techniques may provide information: labelled NMR probes, e.g., ^{15}N urea could be used for HOESY to determine interactions with water. Diffusion experiments already show two different environments for water and deuterated sample of urea and ethylene glycol may indicate partitioning between the two phases.

3.10 Enthalpy of mixing DES with water.

To understand why water may not want to homogeneously mix with the DES it may be useful to understand the thermodynamics of mixing. This can be done by measuring the heat capacity of the liquids. In ionic liquid binary mixtures, the C_p value depends on the type of anion.^{80 81} The C_p values was used here to find the change in enthalpy of DES-water mixtures by application of **Equation (3.21)**.

$$C_{p\,mix} = \text{Real } C_p \text{ mixture} - \text{Ideal } C_p \text{ mixture} \quad \text{Equation (3.21)}$$

Here, $C_{p\,mix}$ is the heat capacity of mixing. Then, the enthalpy of the mixture, $\Delta_{mix}H$, can be found from the heat capacity of the mixture, as per **Equation (3.22)**.

$$\Delta H_{mix} = \Delta C_{p\,mix} \Delta T \quad \text{Equation (3.22)}$$

The enthalpy describes the non-ideal behaviour of real mixtures and it is an important factor in the study of molecular interactions and macroscopic behaviour of fluid mixtures.⁸²

Table 3.5: Heat capacity of deep eutectic solvents with 10% water, and the enthalpy of the mixture. Uncertainty is to one standard deviation.

DESs	C_p (DESs) J/g K at 298 K	C_p DESs+10 wt% H ₂ O J/g K at 298 K	ΔH (kJ/mole)
Ethaline	1.71 ± 0.4	2.36 ± 0.8	19.09
Glyceline	2.18 ± 0.9	2.33 ± 0.4	-1.89
Reline	1.97 ± 0.9	2.58 ± 0.6	12.67

Table 3.5 shows that for Ethaline and Reline the enthalpy of mixing is endothermic, which means that mixing will only occur if there is an increase in entropy. The hydrogen bonding plays an important role in the determining the enthalpy of the mixture, where the –OH group in the choline chloride can function as both a hydrogen bond donor and hydrogen bond acceptor. In a previous study⁸³ the partitioning of species from alkanes into DESs was shown to be endothermic and this is studied in greater detail below for the partitioning of iodine into DESs. The positive enthalpy of mixing DESs with water suggests that the interaction between water molecules in the bulk phase is larger than the interactions between water and either chloride ions or ethylene glycol molecules.

3.11 Extraction using DES-water mixtures.

The solvent properties of DES-water mixture can also provide information about the structure and behaviour of mixed systems. It has recently been shown that the thermodynamics of solute extraction from hexane into DESs is significantly affected by the properties of the DES and the solute. It was found for the extraction of thiophene from

decane into DESs that the partition coefficient was controlled by the surface tension of the liquid. It was shown that DESs with low surface tension such as Ethaline were better at extracting thiophenic compounds than Reline or Glyceline. This was argued in terms of the endothermic enthalpy of transfer arising from the energy required to make a hole in the DES to fit the solute into. It was shown that partition of the solute into the DES was governed by entropy changes.

There has been considerable research into the use of DESs in extraction.⁸⁴⁻⁸⁸ In this section of our work, we used three types of DES, namely Ethaline, Glyceline and Reline, with hexane in order to extract iodine. Iodine is a hydrophobic molecule which would normally be expected to partition into the organic phase. In the DESs, however, it can form I_2Cl^- which should be exothermic on formation. The addition of water would be expected to shift the equilibrium back to the organic phase.

The partitioning of iodine between hexane and three DESs was measured at two temperatures (25°C and 35°C) and this was repeated for a DES-water mixture containing 12.5 wt% water. The results showed that equilibrium was rapidly set up in only 5 minutes. These results corresponded well with a previous study by Gu *et al.* This same group showed that DESs have a much greater enrichment factor (EF) compared with water and DES-water mixtures, due to DESs showing a high capacity to dissolve polar compounds.⁸⁵

To see the effect of the solute polarity on phase transfer, we used iodine as a solute. Iodine is an important solute in DESs as it has been used extensively as an electrocatalyst and is a good oxidising agent.⁸⁹ These partition coefficients were determined at 25°C and 35°C using the Gibbs and van't Hoff **Equation (3.23)** and **Equation (3.25)**.

$$\Delta G = -RT \ln K_p \quad \text{Equation (3.23)}$$

$$\ln \left(\frac{K_2}{K_1} \right) = -\frac{\Delta H}{R} \left(\frac{1}{T_2} - \frac{1}{T_1} \right) \quad \text{Equation (3.24)}$$

$$\Delta S = (\Delta H - \Delta G)/T \quad \text{Equation (3.25)}$$

where R is the universal gas constant, T is the absolute temperature, and K_p is the value of the partition coefficient at equilibrium, defined as:

$$K_p = \frac{(\text{molality of iodine})_{in\ DES}}{(\text{molality of iodine})_{in\ hexane}} \quad \text{Equation (3.26)}$$

The iodine layer was analysed by UV-Vis spectroscopy, the data from which are shown in **Table 3.6**. These data show that despite being non-polar, iodine partitions preferentially into the DES, in some cases decolouring the organic phase almost completely. Interestingly, the enthalpy of transfer to the DES is still endothermic, showing that entropy is driving the transfer of iodine to the polar phase. The enthalpy of transfer is more endothermic in 1 ChCl: 2 urea and 1 ChCl: 2 glycerol than in 1 ChCl: 2 ethylene glycol, and yet iodine partitions preferentially into the DESs with the higher surface tension, which is the opposite to that seen for thiophene in the Kareem study.⁹⁰ It is evident in this case that the enthalpy of hole formation is less important in governing the partitioning of the solute, but the complex formed, I_2Cl^- , is better at breaking up the structure of the DES than thiophene because the entropy of transfer is much higher for I_2 .

Table 3.6: Partition coefficients and Gibbs energy change for iodine partitioning from hexane to DESs. Uncertainty is to one standard deviation.

DES	K_p		ΔG (kJ mol ⁻¹)		ΔH (kJ mol ⁻¹)	ΔS (J mol ⁻¹ K ⁻¹) at 25°C
	25°C	35°C	25°C	35°C		
Ethaline	11.79 ± 0.18	15.3 ± 0.34	-6.1 ± 0.03	-7.0 ± 0.05	+19.9 ± 0.50	+88.0 ± 1.20
Glyceline	19.87 ± 0.41	43.59 ± 1.11	-7.4 ± 0.1	-9.7 ± 0.06	+60.0 ± 1.1	+226.2 ± 3.9
Reline	25.08 ± 0.20	40.40 ± 0.60	-8.0 ± 0.20	-9.2 ± 0.30	+36.40 ± 0.30	+148.9 ± 0.40

Mixing water with a DES-hexane system makes the mixture very complicated due to the partitioning of iodine between three phases, namely DES-water-hexane. The results show a decrease in partition coefficient for all three systems compared with the pure systems.

This is unsurprising as iodine is virtually insoluble in water. **Table 3.7** reports the partition coefficient for iodine in hexane-DESs-water mixtures. As can be seen from this table, the partition coefficient for all DESs decreases when mixed with water.

The data in **Table 3.7** shows that the addition of water to Reline affects the partitioning of iodine less than Ethaline and Glyceline. If the solutions were homogeneous then iodine partitioning should be relatively independent of the HBD. Analysing the data in **Figure 3.17** it can be seen that the dispersed phase is significantly smaller in Reline than in either Ethaline or Glyceline which may explain why the iodine still partitions into Reline with a significant amount of water in it. It could also be that Reline-water mixtures are more heterogeneous than Ethaline-water mixtures.

Table 3.7: partition coefficients for iodine in DES-water (12.5 wt% water) mixtures. Uncertainty is to one standard deviation.

DES-water mixture	K_p		ΔG (kJ mol ⁻¹)		ΔH (kJ mol ⁻¹)	ΔS (J mol ⁻¹ K ⁻¹) at 25°C
	25°C	35°C	25°C	35°C		
Ethaline	+ 0.55 ± 0.04	+ 0.62 ±0.03	+ 1.46 ± 0.17	+ 1.22 ± 0.12	+ 8.51 ± 0.48	+ 23.6 ± 1.54
Glyceline	+ 0.53 ±0.04	+ 0.47 ± 0.07	+ 1.56 ± 0.18	+ 1.91 ± 0.3	- 8.13 ± 0.20	- 32.5 ± 0.69
Reline	+ 6.11 ±0.31	+ 6.90 ± 0.28	- 4.47 ± 0.12	- 4.73 ± 0.10	+1.63 ± 0.52	+ 21.3 ± 1.3

Figure 3.22 shows the comparative extractions of iodine in the two systems. Without water the equilibrium lies towards the DES, whereas when water is added the equilibrium lies almost equally between the two phases.

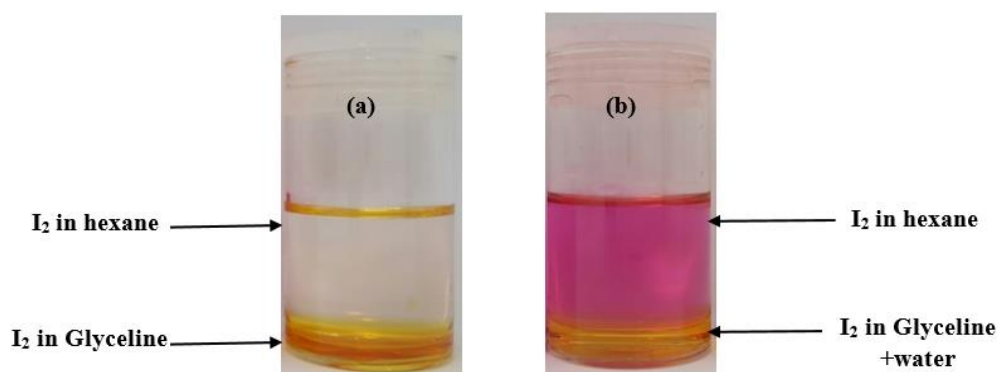


Figure 3.22: Extraction of I_2 in different media (a) pure Glyceline and (b) Glyceline-water mixture.

3.12 Conclusions.

This study has quantified the thermophysical properties of both pure deep eutectic solvents, and deep eutectic solvents with different water content. In pure DESs, the physical properties, including viscosity, surface tension, density and conductivity as a function of temperature, are dependent on the interaction between choline chloride and a hydrogen-bonding donor. The properties can be explained in terms of hole theory and it is clear that the liquids with higher surface tensions have higher viscosities than those with lower values.

The behaviour of DES-water mixtures indicated that DES-water mixtures are not homogeneous as water was found to have a non-continuous and even effect on parameters such as viscosity, conductivity and density. Using Dole-Jones analysis of the viscosity data showed that the B parameter suggested that ChCl acts as a kosmotrope, i.e., increasing the structure of the HBD. The liquids were mostly Newtonian in behaviour but Reline and Oxaline showed some non-Newtonian behaviour at lower temperature due to increased hydrogen bonding.

The most significant results were obtained using dynamic light scattering which provided more evidence that the DES-water mixtures were not homogeneous. Corresponding measurement of ζ potentials suggested values at most compositions which were significantly greater than 10 mV, showing that the colloidal dispersions are stable. It is interesting to note that both water in DES and DES in water emulsions are formed. This might help to explain some of the observations that solutions of DESs and ionic liquids

in water have properties which are different from those that would otherwise be expected for a solution of choline chloride and an HBD in water.

3.13 References.

1. A. R. Neale, S. Murphy, P. Goodrich, C. Hardacre and J. Jacquemin, *ChemPhysChem*, 2017.
2. C. P. Fredlake, J. M. Crosthwaite, D. G. Hert, S. N. Aki and J. F. Brennecke, *Journal of Chemical & Engineering Data*, 2004, **49**, 954-964.
3. H. Tokuda, K. Hayamizu, K. Ishii, M. A. B. H. Susan and M. Watanabe, *The Journal of Physical Chemistry B*, 2005, **109**, 6103-6110.
4. P. Wasserscheid and W. Keim, *Angewandte Chemie International Edition*, 2000, **39**, 3773-3789.
5. S. Aparicio, M. Atilhan and F. Karadas, *Industrial and Engineering Chemistry Research*, 2010, **49**, 9580-9595.
6. A. A. Fannin, D. A. Floreani, L. A. King, J. S. Landers, B. J. Piersma, D. J. Stech, R. L. Vaughn, J. S. Wilkes and J. L. Williams, *The Journal of Physical Chemistry*, 1984, **88**, 2614- 2621.
7. R. B. Leron, A. N. Soriano and M. Li, *Journal of the Taiwan Institute of Chemical Engineers*, 2012, **43**, 551-557.
8. R. Sedev, *Current Opinion in Colloid & Interface Science*, 2011, **16**, 310-316.
9. A. Jarosik, S. R. Krajewski, A. Lewandowski and P. Radzimski, *Journal of Molecular Liquids*, 2006, **123**, 43-50.
10. D. S. Viswanath, T. K. Ghosh, D. L. Prasad, N. K. Dutt and K. Y. Rani, *Viscosity of Liquids Theory, Estimation, Experiment, and Data*, Springer, 2007.
11. G. Yu, D. Zhao, L. Wen, S. Yang and X. Chen, *American Institute of Chemical Engineers*, 2012, **58**, 2885-2899.
12. H. Ghaedi, M. Ayoub, S. Sufian, A. M. Shariff and B. Lal, *Journal of Molecular Liquids*, 2017, **241**, 500-510.

13. P. Wasserscheid and T. Welton, *Ionic Liquids in Synthesis*, Wiley, 2007.
14. A. Andresova, J. Storch, M. Traïkia, Z. Wagner, M. Bendova and P. Husson, *Fluid Phase Equilibria*, 2014, **371**, 41-49.
15. J. Rotrekl, J. Storch, J. Kloužek, P. Vrbka, P. Husson, A. Andresová, M. Bendová and Z. Wagner, *Fluid Phase Equilibria*, 2017, **443**, 32-43.
16. M. Tariq, P. J. Carvalho, J. A. P. Coutinho, I. M. Marrucho, J. N. C. Lopes and L. P. N. Rebelo, *Fluid Phase Equilibria*, 2011, **301**, 22-32.
17. Y. Qiao, F. Yan, S. Xia, S. Yin and P. Ma, *Journal of Chemical and Engineering Data*, 2011, **56**, 2379-2385.
18. S. Panda and R. L. Gardas, *Fluid Phase Equilibria*, 2015, **386**, 65-74.
19. J. O. M. Bockris and A. K. Reddy, *Modern Electrochemistry 2B: Electrodics in Chemistry, Engineering, Biology and Environmental Science*, Springer Science & Business Media, 2000.
20. A. P. Abbott, *ChemPhysChem*, 2004, **5**, 1242-1246.
21. *More Solutionsto StickyProblems, Brookfield Engineering Labs, Inc.*
22. R. Stefanovic, M. Ludwig, G. B. Webber, R. Atkin and A. J. Page, *Physical Chemistry Chemical Physics*, 2017, **19**, 3297-3306.
23. G. García, S. Aparicio, R. Ullah and M. Atilhan, *Energy & Fuels*, 2015, **29**, 2616-2644.
24. A. Yadav and S. Pandey, *Journal of Chemical & Engineering Data*, 2014, **59**, 2221-2229.
25. X. Yujiao, D. Haifeng, Z. Suojiang, L. Xiaohua and J. Xiaoyan, *Journal of Chemical & Engineering Data*, 2014, **59**, 3344-3352.
26. D. Shahi and F. S. Mjalli, *Physical Chemistry Chemical Physics*, 2014, **16**, 23900-23907.

27. O. S. Hammond, D. T. Bowron and K. J. Edler, *Angewandte Chemie*, 2017.
28. G. Jones and M. Dole, *Journal of the American Chemical Society*, 1929, **51**, 2950-2964.
29. G. Jones and S. K. Talley, *Journal of the American Chemical Society*, 1933, **55**, 624-642.
30. D. Feakins, W. E. Waghorne and K. G. Lawrence, *Journal of the Chemical Society, Faraday Transactions 1: Physical Chemistry in Condensed Phases*, 1986, **82**, 563-568.
31. S. J. Davis, PhD Thesis, University of Leicester, 2016.
32. A. Hammadi and D. C. Champeney, *Journal of Chemical & Engineering Data*, 1998, **43**, 1004-1008.
33. Y. Akhtar, *International Journal of Science, Technology and Society*, 2015, **3**, 6.
34. J. Curie and P. Curie, *Comptes Rendus*, 1880, **91**, 294-295.
35. C. O'sullivan and G. Guilbault, *Biosensors and Bioelectronics*, 1999, **14**, 663-670.
36. D. A. Buttry and M. D. Ward, *Chemical Reviews*, 1992, **92**, 1355-1379.
37. J. Curie and P. Curie, *Comptes-rendus de l'Académie des Sciences*, 1881, **93**, 1137-1140.
38. K. A. Marx, *Biomacromolecules*, 2003, **4**, 1099-1120.
39. K. K. Kanazawa and J. G. Gordon, *Analytica Chimica Acta* 1985 **175**, 99-10.
40. J. Smith, G. B. Webber, G. G. Warr and R. Atkin, *The Journal of Physical Chemistry B*, 2013, **117**, 13930-13935.
41. G. L. Burrell, N. F. Dunlop and F. Separovic, *Soft Matter*, 2010, **6**, 2080.

42. P. S. Kulkarni, L. C. Branco, J. G. Crespo, M. C. Nunes, A. Raymundo and C. A. Afonso, *Chemistry - A European Journal*, 2007, **13**, 8478-8488.
43. E. Y. Bormashenko, *Wetting of Real Surfaces*, De Gruyter, 2013.
44. C. Kolbeck, J. Lehmann, K. R. J. Lovelock, T. Cremer, N. Paape, P. Wasserscheid, A. P. Fröba, F. Maier and H.-P. Steinrück, *The Journal of Physical Chemistry B* 2010, **114**, 17025–17036.
45. C. Kolbeck, J. Lehmann, K. R. J. Lovelock, T. Cremer, N. Paape, P. Wasserscheid, A. P. Fröba, F. Maier and H.-P. Steinrück, *Journal of Physical Chemistry* 2010, **114**, 17025–17036.
46. M. Tariq, M. G. Freire, B. Saramago, J. A. Coutinho, J. N. C. Lopes and L. P. N. Rebelo, *Chemical Society Reviews*, 2012, **41**, 829-868.
47. M. G. Freire, P. J. Carvalho, A. M. Fernandes, I. M. Marrucho, A. J. Queimada and J. A. P. Coutinho, *Journal of Colloid and Interface Science* 2007, **314**, 621-630.
48. Q. Zhang, K. D. O. Vigier, S. Royer and F. Jerome, *Chemical Society Reviews*, 2012, **41**, 7108-7146.
49. A. P. Abbott, R. C. Harris and K. S. Ryder, *The Journal of Physical Chemistry B*, 2007, **111**, 4910-4913.
50. A. P. Abbott, G. Capper, D. L. Davies, H. L. Munro, R. K. Rasheed and V. Tambyrajah, *Chemical Communications*, 2001, 2010-2011.
51. A. P. Abbott, *A European Journal of Chemical Physics and Physical Chemistry*, 2005, **6**, 2502-2505.
52. N. V. Plechkova and K. R. Seddon, *Ionic Liquids Completely Uncoiled: Critical Expert Overviews*, John Wiley & Sons, 2015.
53. A.-M. Popescu, C. Donath and V. Constantin, *Bulgarian Chemical Communications*, 2014, **46**, 452-457.

54. A. P. Abbott, D. Boothby, G. Capper, D. L. Davies and R. K. Rasheed, *Journal of the American Chemical Society* 2004, **126**, 9142-9147.
55. Q. Cao, X. Lu, X. Wu, Y. Guo, L. Xu and W. Fang, *Journal of Chemical & Engineering Data*, 2015, **60**, 455-463.
56. J. A. Widegren, E. M. Saurer, K. N. Marsh and J. W. Magee, *The Journal of Chemical Thermodynamics*, 2005, **37**, 569-575.
57. A. Stoppa, O. Zech, W. Kunz and R. Buchner, *Journal of Chemical and Engineering Data*, 2010, **55**, 1768-1773.
58. W. Liu, L. Cheng, Y. Zhang, H. Wang and M. Yu, *Journal of Molecular Liquids*, 2008, **140**, 68-72.
59. L. Ries, F. Do Amaral, K. Matos, E. Martini, M. de Souza and R. de Souza, *Polyhedron*, 2008, **27**, 3287-3293.
60. K. N. Marsh, J. A. Boxall and R. Lichtenthaler, *Fluid Phase Equilibria*, 2004, **219**, 93-98.
61. S. V. Dzyuba and R. A. Bartsch, *Chemphyschem*, 2002, **3**, 161 - 166.
62. C. D'Agostino, R. C. Harris, A. P. Abbott, L. F. Gladden and M. D. Mantle, *Physical Chemistry Chemical Physics*, 2011, **13**, 21383-21391.
63. K. Shahbaz, F. G. Bagh, F. Mjalli, I. AlNashef and M. Hashim, *Fluid Phase Equilibria*, 2013, **354**, 304-311.
64. F. Endres, A. Abbott and D. MacFarlane, *Electrodeposition from Ionic Liquids*, John Wiley & Sons, 2017.
65. B. Mokhtarani, M. M. Mojtahedi, H. R. Mortaheb, M. Mafi, F. Yazdani and F. Sadeghian, *Journal of Chemical & Engineering Data*, 2008, **53**, 677-682.
66. R. B. Leron, A. N. Soriano and M.-H. Li, *Journal of the Taiwan Institute of Chemical Engineers*, 2012, **43**, 551-557.

67. R. Pecora, *Journal of Nanoparticle Research*, 2000, **2**, 123–131.
68. L. Pohjala and P. Tammela, *Molecules*, 2012, **17**, 10774-10790.
69. H. Wang, J. Wang, S. Zhang and X. Xuan, *The Journal of Physical Chemistry B*, 2008, **112**, 16682-16689.
70. K. Saihara, Y. Yoshimura, S. Ohta and A. Shimizu, *Scientific Reports*, 2015, **5**.
71. E. A. Cade, J. Petenuci and M. M. Hoffmann, *ChemPhysChem*, 2016, **17**, 520-529.
72. R. Sheldon, *Chemical Communications*, 2001, 2399-2407.
73. Z. Yang and W. Pan, *Enzyme and Microbial Technology*, 2005, **37**, 19-28.
74. Y. Kohno and H. Ohno, *Chemical Communications*, 2012, **48**, 7119-7130.
75. J. Wang, L. Zhang, H. Wang and C. Wu, *The Journal of Physical Chemistry B*, 2011, **115**, 4955-4962.
76. D. Evans and H. Wennerström, *New York, Wiley-VCH*, 1999, 45-98.
77. M. Kaszuba, J. Corbett, F. M. Watson and A. Jones, *Philosophical Transactions of the Royal Society of London A: Mathematical, Physical and Engineering Sciences*, 2010, **368**, 4439-4451.
78. S. Skoglund, J. Hedberg, E. Yunda, A. Godymchuk, E. Blomberg and I. O. Wallinder, *Plos One*, 2017, **12**, 0181735.
79. A. M. Smith, A. A. Lee and S. Perkin, *The Journal of Physical Chemistry Letters*, 2016, **7**, 2157-2163.
80. J. O. Valderrama, A. Toro and R. E. Rojas, *The Journal of Chemical Thermodynamics*, 2011, **43**, 1068-1073.
81. G. García-Miaja, J. Troncoso and L. Romaní, *The Journal of Chemical Thermodynamics*, 2009, **41**, 161-166.

82. C. Ma, Y. Guo, D. Li, J. Zong, X. Ji, C. Liu and X. Lu, *Journal of Chemical & Engineering Data*, 2016, **61**, 4172-4177.
83. P. López-Porfiri, J. F. Brennecke and M. Gonzalez-Miquel, *Journal of Chemical & Engineering Data*, 2016, **61**, 4245-4251.
84. M. W. Nam, J. Zhao, M. S. Lee, J. H. Jeong and J. Lee, *Green Chemistry*, 2015, **17**, 1718-1727.
85. T. Gu, M. Zhang, T. Tan, J. Chen, Z. Li, Q. Zhang and H. Qiu, *Chemical Communications*, 2014, **50**, 11749-11752.
86. B. Tang, H. Zhang and K. H. Row, *Journal of Separation Science*, 2015, **38**, 1053-1064.
87. L. Duan, L.-L. Dou, L. Guo, P. Li and E.-H. Liu, *ACS Sustainable Chemistry & Engineering*, 2016, **4**, 2405-2411.
88. Y. Dai, J. van Spronsen, G.-J. Witkamp, R. Verpoorte and Y. H. Choi, *Journal of Natural Products*, 2013, **76**, 2162-2173.
89. A. Abbott, G. Frisch, S. Gurman, A. Hillman, J. Hartley, F. Holyoak and K. Ryder, *Chemical Communications*, 2011, **47**, 10031-10033.
90. J. H. Kareem, PhD Thesis, University of Leicester, 2017.

Chapter 4: Diffusion in DES/ water mixtures.

4	Diffusion in DES/ water mixtures.	99
4.1	Overview.....	99
4.2	Objective.....	100
4.3	Results and discussion.	100
4.3.1	Diffusion coefficient by PFG-NMR.....	100
4.4	Study of diffusion coefficients by electrochemical methods.....	109
4.5	Cyclic voltammetry of iron chloride in deep eutectic solvents.	109
4.6	UV-Vis spectroscopy.....	116
4.7	Electrical double layer.	119
4.8	Double layer capacitance.	126
4.8.1	Iodine speciation with in DES-water mixtures.	127
4.9	Conclusion.	128
4.10	References.....	129

4 Diffusion in DES/ water mixtures.

4.1 Overview.

The thermophysical properties of ionic liquids and deep eutectic solvents with water, e.g., ionic conductivity, dynamic viscosity, density, surface tension, solubility and melting point have been investigated in detail.¹⁻³ In the previous chapter, it was shown that there is sufficient data to suggest that water does not form homogeneous mixtures with DESs and by inference the same is true for ionic liquids.

One way to probe the structure of liquids is to measure the movement of both solvent ions/ molecules and solutes dissolved in the DES. Several methods have been used to study diffusion coefficients in solution including nuclear magnetic resonance (NMR), computer simulations, diaphragm cells, optical methods, and a variety of electrochemical methods.⁴⁻¹⁰ In this part of the study, we used NMR and cyclic voltammetry to measure diffusion coefficient of the solvent species themselves and electrochemical probes in solution.

Diffusion coefficients have been measured in dilute IL solutions to provide information about interactions between the ions and the solute.¹¹ Nuclear magnetic resonance (NMR) has been used to probe structure and dynamics of ILs. There are several of NMR techniques available depending on method of use; for example, multinuclear, multidimensional, nuclear Overhauser effects, relaxation times, and self-diffusion measurements.¹²

D'Agostino *et al.* used PFG-NMR to study self-diffusive motion in choline chloride-based DESs, including Ethaline, Glyceline, Reline and Maline. For the first three samples, the hydrogen bonding diffuses faster than the corresponding chlorine cation due to the higher molecular weight of the chlorine chloride compared to the hydrogen bond donor. However, in Maline, the choline chloride diffuses faster than the hydrogen bond donor "malonic acid" due to formation of dimer chains between malonic acid molecules, which has the effect of reducing the molecular mobility of the system. In addition, their study showed the influence of changes in temperature on the system; the self-diffusion coefficient obeyed the Arrhenius equation for all samples under investigation.¹³

Taylor *et al.* argued that ionic liquids behave like glass-forming systems, which means the diffusion occurs via a jumping mechanism when suitable size voids are present, rather

than via a classical random walk mechanism. This due to fact that the diffusion mechanism in DESs depends on the free volume available.¹⁴

4.2 Objective.

Many researchers have characterised the diffusion coefficients of species in ionic liquids.¹⁵⁻²² However, this project is the first to study diffusion coefficients of species in DES-water mixtures. The first part of this study will investigate the self-diffusion coefficients in type III DES-water mixtures using PFG-NMR. The aim is to see whether the species diffuse in a Stokesian manner and whether they behave independently of each other. The second part of the study was to investigate diffusion coefficients by electrochemical methods using iron chloride and potassium ferrocyanide as probes in DES-water systems. Moreover, the study of the double layer in an Ethaline-water mixtures was made using sodium iodide and iodine as probes. Finally, the speciation of these probes in solution was studied using UV-Vis spectroscopy.

4.3 Results and discussion.

4.3.1 Diffusion coefficient by PFG-NMR.

Aqueous DES mixtures have been used in several practical applications²³⁻²⁶ including in the extraction of proteins.²⁴ Different DESs were shown to have different abilities to extract various proteins. Abbott *et al.*²⁶ used water miscible DESs as potential “green” lubricants and investigated the corrosion rate for different metals. It was shown that steel underwent mild corrosion in wet Reline, but was almost inert in wet Glyceline. This was ascribed to differences in cathodic reactions in the liquids resulting from different water “activities”. It would therefore be helpful to better understand the microscopic behaviour of such water-DES mixtures to help capitalise on the properties.

PFG NMR was used to study the molecular mobility of three ChCl-based DESs in the presence of water in order to understand the effect of water composition on the molecular mobility of the different species involved in the system. To probe the mobility of the charged and uncharged species further, the self-diffusion coefficients were determined using NMR spectroscopy. These measurements were carried out at Cambridge University. **Figure 4.1** shows a typical NMR spectrum for the samples used in this study, together with the peak assignment. The peak assignment is consistent with the spectra

previously reported for choline chloride-based DES.²² The NMR peaks are rather broad, which is expected given the high viscosity of such samples.

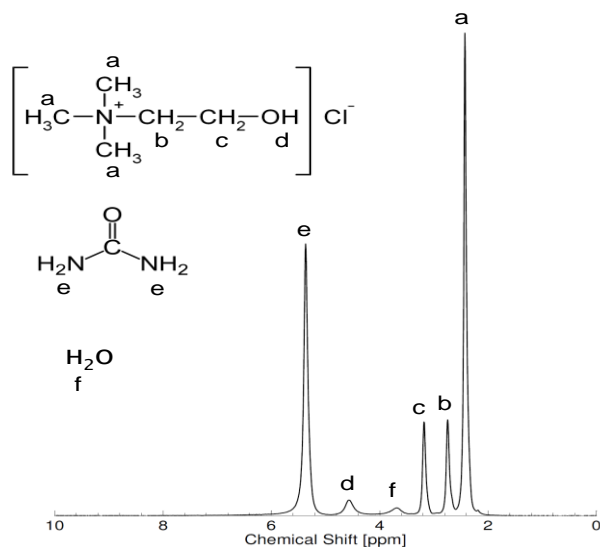


Figure 4.1: ¹H-NMR spectrum of aqueous Reline at 1 wt% water content. The peak positions are (in ppm): a = 2.34; b = 2.75; c = 3.18; d = 4.59; e = 5.38; f = 3.69. All resonances are quoted relative to TMS as the reference standard.

Figure 4.2 reports a typical PFG NMR attenuation plots for the samples studied here, showing the NMR signal attenuation for the various resonances in aqueous Glyceline with a 15 wt% fraction of water. It can be clearly observed as the water resonance shows a much higher slope (i.e., higher NMR signal attenuation) relative to the resonances of Glyceline, indicating a much faster self-diffusion coefficient of water relative to the species present in Glyceline.

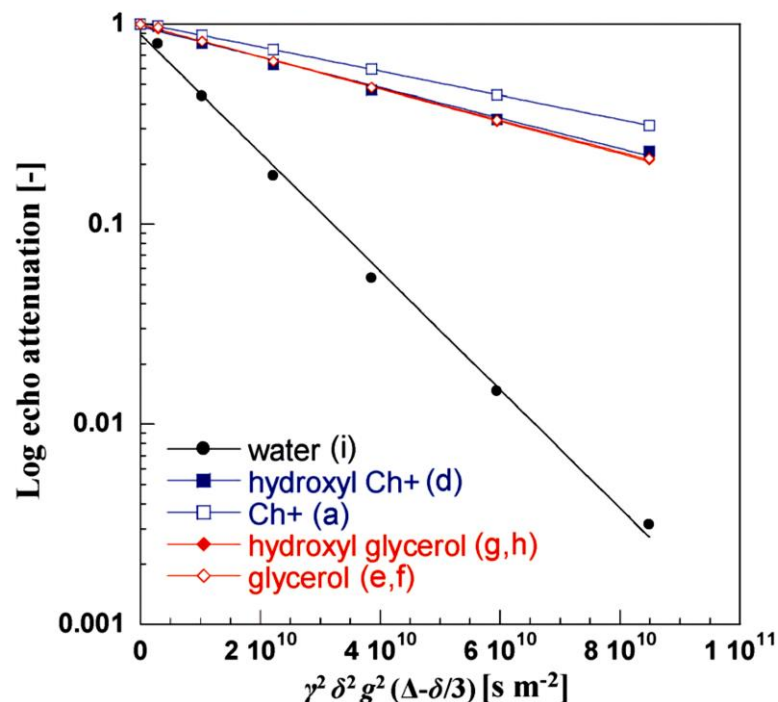


Figure 4.2: PFG NMR log attenuation plots for the various species in aqueous Glyceline with a 15 wt% fraction of water. Note the distinctive diffusion attenuation of water relative to the other species. Solid lines are fittings using Equation 2.7.

The experimental data were fitted using **Equation 2.7** (see chapter two), which allows the determination of the numerical values of self-diffusivity. In the current work it is not only the self-diffusion coefficients of the three main components of the mixture (i.e., ChCl, HBD and water) which are of interest, but we are also interested in the diffusivities of the hydroxyl protons of both Ch⁺ and the HBD molecules. The particular advantage of PFG NMR is that it can probe the diffusion of a certain species by measuring the signal attenuation of the NMR resonances of that species. In the absence of any exchange/interactions with other species, both aliphatic and hydroxyl ¹H resonances of the molecule should yield the same diffusion coefficients (i.e., the molecule moves as a whole). However, if phenomena such as interaction/ pairing/ exchange between hydroxyl protons of different molecules become significant, one may expect a very large difference in the diffusion coefficient values of the aliphatic and hydroxyl protons of the same molecule. In this context, PFG NMR diffusion measurements become a powerful tool by which to elucidate interactions between the different species within the liquids, besides their motion characteristics.²² The values of self-diffusion coefficients as a function of

water content are reported for the different species present in the three different aqueous DES mixtures.

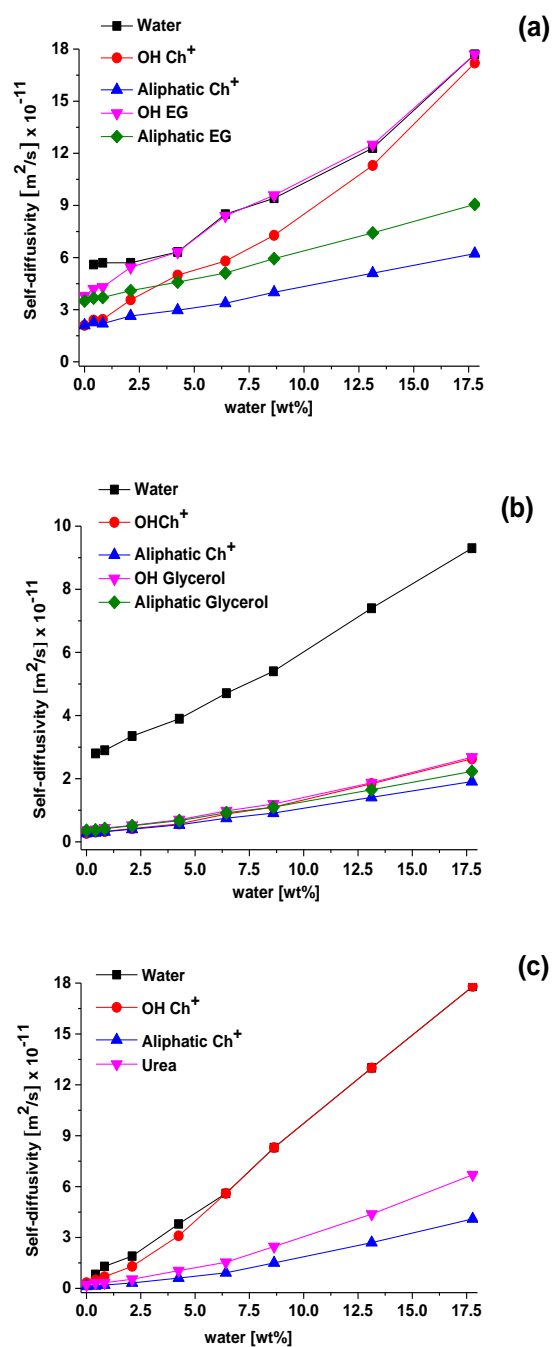


Figure 4.3: Self-diffusion coefficients for different species in (a) Ethaline, (b) Glyceline and (c) Reline as a function of water content.

It may be noted that the only species that cannot be probed with our current set-up is the Cl⁻ anion; this is because its detection via PFG-NMR is complicated by several factors such as the low sensitivity of chloride anions and the presence of nuclear quadrupolar

interactions. For all three DESs, the self-diffusion coefficients of all the species of interest can be measured unambiguously. Diffusion coefficients as a function of water content are reported in **Figure 4.3**.

Ethaline: In the pure liquid (i.e., in the absence of any water) the diffusivity of ethylene glycol is higher than that of Ch^+ . This is in agreement with previous findings²² on pure DES studies and is attributed to the larger size of the Ch^+ cation relative to ethylene glycol. It can also be seen that in each species (i.e., Ch^+ and ethylene glycol), the diffusivity of the hydroxyl proton is the same as that measured for the rest of the molecule, which clearly suggests that there is no significant exchange of hydroxyl protons between the two species in the pure Ethaline sample (i.e., the hydroxyl proton remains bound to the rest of the molecule as it diffuses).

When water is added to the DES, the diffusivities of both Ch^+ and ethylene glycol both increase. However, we now observe a significant deviation for the hydroxyl protons diffusivity of both Ch^+ and ethylene glycol; for each of these species, the hydroxyl proton diffuses faster than rest of the molecule and such a difference becomes more significant as the water content increases, with values approaching those measured for pure water. Indeed, for the highest water content, the diffusion coefficients of the hydroxyl protons of Ch^+ and ethylene glycol are almost identical to that measured for water. This suggests that at higher water content both Ch^+ and ethylene glycols are in equilibrium with some negatively charged species, with their hydroxyl counterpart in strong exchange with water. Were this otherwise, then there would be no difference between the self-diffusion of the hydroxyl proton and that of the rest of the molecule, which is clearly not the case. It may be noted that for the highest water content the -OH resonance of the HBD and water overlap, and the diffusivity reported is the average diffusivity of both species.

Glyceline: In the pure liquid the diffusivity of glycerol is slightly higher than that of Ch^+ , again reflecting the differences in molecular size; however, compared to the case of Ethaline, the diffusivity of the glycerol is much closer to that of Ch^+ and this is also consistent with previous findings.²² Water has a significantly higher and distinct diffusion coefficient in Glyceline relative to all the other species of DES, including the hydroxyl species of the DES components (i.e., Ch^+ and HBD). This suggests that the hydroxyl protons of Ch^+ and glycerol forming Glyceline do not show any significant interaction with water, otherwise a different diffusion coefficient for such protons would be observed

due to chemical exchange of protons, as previously observed in alcohol/water mixtures.²² Conversely, the hydroxyl protons of both Ch^+ and glycerol have a similar value of self-diffusivity, particularly for low water content. As the water content increases, a deviation of the hydroxyl proton diffusivities in both Ch^+ and glycerol is observed, with greater values than those measured for the other molecules; however, such values are nowhere close to the values measured for water. This suggests that the interaction of Ch^+ and the glycerol with water is minimal compared to the Ethaline case; conversely, much stronger correlated motion between Ch^+ and glycerol is observed. This could be attributed to differences in steric hindrance effects between ethylene glycol and glycerol

Reline: A major difference in Reline compared to Ethaline and Glyceline is that urea does not have any hydroxyl protons that may interact with other species. In pure Reline, similar considerations to those made for pure Glyceline can be made in terms of differences in diffusion coefficients between the HBD and Ch^+ ; the diffusivity of urea is faster than that observed for Ch^+ , reflecting again the difference in molecular size. As water is added to the system, the diffusivity of the hydroxyl proton of Ch^+ starts deviating significantly relative to the diffusivity of the rest of the Ch^+ molecule and approaches the larger diffusivity values observed for water. Above 10 wt% water, the resonances of the hydroxyl proton of Ch^+ and water become closer and eventually overlap. Above this water content, the reported diffusivity values for water and the hydroxyl proton of Ch^+ is that of their overlapping NMR peaks. The coalescence of these two NMR peaks indicates a fast exchange between the water protons and the hydroxyl protons of Ch^+ ;²⁷ in addition to the finding that the diffusion coefficients of such peaks become similar, this suggests a strong interaction between water and the hydroxyl proton of Ch^+ .

To compare the systems more clearly the data of viscosity **Figure 3.2** (see Chapter 3) and **Figure 4.3** are combined in **Figure 4.4**. In principle, if a Stokesian model of diffusion is valid then the diffusion coefficient should be inversely proportional to the viscosity. **Figure 4.4(a)** shows that for the aliphatic protons on choline this behaviour is valid, although there is a slightly different slope for the first three data points (up to 2.5 wt %). In the dry ionic liquids and DESs we have previously shown that diffusion is non-Stokesian and this may be due to the large size of the diffusing species and the lack of suitable spaces for them to diffuse into.²²

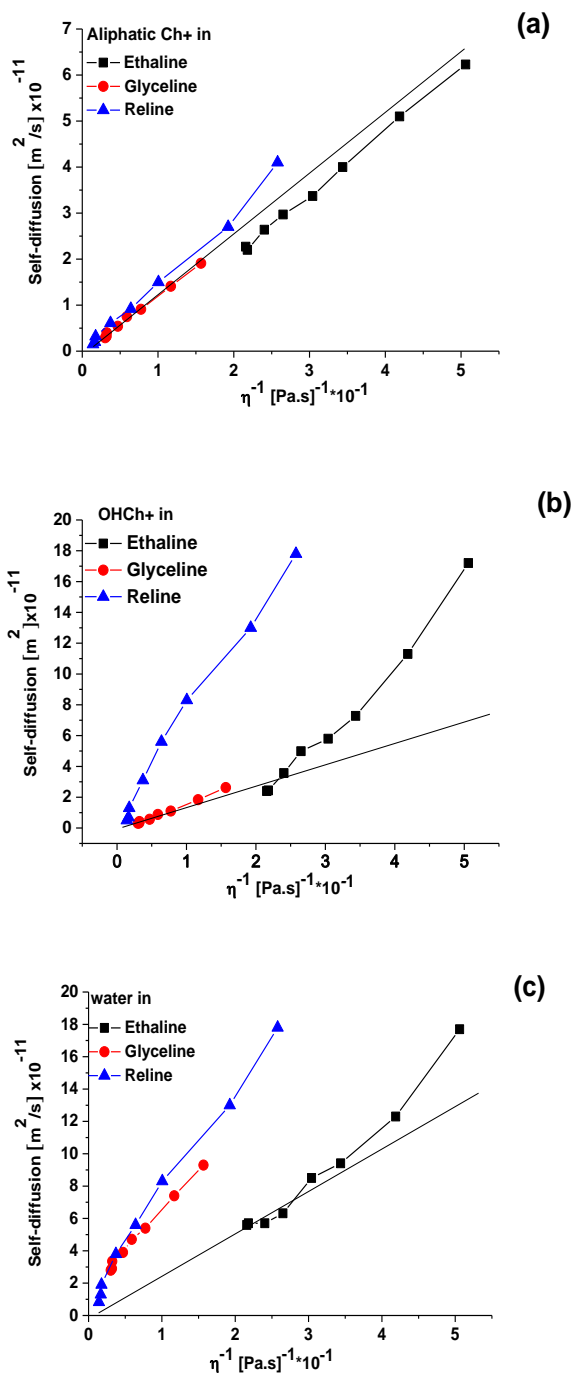


Figure 4.4: Diffusion coefficients as a function of inverse viscosity for (a) aliphatic Ch^+ (b) OH on Ch^+ and (c) water in Ethaline, Glyceline and Reline. Straight lines correspond to ideal Stokesian responses in (a) and (b) for Ch^+ and in (c) for water.

Application of the Stokes-Einstein **Equation 2.6** (see chapter two). **Figure 4.4** shows also the theoretical line calculated for Ch^+ using **Equation 2.6** assuming a hard sphere radius of 3.29 \AA and calculated using a Hartree-Fock model.²⁸ It can be seen that the aliphatic

protons all give responses that were very similar to those predicted by the Stokes-Einstein equation.

Figure 4.4(b) shows the response for the OH proton in Ch^+ , where there is a difference between the behaviour of Glyceline and the other two liquids. At low water concentrations, all liquids show a behaviour which is roughly similar to the theoretical slope for Ch^+ , but where Ethaline and Reline deviate significantly as the water content increases above 2 wt% (a 1:1 $\text{H}_2\text{O}:\text{Cl}^-$).

With a high water content, the diffusion coefficients become similar to those expected for water, i.e., with a low water content the water associates with the halide anion whereas with a higher water content it acts essentially as free water. The corrosion of metals in these three liquids have recently been tested and it was shown that steel underwent mild corrosion in wet Reline but was almost inert in wet Glyceline. This was ascribed to differences in cathodic reactions in the liquids. The data in **Figure 4.4** suggest that aqueous solutions of Ethaline and Reline enable dissociation of the OH proton of Ch^+ , which could make the liquids more acidic than Glyceline.²⁹ **Figure 4.5** shows solutions of the three DESs containing a 20 wt% water and universal indicator paper as a pH indicator. It can clearly be seen that there is a significant difference in the colour of the solutions, indicating that Reline is considerably more basic than the other two liquids. Use of a pH electrode shows the pH of the three solutions, each with 20 wt% water, to be 3.97 ± 0.04 , for Ethaline, 7.02 ± 0.07 for Glyceline and 12.20 ± 0.01 for Reline. The Glyceline solution is roughly neutral, confirming that the OH on the Ch^+ remain associated while the Ethaline solution is slightly acidic, which is confirmed by the larger diffusion coefficient observed in **Figure 4.4**. The pH of Reline can only be explained by the partial decomposition of urea to form $\text{NH}_3/\text{NH}_4\text{OH}$. It should, however, be noted that the dissociation is relatively small with an OH^- concentration of $0.016 \text{ mol. dm}^{-3}$. It is therefore unsurprising that only a trace NMR signal is observed.

These pH data also tie in with the corrosion studies recently reported for the three liquids²⁶ where it was shown that almost no corrosion was observed in wet Glyceline even after one year, whereas mild corrosion was noted in both wet Reline and Ethaline. The formation of NH_4OH in dilute Reline would also explain the deviation from linear behaviour in **Figure 3.14** (see chapter three) since there will be more charge carriers, which are considerably smaller and have a larger molar conductivity.



Figure 4.5: Samples of Ethaline (left) Glyceline (middle) and Reline (right) with 20 wt% water, each containing a sample of universal indicator paper.

Figure 4.4(c) shows the diffusion coefficient for water as a function of fluidity. The responses for Reline and Glyceline are relatively similar and show a high diffusivity for water, which is similar in both liquids. The self-diffusion coefficient of pure water is $2.299 \times 10^{-9} \text{ m}^2 \text{ s}^{-1}$ at 2°C .³⁰ Using this value and scaling for viscosity produces the solid line seen in **Figure 4.4(c)**.

The data for Ethaline fit this quite well but the data for Glyceline and Reline are anomalously high. These results are difficult to reconcile with the liquids being homogeneous, which leads to the suggestion that the anomalous behaviour of water/DES mixtures arises because the water is not homogeneously mixed with the DESs but instead forms separate phases at high concentrations of water. Similar studies have been carried out using hydrophobic ionic liquids. Rollet *et al.*³¹ used NMR spectroscopy to study water diffusion in $[\text{C}_4\text{mim}][(\text{CF}_3\text{SO}_2)_2\text{N}]$ and found a diffusion coefficient for water which was 25 times higher than predicted. They concluded that this was due to phase separation at the microscopic scale. This phase separation has been predicted by molecular dynamics simulations and is somewhat unsurprising given the hydrophobicity of the ionic liquids.³² The hydrophilicity of DESs might lead to the assumption that aqueous mixtures as homogeneous, but these diffusional studies show that phase separation still occurs. The pH and the ability of water in these mixtures to form separate micro-phases could be responsible for some of the observations in biochemical and mineral processing applications.

These data confirm that dynamic light scattering observations that ionic liquids and water form phases which are heterogeneous on the microscopic scale.

4.4 Study of diffusion coefficients by electrochemical methods.

Electrochemical methods are commonly used to probe mass transport in liquids.³³ This part of the study used cyclic voltammetry to quantify the diffusion coefficients for two different probes; iron chloride and potassium ferrocyanide as hydrophilic compounds and iodine as a hydrophobic compound. Taylor *et al.* used two different electrochemical methods to study diffusion coefficients in ILs, namely cyclic voltammetry and potential step chronoamperometry, to study diffusion in [FcC₁C₁Im][Tf₂N] in [C₂C₁Im][Tf₂N]. Their results illustrate that the diffusion coefficient of [FcC₁C₁Im][Tf₂N] in [C₂C₁Im][Tf₂N] was $1.18 \times 10^{-7} \text{ cm}^2 \text{ s}^{-1}$; however, the diffusion coefficient found by using potential step chronoamperometry was $1.71 \times 10^{-7} \text{ cm}^2 \text{ s}^{-1}$. It is clear that the diffusion coefficient found by the potential step chronoamperometry method is higher by about 1.5 times than that found by cyclic voltammetry. The difference between the diffusion coefficients found by cyclic voltammetry and potential step chronoamperometry was due to correcting for the effect of the capacitive current which is removed in chronoamperometry experiments, but is completely absent in the redox probe.¹⁴

4.5 Cyclic voltammetry of iron chloride in deep eutectic solvents.

Cyclic voltammetry is a standard technique used to obtain qualitative information about electrochemical reactions. It can provide information about the thermodynamics of redox processes, kinetics of heterogeneous electron-transfer reactions and analysis of coupled electrochemical reactions or adsorption processes. Cyclic voltammograms of 0.02 mol dm^{-3} of iron chloride in deep eutectic solvents containing various amounts of water were studied using a 0.5 mm diameter platinum electrode at different scan rates (5, 10, 15, 20 and 25 mVs^{-1}) at 25°C . The potential window was from 0.0 - 0.8 V for Ethaline, and -0.2 - 0.8 V for Glyceline and Reline, all of which were within the electrochemical window of the DESs.³⁴ These data are shown in **Figure 4.6 (a), (b), (c) and (d)**.

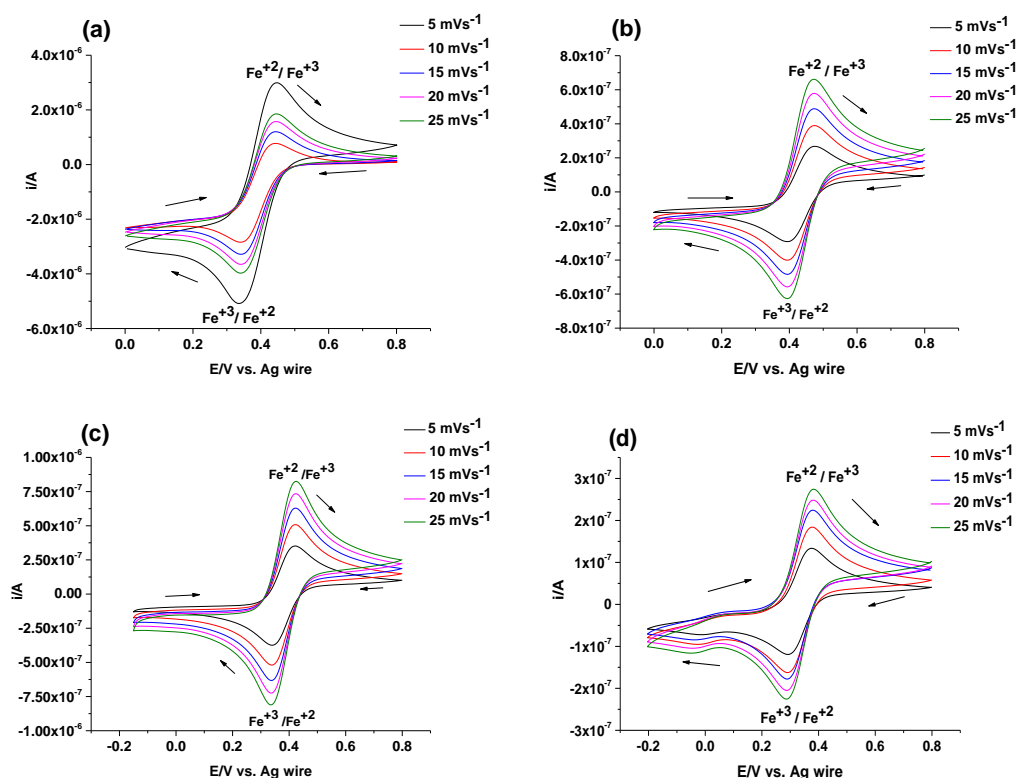


Figure 4.6: Cyclic voltammograms of $0.02 \text{ mol dm}^{-3} \text{ FeCl}_3$ in four systems: (a) water, (b) Ethaline, (c) Glyceline and (d) Reline.

It is important to note that the experiment for each mix was repeated at each scan rate three times. In one of the most recent studies, Yamagata *et al.* investigated the interaction of iron bromide in bromide-based ionic liquids. A complex formed between the iron bromide and bromide ions to give $\text{FeBr}_4^- / \text{FeBr}_4^{2-}$; moreover, this complex was found to be dependent on the concentration Br^- . Iron chloride will give a similar complex in ionic liquids, namely $\text{FeCl}_4^- / \text{FeCl}_4^{2-}$.³⁵ In contrast, there are sometimes other complexes that can be formed for the redox of FeCl_3 with ionic liquids, which is $\text{FeCl}_4^- / \text{Fe}_3\text{Cl}_7^-$. **Equation (4.1)** and **Equation (4.2)** illustrate these reactions.



The possibility of forming Fe_3Cl_7^- is dependent on the concentration of both Cl^- and Fe (II)-ILs. In the case of Fe-DESSs, no Fe_3Cl_7^- can be formed due to the high concentration of DESs used and the lower concentration of FeCl_3 , where the DESs surround FeCl_4^- and this effect prevents formation Fe_3Cl_7^- .³⁶

When water was added to the DESs (Ethaline, Glyceline and Reline), the resultant cyclic voltammograms are shown in **Figure 4.7** for both pure DESs, 80 wt% DESs: 20 wt% water mixtures, 60 wt% DESs: 40 wt% water and in pure water. The results show that with an increasing amount of water there was a shift towards more positive redox potentials for FeCl_3 in all three systems. This process was repeated to give cyclic voltammograms for all 16 solutions involved in this part of the study.

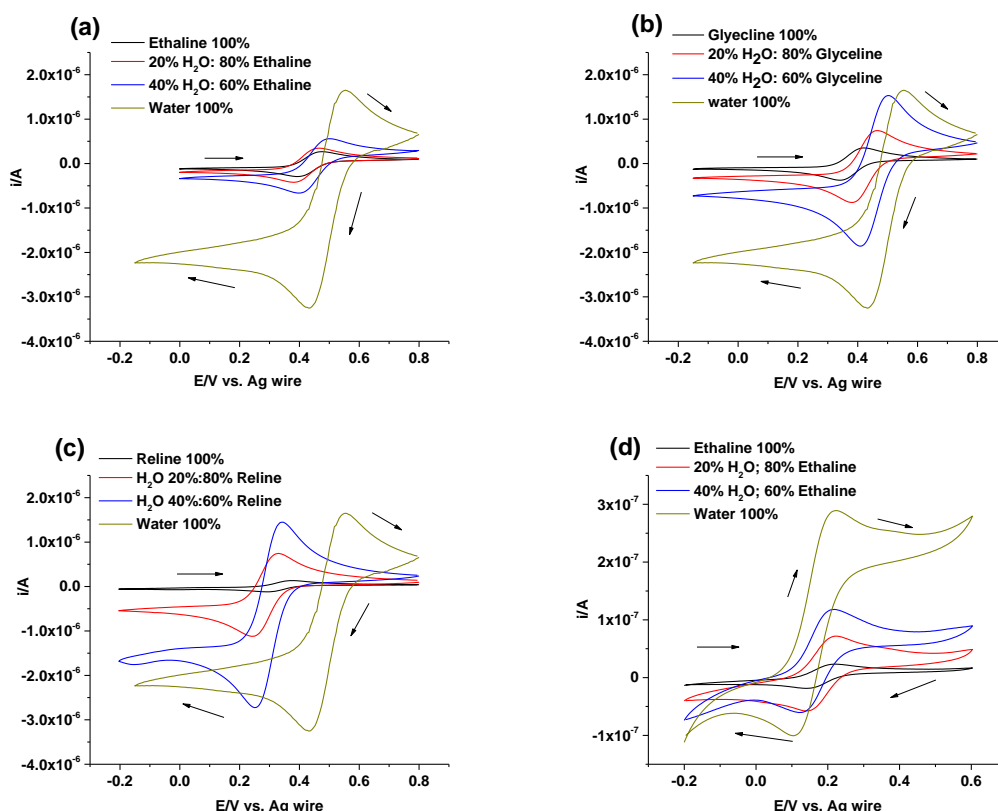


Figure 4.7: Cyclic voltammograms of $0.02 \text{ mol dm}^{-3} \text{FeCl}_3$ in three systems: (a) Ethaline, (b) Glyceline and (c) Reline, both and with different proportions of water; (d) shows $0.002 \text{ mol dm}^{-3}$ potassium ferrocyanide in Ethaline, both pure and with different amounts of water.

The oxidation current to reduction current ratio, $i_{p,a}/i_{p,c}$, and E_p for the data in **Figure 4.7** for pure DESs and water-DES mixtures are shown in **Table 4.1**.

Table 4.1: $i_{p,a}/i_{p,c}$ and E_p the difference in redox potential of three DESs with different water content for FeCl_3 and $\text{K}_4\text{Fe}(\text{CN})_6 \cdot 3\text{H}_2\text{O}$ solutions.

System FeCl_3	Water content /wt%	$E_{p,c}$ /V	$i_{p,a}/i_{p,c}$
Ethaline	0%	0.47	1.01
	20%	0.46	1.00
	40%	0.49	1.02
	100%	0.55	1.06
Glyceline	0%	0.42	1.03
	20%	0.46	1.03
	40%	0.50	1.03
Reline	0%	0.37	1.07
	20%	0.32	1.02
	40%	0.34	1.01
$\text{K}_4\text{Fe}(\text{CN})_6 \cdot 3\text{H}_2\text{O}$ in Ethaline	0%	0.22	1.04
	20%	0.22	1.01
	40%	0.21	1.03
	100%	0.22	1.02

It is clear from the results that the electrochemical behaviour of FeCl_3 and $\text{K}_4\text{Fe}(\text{CN})_6 \cdot 3\text{H}_2\text{O}$ is largely that of reversible systems.

The shift in the redox potential in iron chloride compared with that of potassium ferrocyanide is due here to the change in the speciation of iron chloride in the DES-water mixture. However, this change does not occur with the potassium ferrocyanide in Ethaline system, as was clear from the associated E_p values. There was no shift for potassium ferrocyanide due to cyanide being a strong ligand; it cannot be replaced by the hydroxyl group from water that would otherwise have the effect of keeping the redox potential essentially unchanged. However, for the other three liquids it is clear that there is a shift to more positive values with the increased amount of water in iron chloride in the three DESs.

The phenomena that occur between two electrolyte solutions of different compositions that come in contact with each other is called the liquid junction potential (LJP). To put this more clearly, the difference in the ion activities of two electrolytes generates an LJP. Several reports have shown the error in the electrochemical methods was caused by the LJP.³⁷ Several reports have shown that the use of Ag or Pt wires as pseudo-reference

electrodes by directly immersing them into DESs rather than using Ag/AgCl.³⁸⁻⁴⁰ In our study an Ag pseudo-reference electrode was used as the reference electrode to reduce the effect of the liquid junction potential formed when using Ag/AgCl.

The Randles-Sevcik, **Equation (4.3)**, can be applied to calculate the diffusion coefficients using the results of cyclic voltammetry for the 0.02 mol dm⁻³ FeCl₃ in the three DESs and 0.002 mol dm⁻³ K₄Fe(CN)₆·3H₂O in Ethaline (note the lower concentration with potassium ferricyanide due to lower solubility).

$$i_p = 269,000 n^{3/2} AD^{1/2} C v^{1/2} \quad \text{Equation (4.3)}$$

Where i_p is the peak current, n is the number of electrons involved in the reduction process, A is the area of the electrode surface, D is the diffusion coefficient, c is the concentration of species in solution and v is the voltage scan rate. **Figure 4.8** shows the correlation between the peak current and the square root of the sweep rate as a test of **Equation (4.3)**. A clear linear correlation is observed in pure DESs and DES-water mixtures.

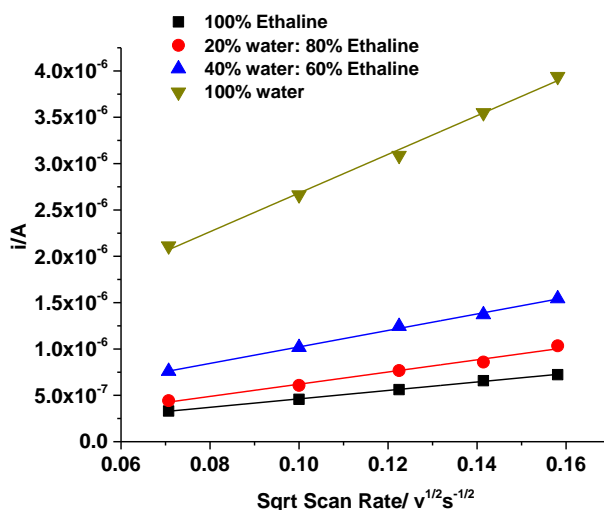


Figure 4.8: Plot of oxidation peak currents versus the square root of sweep rate for 0.02 mol dm⁻³ FeCl₃ in pure Ethaline, pure water and Ethaline with different water content.

The gradients of the plots in **Figure 4.8** can be used to determine the diffusion coefficient. As an example, the diffusion coefficient of iron chloride in Ethaline at 25°C was

$1.859 \times 10^{-7} \text{ cm}^2 \text{ s}^{-1}$. A plot of the diffusion coefficient versus water content is shown in **Figure 4.9** for iron chloride in Ethaline, Glyceline and Reline, as well as for the potassium ferrocyanide in Ethaline system. It is clear from the results that there is an increased rate of diffusion for iron chloride when the amount of water was increased in each of the systems.⁴¹ In addition, 20 wt% water represents a critical point; it is clear from the results that diffusion increased significantly after this amount. Diffusion of both iron chloride and potassium ferrocyanide in Ethaline showed the same trend. However, the diffusion of iron chloride in both Glyceline and Reline is different. This is most likely because Glyceline and Reline mixtures with water are more heterogeneous than Ethaline, as mentioned in chapter three. This suggests that iron chloride and potassium ferricyanide diffuse in a more ionic phase rather than a water dominated phase in Ethaline. However, in Reline and Glyceline, the iron species moves from the ionic phase to the aqueous phase when more than 20 wt% water is present in the mixture.

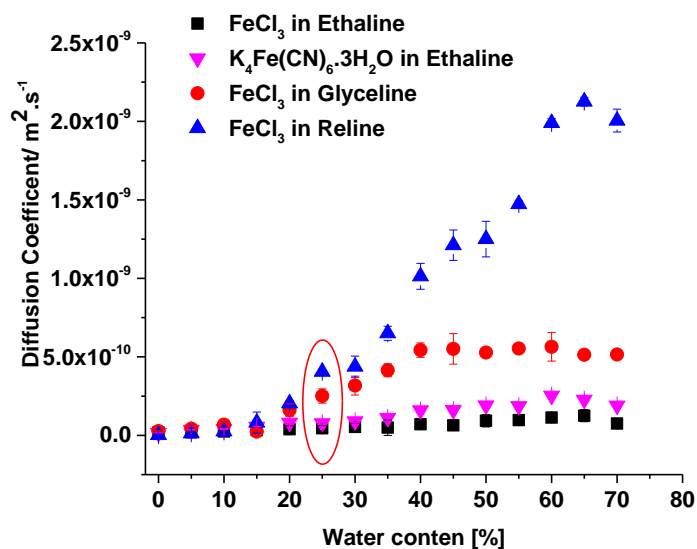


Figure 4.9: Diffusion coefficient of FeCl₃ in Ethaline, Glyceline and Reline and K₄Fe(CN)₆ in Ethaline system as a function of water content. Error bars indicate one standard deviation.

Previous studies have illustrated the diffusion coefficient for [C₄mim][CF₃SO₂]₂N with water. The results showed the diffusion coefficient for water was higher than expected.¹⁵

A plot of diffusion coefficient versus fluidity (viscosity⁻¹) should produce a linear plot if the medium through which the species is diffusing is homogeneous in accordance with the Stokes–Einstein **Equation (4.4)**.

$$D = kT / 6\pi\eta r$$

Equation (4.4)

Figure 4.10 shows plots of diffusion coefficient versus fluidity for FeCl_3 in three DESs and a $\text{K}_4\text{Fe}(\text{CN})_6 \cdot 3\text{H}_2\text{O}$ in Ethaline system. If there is a linear relationship between diffusion coefficient and fluidity, this means the system will obey the Stokes-Einstein Equation. The results indicate that for all systems, diffusion in DESs as a function of water content is non-Stokesian. There could be several reasons for this, e.g., the change from diffusion governed by holes in the pure DES to more classical diffusion in the water mixture, or it could result from a change in the hydrodynamic radius of ferric chloride.

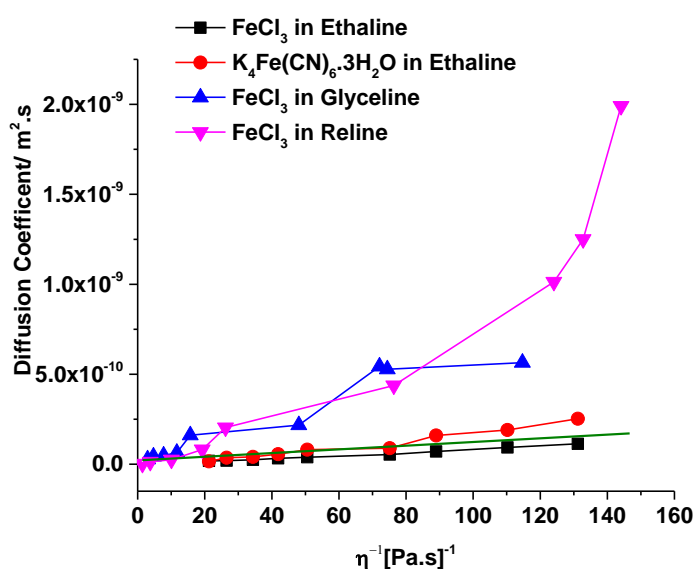


Figure 4.10: Diffusion coefficients of iron chloride in different systems (Ethaline, Glyceline, Reline and potassium ferrocyanide in Ethaline) versus fluidity. The solid green line shows expected Stokesian behaviour.

As discussed above for the self-diffusion coefficients, the most probable cause for the non-Stokesian behaviour is that the medium is non-homogeneous. **Figure 4.4(c)** shows the highest self-diffusion coefficient for water is in Reline which was similar but slightly higher than Glyceline, followed by Ethaline. This is the same order as that seen in **Figure 4.10**. This seems to suggest that either ferric chloride partitions more into the water phase in Reline than Ethaline or that the water phases are larger and more heterogeneous in Reline than Ethaline. Dynamic light scattering experiments in chapter three showed that while the water droplets were somewhat larger in Ethaline at low water contents than in Reline or Glyceline at higher water contents the dispersed phase (which, above 20 wt%,

is almost certainly DES) is about the same size. This would tend to suggest a change in the partition of ferric chloride.

4.6 UV-Vis spectroscopy.

To investigate the behaviour of ferric chloride in the different DES-water mixtures, UV-Vis spectroscopy was used to probe solute speciation. Previous research has established that in aqueous solution, iron chloride forms a variety of series with differing numbers of water and chloride ligands in acidic chloride media, for example, $[\text{Fe}\cdot 6\text{H}_2\text{O}]^{3+}$, $[\text{FeCl}\cdot 5\text{H}_2\text{O}]^{2+}$, $[\text{FeCl}_2\cdot 4\text{H}_2\text{O}]^+$, $[\text{FeCl}_3\cdot 3\text{H}_2\text{O}]$, and $[\text{FeCl}_4\cdot 2\text{H}_2\text{O}]^-$, depending on the chloride concentrations and solution conditions. In addition, with an increased concentration of chloride, this can lead to an increased intensity of the UV-Vis peaks in aqueous solutions of iron chloride⁴²⁻⁴⁴ **Figure 4.11** shows the UV-Vis absorption spectra for FeCl_3 in the Ethaline and Glyceline systems and their mixtures with different amounts of water. Each spectrum consists of two parts: the region between 200-500 nm (UV-Visible) contains charge-transfer bands. The second part is between 600-1000 nm (visible-near IR) which contains metal-based *d-d* transitions.

A strong peak was observed at 241 nm for iron chloride in pure Ethaline solution with a molar absorptivity of $8770 \text{ L cm}^{-1} \text{ mol}^{-1}$. Also, two peaks associated with iron chloride appeared at 313 nm, with a molar absorptivity of $8384 \text{ L cm}^{-1} \text{ mol}^{-1}$, and 359 nm, with a molar absorptivity of $5580 \text{ L cm}^{-1} \text{ mol}^{-1}$. According to previous studies, peaks appearing between 249-367 nm are related to $[\text{FeCl}_4]^-$.³⁶ In terms of this work, for iron chloride in Ethaline without water there can only be three species; these results are similar to previous studies of iron chloride, which gave three peaks in organic media.⁴² The first and second peaks at 241 nm and at 313 nm might be related to $[\text{FeCl}_4]^-$. The third peak at 359 nm is related $[\text{FeCl}_4]^{2-}$. An EXAFS study by Hartley studied this system and showed some evidence for $[\text{FeCl}_4]^-$ but there was also some evidence for an oxygen ligand being involved, which was possibly from an ethylene glycol being bound to the metal centre.

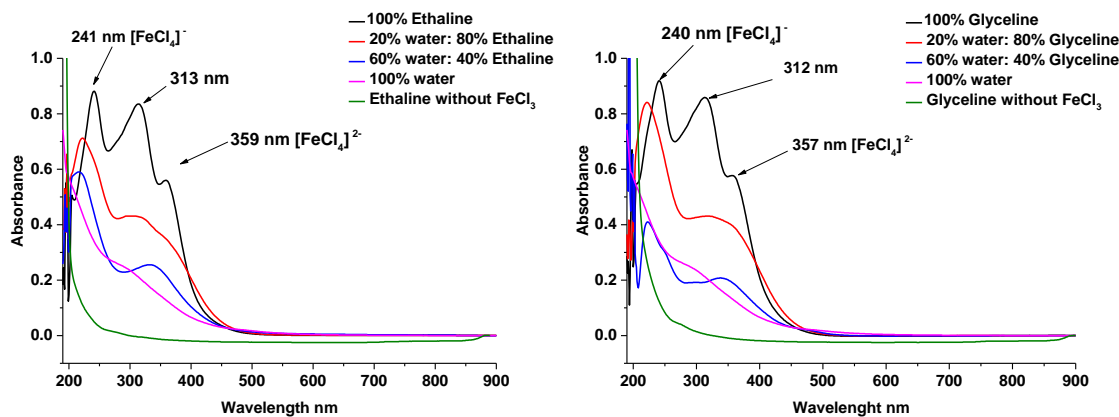


Figure 4.11: UV-Vis spectrum of 1×10^{-4} mol dm^{-3} FeCl_3 in pure Ethaline and Glyceline and their mixtures with different amounts of water (20 wt%, 60 wt% and 100 wt%).

It is important to note that the UV-Vis spectra for the other two DESs also have absorbance peaks at similar wavelengths so if there is mixed speciation, it does not significantly affect the absorbance spectra. However, when 20 wt% of water was added to the iron chloride-Ethaline mixture, the peak intensity decreased with an increasing amount of water, and furthermore the peaks shifted towards lower wavelengths and became less intense.

This discrepancy could be attributed to a change in the coordination of the iron cation in DES-water mixtures. In addition, the third peak at 359 nm decreased more markedly in magnitude, and ultimately almost disappeared in pure water.⁴⁵ In pure water, there was just one shoulder at about 320 nm which is known to be due to $[\text{Fe}(\text{H}_2\text{O})_6]\text{Cl}_3$. This tends to suggest that the speciation changes as water is added but interestingly the speciation seems unrelated to the HBD so the equilibria are governed solely by the relative water and chloride concentrations, which is logical.

An unusual observation arose when measuring the UV-Vis spectra for FeCl_3 in Reline. At the usual concentration of 1×10^{-3} mol dm^{-3} . A separate orange coloured phase formed. This continued to be biphasic up to a concentration of 0.01 mol dm^{-3} when the concentration was raised to 0.02 mol dm^{-3} the systems became monophasic. It was interesting that the FeCl_3 partitioned into the ionic phase rather than the less dense water phase. This phase change is depicted pictorially in **Figure 4.10**.

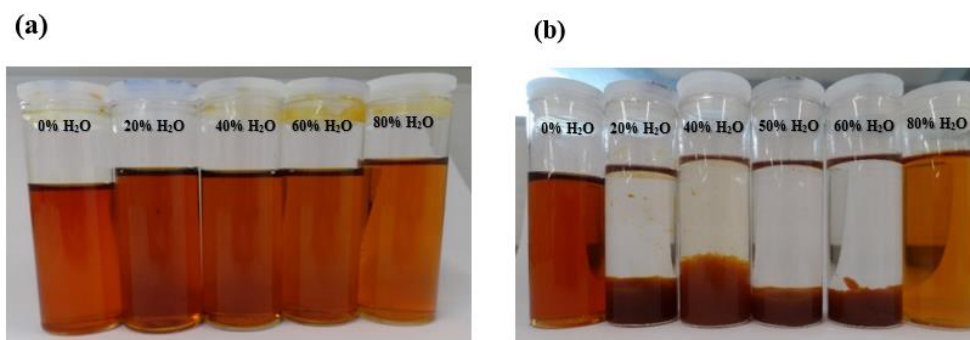


Figure 4.12: (a) Images of iron chloride 0.02 mol dm^{-3} in pure Reline and Reline with various amount of water, (b) as (a) but with an iron chloride concentration of 0.01 mol dm^{-3} .

In all cases, the volume of the lower phase does not appear to change which suggests that some type of chathrate (super-saturated phase) is formed. The separation of liquids into two phases arise from chathrate formation. A chathrate is a complex that forms at a specific molar ratio of two components. If one component has a significantly larger density it can settle to the bottom of the container as a separate phase. In the ionic liquid system, the chathrate phenomenon occurs due to associative interactions between aromatic molecules and salt ions which separate cation–anion packing interactions to a sufficient degree that localized cage-structures are formed. In addition, if there is a strong ion–ion interaction, crystallization of the salt occurs. The classic example of this is $[\text{C}_1\text{mim}][\text{PF}_6]$, $[\text{C}_2\text{mim}][\text{PF}_6]$ and $[\text{C}_4\text{mim}]\text{Cl}$ and an organic solvent such as benzene.⁴⁶ In this study, the chathrate phenomenon formed between FeCl_3 and urea “type 4 DESs” could be due to the difference in density between the aqueous phase, $1.12 \pm 0.02 \text{ g cm}^{-3}$, and the ionic phase, $1.92 \pm 0.03 \text{ g cm}^{-3}$.

Figure 4.12 presents the experimental data on mixing water with Reline at a 20 wt% composition, as two layers were formed. **Figure 4.12(a)** shows 0.02 mol dm^{-3} of iron chloride in pure Ethaline and Ethaline with different amounts of water. **Figure 4.12(b)** illustrates 0.01 mol dm^{-3} iron chloride in pure Ethaline and in an Ethaline with water mixture; it is clear that two layers are formed, namely an upper, aqueous layer and a lower, ionic layer. This could be that due to the change in density of the mixtures with increasing dilution. The phase behaviour and speciation of these metal salts in these systems is very complex and requires further investigation.

Figure 4.13 also shows the behaviour of $2 \times 10^{-5} \text{ mol dm}^{-3} \text{ K}_4\text{Fe}(\text{CN})_6 \cdot 3\text{H}_2\text{O}$ in pure Ethaline and Ethaline-water mixtures. The results reveal that there is one peak at 214.7 nm. Potassium ferrocyanide clearly does not change its speciation in DESs and in DESs with water which would be expected since the cyanide ligand is strong and does not exchange with water in solution. This tends to suggest that since a Stokesian diffusion is seen in **Figure 4.10** for both FeCl_3 and $\text{K}_4\text{Fe}(\text{CN})_6 \cdot 3\text{H}_2\text{O}$ in Ethaline despite the speciation changing for the former and not the latter, that the changes in diffusion with fluidity are not related to speciation differences.

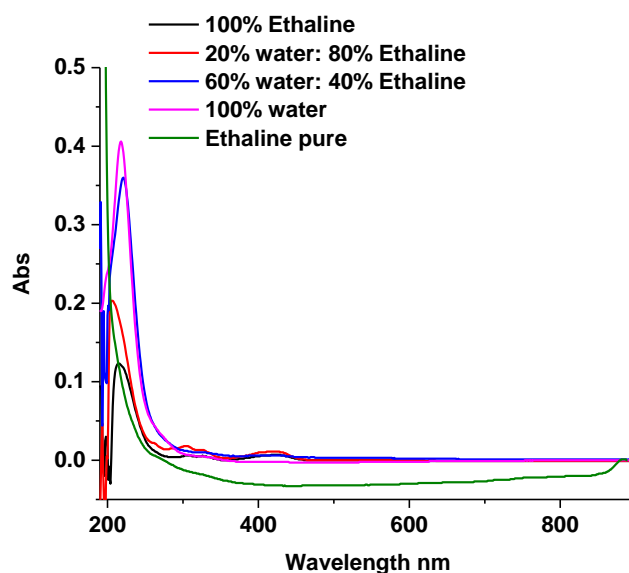


Figure 4.13: UV-Vis spectrum of $2 \times 10^{-5} \text{ mol dm}^{-3} \text{ K}_4\text{Fe}(\text{CN})_6 \cdot 3\text{H}_2\text{O}$ in Ethaline and Ethaline–water mixture.

4.7 Electrical double layer.

The electrostatic interactions which occur between a charged interface and electrolyte result in a so-called double layer.^{47, 48} The structure of this double layer region depends significantly on the type and concentration of the ions and the type of solvent. In a classical aqueous electrolyte, the electrical double layer can be divided into two distinct parts; an inner layer that lies very close to the electrode phase (the inner Helmholtz plane (IHP)), which is very thin, approximately 10 \AA , and is highly organised. The composition of the inner Helmholtz plane depends on the composition of the bulk in the solution phase. This layer may also include specific adsorption which depends on the nature of the ions

and the electrode material. Specific adsorption may occur through covalent bond formation.⁴⁹ Another possibility to the forces of interaction between the ions and surface of electrode is electrical image energy⁵⁰ or a type of “ionic solvation”.⁵¹ The excess charge density, q^m , on the surface of the electrode can be described in two ways. Firstly, if the charge of the electrode is lower than zero, $q^m < 0$, this reveals that there is an excess of electrons. Secondly, if the electrode surface charge is higher than zero, $q^m > 0$, this suggests that there is a deficiency of electrons. In general, the inner Helmholtz layer contains solvent molecules and specifically adsorbed ions which are not hydrated within the aqueous solution, such as I^- and Br^- .^{47, 51, 52}

The second layer is the outer Helmholtz plane (OHP), which is the plane which passes through the electrical centres of solvated ions at a minimum distance from the electrode surface. In this plane, the interaction between solvated ions and electrode phase is one of coulombic forces. Most the electrode charge (typically 90 wt%) is neutralised by the OHP. What residual charge remains is neutralised by the diffuse layer which is a slightly more concentrated electrolyte solution than that of the bulk. This diffuse layer is typically 1-10 nm in thickness. **Figure 4.14** shows a model of electrical double layer for an aqueous electrolyte solution.

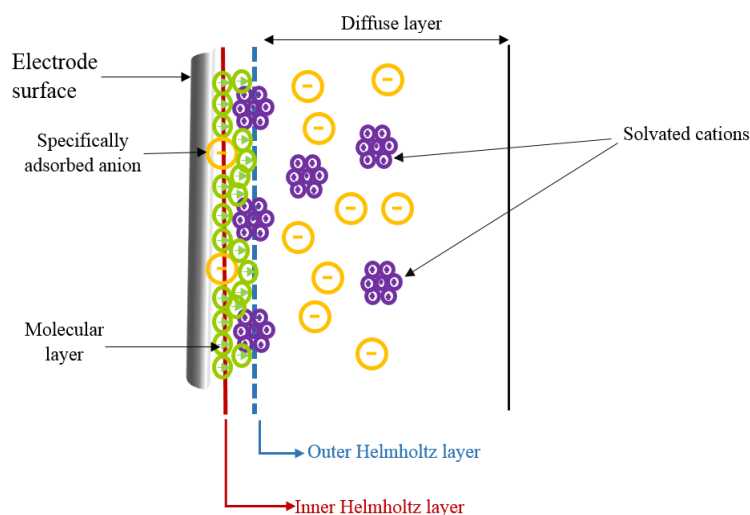


Figure 4.14: The electrical double layer model.

The double layer for ionic liquids and deep eutectic solvents has also been studied by several groups. Prior studies have noted the importance of the influence of anions and cations on the double layer structure of ionic liquids and deep eutectic solvents. For example, using $[F_3CSO_2]_2$ and $[BF_4]^-$ -based ionic liquids showed the presence of

alternating anionic and cationic layers close to the electrode surface. In addition, the double layer capacitance for ionic liquids is smaller and somewhat different from aqueous solution, which could be due to the presence of ion pairs at the electrode surface at different potentials although the main difference between ionic liquids and aqueous solution is the size of the ions. This factor is important when studying the mechanism of nucleation and growth for metal deposition in ionic liquids. Ionic radii are typically between 1 and 2 Å for metal ions in aqueous solution; however, typical cations for ionic liquids are between 3 and 5 Å. As a result, the thickness of the electrode layer in ionic liquids is typically 6-7 Å.⁵³

Atkin *et al.* studied the double layer using scanning probe microscopy. The force required to bring an atomically sharp probe close to the electrode surface increased significantly in a number of steps in an ionic liquid. The size of these steps corresponded to the dimensions of the ions of the ionic liquid. From this, it was concluded that organised and alternating ionic layers occurred at the electrode-ionic liquid interface. These layers could be 4-8 ions thick depending on the type of ion used. Atkin also studied DESs and found that, unlike ionic liquids, there appeared to be only one or two molecular layers thick and it was concluded that the HBD and anion were specifically adsorbed to the electrode. In addition, their study argues as to the effect of a trace amount of water on the double layer. They found the concentration of water in near surface layers was similar to that in the bulk layer.⁵⁴

Empirical results from the Abbott group have found that the electrochemical response in water DES mixtures can change significantly with a critical concentration of water changing the electrode solution interface from ionic to aqueous. To probe this, it was decided to study the iodide/iodine (I⁻/I₂) redox couple as the reduced form is hydrophilic and the oxidised form is hydrophobic. The mechanism of formation of I⁻/I₃⁻/I₂ occurs over two steps, as per **Equation (4.5)** and **Equation (4.6)**.



There is totally different behaviour between I⁻, which is a nucleophile, and I₂, which is an electrophile.⁵⁵ It is useful to understand the phase changes when water is added to the

system. According to previous studies, when iodine is dissolved in different media, a small layer is formed between the surface of the electrode and the electrolyte solution. There are three assumptions required to understand the behaviour of iodine on the surface of the electrode; firstly, there is a complex formed with the products of triiodide and free iodine. Secondly, the amount of iodine formed depends on the amount of iodine dissolved in the supporting electrolyte. Finally, there is an equilibrium between three species $I^-/I_2/I_3^-$.⁵⁶

Sodium iodide and iodine were used as probes to understand the double layer and phase changes in DES-water mixtures. In this section, a series of DES-water solutions of NaI (0 wt%-100 wt%) and (0 wt%-50 wt%) for I_2 were prepared.

Cyclic voltammograms of 0.1 mol dm⁻³ sodium iodide and 0.02 mol dm⁻³ iodine were investigated using a 0.5 mm diameter platinum electrode at different scan rates (4, 5, 8 and 10 mVs⁻¹) in DESs and DES-water mixtures at room temperature. In the pure DESs, two well-defined electrochemically reversible redox peaks could be observed for both NaI and I_2 . There are two possible explanations for this: firstly, the first peak is related to the electrochemical reduction of iodine to iodide to form triiodide. The dissociation of triiodide can give iodide which clearly appears as the second peak;⁵⁷ this suggestion is illustrated in **Equation (4.7)** and **Equation (4.8)**.



Secondly, there is a polyanion species (I_3^- , I_2Cl^- , ICl_2^- , etc.) that leads to the formation of iodine^{55, 58}; this will be discussed in more detail when considering the associated UV-Vis spectra. **Figure 4.15(a)** and **(b)** shows the cyclic voltammograms obtained from NaI and I_2 in solutions of different water content.

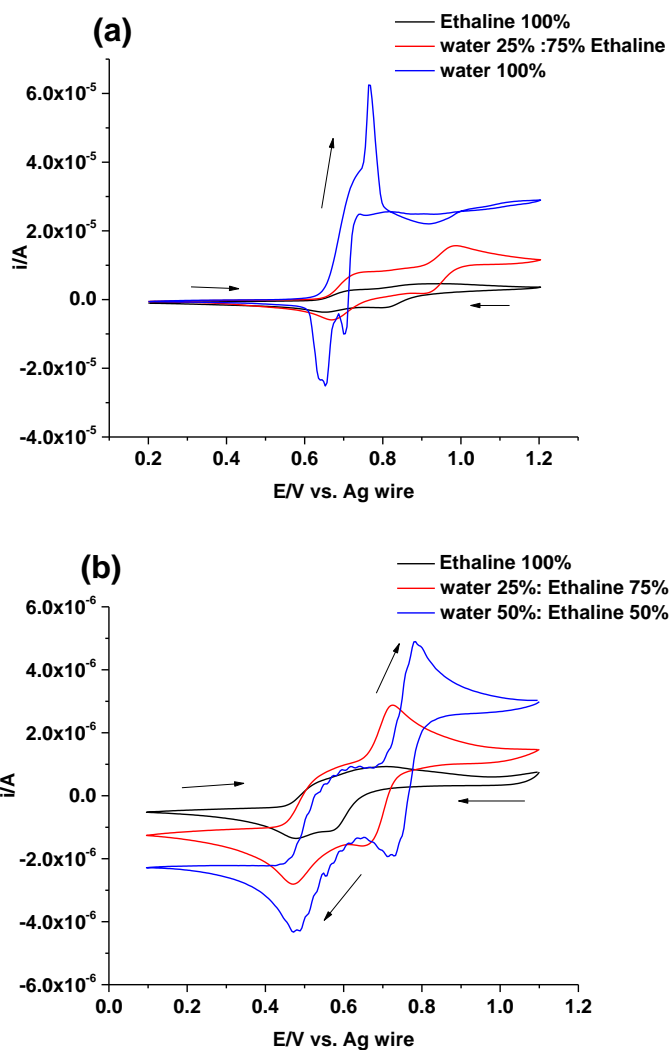


Figure 4.15: Cyclic voltammograms of (a) $0.1 \text{ mol dm}^{-3} \text{NaI}$ and (b) $0.02 \text{ mol. dm}^{-3} \text{I}_2$ in Ethaline with different water contents.

As the water content increases, the peak current of both oxidative processes also increases. Iodine dissolves in water-DES mixtures due to the formation of I_2Cl^- . Iodine is uncharged and has no dipole moment and so dissolution in water is poor as the solvation enthalpy is low. The presence of a halide anion leads to the formation of the trihalide anion either I_3^- or I_2Cl^- . This will be ionic and so have a larger solvation enthalpy, as shown in chapter three.

The diffusion coefficients have been studied here by applying the Randles-Sevcik equation, the results of which show a similar magnitude to that obtained in a previous study.⁵⁸ The peak currents were obtained by running background CVs with no electroactive species and subtracting the capacitive current from the peak to peak current in **Figure 4.15** then dividing the current by 2. **Table 4.2** and **Figure 4.16** show the

diffusion coefficient for NaI with different water content from 0 wt% to 35 wt%. The first diffusion coefficient is that for the oxidation of I_2 to I_3^- as shown in **Equation (4.7)** and the second is for the oxidation I_3^- to I^- . It is clear that for water content below 10 wt%, both ions have approximately the same value of diffusion coefficient. However, with increasing water content above 10 wt%, the diffusion coefficient for the I_3^- does not rise as rapidly as that for I^- . I^- is more likely to partition into the water-rich phase which will mean it has a higher diffusion coefficient than I_3^- .⁵⁹

Table 4.2: I_3^-/I^- diffusion coefficient in Ethaline system. Uncertainties are to one standard deviation.

water content %	Diffusion coefficient m^2/s			
	Peak 1 (I_3^-)	SD	Peak 2 (I^-)	SD
0	7.82×10^{-12}	1.5×10^{-13}	5.81×10^{-11}	1.61×10^{-12}
5	2.01×10^{-11}	4.67×10^{-12}	2.12×10^{-11}	8.92×10^{-12}
10	2.98×10^{-11}	8.75×10^{-12}	2.54×10^{-11}	1.16×10^{-11}
15	4.95×10^{-11}	3.11×10^{-12}	8.26×10^{-11}	7.91×10^{-12}
20	1.68×10^{-10}	8.50×10^{-12}	3.69×10^{-11}	9.23×10^{-12}
25	1.92×10^{-10}	4.61×10^{-12}	4.31×10^{-11}	6.46×10^{-12}
30	2.36×10^{-10}	3.45×10^{-12}	4.71×10^{-11}	5.97×10^{-12}
35	2.81×10^{-10}	5.91×10^{-12}	6.21×10^{-11}	1.10×10^{-11}

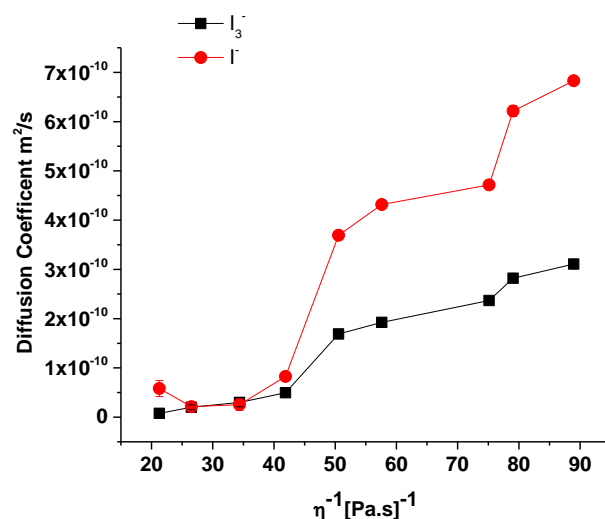


Figure 4.16: Diffusion coefficient of I_3^-/I^- versus fluidity in Ethaline system. Error bars indicate one standard deviation.

Figure 4.17 shows the cyclic voltammograms for 0.1 mol dm⁻³ sodium iodide in 25 wt% water: 75 wt% Ethaline (black colour) and 40 wt% water: 60 wt% Ethaline (red colour) at a scan rate of 4 mVs⁻¹. It can be seen that the electrochemical response changes for the two compositions with the second peak becoming much sharper with an increased amount of water in the mixture. It is also clear that with cycling the solution becomes red in colour rather than black. This could be due to the formation of solid iodine on the surface of electrode, which decreases the number of iodide ions in solution.

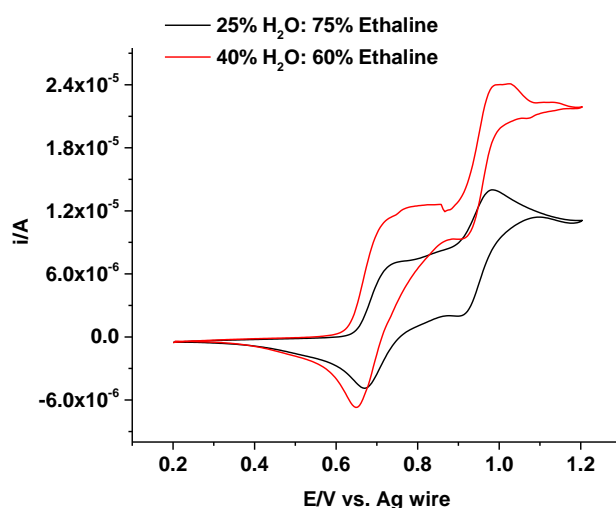


Figure 4.17: Cyclic voltammograms of 0.1 mol dm⁻³ sodium iodide in a 25 wt% water: 60 wt% Ethaline and 40 wt% water-60 wt% Ethaline mixture at 4 mVs⁻¹ scan rate.

This change in electrochemical behaviour from forming a soluble I_2Cl^- in an ionic medium to forming solid I_2 in an aqueous medium can be seen in Error! Reference source not found.(a). The change in voltammogram shape observed in **Figure 4.17** suggests that at some point between 25 wt% and 40 wt% water the double layer changes from being ion dominated to being water dominated. It is interesting to note that even with 25 wt% water, the double layer is still dominated by the DES.

4.8 Double layer capacitance.

There are many factors that can have an effect on the double layer capacitance; for example, electrode potential, temperature, ionic concentrations, types of ions, oxide layers, electrode roughness and impurity adsorption.⁶⁰ Carrying out cyclic voltammetry at a very slow sweep rate in the region where no Faradaic processes occur enables the charging currents to be measured. The double layer capacitance for pure Ethaline and Ethaline with different amounts of water content (varying from 0 wt% - 95 wt%) was determined and are shown in **Figure 4.18**. The double layer capacitance increases as water is added to the DES. This presumably occurs because small water molecules replace the large HBD and some of the large ions in the double layer. There appears to be a larger increase in capacitance above 20 wt% water. Interestingly, the capacitance of the DESs are different from each other at high water content, showing that there must be some HBD incorporated into the structure of the double layer.

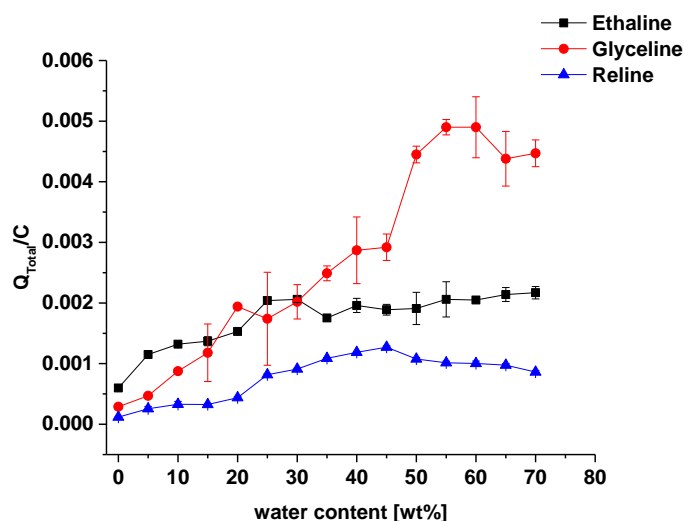


Figure 4.18 : Double layer capacitance calculated from slow sweep rate cyclic voltammograms in three DESs as a function of water content. Error bars indicate one standard deviation.

4.8.1 Iodine speciation with in DES-water mixtures.

UV-Vis spectra for iodine have been recorded to study the kinds of species formed when dissolving I_2 in mixtures of Ethaline with different amounts of water (0, 10, 20, 30, 40 and 100 wt%). **Figure 4.19** shows that there are different peaks for I_2 , I^- and I_3^- , where the kind of peaks formed were dependent on the solvent used. For example, pure Ethaline gave two peaks, the first absorption peak at 408 nm was related to I_2 absorption, whilst the second peak at 224 nm was related to I^- . Conversely, three peaks were observed in Ethaline-water mixtures, the first peaks at 416- 422 nm for I_2 absorption, and the third peaks at 220-223 nm for I^- . The second peak at 257 - 258 nm arose for two possible reasons; recent research has suggested that this peak is related to the formation of I_3^- ,⁶¹ although in these liquids it is most likely to be I_2Cl^- .⁶² As mentioned above in section 4.12.1, the intensity and wavelength of the peaks will be shifted to towards lower wavelength and become less intense with increasing amounts of water in the mixture. The same behaviour has been shown for sodium iodide in DESs mixed with different amounts of water.

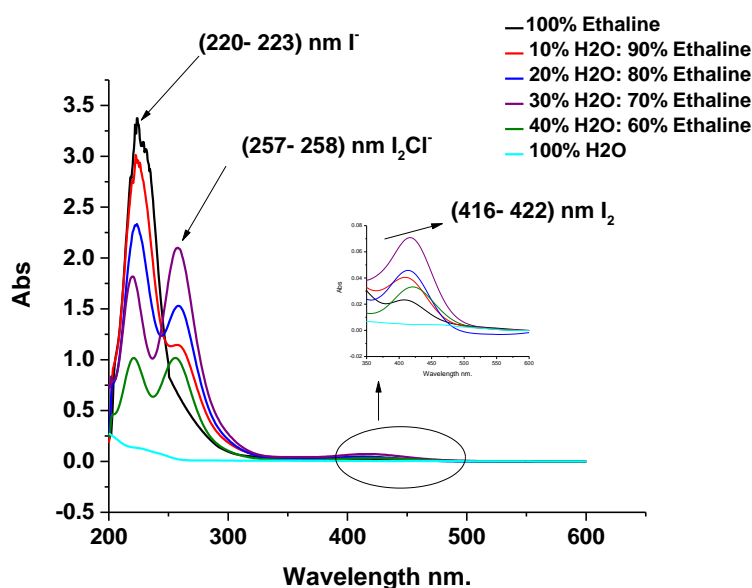


Figure 4.19: UV-Vis spectra of $1 \times 10^{-5} \text{ mol dm}^{-3} I_2$ in pure Ethaline and mixtures of Ethaline with different amounts of water.

4.9 Conclusion.

As previously observed, one issue in dealing with ILs is due to their high viscosities and lower conductivities. In this chapter, it has been shown that water can significantly increase the diffusion coefficients of species in DES-water mixtures. Diffusion studies can be used to provide information about the structure of these liquids. The results of self-diffusion coefficients showed non-Stokesian behaviour for DES-water mixtures, which tells us the medium is non-homogeneous, as suggested in chapter three. This was very clear from the self-diffusion coefficient for the water in Reline system, the self-diffusion coefficient is higher than in Glyceline and Ethaline. Electrochemistry studies showed the same order, and it has been suggested that the ferric chloride partitions more into the water phase in Reline than for Glyceline, and then Ethaline. This gives further evidence that the Reline system is more heterogeneous than the Ethaline system.

The heterogeneity of DES-water mixtures also exists at interfaces. In chapter three, the surface tension showed that the gas liquid interface could become enriched with one component and the same has been demonstrated at the solid-liquid interface. This has significant implications for electrochemical applications of DESs. This has been known empirically within our group for many years, but the extent of the heterogeneity was unknown. In the next chapter, the aim is to demonstrate how this heterogeneity affects the way in which metals nucleate on an electrode surface during electrodeposition.

4.10 References.

1. V. Losetty, B. K. Chennuri and R. L. Gardas, *The Journal of Chemical Thermodynamics*, 2015, **90**, 251-258.
2. E. L. Smith, A. P. Abbott and K. S. Ryder, *Chemical Reviews*, 2014, **114**, 11060-11082.
3. S. Tang, G. A. Baker and H. Zhao, *Chemical Society Reviews*, 2012, **41**, 4030-4066.
4. A. W. Taylor, F. Qiu, J. Hu, P. Licence and D. A. Walsh, *The Journal of Physical Chemistry B*, 2008, **112**, 13292-13299.
5. P. Wachter, C. Schreiner, M. Zistler, D. Gerhard, P. Wasserscheid and H. J. Gores, *Microchimica Acta*, 2008, **160**, 125-133.
6. C. A. Brooks and A. P. Doherty, *Electrochemistry communications*, 2004, **6**, 867-871.
7. D. Kruk, R. Meier, A. Rachocki, A. Korpała, R. Singh and E. Rössler, *The Journal of Chemical Physics*, 2014, **140**, 244509.
8. R. Brookes, A. Davies, G. Ketwaroo and P. A. Madden, *The Journal of Physical Chemistry B*, 2005, **109**, 6485-6490.
9. A. N. Soriano, A. M. Agapito, L. J. L. I. Lagumbay, A. R. Caparanga and M.-H. Li, *Journal of the Taiwan Institute of Chemical Engineers*, 2011, **42**, 258-264.
10. C.-L. Wong, A. N. Soriano and M.-H. Li, *Fluid Phase Equilibria*, 2008, **271**, 43-52.
11. A. Heintz, R. Ludwig and E. Schmidt, *Physical Chemistry Chemical Physics*, 2011, **13**, 3268-3273.
12. G. A. Webb, *Annual Reports on NMR Spectroscopy*, Academic Press, 2017.
13. A. P. Abbott, R. C. Harris, K. S. Ryder, C. D'Agostino, L. F. Gladden and M. D. Mantle, *Green Chemistry*, 2011, **13**, 82.
14. A. W. Taylor, P. Licence and A. P. Abbott, *Physical Chemistry Chemical Physics*, 2011, **13**, 10147-10154.
15. A.-L. Rollet, P. Porion, M. Vaultier, Isabelle Billard, M. Deschamps, C. Bessada and L. Jouvensal, *The Journal of Physical Chemistry B*, 2007, **111**, 11888-11891.
16. D. Kruk, R. Meier, A. Rachocki, A. Korpała, R. K. Singh and E. A. Rossler, *Journal of Chemical Physics*, 2014, **140**, 244509.

17. J. Sangoro, C. Iacob, S. Naumov, R. Valiullin, H. Rexhausen, J. Hunger, R. Buchner, V. Strehmel, J. Kärger and F. Kremer, *Soft Matter*, 2011, **7**, 1678-1681.
18. T. A. Fadeeva, P. Husson, J. A. DeVine, M. F. Costa Gomes, S. G. Greenbaum and E. W. Castner Jr, *The Journal of Chemical Physics*, 2015, **143**, 064503.
19. J. Sangoro, A. Serghei, S. Naumov, P. Galvosas, J. Kärger, C. Wespe, F. Bordusa and F. Kremer, *Physical Review E*, 2008, **77**, 051202.
20. A. Noda, K. Hayamizu and M. Watanabe, *The Journal of Physical Chemistry B*, 2001, **105**, 4603-4610.
21. A. P. Abbott, C. D'Agostino, S. J. Davis, L. Gladden and M. Mantle, *Physical Chemistry Chemical Physics*, 2016, **18**, 25528-25537.
22. C. D'Agostino, R. C. Harris, A. P. Abbott, L. F. Gladden and M. D. Mantle, *Physical Chemistry Chemical Physics*, 2011, **13**, 21383-21391.
23. Y.-H. Hsu, R. B. Leron and M.-H. Li, *The Journal of Chemical Thermodynamics*, 2014, **72**, 94-99.
24. Q. Zeng, Y. Wang, Y. Huang, X. Ding, J. Chen and K. Xu, *Analyst*, 2014, **139**, 2565-2573.
25. R. Esquembre, J. M. Sanz, J. G. Wall, F. del Monte, C. R. Mateo and M. L. Ferrer, *Physical Chemistry Chemical Physics*, 2013, **15**, 11248-11256.
26. A. P. Abbott, E. I. Ahmed, R. C. Harris and K. S. Ryder, *Green Chemistry*, 2014, **16**, 4156-4161.
27. P. J. Hore, Davies, S. G., Compton, R. G., Evans, J., Gladden, L. F., *Nuclear Magnetic Resonance*, Oxford Science Publications, Oxford, UK, 1995.
28. A. P. Abbott, R. C. Harris, K. S. Ryder, C. D'Agostino, L. F. Gladden and M. D. Mantle, *Green Chemistry*, 2011, **13**, 82-90.
29. E. I. Ahmed, PhD Thesis, University of Leicester, 2015.
30. M. Holz, S. R. Heil and A. Sacco, *Physical Chemistry Chemical Physics*, 2000, **2**, 4740-4742.
31. A.-L. Rollet, P. Porion, M. Vaultier, I. Billard, M. Deschamps, C. Bessada and L. Jouvencal, *Journal of Physical Chemistry B*, 2007, **111**, 11888-11891.
32. C. G. Hanke and R. M. Lynden-Bell, *Journal of Physical Chemistry B*, 2003, **107**, 10873-10878.
33. A. A. Torriero, *Electrochemistry in Ionic Liquids.*, Springer, 2015.

34. M. Azam, PhD Thesis, University of Leicester, 2011.
35. M. Yamagata, N. Tachikawa, Y. Katayama and T. Miura, *Electrochimica acta*, 2007, **52**, 3317-3322.
36. Z. Guo, T. Zhang, M. Khan, S. Gao, T. Liu and J. Yu, *Electrochimica Acta*, 2014, **142**, 132-143.
37. A. Yamada, S. Mohri, M. Nakamura and K. Naruse, *Sensors*, 2015, **15**, 7898-7912.
38. U. Schröder, J. D. Wadhawan, R. G. Compton, F. Marken, P. A. Suarez, C. S. Consorti, R. F. de Souza and J. Dupont, *New Journal of Chemistry*, 2000, **24**, 1009-1015.
39. B. Huber and B. Roling, *Electrochimica Acta*, 2011, **56**, 6569-6572.
40. L. Barrosse-Antle, A. Bond, R. Compton, A. O'Mahony, E. Rogers and D. Silvester, *Chemistry—An Asian Journal*, 2010, **5**, 202-230.
41. Y. Gao, S. Han, B. Han, G. Li, D. Shen, Z. Li, J. Du, W. Hou and G. Zhang, *Langmuir*, 2005, **21**, 5681-5684.
42. L. Cui, F. Cheng and J. Zhou, *Industrial & Engineering Chemistry Research*, 2015, **54**, 7534-7542.
43. G. A. Gamlen and D. Jordan, *Journal of the Chemical Society*, 1953, 1435–1443.
44. T. Vander Hoogerstraete, S. Wellens, K. Verachtert and K. Binnemans, *Green Chemistry*, 2013, **15**, 919.
45. P. De Vreese, N. R. Brooks, K. Van Hecke, L. Van Meervelt, E. Matthijs, K. Binnemans and R. Van Deun, *Inorganic Chemistry* 2012, **51**, 4972-4981.
46. J. D. Holbrey, W. M. Reichert, M. Nieuwenhuyzen, O. Sheppard, C. Hardacre and R. D. Rogers, *Chemical Communications*, 2003, 476-477.
47. J. Wang, *Analytical Electrochemistry*, John Wiley & Sons, 2006.
48. F. G. Thomas and G. Henze, *Introduction to Voltammetric Analysis: Theory and Practice*, Csiro Publishing, 2001.
49. D. C. Grahame, *Chemical Reviews*, 1947, **41**, 441-501.
50. S. Levine, G. M. Bell and D. Calvert, *Canadian Journal of Chemistry*, 1962, **40**, 518-538.
51. T. Andersen and J. M. Bockris, *Electrochimica Acta*, 1964, **9**, 347-371.

52. H. B. Mark, *Analyst*, 1990, **115**, 667-678.
53. F. Endres, A. Abbott and D. MacFarlane, *Electrodeposition from Ionic Liquids*, John Wiley & Sons, 2017.
54. Z. Chen, B. McLean, M. Ludwig, R. Stefanovic, G. G. Warr, G. B. Webber, A. J. Page and R. Atkin, *The Journal of Physical Chemistry C*, 2016, **120**, 2225-2233.
55. C. L. Bentley, A. M. Bond, A. F. Hollenkamp, P. J. Mahon and J. Zhang, *Analytical Chemistry*, 2016, **88**, 1915-1921.
56. S. Swathirajan and S. Bruckenstein, *Journal of Electroanalytical Chemistry*, 1981, **125**, 63-71.
57. E. I. Rogers, I. Streeter, L. Aldous, C. Hardacre and R. G. Compton, *The Journal of Physical Chemistry C*, 2008, **112**, 10976–10981.
58. A. Ejigu, K. R. J. Lovelock, P. Licence and D. A. Walsh, *Electrochimica Acta*, 2011, **56**, 10313-10320.
59. C. L. Bentley, A. M. Bond, A. F. Hollenkamp, P. J. Mahon and J. Zhang, *The Journal of Physical Chemistry C*, 2015, **119**, 22392-22403.
60. M. Singh, K. Manoli, A. Tiwari, T. Ligonzo, C. Di Franco, N. Cioffi, G. Palazzo, G. Scamarcio and L. Torsi, *Journal of Materials Chemistry C*, 2017, **5**, 3509-3518.
61. Z. Kebede and S. Lindquist, *Solar Energy Materials and Solar Cells*, 1999, **57**, 259-275.
62. J. M. Hartley, PhD Thesis, University of Leicester, 2013.

Chapter 5: Effect of water on copper electrodeposition in Ethaline.

5	Effect of water on copper electrodeposition in Ethaline.....	134
5.1	Introduction.....	134
5.2	Objective.....	136
5.3	Electrochemistry study.	137
5.3.1	Effect of water on the electrochemical window of Ethaline.....	137
5.3.2	Effect of water on the bulk electrolysis of copper.....	138
5.4	X-Ray diffraction analysis (XRD).....	142
5.5	Cyclic voltammetry.....	144
5.6	Diffusion coefficient in copper-water system.....	152
5.7	Chronoamperometry.	156
5.8	Effect of the anode.....	160
5.9	Conclusion.....	167
5.10	References.....	168

5 Effect of water on copper electrodeposition in Ethaline.

5.1 Introduction.

Copper is an important metal due to its resistance to corrosion, it is a good conductor of heat and electricity, and it is malleable and relatively soft. It has found in use in many systems such as building construction, power generation and transmission, electronic components, heating and cooling devices, telecommunications links, motor components, wiring, radiators, connectors, brakes and bearings.

While electrodeposition of copper in aqueous media is routinely carried out, the associated narrow potential window makes it difficult to deposit metals with larger negative reduction potentials such as Cr and Zn.^{1, 2} Various aqueous electrolytes have been used to deposit copper, for instance acid baths, cyanide baths, alkaline non-cyanide baths and pyrophosphate baths. However, dealing with such baths requires caution due to the high toxicity of the electrolytes. Moreover, the alkaline bath gives rise to other difficulties such as sensitivity to impurities, and chemistries that are difficult to control. These baths are also very sensitive to the concentrations of additives required to obtain a good surface finish.³

An alternative to the use of aqueous media for metal electrodeposition is ionic liquids and DESs. Their wide potential windows, relatively high conductivity compared to non-aqueous solvents, and high solubility of metals salts makes them useful for the electrodeposition of metals such as aluminium.^{1,4} While the electrodeposition of copper using ionic liquids is not necessarily an important technical advance due to the disparity in the cost of the electrolytes, it is a useful model system as it gives a different deposit morphology when deposited from water as compared to from an ionic liquid. Mixtures of the two liquids should provide information about the causes of these morphological differences.

Previous studies have focussed on kinetic factors, nucleation mechanism and the crystalline structure of electrodeposited copper.^{5,6} Several reports have shown that the behaviour of $\text{Cu}^{2+/+}$ is reversible in aluminium chloride-*N*-methylpyridinium chloride acidic RTIL.⁷ However, the use of butylpyridinium chloride-aluminium chloride in 1-ethyl-3-methylimidazolium tetrafluoroborate RTIL containing excess 1-ethyl-3-

methylimidazolium chloride shows quasi-reversible behaviour for $\text{Cu}^{2+/+}$,^{8, 9} while the $\text{Cu}^{2+/+}$ redox couple exhibits irreversible behaviour in a binary mixture of ionic liquid/organic solvent (tri-n-octylmethylammonium chloride (TOMAC))/chloroform (CHCl_3).¹⁰ There are several ionic liquids have been used to electroplate of Cu; however, the cost and toxicity of the liquids has meant that none of them are practically viable.^{8,9,11-14}

Abbott and co-workers have used DESs rather than ionic liquids to deposit metals.^{15, 16} There are several reasons to use DESs instead of ionic liquids in electrochemistry; for example, DESs are typically, less expensive, more synthetically accessible, nontoxic, biodegradable and easy to prepare. In addition, DESs are green solvents due to there being no waste in the process of preparation and the lack of any need for purification.¹⁷ Moreover, DESs includes a variety of abundant cellular constituents for example, fructose, sugars, alcohols and amino acids, which have low inherent toxicity. Furthermore, both choline chloride and hydrogen bond donors such as ethylene glycol are non-harmful to the environment, and both are readily biodegradable, with the resultant DES also readily biodegradable.^{18, 19} Popescu *et al.* argued that the use of choline chloride as a base varies depending on the hydrogen bonding, such as with ethylene glycol, malonic acid, oxalic acid and urea, to deposit copper. Their results showed that both liquids, ChCl: ethylene glycol and ChCl: oxalic acid, gave the best homogeneous and adherent copper deposits compared to other liquids.²⁰ Lloyd *et al.* used DESs to study the electron transfer kinetics of the $\text{Cu}^+/\text{Cu}^{2+}$ redox couple. They used cyclic voltammetry, chronoamperometry and impedance spectroscopy, and proposed that there two species formed in ChCl: ethylene glycol-based ionic liquids, namely $[\text{CuCl}_3]^{2-}$ and $[\text{CuCl}_4]^{2-}$. They also reported that $\text{Cu}^+/\text{Cu}^{2+}$ redox couple was only quasi-reversible.²¹

Abbott and McKenzie summarised the parameters that can influence deposition characteristics, for example, temperature, cation, anion, electrolyse, metal salts, hydrogen bond donor, diluents, anode material, brighteners, pre-treatment protocols, and complexing agents.¹ The mechanisms of electrodeposition of metals have been investigated a number of authors.²² In general, the electrodeposition process occurs by the crystallization of metal at the surface of the substrate. Briefly, the method starts with the reduction of metal ions at the surface which help to form metal atoms, “adatoms”, on the surface of substrate. If the interaction energy between the atoms of surface and the

adatom is not adequate to keep the adatom attached to the surface, the adatom will dissolve again. However, the adatom is stabilized on the substrate by specific sites such as imperfections in the crystal lattice of the substrate. These specific sites are called “kink sites”, and it is important to note here the step dislocations as per **Figure 5.1**. A stable nucleus can be formed after the conjunction of the adatoms in a kink site followed by growth of a nucleus. Hence, this leads to the formation of a metal crystal.²²

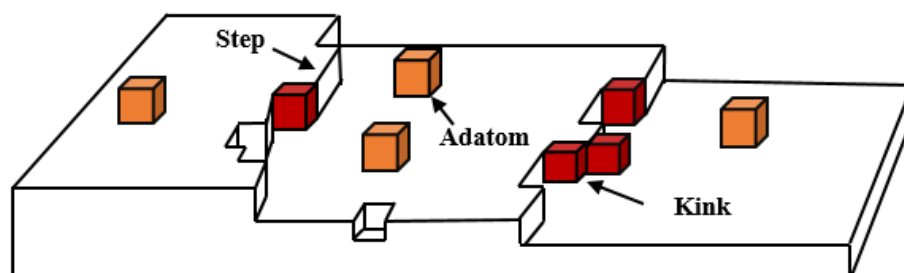


Figure 5.1: An illustration of stabilisation of adatoms at kink sites.²³

The implications for this project are that the energy of adsorption sites will depend critically on the liquid state species which are in contact with the surface. When the surface is charged then ions in the electrolyte will neutralise the surface charge and structure will arise in the first 1 - 20 molecular dimensions from the electrode-solution interface. The neutralisation of the charge will depend on the size and charge of the ions in the electrolyte. Water can also play a crucial role in the structure at the electrode-electrolyte interface since it has a large dipole moment and can thus strongly solvate ions and interact with charged surfaces.

5.2 Objective.

The main objective of this chapter is to quantify and explain some unusual observations with metal electrodeposition that have been seen within the group. It has been found that a small amount of water added to a DES has a significant effect on the deposit morphology. It has also been proposed that the anodic reaction in DESs can significantly influence the cathodic reaction, and finally it was shown with aluminium deposition that the presence of group I metals salts can also have a significant effect on deposit morphology.

To investigate these parameters, it was chosen to use copper as a test metal and to deposit it from $\text{CuCl}_2 \cdot 2\text{H}_2\text{O}$ in DES-water mixtures. This system has been studied previously and is interesting as it has the internal $\text{Cu}^{\text{II}}/\text{Cu}^{\text{I}}$ couple which can be used to study mass transport. The intention was to investigate if mixing DESs with water changes the morphology of the copper deposit and to try to quantify the effects of water on mass transport, the double layer structure and speciation. The effect of added NaCl was also studied. Finally, it has been shown that the rates of anodic dissolution processes can be very slow in DESs and so deposition was carried out using exactly the same conditions but using two types of anode material; a copper sheet and an iridium oxide-coated titanium mesh.

5.3 Electrochemistry study.

5.3.1 Effect of water on the electrochemical window of Ethaline.

Several reports have shown that influence of water on electrochemical window of ionic liquids and DESs.²⁴⁻²⁶ Du *et al.* investigated the influence of water on the electrochemical window of Reline. Their results showed that the anodic potential moved to more negative values, 1.40 V to 1.22 V, with increased amounts of water up to 6 wt%, and the cathodic potential moved to more positive values from -1.10 V to -0.23 V, thus decreasing the electrochemical window from 2.50 V to 1.45 V.²⁷

The electrochemical window for Ethaline was measured with different amounts of water and in pure water with 0.1 mol dm^{-3} choline chloride using a three electrode cell, a platinum working electrode, a platinum flag counter electrode and an Ag wire reference electrode at room temperature. **Figure 5.2** shows the effect of water on the electrochemical window of the different solutions. The results indicate there is no significant decrease in the potential window when water is added, showing that choline is dominating the double-layer structure. However, in pure water (olive-coloured line) with 0.1 mol dm^{-3} choline chloride the electrochemical window decreased to about 2 V. It is also clear that there are some adsorptive processes occurring (**Figure 5.2** (insert)) means the electrolyte changes the behaviour of solution, which is a very important finding as it shows the choline chloride is very surface active; this result confirms Atkin *et al.*'s study which showed that the surface of an electrode is rich in molecular components, and the choline cation is attracted to a surface with a negative potential.²⁸

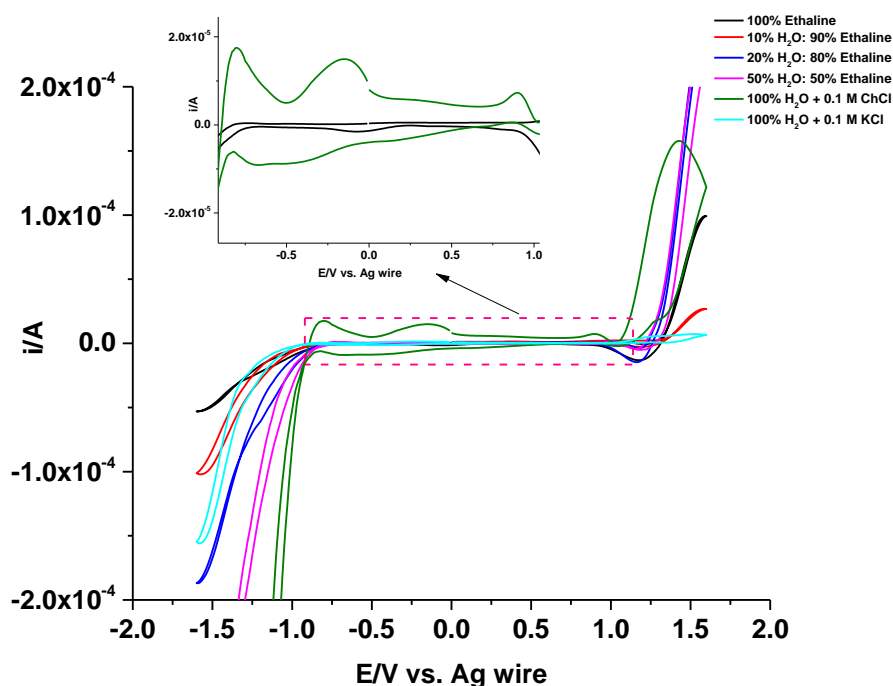


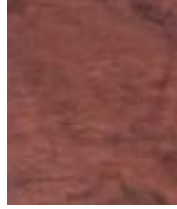
Figure 5.2: Potential window for different Ethaline-water mixtures on a Pt electrode.

5.3.2 Effect of water on the bulk electrolysis of copper.

To demonstrate the effect of water on the electrodeposition of copper in mixed Ethaline-water systems, bulk electrolysis was carried out under the same conditions, namely $0.1 \text{ mol kg}^{-1} \text{ CuCl}_2 \cdot 2\text{H}_2\text{O}$ in Ethaline-water mixtures. All experiments were performed for 1 h at 35°C and at a current density of 50 mA cm^{-2} on a Ni substrate. Experiments were carried out with either a copper anode or an iridium oxide-coated titanium mesh anode. **Table 5.1** clearly shows that water has an effect on the appearance of the copper deposit. In the absence of water, a dull, red-orange deposit is obtained. This increases in brightness up to 20 wt% water but becomes dull brown when 100 wt% water is used with ChCl. This confirms the qualitative observations seen earlier in our group, but which have not as yet been reported in the literature.

Table 5.2 shows the SEM images of the same samples shown in **Table 5.1**. It can be seen that the copper crystallites are very small in pure Ethaline but very large in pure water. The addition of 10 wt% and 20 wt% do not significantly affect the grain structure. This could be due to changes in speciation, mass transport or double layer properties.

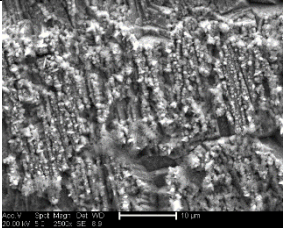
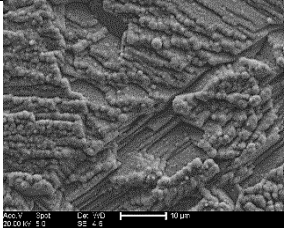
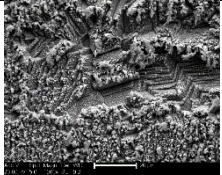
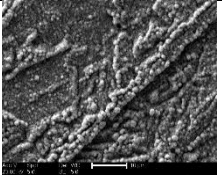
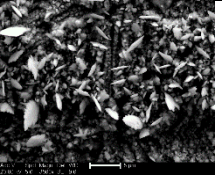
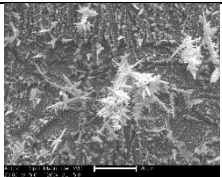
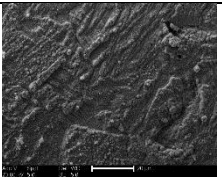
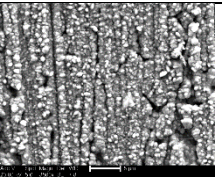
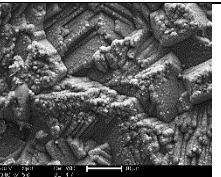
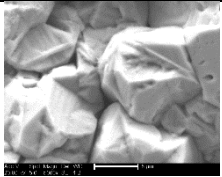
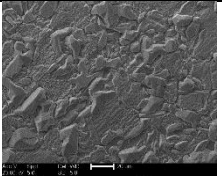
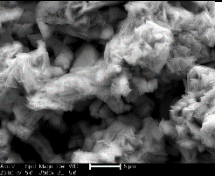
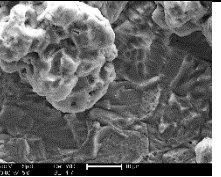
Table 5.1: Deposit of copper obtained from $0.1 \text{ mol kg}^{-1} \text{ CuCl}_2 \cdot 2\text{H}_2\text{O}$ in Ethaline-water mixtures. All experiments were performed for 1 h at 35°C and at a current density of 50 mA cm^{-2} . Experiments were carried out with either a copper anode or an iridium oxide-coated titanium mesh anode.

Water wt%	Copper anode		Iridium oxide coated titanium mesh anode	
0%				
With NaCl			Without NaCl	
Water wt%	Copper anode	Iridium oxide coated titanium mesh anode	Copper anode	Iridium oxide coated titanium mesh anode
10%				
20%				
100%				

As observed qualitatively previously, the anode material can affect the cathode deposit morphology. **Table 5.1** shows exactly the same experiment repeated using an iridium oxide-coated titanium mesh anode. It is assumed in this case that the anodic reaction is

the oxidation of water. What is immediately apparent is that the copper deposit has changed colour from a red-orange colour with a copper anode to a yellow/brown colour with an IrO_2/Ti electrode. It is, however, notable that the brightest deposit is again obtained with 20 wt% water added. **Table 5.2** shows that the deposit morphology also changes. The crystallite dimensions are once again changed which changes the absorbance and reflectance of visible light. It can also affect the scattering of light from the surface, making it appear dull.

Table 5.2: SEM images of the samples shown in Table 5.1.

Water wt%	Copper anode		Iridium oxide coated titanium mesh anode	
0%				
	With NaCl		Without NaCl	
Water wt%	Copper anode	Iridium oxide coated titanium mesh anode	Copper anode	Iridium oxide coated titanium mesh anode
10%				
20%				
100%				

It could be argued that the addition of water affects the speciation of copper in solution. To differentiate speciation effects from double layer effects, the total molality of chloride was kept constant in solution by adding a 5.2 mol kg⁻¹ aqueous solution instead of pure water. The results with a copper anode confirm that the deposit was very dark brown as opposed to a red-orange.

5.4 X-Ray diffraction analysis (XRD).

Figure 5.3 shows the X-ray diffraction spectra for Cu films obtained from 0.1 mol kg^{-1} $\text{CuCl}_2 \cdot 2\text{H}_2\text{O}$ in pure Ethaline and Ethaline with different amounts of water (10 wt% and 20 wt%) and in pure water at 35°C on a nickel substrate and applying a current density of 50 mA cm^{-2} for 1 h using an IrO_2/Ti anode. The XRD pattern of the sample deposited is a good match to the standard JCPDS card for Cu.^{29, 30} The crystallographic texture of the deposits clearly change with the amount of water. The texture coefficients calculated for the Cu deposits obtained with pure Ethaline, with 10 wt% and 20 wt% water, and with pure water are listed in **Table 5.3** and have been normalised to the relative intensity of the [111] signal.

The results showed that in all cases the [111] diffraction peak is the largest observed, as followed by the [200] and the [220] diffraction peaks. As the water content increases, the relative intensities of the [200] and [220] peaks both increase. This could be due to the double-layer structure favouring one form of crystal growth or due to speciation affecting the kinetics of different crystal growth rates. It should be noted that in pure water a diffraction signal was observed at a 2θ value of 47° which could not be identified. It is slightly too low to be CuO [200] and there are no nickel-based signals in the region.

Table 5.3: Texture coefficients of the Cu deposits prepared from pure Ethaline, mixtures with water, and in pure water containing 0.1 mol kg^{-1} $\text{CuCl}_2 \cdot 2\text{H}_2\text{O}$. All experiments were performed for 1 h at 35°C and at a current density of 50 mA cm^{-2} .

Component	Relative intensity [111]	Relative intensity [200]	Relative intensity [220]
Cu in pure Ethaline	1	0.45	0.27
Cu in 10 wt% H_2O	1	0.48	0.34
Cu in 20 wt% H_2O	1	0.51	0.34
Cu in 100 wt% H_2O	1	0.64	0.43

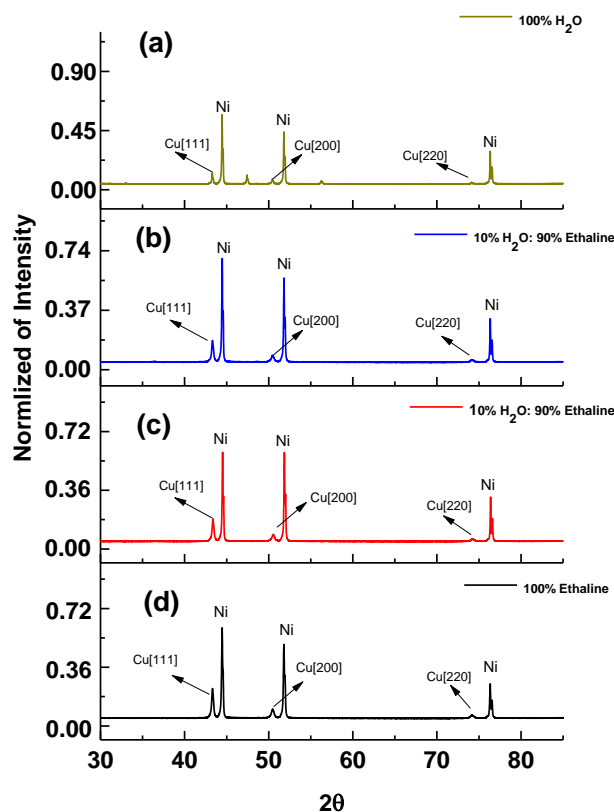


Figure 5.3: XRD patterns of Cu film in (a) pure water, (b) 10 wt% water, (c) 20 wt% water and (d) pure Ethaline at 35°C for 1 h on a nickel electrode at an applied current density of 50 mA cm⁻² using an ItO₂/Ti electrode.

The morphology depends on the rate at which the electroactive species travels to the electrode surface, the ease of reduction when it gets there, which is usually dependent on the speciation and the reactivity at the electrode solution interface and which itself depends on the double-layer structure. To investigate these factors, the effects of water and added sodium chloride were measured on the electrochemical response of the electrode. These data were also used to investigate mass transport by calculating the diffusion coefficient. The speciation of copper salts in solution was determined using UV-Vis spectroscopy and the mechanism of nucleation was investigated using chronoamperometry.

5.5 Cyclic voltammetry.

Cyclic voltammetry (CVs) experiments were carried out using three electrodes, a platinum working electrode, a platinum flag counter electrode and an Ag wire reference electrode. The working electrode was immersed in 0.1 mol kg⁻¹ CuCl₂·2H₂O in pure Ethaline, 10 wt% water, 20 wt% water and pure water; the potential was scanned from 1 V to -1 V and back to 1 V. In the pure Ethaline system two peaks were observed; one for the deposition of Cu at -0.40 V and the other for Cu^{II}/Cu^I, at +0.47 V, which is in good agreement with previous studies,^{20, 31} see **Figure 5.4(a)**. It is important to note here that the concentrations are expressed in terms of molality rather than molarity to reduce the effects of changing concentration with increasing temperature and the different densities between Ethaline and water. The advantage of studying copper reduction is that the Cu^{II/I} acts as an internal standard against which changes in redox potential and diffusion kinetics can be measured.

The addition of water has the ability to affect the speciation of copper in the mixtures. It has been shown that [CuCl₃]⁻ and [CuCl₄]²⁻, are formed in the pure DESs. **Figure 5.4(b)** shows the voltammetry as a function of water content. It is apparent that the potential for the Cu^{II}/Cu^I couple remains roughly constant, whereas the onset potential for reduction to the metal becomes less negative as water is added to the solution.

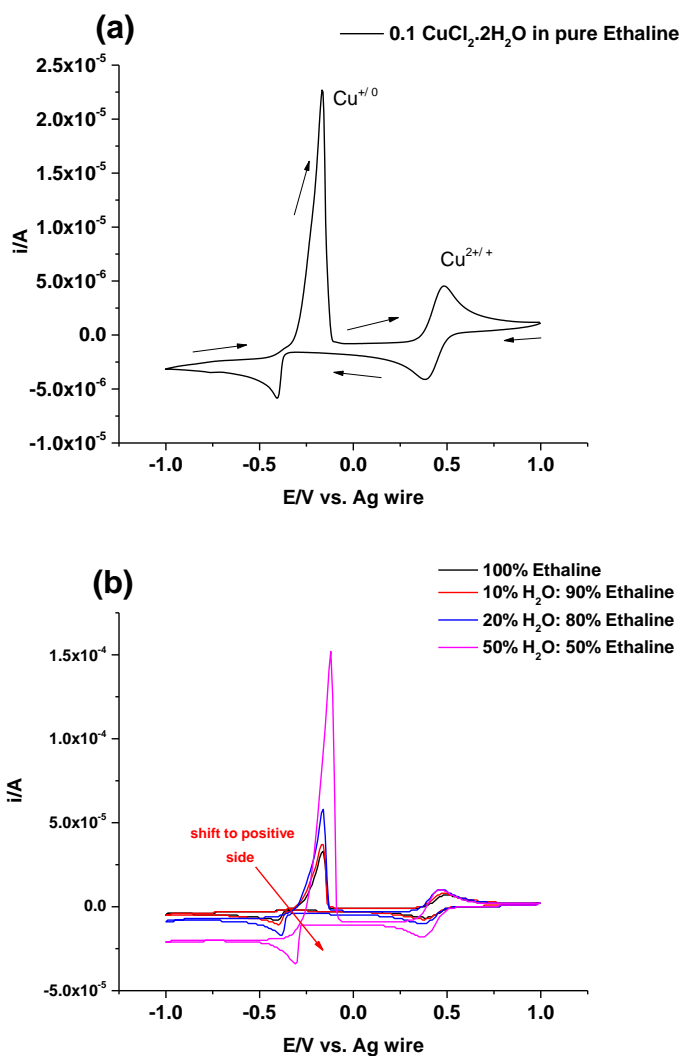


Figure 5.4: (a) Cyclic voltammograms of $0.1 \text{ mol kg}^{-1} \text{ CuCl}_2 \cdot 2\text{H}_2\text{O}$ in pure Ethaline and (b) of $0.1 \text{ mol kg}^{-1} \text{ CuCl}_2 \cdot 2\text{H}_2\text{O}$ in pure Ethaline and with 10 wt%, 20 wt% and 50 wt% at 35°C on a (dia. 5 mm) Pt working electrode at a sweep rate of 20 mVs^{-1} .

This shows that the Ag pseudo-reference potential is relatively stable with respect to the $\text{Cu}^{\text{II}}/\text{Cu}^{\text{I}}$, which is surprising given previous studies of redox couples.³² This would tend to suggest that either water does not affect speciation or that the changes in speciation affect the reference potential and the redox potential to an equal extent.

Table 5.4: $E_{1/2}$ for $\text{Cu}^{\text{II/I}}$ versus onset potential for $\text{Cu}^{\text{I/0}}$ with different amounts of water.

Water wt%	$E_{1/2} \text{Cu}^{\text{II/I}} / \text{V}$	$E_{\text{onset}} \text{Cu}^{\text{I/0}} / \text{V}$
0	0.43	-0.35
10	0.41	-0.35
20	0.41	-0.33
50	0.41	-0.27

As mentioned previously in chapter three, a change in the viscosity of liquids due to increased water content influence the rate of mass transport. It is clear the Cu^{+0} current increased with increasing water content due to the associated change in viscosity of the DESs. Moreover, new species will form when mixing DESs with water, and this could influence the shift in the redox potentials, as per **Table 5.4**; the same was observed in Chapter four.

Comparing the two extremes; pure DES and pure water, **Figure 5.5** shows that the colour of copper chloride in the two liquid changes from yellow to blue. This is because the dominant species in pure DESs is $[\text{CuCl}_4]^{2-}$, and in pure water is $[\text{Cu}(\text{H}_2\text{O})_6]^{2+}$. At 20 wt% water the solution is green due to a mixture of species being present. In an analogous experiment the molality of chloride was kept constant by mixing the DES with a NaCl brine solution of the same molality of chloride as that found in Ethaline (5.2 mol kg^{-1}). It can be seen that copper chloride in a NaCl solution is pale green, showing an equilibrium between the tetrachloro and hexa-aquo species.

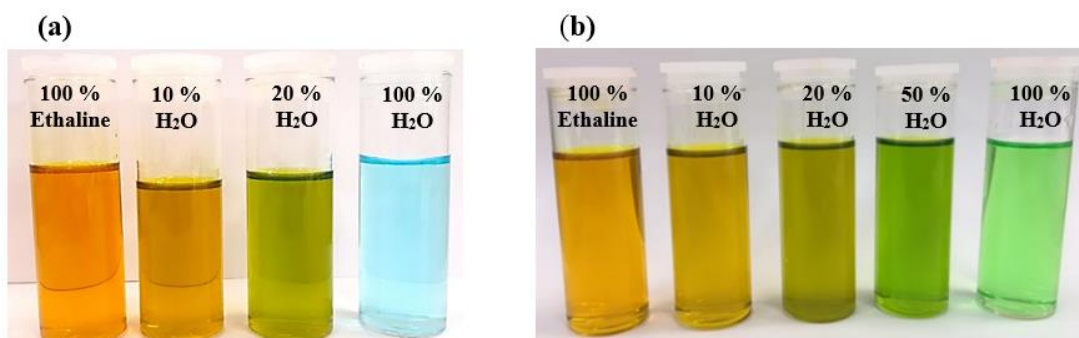


Figure 5.5: (a) $0.1 \text{ mol kg}^{-1} \text{ CuCl}_2 \cdot 2\text{H}_2\text{O}$ in different DES-water mixtures, (b) $0.1 \text{ mol kg}^{-1} \text{ CuCl}_2 \cdot 2\text{H}_2\text{O}$ in different DES-brine solutions all with $5.2 \text{ mol kg}^{-1} \text{ Cl}^-$.

UV-Vis studies were undertaken for $0.1 \text{ mol kg}^{-1} \text{ CuCl}_2 \cdot 2\text{H}_2\text{O}$ in pure Ethaline and Ethaline with various amounts of water (20 wt% and 50 wt%) and in pure water with and without NaCl. For the pure Ethaline and the Ethaline-water mixtures without NaCl, the characteristic absorption bands of the various Cu^{2+} chloro complexes appear in the range between 206 nm and 500 nm, as per **Figure 5.6(a)**. Copper chloride in pure Ethaline shows a strong peak at 293.60 nm. Also, two other peaks associated with copper chloride appeared at 406.97 nm and 240.11 nm. According to previous studies, the complex in pure Ethaline is $[\text{CuCl}_4]^{2-}$.³²⁻³⁴ However, on addition of water, this complex will change depending on the amount of water added to the mixture. The results indicated that peaks will be shifted to shorter wavelengths and decrease in intensity, which is very clear with 20 wt% water and 50 wt% water mixtures.

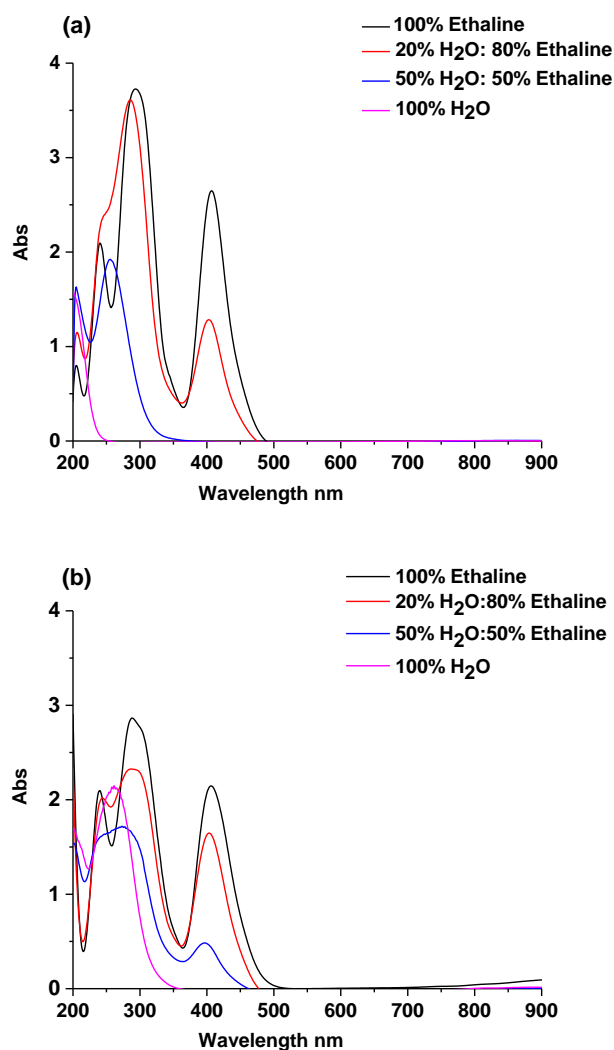


Figure 5.6: UV-Vis spectra of (a) $0.1 \text{ mol kg}^{-1} \text{ CuCl}_2 \cdot 2\text{H}_2\text{O}$ in pure Ethaline and mixtures with different amounts of water (20 wt%, 50 wt% and 100%), (b) $0.1 \text{ mol kg}^{-1} \text{ CuCl}_2 \cdot 2\text{H}_2\text{O}$ in pure Ethaline and Ethaline with different amounts of water (20 wt%, 50 wt% and pure water) with NaCl.

De Vreese *et al.* showed that at 50 wt% water 50 wt% Ethaline, the $[\text{CuCl}_4]^{2-}$ complex will be changed due to the increasing number of water molecules as they enter the coordination sphere of the Cu^{2+} ion, which shifts the UV-Vis peaks to shorter wavelength and decreases their intensity.³⁵ In fact, previous studies have shown that copper chloride in aqueous media with high chloride concentrations forms three complexes, CuCl^+ , CuCl_2 and CuCl_3 . This complexes show absorption bands in the 250-280 nm region.³⁶ In addition, there is an equilibrium between $[\text{Cu}(\text{H}_2\text{O})_4]^{2+}$ and the $[\text{CuCl}_4]^{2-}$, which is very clear due to the colour of copper chloride, with a high concentration of chloride ions being green.³⁷ The results are consistent with these studies, and this could be considered

evidence as to why we have a broad peak at 261 nm in pure water, as seen in **Figure 5.6(b)**. As mentioned previously, water is a good leaving ligand, and which helps to change mass transport properties; however, the system is not completely saturated with water. The speciation will clearly affect the redox potentials of both the $\text{Cu}^{\text{II}}/\text{Cu}^{\text{I}}$ and $\text{Cu}^{\text{I}}/\text{Cu}^0$ couples. **Figure 5.7(a)** and **(b)** shows the cyclic voltammograms for the reduction of copper from a chloride containing medium ($5.2 \text{ mol kg}^{-1} \text{ NaCl}$) and one with just water. The chloride containing solution shows the separate $\text{Cu}^{\text{II}}/\text{Cu}^{\text{I}}$ and $\text{Cu}^{\text{I}}/\text{Cu}^0$ processes, as per **Figure 5.7(b)**, which is the same way as the pure DESs in **Figure 5.4**. In a pure aqueous solution, disproportionation “self-oxidation-reduction” can occur between Cu^{2+} and Cu metal due to the difference in standard aqueous redox potentials ($+0.52 \text{ V}$ for the Cu^{+0} redox couple versus $+0.16 \text{ V}$ for the $\text{Cu}^{2+/+}$ redox couple).¹⁶

Figure 5.7(a) shows cyclic voltammograms of $\text{CuCl}_2 \cdot 2\text{H}_2\text{O}$ in pure water. The results show direct reduction of Cu^{2+} to Cu^0 at -0.2 V without the formation of Cu^+ as an intermediate. Moreover, on the reverse scan three separate oxidation peaks were observed. The two main oxidation peaks are related to the oxidation of Cu^0 to an insoluble Cu^+ chloride salt on the electrode surface followed by oxidation of this Cu^+ species to a soluble Cu^{2+} species.

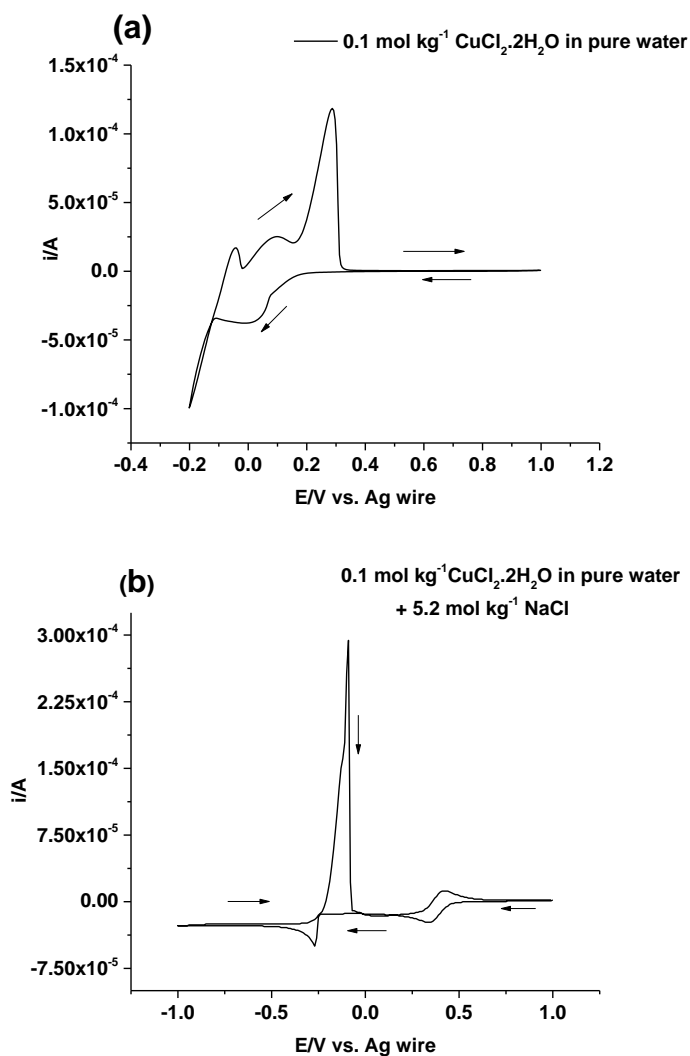


Figure 5.7: (a) Cyclic voltammograms of 0.1 mol kg⁻¹ CuCl₂·2H₂O in pure water with no NaCl at a scan rate of 20 mVs⁻¹ and (b) cyclic voltammograms of 0.1 mol kg⁻¹ CuCl₂·2H₂O in pure water with NaCl (5.2 mol kg⁻¹) at a scan rate of 40 mVs⁻¹.

Figure 5.7(a) shows that in pure water the reduction potential is less cathodic than that when NaCl is added to the solution showing that [Cu(H₂O)₆]²⁺ is easier to reduce than [CuCl₄]²⁻. While it may appear that the stripping charge in pure water than in the NaCl solution, it should be noted that the time spent in the deposition region in **Figure 5.7(b)** is half that of **Figure 5.7(a)**. It should be noted that the reduction current for copper reduction in NaCl solution reaches a steady state value which the CV in pure water does not.

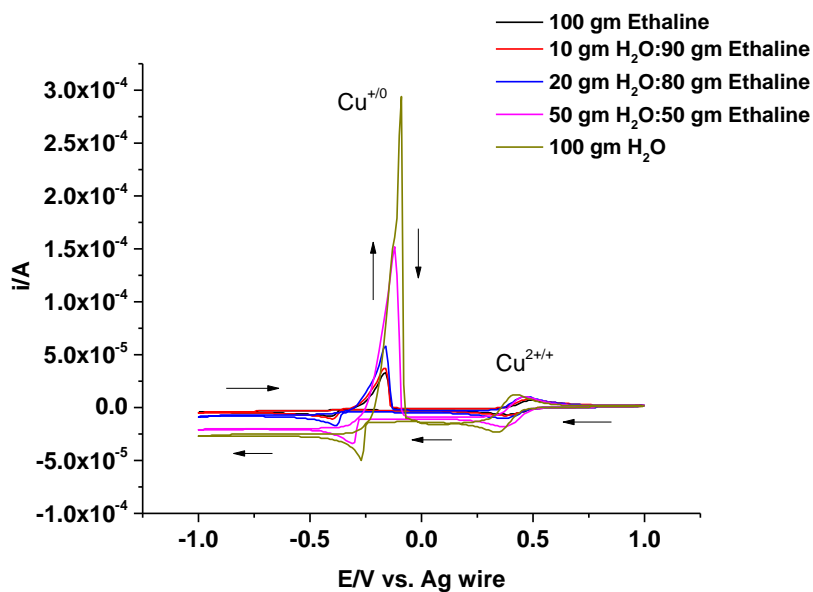


Figure 5.8: Cyclic voltammograms of $0.1 \text{ mol kg}^{-1} \text{ CuCl}_2 \cdot 2\text{H}_2\text{O}$ in pure Ethaline and Ethaline with different water amount and pure water with NaCl (5.2 mol kg^{-1}) at a scan rate of 30 mVs^{-1} .

Figure 5.8 show the CVs of copper chloride in pure Ethaline and Ethaline with different amounts of NaCl brine solutions. While the $\text{Cu}^{\text{II/I}}$ redox couple is relatively unchanged in potential, the onset potential for the $\text{Cu}^{\text{I/0}}$ was shifted by up to 0.2 V to less negative potential from pure Ethaline to brine. The water complexes are easier to reduce to the metal than the chloro-species, probably because water is a better leaving ligand than chloride.

The effect of chloride ions on the electrodeposition of copper in aqueous solutions have been studied previously.^{38, 39} Kao *et al.* studied the effects of adding chloride ions on the electrocrystallisation of copper plated in aqueous solutions at 65°C at a current density of 0.7 A cm^{-2} on a titanium substrate. The results indicated that the presence of the chloride ions in the plating bath influenced the formation of the high-density precipitation of CuCl on the titanium cathode surface. Hence, the CuCl precipitation would lead to higher charge-transfer resistance for cupric ions' reduction on the cathode.⁴⁰ Other studies have shown the impact adding the chloride ion on the morphology of copper deposits on copper substrates at room temperature and applying a current density of 50 mA cm^{-2} to be that small particles appeared on the surface of the substrate.⁴¹ By contrast, electrodeposition of Cu_2O in DMSO in the presence of chloride ions was also studied, the results of which

showed that in the presence of chloride ions, the film took on a crystalline character compared with films electrodeposited in the absence of chloride ions.⁴²

As mentioned previously, ionic liquids have lower conductivities compared to aqueous solutions; increasing their conductivities can be achieved by the addition of small inorganic cations such as Li^+ .¹ Obviously, when water is added to a $\text{CuCl}_2 \cdot 2\text{H}_2\text{O}$: DES mixture, this leads to the dilution of the chloride ion concentration in the DES (the concentration of chloride ions in Ethaline is equal to 5.2 mol kg^{-1}). In this investigation, DESs were used in the electrodeposition of copper due to the fact that DESs have wide potential windows compared with aqueous media. However, the addition of water to the DESs result in an enhancement of the brightness of deposit and an increase in conductivity.

5.6 Diffusion coefficient in copper-water system.

Figure 5.9 shows the CVs for $0.1 \text{ mol kg}^{-1} \text{ CuCl}_2 \cdot 2\text{H}_2\text{O}$ with different amounts of water containing NaCl. CV experiments were carried out using three electrodes, a platinum working electrode, a platinum flag counter electrode and an Ag wire reference electrode. CVs of copper showed an increase in current with increasing amounts of water due to the associated change in viscosity of the liquids; the same behaviour was observed for iron chloride in chapter four.

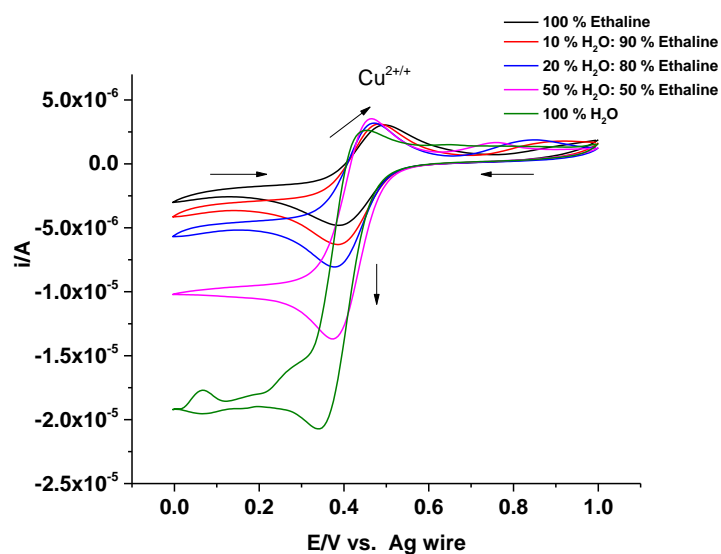


Figure 5.9: $\text{CuCl}_2 \cdot 2\text{H}_2\text{O}$ in different media at a scan rate of 20 mVs^{-1} with NaCl (5.2 mol kg^{-1}).

Previous studies have suggested that the reduction of copper in ionic liquid-water systems is an irreversible process. This conclusion was based on the cyclic voltammograms of the deposition of metallic Cu in the binary mixture ionic of liquid/organic solvent showing unsymmetrical peaks on the reverse scan. This was particularly noticeable at slow scan rates. A self-inhibition process was noted coinciding with the initial growth region. Additionally, the results illustrate that the cathodic peak current is increased and shifted to more negative values with increasing scan rate, as the reduction of copper (II) represents an irreversible system.¹⁰ De Vreese *et al.* showed the behaviour of copper chloride in DES-water mixtures was irreversible, and the irreversibility increased with increasing amounts of water, as per the change from 25 wt% to 73 wt%, as evidenced by the ratio of the oxidation current to the reduction current becoming larger with increasing amounts of water.³⁵

However, in this study the electrochemical behaviour of copper chloride in DES-water mixtures was studied with a platinum working electrode. It can clearly be seen that the $\text{Cu}^{\text{II/I}}$ process was a reversible process, from the ratio of the oxidation current to the reduction current, as seen **Table 5.5**. The diffusion coefficient of copper chloride in the different mixtures was determined using the Randles-Sevcik equation for the $\text{Cu}^{\text{II/I}}$ couple. The peak currents of the reversible process were plotted against the square root

of the scan rate, with the resultant graph showing a good linear correlation between peak currents and the square root of the scan rate, as can be seen in **Figure 5.10**.

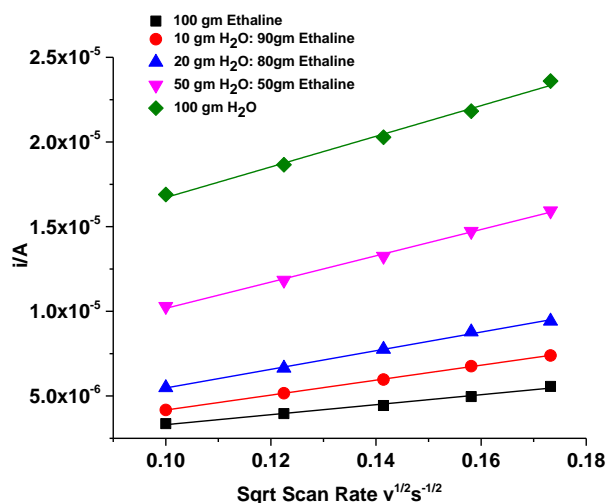


Figure 5.10: Plot of oxidation peak currents versus the square root of sweep rate for $0.1 \text{ mol kg}^{-1} \text{ CuCl}_2 \cdot 2\text{H}_2\text{O}$ in pure Ethaline, pure water and mixes of Ethaline with different amounts of water.

The diffusion coefficients of $\text{Cu}^{2+/+}$ species were calculated with different amounts of water, as reported in **Table 5.5**. These results are consistent with the earlier observation of De Vreese *et al.* who, with their studies using EXAFS, indicated that with increasing water content the water molecules can enter the coordination sphere of Cu^{II} and this can influence increased diffusion due to changes of the complex of Cu^{II} .³⁵

Table 5.5: Diffusion coefficients of $\text{Cu}^{2+/+}$ with different amounts of water.

Water content / wt%	Diffusion Coefficient/ m^2/s	SD	$i_{p,a}/i_{p,r}$
0	3.12×10^{-11}	1.58×10^{-12}	1.0
10	6.98×10^{-11}	3.72×10^{-12}	1.1
20	1.00×10^{-10}	1.54×10^{-12}	1.1
50	1.08×10^{-10}	2.14×10^{-12}	1.0
100	2.93×10^{-10}	4.07×10^{-11}	0.99

The diffusion coefficient data were plotted as a function of fluidity (viscosity⁻¹) as a test of the Stoke-Einstein equation. **Figure 5.11(a)** shows the diffusion coefficient for copper chloride in pure Ethaline, Ethaline with different amounts of water (10 wt%, 20 wt% and 50 wt%). The results illustrate that for pure Ethaline, and Ethaline with smaller amounts of water (10 wt% and 20 wt%), copper chloride diffuses in accordance with what would be expected from the Stokes-Einstein equation; however, on increasing the amount of water to 50 wt%, it is clear there is a deviation from the linearity anticipated on the basis of Stokes-Einstein behaviour which could be due to changes in speciation as shown above.

Figure 5.11(a) also shows the diffusion coefficient for FeCl₃ calculated in chapter four. It may be expected that since the ionic radii of Fe^{III} and Cu^{II} are not overly dissimilar then the diffusion coefficients of the two species should be relatively similar. Any deviation between the two species could be due to either differences in speciation, i.e., replacing more chloride ligands with water ligands as the water content is increased or because the species partitions on average more into a primarily aqueous or primarily ionic phase. **Figure 5.11(a)** shows that the diffusion coefficient of CuCl₂ is larger than that of FeCl₃ in the mixed phases despite the values being similar in pure Ethaline. This could suggest that the Cu^{II} species more preferentially partitions into the water phase than the corresponding Fe^{III} complex.

To see whether the copper deposition process is also diffusion controlled the cathodic charge was also plotted as a function of fluidity and this is plotted in **Figure 5.11(b)**. It can be seen that when water is added to Ethaline the process does appear to be diffusion controlled but there is some deviation when there is no water present. This could be due to differences in speciation and nucleation mechanisms (see below).

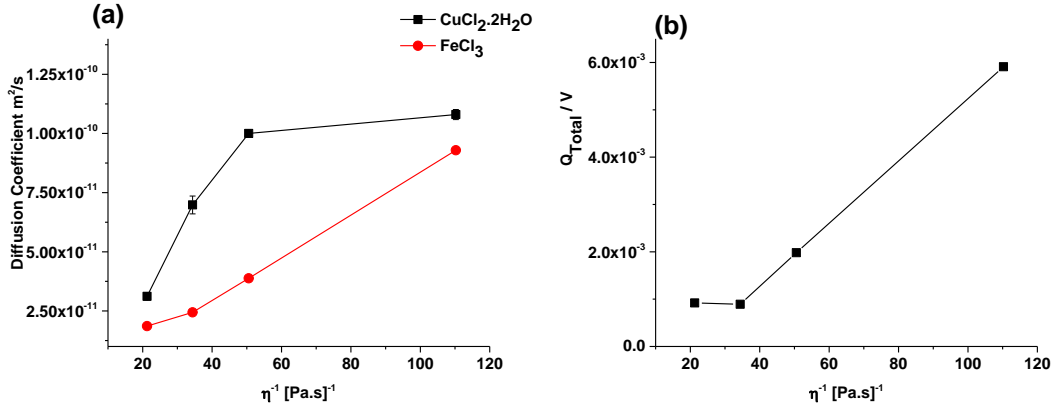


Figure 5.11: (a) plot of D vs. $1/\text{viscosity}$ (b) total charge for reduction versus fluidity of copper chloride for different water contents.

5.7 Chronoamperometry.

To study the nucleation and growth mechanism, chronoamperometry was used for $\text{CuCl}_2 \cdot 2\text{H}_2\text{O}$ in Ethaline and an Ethaline-water mixture at a concentration of 0.1 mol kg^{-1} . A Pt working electrode, Pt flag counter electrode and Ag wire pseudo-reference electrode were used for this study. The relationship between current-time depends on the concentration gradients in the region around the electrode surfaces. Previous studies by Scharifker and Hills defined the mathematical model for current transients. The data can be fitted to two models of nucleation and growth: instantaneous and progressive. The instantaneous mechanism results in rapid growth of nuclei with many active sites and these active sites will activate in a short time; however, the progressive mechanism corresponds to slow growth of nuclei with a limited number of active sites, and these will be activated during the electroreduction process. **Equation (5.1)** and **Equation (5.2)** show, respectively, the Scharifker and Hills mathematical models for these two nucleation and growth cases.⁴³⁻⁴⁵

$$\left(\frac{i}{i_m}\right)^2 = 1.9542 / \left(\frac{t}{t_m}\right) \left\{ 1 - \exp \left[-1.2654 \left(\frac{t}{t_m}\right) \right] \right\}^2 \quad \text{Equation (5.1)}$$

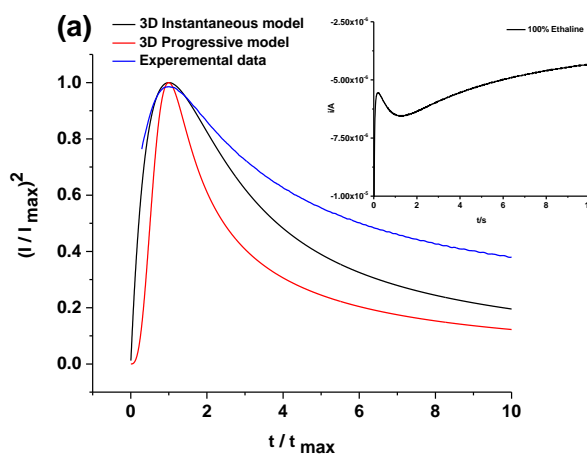
$$\left(\frac{i}{i_m}\right)^2 = 1.2254 / \left(\frac{t}{t_m}\right) \left\{ 1 - \exp \left[-2.3367 \left(\frac{t}{t_m}\right)^2 \right] \right\}^2 \quad \text{Equation (5.2)}$$

In chronoamperometry, at the start of the experiment at time t_0 , there is no current and no electroactive species, and hence there is no reduction of Cu^{2+} . The beginning of the

growth of the nuclei leads to a rising current until a current maximum, i_m , is reached at a time t_m , at which time the crystallites begin to grow.

The electrochemical mechanism can be described as proceeding in three steps: the first ($t/t_{max} < 1$) is when the nuclei start their growth on the surface of the substrate; the second is the coalescence step ($t/t_{max} \approx 1$), when nuclei associate with the surface of the substrate; and the third ($t/t_{max} > 1$) is the growth of the metal layer. The relationship between current i and t are shown in **Figure 5.12**, where the maximum current t_{max} is plotted against the theoretical models for instantaneous and progressive nucleation. It is clear from the results that the growth mechanism of the nuclei is 3D progressive for $\text{CuCl}_2 \cdot 2\text{H}_2\text{O}$ in pure Ethaline, as seen in **Figure 5.12(a)**, and instantaneous for Ethaline-water mixtures (10 wt% and 20 wt% water), as per **Figure 5.12(b)** and **(c)**. However, for pure water the mechanism was entirely different from Ethaline and Ethaline with water mixtures. This unusual behaviour could be due to the rapid growth of copper in pure water completely blocking the surface of the electrode, which would lead to an associated decrease in the total current, as per **Figure 5.12(d)**.

It should, however, be noted that these experiments cannot be compared directly as the experiments were all made at the same potential of -0.37 V vs. Ag . To be strictly comparable, the measurements should have been made at the same over-potentials and so some of the differences observed may also be due to slight differences in over-potential.



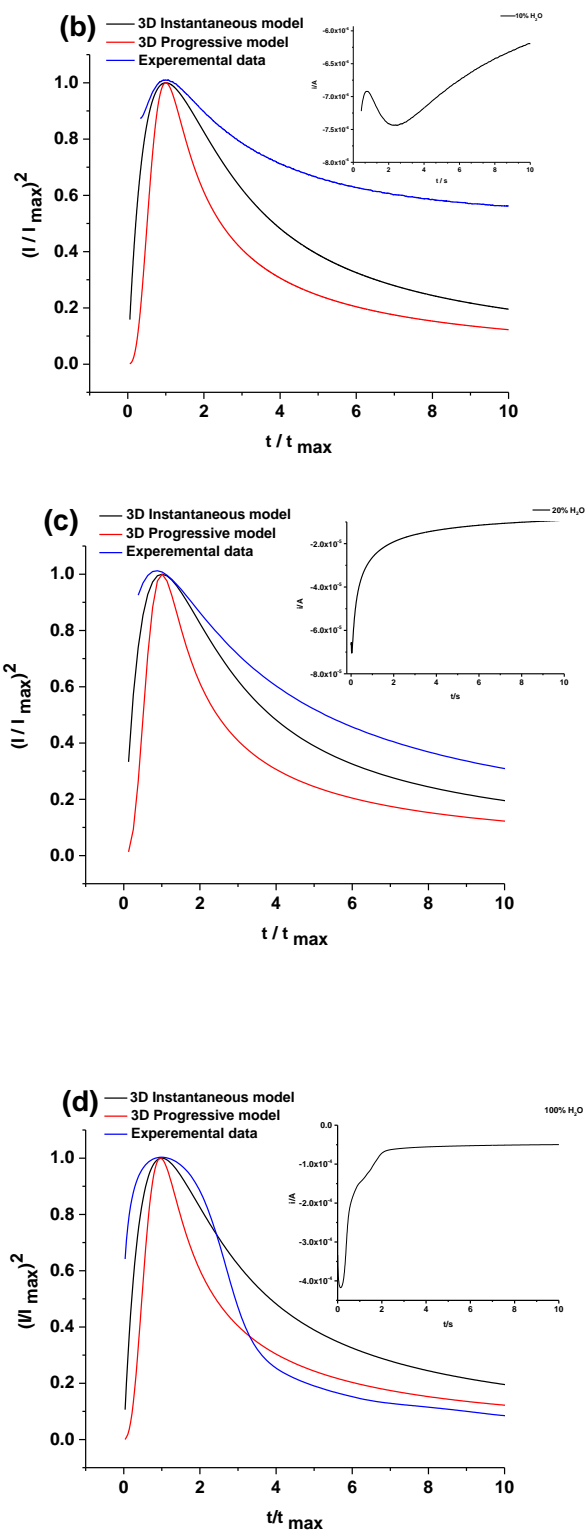


Figure 5.12: Comparison of dimensionless time versus dimensionless current for $0.1 \text{ mol kg}^{-1} \text{ CuCl}_2 \cdot 2\text{H}_2\text{O}$ in (a) pure DES and DES-water mixtures (b) 10 wt%, (c) 20 wt% water and (d) pure water with $0.1 \text{ mol dm}^{-3} \text{ NaCl}$ as a supporting electrolyte at -0.370 V using an Ag wire pseudo-reference electrode.

Additionally, chronoamperometry for copper reduction in the presence of NaCl brine solutions was undertaken to determine the effects of Na^+ in the nucleation and growth processes. **Figure 5.13** shows the growth mechanism of $\text{CuCl}_2 \cdot 2\text{H}_2\text{O}$ nuclei.

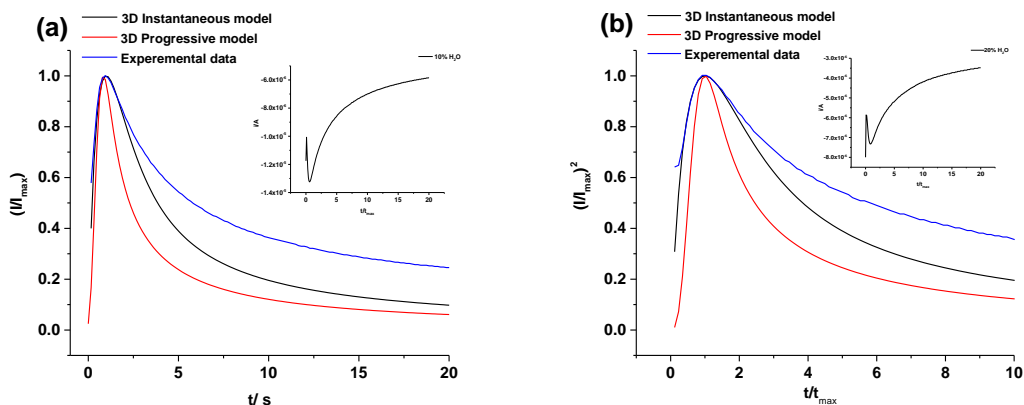


Figure 5.13: Comparison of dimensionless time versus dimensionless current for $0.1 \text{ mol kg}^{-1} \text{ CuCl}_2 \cdot 2\text{H}_2\text{O}$ with $5.2 \text{ mol kg}^{-1} \text{ NaCl}$ in (a) 10 wt% and (b) 20 wt% Ethaline-water mixture, respectively at -0.350 V using an Ag wire pseudo-reference electrode.

The results showed that there is a change in the growth mechanism for copper deposition from solutions of $\text{CuCl}_2 \cdot 2\text{H}_2\text{O}$ nuclei in 10 wt% and 20 wt% compared with results in absence of NaCl, as per **Figure 5.13(a)** and **(b)**. The results are also similar to those for the brine solution without Ethaline. This shows that the presence of Na^+ ions is presumably affecting the double layer structure as Na^+ ions replace Ch^+ ions close to the electrode surface. The presence of Na^+ ions can be most strikingly seen by comparing the dimensionless time versus dimensionless current plots with and without NaCl in pure water as shown in **Figure 5.14(a)** and **(b)**.

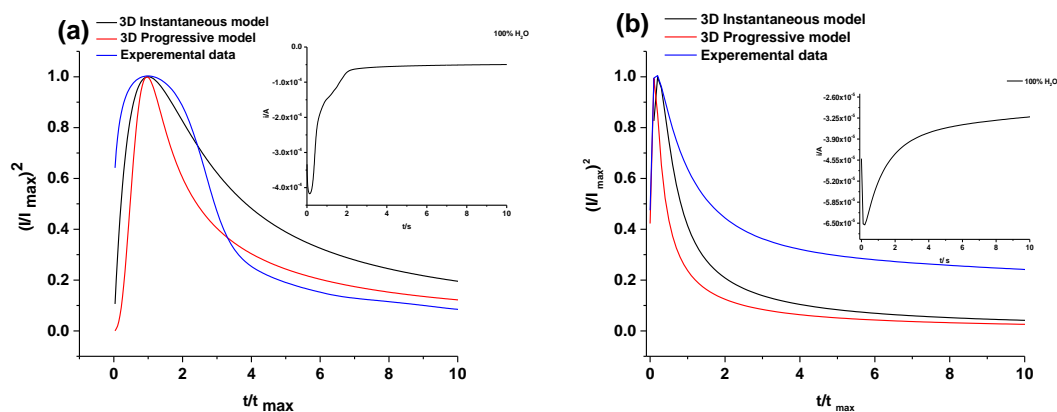


Figure 5.14: Comparison of dimensionless time versus dimensionless current for $0.1 \text{ mol kg}^{-1} \text{ CuCl}_2 \cdot 2\text{H}_2\text{O}$ in (a) pure water without NaCl and (b) pure water with $5.2 \text{ mol kg}^{-1} \text{ NaCl}$.

5.8 Effect of the anode.

As shown in section 5.3.2, the anodic reaction appears to have an influence on the morphology of the metal deposit. The use of a dimensionally stable anode (iridium oxide coated titanium) produces a dull brown looking deposit in contrast to a red-orange coating when a soluble copper anode is used. Karim has recently studied the electrodisolution of metals in DESs and found that for most metals an insoluble film was formed on the electrode surface under anodic polarisation. For some of the metals, the layer was identified as being an insoluble halide layer. While metal halides are generally very soluble in DESs due to the formation of negatively charged species, it was found that the high viscosity and low mobility of the ligands meant neutral species were formed, i.e., for the anodic dissolution of Cu, CuCl_2 was formed instead of CuCl_4^{2-} .⁴⁶ The layer of CuCl_2 leads to significant resistance at the electrode surface.

The electrodeposition experiments shown in **Table 5.1** were repeated in using a soluble copper anode and the anode was studied after bulk electrolysis at 35°C and at a current density of 50 mA cm^{-2} on a Ni substrate. **Table 5.6** shows that water has a significant effect on the morphology of the copper anode. In the absence of water etching of the copper occurs. When 10 wt% water is added some areas of the copper anode appear to be bright as if polishing occurs. Electropolishing of metals has previously been studied in Ethaline and it was found that small amounts of water had a beneficial effect on the quality of the polish obtained.

In terms of using the soluble anode, previous studies have shown the influence of the formation of a brownish or black passive layer on the surface of the anode, where these studies were completed in aqueous media.⁴⁷ Moreover, Cobley and Gabe have shown that the use of an insoluble anode can affect the morphology, chemical composition, electrochemistry and brightness of any subsequent copper deposition.⁴⁸ The same behaviour was observed on the anode surface in pure water. CuO has a relatively small band gap of 1.3 - 2.1 eV⁴⁹ which should lead to a relatively small resistive element in the circuit compared to CuCl₂.⁴⁶

Table 5.6 also shows the effect of increasing the copper chloride concentration to 0.5 mol kg⁻¹. If the copper chloride concentration increases then it would be expected that it would be easier for the double layer next to the anode to passivate with CuCl₂ as the solution is already almost completely saturated with copper chloride. It is clear that CuCl₂ forms on the electrode surface because of the green colouration.

Table 5.6: Photos of the copper anode in pure Ethaline, Ethaline with different amounts of water and in pure water at two different concentrations of 0.1 mol kg⁻¹ and 0.5 mol kg⁻¹ of CuCl₂·2H₂O.

wt% water				
	0%	10%	20%	100%
0.1 mol kg ⁻¹				
0.5 mol kg ⁻¹				

Figure 5.15 shows the cyclic voltammetry of a copper electrode in pure Ethaline, Ethaline with different amounts of water and in pure water with NaCl. The results are the same as those shown by Karim for pure Ethaline.⁴⁶

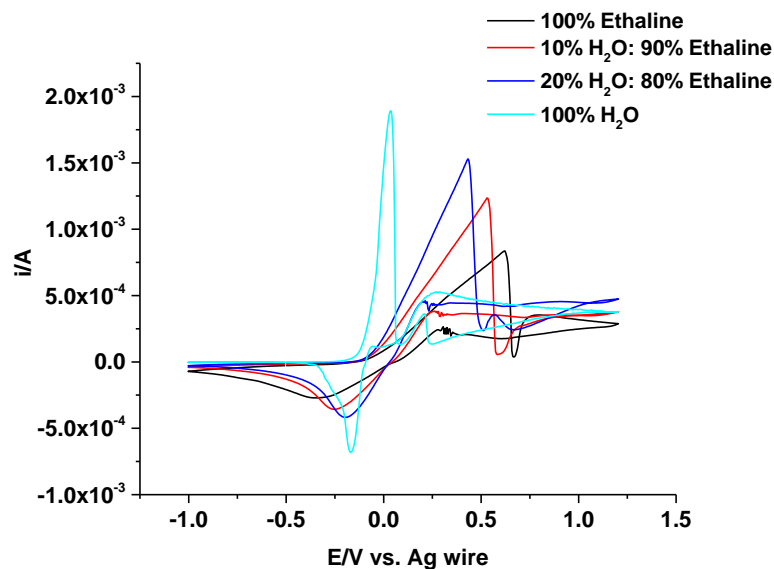


Figure 5.15: Cyclic voltammograms of a copper electrode in pure Ethaline and Ethaline with different amounts of water of 10 wt% and 20 wt% and in pure water with NaCl, at a scan rate of 50 mVs^{-1} .

Anodic dissolution of copper is observed up to a potential of *ca.* 0.6 V where a sudden decrease in current is observed due to passivation. There is a shift in the onset potential for anodic dissolution which shifts to less positive values with increasing amounts of water. The charge for anodic dissolution in Ethaline is less than that for the aqueous mixtures, most probably due to the slower mass transport. At potentials to the positive of +0.7 V the current increases for Ethaline which is due to a breakdown in the anodic film formed on the electrode surface.

The same trend was also observed for Ethaline-water mixtures, but again the potentials were shifted to less positive values. Moreover, copper dissolution in pure water with NaCl showed similar behaviour but the initial anodic dissolution peak was much sharper and appeared at +0.06 V as opposed to +0.6 V in pure Ethaline. Karim showed that the passivating film on the copper surface was quite thick ($3.75 \mu\text{m}$) and so it can be concluded that although in Ethaline a film forms, it must have different characteristics to those found in water. This is in agreement with the results in **Table 5.1**, where it can be seen that the films are different purely by visual inspection. The presence of a more resistive film on the anode will affect the total applied cell potential for a given applied current density and result in different potential profiles at both the anode and cathode

surfaces. This is thought to be one of the major reasons that a small amount of water is beneficial to electrochemical processes in DESs.

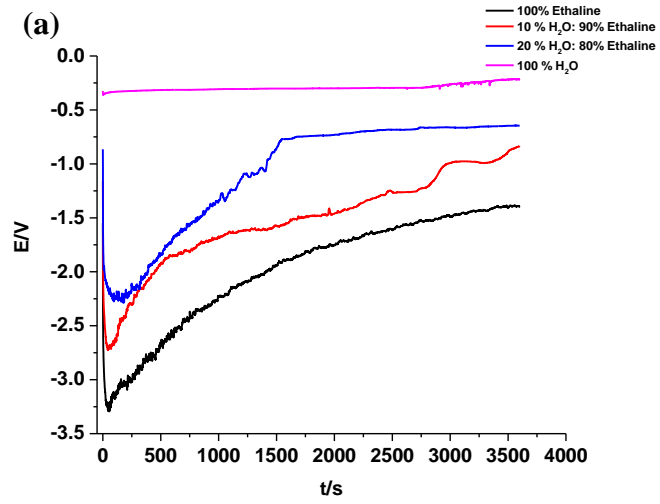
A galvanostatic study was undertaken to examine the changes in potential as a function of time using a 1 cm² nickel working electrode, copper and iridium oxide-coated titanium anodes, a counter electrode and an Ag wire reference electrode at a current density of 50 mA cm² for 0.5 mol kg⁻¹ copper chloride.

Figure 5.16 shows the chronopotentiometric curves obtained for different solutions in pure Ethaline, Ethaline with different amounts of water (10 wt% and 20 wt%), and pure water with/without NaCl. For the Ethaline containing liquids there was a sudden increase in the reduction potential required to achieve a current density of 50 mA cm². This was almost certainly due to the slow diffusion rate of copper to the electrode and the increase in potential required to reduce water or ethylene glycol. Some gassing could be seen on the electrode surface during this part of the experiment. The potential slowly fell in all three Ethaline-containing liquids, presumably because copper was deposited and copper deposition became easier. In addition to the standard potential required to reduce the metal E^0 , the cell voltage E_{cell} will be made up of the resistive component for the electrodes, $iR_{electrodes}$, and the solution, iR_{soln} , as well as the over-potential required to achieve the required reduction kinetics, η , as per **Equation (5.3)**.

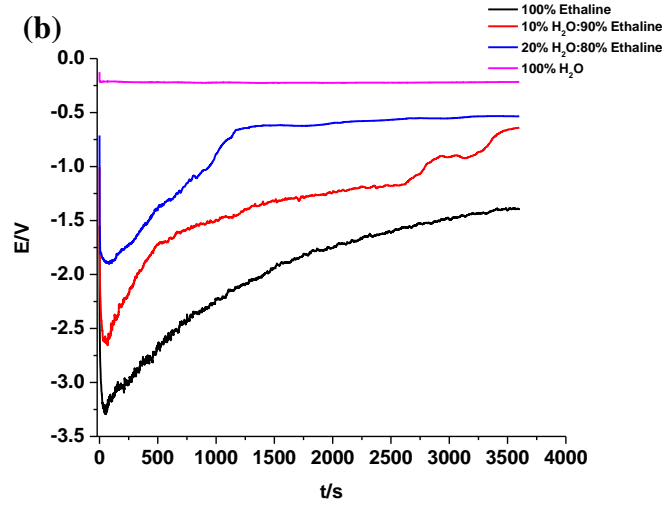
$$E_{cell} = E^0 + iR_{soln} + iR_{electrodes} + \eta \quad \text{Equation (5.3)}$$

In Ethaline, iR_{soln} will be largest due to its lower conductivity. If the anodic film grows on the copper surface, it will also increase $iR_{electrodes}$. **Figure 5.16** shows that the anode material, the water content and the presence of NaCl all cause a change in the cell potential which will change the growth mechanism of the copper on the electrode surface.

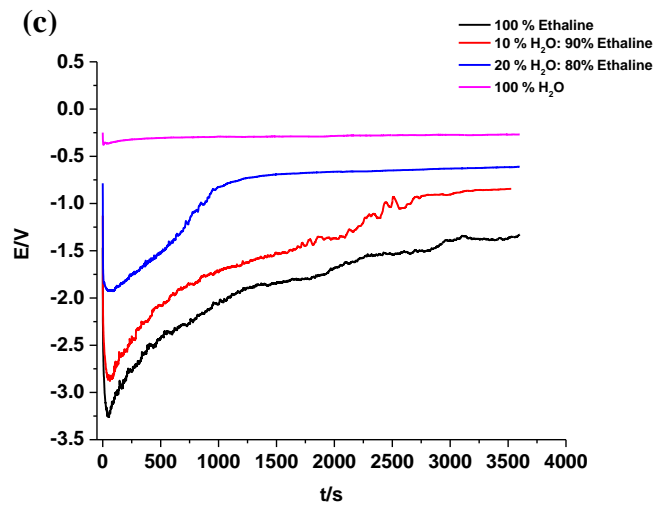
Without NaCl



With NaCl



Without NaCl



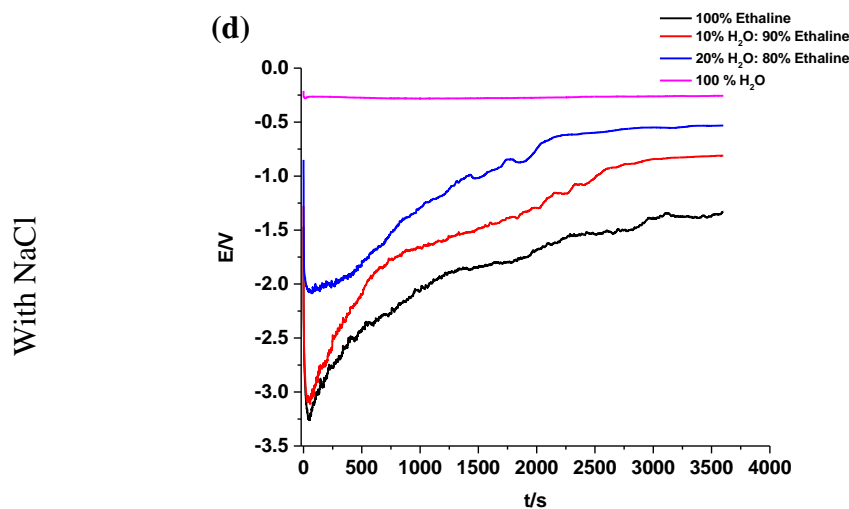


Figure 5.16: Chronopotentiometric curves obtained during electrodeposition of copper in pure Ethaline, Ethaline with different amounts of water and in pure water at a current density of 50 mA cm^{-2} at different electrodes (a) and (b) copper anode with/without NaCl and (c) and (d) iridium oxide-coated titanium anode with/without NaCl.

Amaral and Müller used chronopotentiometry for the deposition of iron in alkaline solutions. Their study showed two potential plateaus which suggested that galvanostatic film formation occurs in two steps. The first plateau shows the formation of a ferrous species, whilst the second indicates a ferric species.⁵⁰ By analogy, the steps in the potential observed in **Figure 5.16** could be due to the formation of cuprous chloride ion which could saturate the area next to the electrode. The deposition of copper in pure DESs was recently studied by Cihangir⁵¹ who used both optical microscopy and impedance spectroscopy to study film formation during deposition. It was found that no films were observed for copper deposition. This is in contrast to zinc deposition, where film formation was observed when the zinc deposited was reactive to both water and ethylene glycol.

The results in **Figure 5.16** are in accordance with the results reported in **Table 5.6**, which show there is a thin layer observed at the anode in pure Ethaline and Ethaline with 10 wt% and 20 wt% water compared with pure water. This explanation is valid for the use of a copper anode; however, for an iridium oxide-coated titanium anode, the mechanism is different due to the titanium anode being insoluble compared with the copper anode.⁵² The reaction is as yet unknown on the titanium anode, but as the surface is good at

catalysing water decomposition it is likely that the water acts as a sacrificial reagent. This does, however, imply that there will be a change in the pH of the liquid as oxygen is evolved, as per **Equation (5.4)**.



This section has not been able to identify the mechanism by which the morphology changes, but it has categorically shown that water, brine and the anode material have a profound effect on the structure of the copper deposit. It is highly probable that speciation, mass transport and double-layer structure all have an effect on the way in which copper nucleates and grows on the electrode surface.

5.9 Conclusion.

In this part of the study, the electrodeposition of copper from a choline chloride-ethylene glycol-based DES was investigated as a function of water content. The addition of water was seen to significantly change the deposit morphology. Most notably, the colour and hue of the copper deposit changed when water was added to the DES. Less obviously, the anode material itself was seen to have a significant effect on the deposit morphology. This study has also shown that the inclusion of a simple electrolyte such as NaCl can affect the deposit morphology, changing it to a dark brown/ black deposit. The causes for these observations were investigated in terms of mass transport (diffusion coefficient), copper speciation and the double-layer structure.

Electrochemical studies have shown that the diffusion of copper chloride increased with increasing water content as expected, while water was found to change the speciation of copper in solution; this was not thought to be a significant issue, except in pure water. The addition of chloride to pure water made the deposition process less easy but resulted in a deposit morphology that had a greater degree of similarity to that of a DES than that of pure water.

Mass transport clearly affected the growth of different crystal face. Water promoted the growth of crystal faces which were non-diagonal, i.e., more [200] and [222] than [111]. One of the biggest factors in affecting the deposit morphology was the anodic reaction which appears to be dominated by dissolution of metal and the diffusion of a ligand to solubilise it. This led to a passivating film on the anode surface which in turn changed the potential profile across the cell.

SEM results indicated that water changes the size of the crystallites which changes the colour and hue of the deposit. In DESs, the crystals were much smaller than in pure water. This can be seen as a change in the nucleation and growth mechanism for metals in the liquid. The main conclusion was, therefore, to confirm that small amounts of water were beneficial to metal deposition from DESs as this modified mass transport, anodic reactions and speciation in solution.

5.10 References.

1. A. P. Abbott and K. J. McKenzie, *Physical Chemistry Chemical Physics*, 2006, **8**, 4265-4279.
2. M. Nair, L. Guerrero, O. L. Arenas and P. Nair, *Applied Surface Science*, 1999, **150**, 143-151.
3. M. Schlesinger and M. Paunovic, *Modern Electroplating*, John Wiley & Sons, 2011.
4. F. Endres, *ChemPhysChem*, 2002, **3**, 144-154.
5. K. Elttaib, PhD Thesis, University of Leicester, 2011.
6. F. Liu, Y. Deng, X. Han, W. Hu and C. Zhong, *Journal of Alloys and Compounds*, 2016, **654**, 163-170.
7. C. Hussey, L. King and R. Carpio, *Journal of the Electrochemical Society*, 1979, **126**, 1029-1034.
8. C. Nanjundiah and R. Osteryoung, *Journal of The Electrochemical Society*, 1983, **130**, 1312-1318.
9. P.-Y. Chen and I.-W. Sun, *Electrochimica Acta*, 1999, **45**, 441-450.
10. I. B. Assaker and M. Dhahbi, *Journal of Molecular Liquids*, 2011, **161**, 13-18.
11. F. Qiu, A. W. Taylor, S. Men, I. J. Villar-Garcia and P. Licence, *Physical Chemistry Chemical Physics*, 2010, **12**, 1982-1990.
12. K. Murase, K. Nitta, T. Hirato and Y. Awakura, *Journal of Applied Electrochemistry*, 2001, **31**, 1089-1094.
13. B. J. Tierney, W. R. Pitner, J. A. Mitchell, C. L. Hussey and G. R. Stafford, *Journal of The Electrochemical Society*, 1998, **145**, 3110-3116.

14. F. Endres and A. Schweizer, *Physical Chemistry Chemical Physics*, 2000, **2**, 5455-5462.
15. A. P. Abbott, K. E. Ttaib, G. Frisch, K. J. McKenzie and K. S. Ryder, *Physical Chemistry Chemical Physics*, 2009, **11**, 4269-4277.
16. A. Abbott, G. Frisch, S. Gurman, A. Hillman, J. Hartley, F. Holyoak and K. Ryder, *Chemical Communications*, 2011, **47**, 10031-10033.
17. D. V. Wagle, H. Zhao and G. A. Baker, *Accounts of Chemical Research*, 2014, **47**, 2299-2308.
18. E. L. Smith, A. P. Abbott and K. S. Ryder, *Chemical Reviews*, 2014, **114**, 11060-11082.
19. M. Espino, M. de los Ángeles Fernández, F. J. Gomez and M. F. Silva, *TrAC Trends in Analytical Chemistry*, 2016, **76**, 126-136.
20. A.-M. J. Popescu, V. Constantin, M. Olteanu, O. Demidenko and K. Yanushkevich, *Revista De Chime*, 2011, **62**, 626-632.
21. D. Lloyd, T. Vainikka, L. Murtomäki, K. Kontturi and E. Ahlberg, *Electrochimica Acta*, 2011, **56**, 4942-4948.
22. E. B. Budevski, G. T. Staikov and W. J. Lorenz, *Electrochemical Phase Formation and Growth: An Introduction to the Initial Stages of Metal Deposition*, John Wiley & Sons, 2008.
23. G. Zangari, *Coatings*, 2015, **5**, 195-218.
24. U. Schröder, J. D. Wadhawan, R. G. Compton, F. Marken, P. A. Suarez, C. S. Consorti, R. F. de Souza and J. Dupont, *New Journal of Chemistry*, 2000, **24**, 1009-1015.
25. A. P. Abbott, R. C. Harris, Y.-T. Hsieh, K. S. Ryder and I.-W. Sun, *Physical Chemistry Chemical Physics*, 2014, **16**, 14675-14681.

26. H. Matsumoto, *Electrochemical Windows of Room-Temperature Ionic Liquids*, John Wiley & Sons, Inc., Hoboken, New Jersey, 2005.
27. C. Du, B. Zhao, X.-B. Chen, N. Birbilis and H. Yang, *Scientific Reports*, 2016, **6**, 29225.
28. Z. Chen, B. McLean, M. Ludwig, R. Stefanovic, G. G. Warr, G. B. Webber, A. J. Page and R. Atkin, *The Journal of Physical Chemistry C*, 2016, **120**, 2225-2233.
29. Q. Zhang, Y. Hua, Y. Wang, H. Lu and X. Zhang, *Hydrometallurgy*, 2009, **98**, 291-297.
30. Q. Zhang, X. Yu, Y. Hua and W. Xue, *Journal of Applied Electrochemistry*, 2015, **45**, 79-86.
31. S. Ghosh and S. Roy, *Surface and Coatings Technology*, 2014, **238**, 165-173.
32. J. M. Hartley, PhD Thesis, University of Leicester, 2013.
33. A. P. Abbott, K. El Ttaib, G. Frisch, K. J. McKenzie and K. S. Ryder, *Physical Chemistry Chemical Physics*, 2009, **11**, 4269-4277.
34. C. Amuli, M. Elleb, J. Meullemeestre, M. J. Schwing and F. Vierling, *Inorganic Chemistry*, 1986, **25**, 856-861.
35. P. De Vreese, N. R. Brooks, K. Van Hecke, L. Van Meervelt, E. Mattheijs, K. Binnemans and R. Van Deun, *Inorganic Chemistry*, 2012, **51**, 4972-4981.
36. M. Wang, Y. Zhang and M. Muhammed, *Hydrometallurgy*, 1997, **45**, 53-72.
37. T. Moeller, *The Journal of Physical Chemistry*, 1944, **48**, 111-119.
38. D. Lloyd, T. Vainikka, L. Murtomäki, K. Kontturi and E. Ahlberg, *Electrochimica Acta*, 2011, **56**, 4942-4948.
39. W. H. Gauvin and C. A. Winkler, *Journal of The Electrochemical Society*, 1952, **99**.

40. Y. Kao, K. Li, G. Tu and C. Huang, *Journal of The Electrochemical Society*, 2005, **152**, C605-C611.
41. M. Delgosh, S. Salehi, L. U. borujeni and S. Sharifi, *Optics*, 2014, **3**, 15.
42. G. Riveros, M. León and D. Ramírez, *Journal of the Chilean Chemical Society*, 2016, **61**, 3219-3223.
43. D. Grujicic and B. Pesic, *Electrochimica Acta*, 2002, **47**, 2901-2912.
44. B. Scharifker and G. Hills, *Electrochimica Acta*, 1983, **28**, 879-889.
45. G. Saravanan and S. Mohan, *New Journal of Chemistry*, 2013, **37**, 2564.
46. W. O. Karim, PhD Thesis, University of Leicester, 2016.
47. Y.-H. Lee, H. Ju, S.-K. Rha, S.-H. Lee and Y.-S. Lee, *Journal of Surface Analysis*, 2011, **17**, 282-286.
48. A. Cobley and D. Gabe, *Transactions of the IMF*, 2003, **81**, 37-44.
49. B. Balamurugan and B. Mehta, *Thin Solid Films*, 2001, **396**, 90-96.
50. S. Amaral and I. Müller, *Corrosion Science*, 1999, **41**, 747-758.
51. S. Cihangir, PhD Thesis, University of Leicester, 2018.
52. M. Palaniappa, M. Jayalakshmi, P. Prasad and K. Balasubramanian, *International Journal of Electrochemical Science*, 2008, **3**, 452-461.

Chapter 6: Conclusions and future work.

6	Conclusions and future work.	173
6.1	Conclusion.	173
6.2	Future work.	176

6 Conclusions and future work.

6.1 Conclusion.

Prior to this study, the perceived wisdom was that ionic liquid-water mixtures were largely homogeneous. It had been suggested that some nano-heterogeneity may occur where the cation of the ionic liquid has long alkyl chains which form hydrophobic domains akin to the behaviour in surfactant systems. It was not, however, thought possible that a chloride salt, a polar organic compound and water would be anything other than a homogeneous solution. While some studies carried out at the same time as this thesis reported the physical characteristics of pure deep eutectic solvent mixtures with water, they simply reported the data without providing any particular insight into the causes for the changes.

The present study measured viscosity, conductivity, surface tension and density of DES-water mixtures as a function of temperature. The systems clearly showed non-ideal behaviour in some parameters. Viscosity studies were carried out using two different techniques, namely with a rotating cylinder viscometer and a quartz crystal microbalance (QCM); both techniques gave identical results. Physical properties could be explained in terms of hole theory, and it is clear that the liquids with higher surface tensions have higher viscosities than those whose viscosities are lower.

The rheological study showed that both Ethaline and Glyceline exhibited Newtonian behaviour; however, Oxaline and Reline showed non-Newtonian behaviour due to the difference in hydrogen bonding between them, with increasing non-Newtonian behaviour with an increasing number of hydrogen bonds. At elevated temperatures, the rheological behaviour of Oxaline and Reline became more Newtonian due to the breaking of these hydrogen bonds.

Since deep eutectic solvents are relatively hygroscopic it was previously thought that the absorbance of water could destroy the solvent properties of DES, having a significant impact on DESs properties; for example, viscosity was decreased with an increasing amount of water due to decreased hydrogen bonding between the chloride anion in choline chloride and a decreased columbic attraction in wet DESs compared with pure

DESs. The results also suggested that the relationship between viscosity and water content is not a linear one.

An alternative approach used to analyse the effect of water on the viscosity of DESs is to use the method employed for aqueous electrolyte solutions by following the Dole-Jones model. The results showed that there is a nonlinear relationship between ChCl: HBD mixtures and the square root of salt concentration due to the increase in concentration of salts due to their influence on increasing the charge-charge interactions.

The conductivities of DES-water mixtures were investigated in this study, with an inverse relationship between viscosity and conductivity being observed. This so-called Walden plot is characteristic of the behaviour on non-diluted ionic liquids. The observation that it also holds for diluted DESs shows that charge mobility, rather than the number of charge carriers, still dominates charge mobility. Conductivity increased with increasing amounts of water for all three systems, namely Ethaline, Glyceline and Reline. Both Ethaline and Glyceline showed the same trend; however, Reline rapidly increased in conductivity with increasing amounts of water. A plot of molar conductivity against fluidity, or a Walden plot, showed that a greater deviation occurs for the Reline system than the other two liquids due to Reline being more heterogeneous than Ethaline and Glyceline. Surface tensions of the DESs were investigated in this study where Reline showed different behaviour to the other two liquids, again reflecting the fact that Reline is more heterogeneous than Ethaline and Glyceline. Additionally, the density of the DESs was found to decrease with an increasing amount of water for all three liquids.

Dynamic light scattering (DLS) was used to investigate the aggregation phenomenon in liquids; in this study, DLS was used to provide further evidence that the DES-water mixtures were not homogenous. It is important to note that for both water in DESs and DESs in water microemulsions are formed. This tells us that the properties of DESs and ionic liquids in water are different from those expected for a solution of choline chloride and an HBD in water. One of the most surprising discoveries of this study was the magnitude of dispersed phases, which were in the order of 10^{-7} m. While these domains will by no means be pure phases, they were sufficiently heterogeneous to affect species mobility. ζ potentials were greater than 10 mV, demonstrating that the colloidal dispersions were stable.

Taken together, these results suggest that the physical properties of DESs with water showed that the Reline-water mixture is more heterogeneous than Ethaline and Glyceline. This result was confirmed via two different methods, namely PFG-NMR and electrochemistry.

Diffusion coefficients was studied via two different methods: PFG-NMR and electrochemistry. The diffusion coefficients of a given species increased with an increasing amount of water in the DES-water mixtures. Glyceline and Reline both showed non-Stokesian behaviour in their associated DES-water mixtures. Electrochemistry was undertaken using iron chloride and potassium ferrocyanide. Results of diffusion through the use of these two probes showed the same order for the associated self-diffusion coefficients, which is that the Reline is more heterogeneous than Ethaline and Glyceline. Moreover, the ionic phase dominated the double layer structure between 25 wt% and 40 wt%, which was subsequently dominated by water at greater than 45 wt%.

In the final part of the study, the electrodeposition of copper was studied in Ethaline-water mixtures. It was shown that several parameters had a significant influence on the deposit morphology. Water was shown to increase the brightness of the deposit due to the changes in the crystallite size. The anode material was also shown to change the deposit morphology. The inclusion of NaCl caused the deposit to change colour from an orange-red to a dark brown-black deposit. The causes for these observations were investigated in terms of mass transport (diffusion coefficient), copper speciation and the double layer structure. In pure Ethaline, the copper complex formed was $[\text{CuCl}_4]^{2-}$; however, when water was added to the Ethaline, $[\text{Cu}(\text{H}_2\text{O})_n]^{2+}$ was formed but $[\text{CuCl}_4]^{2-}$ was also present. When 5.2 mol kg^{-1} NaCl in water was used in place of water the equilibrium between the copper complexes shifted towards $[\text{CuCl}_4]^{2-}$, which prevented the disproportionation of Cu^+ in pure water and changed the electrochemical response.

Electrochemical studies have shown that the diffusion of copper chloride increased with increasing water content as expected. While water was found to change the speciation of copper in solution, this was not thought to be a significant issue, except in pure water. The addition of chloride to pure water made the deposition process less easy but resulted in a deposit morphology that bore a greater resemblance to that from a DES than from pure water.

Mass transport was found to affect the growth of different crystal face. Water promotes the growth of crystal faces which are non-diagonal, i.e., more [200] and [222] rather than [111] in character. One of the biggest factors in affecting the deposit morphology was the anodic reaction, which appeared to be dominated by dissolution of metal and the diffusion of ligand to solubilise it. This led to a passivating film on the anode surface which in turn changed the potential profile across the cell.

SEM results indicated that water changes the size of the crystallites which changes the colour and hue of the deposit. In DESs, the crystals are much smaller than in pure water. This can be seen as a change in the nucleation and growth mechanism for metals in the liquid. The main conclusion is therefore to confirm that small amounts of water are beneficial for metal deposition from DESs as it modifies mass transport, anodic reactions and speciation in solution.

6.2 Future work.

The discovery that DES-water mixtures are not simply solutions of the two components in water means that mixed systems can now be investigated in areas where pure DESs have previously been applied. It is clear that water improves the mass transport properties of DESs, and it may also affect the solubility of different solutes.

This thesis has highlighted that water forms heterogeneous phases in DESs. It is important to investigate the structure within these phases particularly in understanding the length-scales over which order occurs. This can be done using both theoretical and practical methods. Molecular dynamic simulations have been used for IL-water mixtures and these show domains which are continuous over a few molecular dimensions. The problem with this approach is the number of molecular and ionic components which can be fitted in a sample volume. Dynamic light scattering has observed structures in the hundreds of nanometres scale, but it would be interesting to try different light scattering techniques such as neutron or X-ray scattering techniques.

The study here has highlighted some fundamental aspects that could be studied to reveal more information about structure. The study has left some questions about the size of the water droplets in DES and DES in water microemulsions. Measurement of the shape of the droplet formed in the DES-water mixtures could be carried out using different

cryogenic techniques such as cold stage transmission electron microscopy (TEM) and field emission scanning electron microscopy (FE-SEM). Studies of surfactants in DESs have shown that rod-like aggregates form in DESs and it may be possible that strange shaped micro-domains may form as a result of the unusual Stern layer.

Recently an area of particular interest has been in the field of natural product extraction. It has been shown that DESs are effective at carrying out selective extraction from plant-based materials. It tends to be polar molecules, particularly with carboxylic acids and alcohols, which are preferentially extracted. Less polar molecules such as esters and ketones show less favourable extraction. It was found that the partitioning of materials was governed by the energy to create a hole in the DES, i.e., DESs with lower surface tensions seemed to be the most effective at extracting polar molecules. It would be interesting to study the effects of water on the thermodynamics of extraction using the method described in chapter three. It would be interesting to determine the types of solutes for which water acts as a pro-solvent and for which ones it is an anti-solvent.

It has been shown that DES-water mixtures are useful for the extraction and dissolution of DNA and enzymes due to increasing the stability of such systems. It would be useful to study the structure of such systems and see whether the water buffers the enzyme from the ionic phase and whether the ionic phase constrains the shape of the enzyme. The creation of micro-environments may be useful for the synthesis of nanomaterials. It may be possible to put metal ions into mixed DES-water systems and, depending on where they partition, they could be grown in novel architectures. The same could be the case for polymer growth depending on where the monomer partitions. The ability of QAS to stabilise colloidal dispersions may lead to interesting particle sizes and molecular weight dispersions.

Current work within the group has found a way of quantifying pH values in DESs. It would be interesting to determine the pH values of DES-water mixtures to see whether acids partition into a specific phase and whether this affects dissociation. Work within the groups has found that polyaniline grows better in DESs when aqueous acids are added to them and the mechanism behind this would be interesting to study.

The Leicester group has pioneered the use of DESs for mineral processing. One issue with this application has been the relatively high viscosity and the loss of material on the

ore. If water-DES mixtures could be used to perform the same chemistry then this could represent a considerable cost saving and have numerous environmental applications, as it would allow the technology to be applied to large-scale environmental applications. It may also aid in the separation of metals. The study in chapter four which shows that water may act as an anti-solvent for some metal complexes, and thus may simplify separation.

Chapter 7: Appendices.

7	Appendices.....	180
7.1	Appendix A.....	180
7.1.1	Thermophysical properties of pure DESs raw data.	180
7.1.2	Thermophysical properties of DESs with water raw data.	182
7.1.3	Dynamic light scattering.	183
7.2	Appendix B.....	188
7.2.1	Electrochemistry study.	188

7 Appendices

7.1 Appendix A

7.1.1 Thermophysical properties of pure DESs raw data.

Table 7.1: Raw data for viscosity of Ethaline, Glyceline, Oxaline and Reline at different temperatures.

T by K	Ethaline cP	SD	Glyceline cP	SD	Oxaline cP	SD	Reline cP	SD
343	13.36	0.15	34.25	0.09	37.13	0.12	40.04	0.19
338	14.47	0.04	40.82	0.09	40.99	0.19	48.03	0.20
333	16.02	0.08	49.15	0.10	47.86	0.15	59.56	0.23
328	17.66	0.03	59.99	0.30	56.13	0.24	74.16	0.31
323	19.71	0.08	74.02	0.28	61.70	0.28	96.96	0.53
318	22.09	0.04	89.23	0.28	77.17	0.29	128.94	0.60
313	25.04	0.03	112.48	0.46	96.37	0.39	178.81	0.88
308	28.77	0.05	145.86	0.62	133.50	0.39	249.71	1.26
303	33.80	0.05	248.18	1.00	180.52	0.69	400.62	0.76
298	36.05	0.03	313.14	1.60	212.28	0.16	591.73	3.93

Where SD is the standard deviation of the measurements, T is temperature in Kelvin.

Table 7.2: Raw data for conductivity of Ethaline, Glyceline, Oxaline and Reline at different temperatures.

T by K	Ethaline mS cm ⁻¹	SD	Glyceline mS cm ⁻¹	SD	Oxaline mS cm ⁻¹	SD	Reline mS cm ⁻¹	SD
343	22.50	0.01	8.35	1.07	11.67	3.06	8.93	0.51
338	22.00	1.27	7.31	1.41	11.26	2.57	7.81	0.76
333	20.28	1.14	6.60	1.25	9.82	2.02	6.56	0.56
328	18.52	0.84	5.68	1.19	8.36	1.70	5.34	0.27
323	17.05	0.76	4.80	1.08	7.28	1.54	4.48	0.38
318	15.61	0.73	4.08	0.94	6.40	1.53	3.50	0.26
313	14.13	0.50	3.43	0.86	5.39	1.28	2.63	0.13
308	12.64	0.50	2.84	0.72	4.19	0.86	1.90	0.19
303	11.55	0.37	2.21	0.47	3.26	0.67	1.40	0.07
298	9.75	0.26	1.64	0.23	2.54	0.68	1.04	0.02

Table 7.3: Raw data for density of Ethaline, Glyceline, Oxaline and Reline at different temperatures.

T by K	Ethaline g cm ⁻³	SD	Glyceline g cm ⁻³	SD	Oxaline g cm ⁻³	SD	Reline g cm ⁻³	SD
298	1.111	0.002	1.190	0.001	1.198	0.006	1.192	0.008
303	1.109	0.010	1.177	0.001	1.185	0.007	1.181	0.003
308	1.098	0.008	1.172	0.002	1.183	0.009	1.178	0.003
313	1.093	0.008	1.167	0.001	1.174	0.008	1.173	0.006
318	1.083	0.001	1.162	0.002	1.164	0.004	1.168	0.005
323	1.077	0.005	1.157	0.001	1.160	0.005	1.163	0.004
328	1.068	0.009	1.152	0.003	1.152	0.005	1.159	0.004
333	1.065	0.009	1.147	0.002	1.145	0.014	1.152	0.005
338	1.064	0.009	1.144	0.002	1.142	0.013	1.150	0.006
343	1.058	0.013	1.144	0.002	1.133	0.010	1.149	0.007

Table 7.4: Raw data for Surface tension of Ethaline, Glyceline, Oxaline and Reline at different temperatures.

T by K	Ethaline mN m ⁻¹	SD	Glyceline mN m ⁻¹	SD	Oxaline mN m ⁻¹	SD	of Reline mN m ⁻¹	SD
298	56.53	0.35	68.73	0.55	60.76	1.30	71.63	0.15
303	55.86	0.15	66.96	1.01	55.26	2.43	68.4	1.21
308	53.43	0.05	63.56	1.45	55.1	0.7	66.1	1.9
313	52.8	0.17	64.53	0.05	51.86	1.0	63.36	0.35
318	52.3	0.2	63.66	1.20	51.23	3.90	57.2	1.08
323	51.86	1.56	56.46	2.47	50.63	0.56	56.2	0.10
328	48.7	3.23	52.56	1.30	49.13	2.10	51.33	1.00
333	49.53	0.05	52.06	0.66	47.36	0.40	49.13	0.72

7.1.2 Thermophysical properties of DESs with water raw data.

Table 7.5: Raw data for viscosity of Ethaline, Glyceline and Reline with different amounts of water.

Amount of water %	Ethaline cP	SD	Glyceline cP	SD	Reline cP	SD
0.5	46.35	0.16	330.40	0.55	702.10	0.92
1	45.86	0.08	313.60	0.22	599.77	1.06
2.5	41.60	0.11	309.53	0.02	566.27	0.53
5	37.73	0.07	212.78	0.21	267.98	0.17
7.5	32.88	0.09	169.90	0.39	155.98	0.11
10	29.09	0.06	129.05	0.38	99.42	0.37
15	23.87	0.05	85.57	0.04	51.93	0.10
20	19.76	0.11	63.79	0.03	38.16	0.27
30	13.31	0.03	20.82	0.02	13.10	0.02
40	11.24	0.05	13.71	0.06	8.09	0.03
50	9.07	0.05	13.44	0.05	7.53	0.13
60	7.62	0.08	8.72	0.07	6.82	0.04
70	6.65	0.03	6.83	0.03	6.49	0.02

Table 7.6: Raw data for conductivity of Ethaline, Glyceline and Reline with different amounts of water.

Amount of water %	Ethaline mS cm ⁻¹	SD	Glyceline mS cm ⁻¹	SD	Reline mS cm ⁻¹	SD
0.5	8.72	0.07	1.35	0.02	0.99	0.00
1	8.41	0.03	1.38	0.00	1.00	0.01
2.5	8.86	0.03	1.38	0.01	1.41	0.02
5	9.74	0.02	1.83	0.01	2.11	0.02
7.5	11.13	0.05	2.43	0.04	3.82	0.06
10	12.43	0.12	2.96	0.02	5.59	0.25
15	14.81	0.02	4.39	0.01	10.32	0.02

Table 7.7: Raw data for density of Ethaline, Glyceline and Reline with different amounts of water.

Amount of water %	Ethaline gm cm ⁻³	SD	Glyceline gm cm ⁻³	SD	Reline gm cm ⁻³	SD
0.5	1.20	0.02	1.19	0.003	1.11	0.007
1	1.20	0.02	1.19	0.004	1.11	0.001
2.5	1.193	0.006	1.19	0.007	1.10	0.004
5	1.18	0.003	1.17	0.006	1.10	0.006
7.5	1.18	0.006	1.17	0.004	1.10	0.004
10	1.17	0.001	1.18	0.017	1.10	0.008
15	1.16	0.009	1.16	0.010	1.10	0.006
20	1.15	0.001	1.15	0.001	1.08	0.008

Table 7.8: Raw data of surface tension for Ethaline, Glyceline and Reline with different amounts of water.

Amount of water %	Ethaline mN m ⁻¹	SD	Glyceline mN m ⁻¹	SD	Reline mN m ⁻¹	SD
0.5	57.2	0.60	68.2	0.78	48.26	1.53
1	56.46	0.40	69.06	0.11	53.1	0.26
2.5	56.5	0.52	61.56	1.72	65.3	1.47
5	56.13	0.20	69.36	0.28	68.46	2.12
7.5	56.5	0.2	65.53	1.58	64.53	0.85
10	56.66	0.15	69.53	0.40	80.00	0.43
15	57.4	0.1	67.96	1.55	65.9	0.55
20	58	0	68.56	0.11	63.9	0.17

7.1.3 Dynamic light scattering.

Table 7.9: Raw data of DLS for Ethaline, Glyceline and Reline with different amounts of water.

Water amount %	Ethaline system	SD	Glyceline system	SD	Reline system	SD
5	310.9	17.56	105.0	12.22	38.76	2.36
10	108.8	9.22	119.4	19.69	46.00	2.73
20	64.42	8.00	75.25	6.38	47.6	4.30
50	20.34	0.67	83.2	7.40	79.22	11.20
70	119.7	11.55	347.6	23.32	217.9	29.25
90	251.0	14.93	166.7	9.15	108.4	9.39
95	285.5	28.81	168.6	13.66	131.9	17.03

1- Ethaline system.

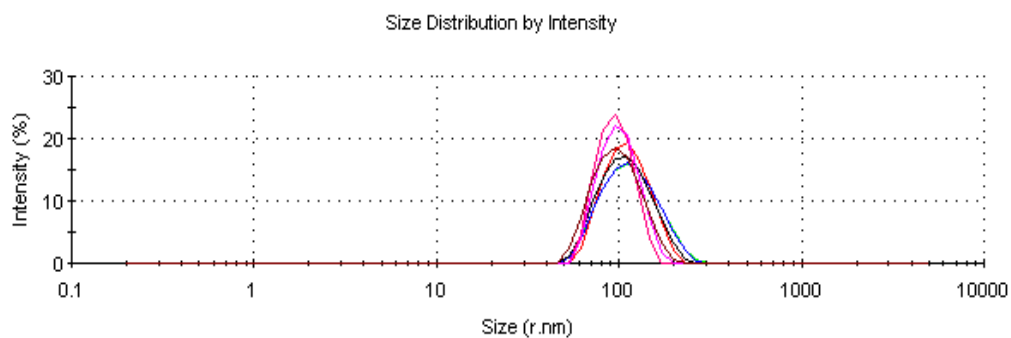


Figure 7.1: Dynamic light scattering of Ethaline with 10 wt% water.

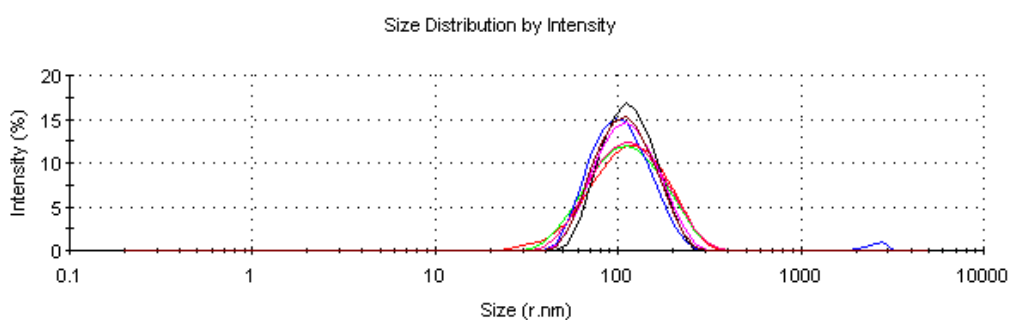


Figure 7.2: Dynamic light scattering of Ethaline with 70 wt% water.

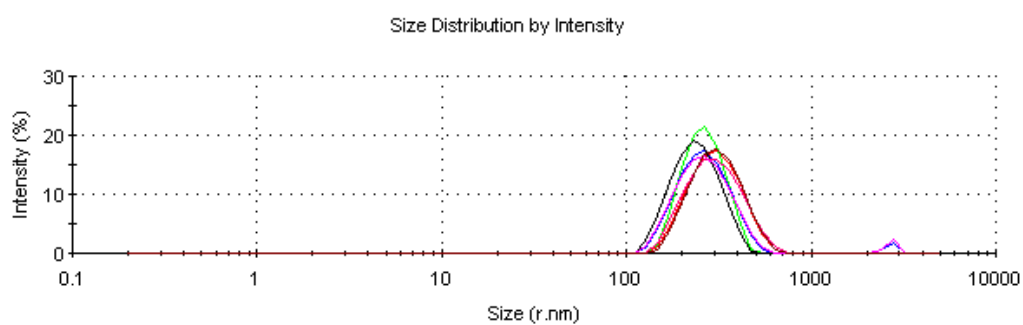


Figure 7.3: Dynamic light scattering of Ethaline with 95 wt% water.

2- Glyceline system.

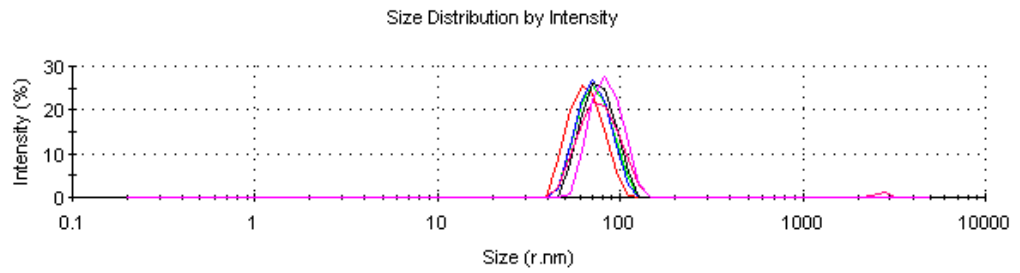


Figure 7.4: Dynamic light scattering of Glyceline with 20 wt% water.

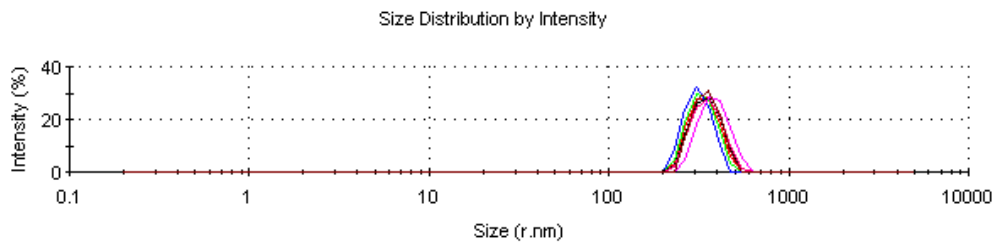


Figure 7.5: Dynamic light scattering of Glyceline with 70 wt% water.

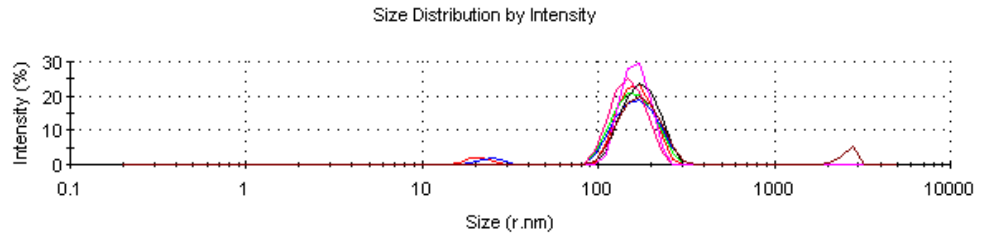


Figure 7.6: Dynamic light scattering of Glyceline with 90 wt% water.

3- Reline system.

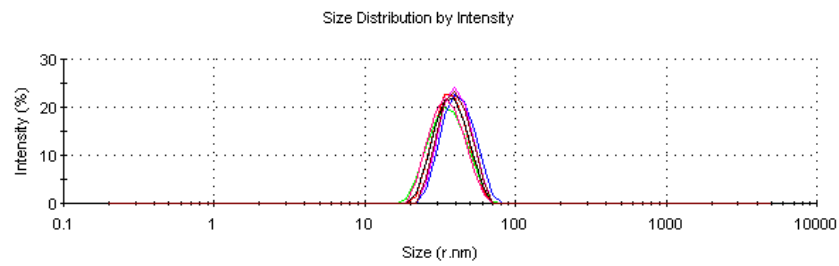


Figure 7.7: Dynamic light scattering of Reline with 5 wt% water.

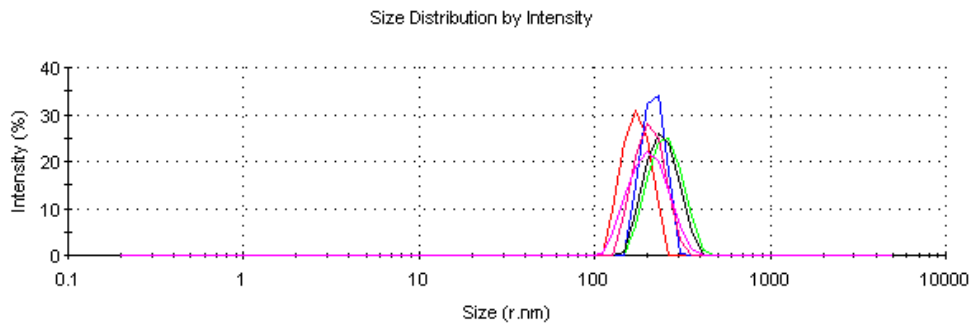


Figure 7.8: Dynamic light scattering of Reline with 70 wt% water.

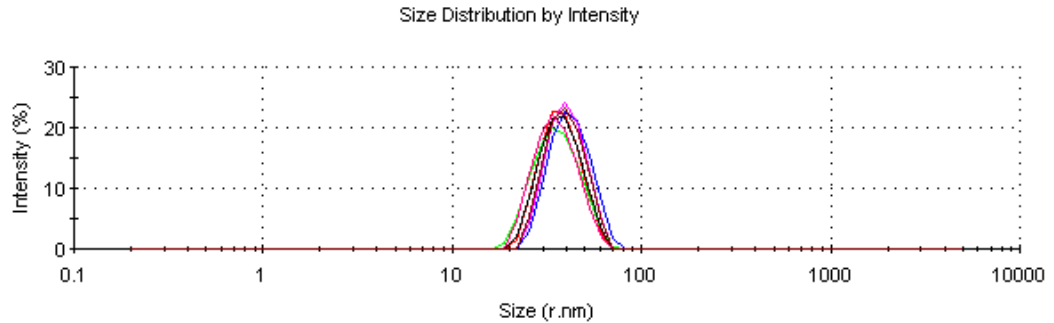


Figure 7.9: Dynamic light scattering of Reline with 90 wt% water.

4- Ionic liquids.

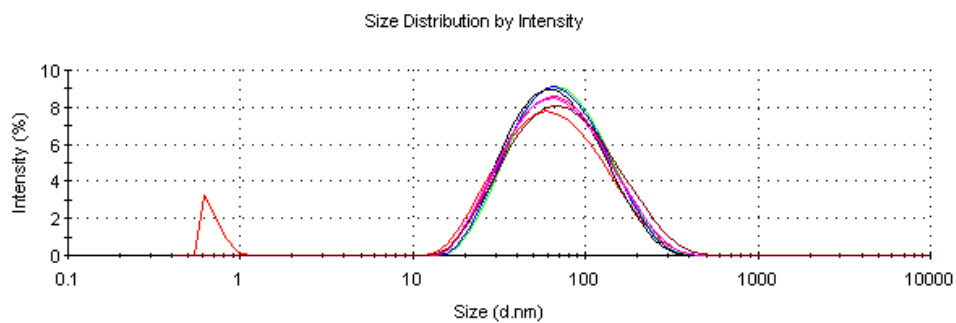


Figure 7.10: Dynamic light scattering of Bmim [BF₄] with 5 wt% water.

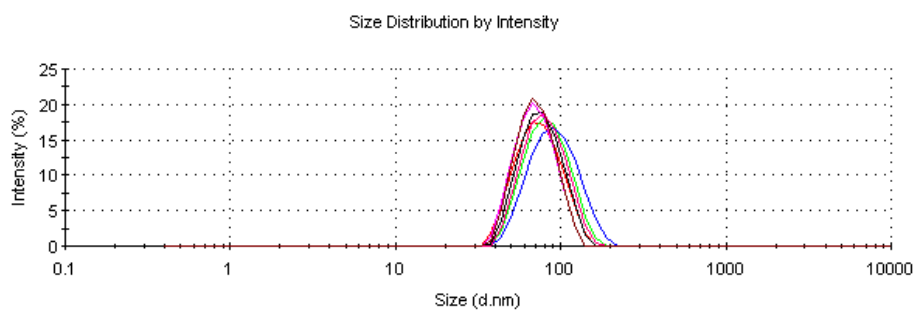


Figure 7.11: Dynamic light scattering of Emim [OAc] with 5 wt% water.

7.2 Appendix B.

7.2.1 Electrochemistry study.

7.2.1.1 Diffusion coefficient.

Table 7.10: Raw data of Diffusion coefficient for Ethaline, Glyceline and Reline with different amounts of water.

Water content %	Diffusion coefficient of FeCl ₃ in Ethaline m ² s ⁻¹	Diffusion coefficient of Fe(CN) ₆ ·3H ₂ O in Ethaline m ² s ⁻¹	Diffusion coefficient of FeCl ₃ in Glyceline m ² s ⁻¹	Diffusion coefficient of FeCl ₃ in Reline m ² s ⁻¹
0	1.85×10^{-11}	1.55×10^{-11}	2.74×10^{-11}	2.08×10^{-12}
5	1.94×10^{-11}	3.60×10^{-11}	4.27×10^{-11}	1.27×10^{-11}
10	2.44×10^{-11}	4.09×10^{-11}	6.84×10^{-11}	2.52×10^{-11}
15	3.24×10^{-11}	5.54×10^{-11}	2.37×10^{-11}	8.14×10^{-11}
20	3.88×10^{-11}	8.07×10^{-11}	1.61×10^{-10}	2.03×10^{-10}
25	4.52×10^{-11}	7.69×10^{-11}	2.51×10^{-10}	4.05×10^{-10}
30	5.36×10^{-11}	8.93×10^{-11}	3.17×10^{-10}	4.37×10^{-10}
35	4.94×10^{-11}	1.11×10^{-10}	4.14×10^{-10}	6.50×10^{-10}
40	7.09×10^{-11}	1.59×10^{-10}	5.43×10^{-10}	1.01×10^{-9}
45	6.40×10^{-11}	1.61×10^{-10}	5.51×10^{-10}	1.21×10^{-9}
50	9.30×10^{-11}	1.90×10^{-10}	5.27×10^{-10}	1.25×10^{-9}
55	9.69×10^{-11}	1.86×10^{-10}	5.53×10^{-10}	1.47×10^{-9}
60	1.14×10^{-10}	2.52×10^{-10}	5.64×10^{-10}	1.99×10^{-9}
65	1.25×10^{-10}	2.27×10^{-10}	5.13×10^{-10}	2.12×10^{-9}
70	7.57×10^{-11}	1.89×10^{-10}	5.15×10^{-10}	2.00×10^{-9}

1- Cyclic voltammograms of Ethaline system.

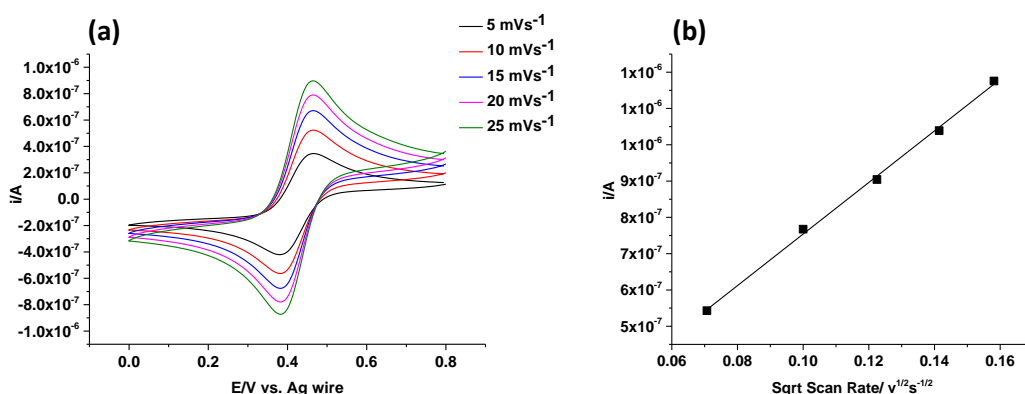


Figure 7.12: (a) Cyclic voltammograms of 0.02 mol dm⁻³ FeCl₃ in 25 wt% water: 75 wt% Ethaline and (b) plot of oxidation peak currents versus the square root of sweep rate.

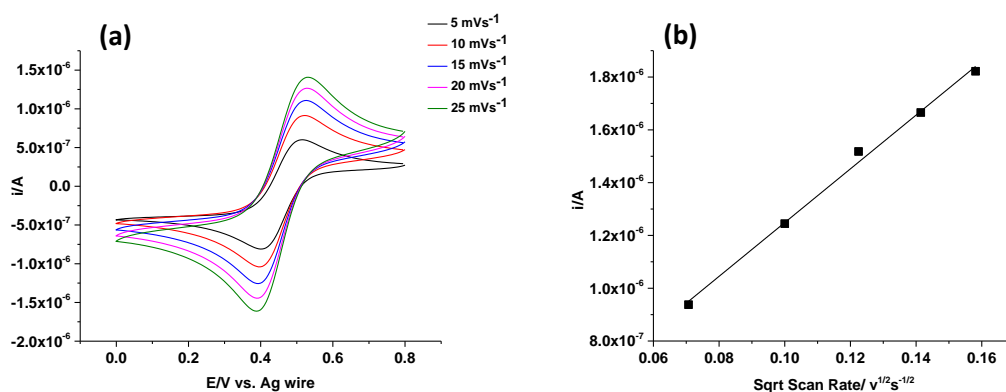


Figure 7.13: (a) Cyclic voltammograms of 0.02 mol dm⁻³ FeCl₃ in 50 wt% water: 50 wt% Ethaline and (b) plot of oxidation peak currents versus the square root of sweep rate.

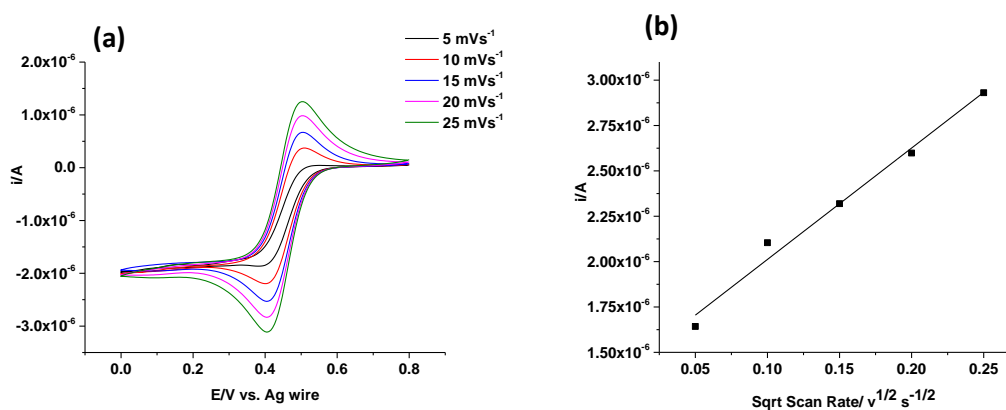


Figure 7.14: (a) Cyclic voltammograms of $0.02 \text{ mol dm}^{-3} \text{ FeCl}_3$ in 70 wt% water: 30 wt% Ethaline and (b) plot of oxidation peak currents versus the square root of sweep rate.

2- Cyclic voltammograms of Glyceline system.

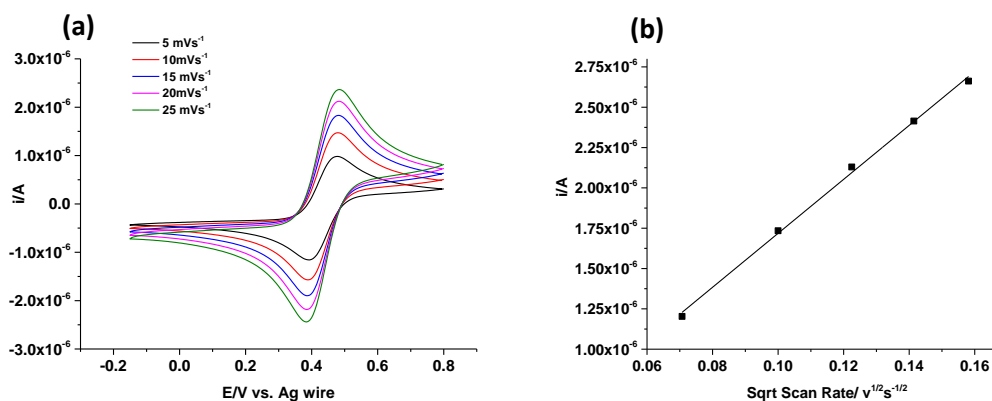


Figure 7.15: (a) Cyclic voltammograms of $0.02 \text{ mol dm}^{-3} \text{ FeCl}_3$ in 25 wt% water: 75 wt% Glyceline and (b) plot of oxidation peak currents versus the square root of sweep rate.

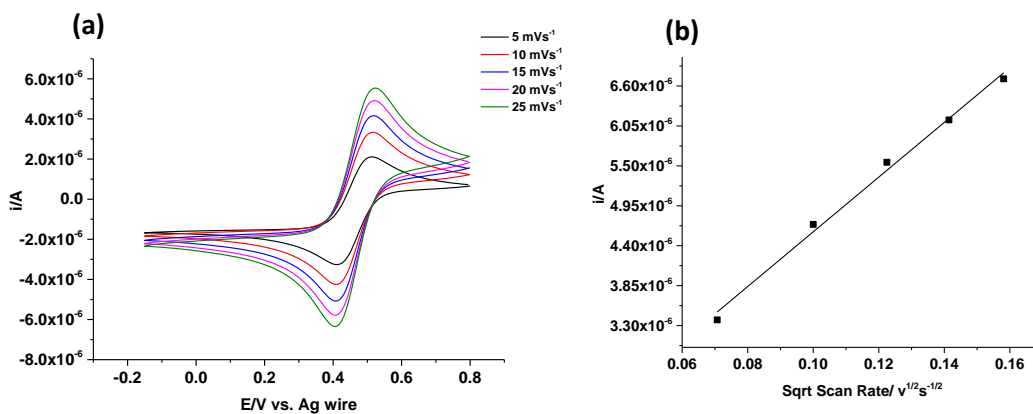


Figure 7.16: (a) Cyclic voltammograms of 0.02 mol dm⁻³ FeCl₃ in 50 wt% water: 50 wt% Glyceline and (b) plot of oxidation peak currents versus the square root of sweep rate.

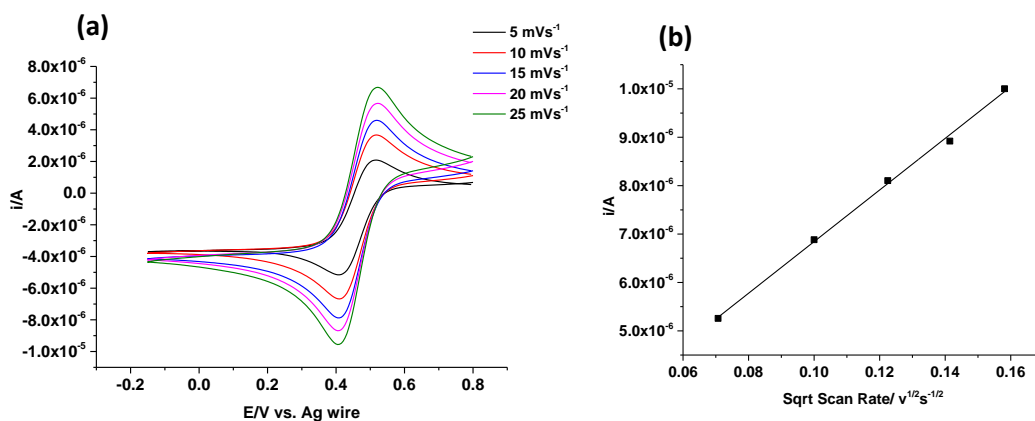


Figure 7.17: (a) Cyclic voltammograms of 0.02 mol dm⁻³ FeCl₃ in 70 wt% water: 30 wt% Glyceline and (b) plot of oxidation peak currents versus the square root of sweep rate.

3- Cyclic voltammograms of Reline system.

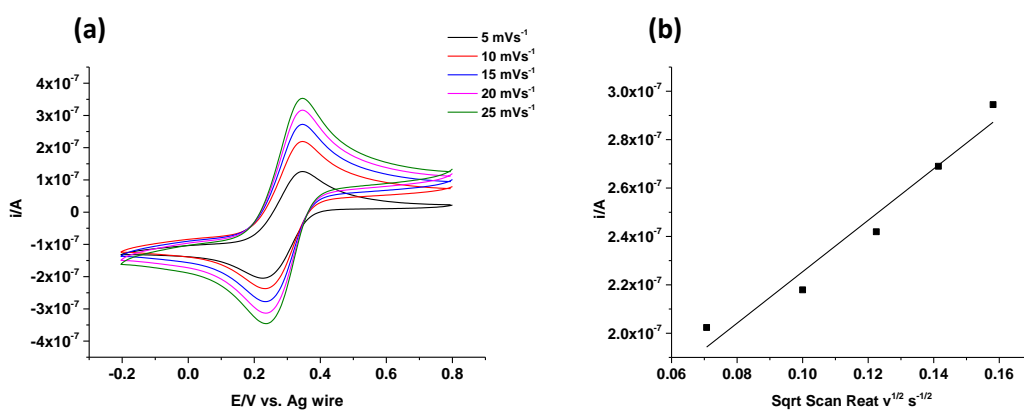


Figure 7.18: (a) Cyclic voltammograms of 0.02 mol dm⁻³ FeCl₃ in 25 wt% water: 75 wt% Reline and (b) plot of oxidation peak currents versus the square root of sweep rate.

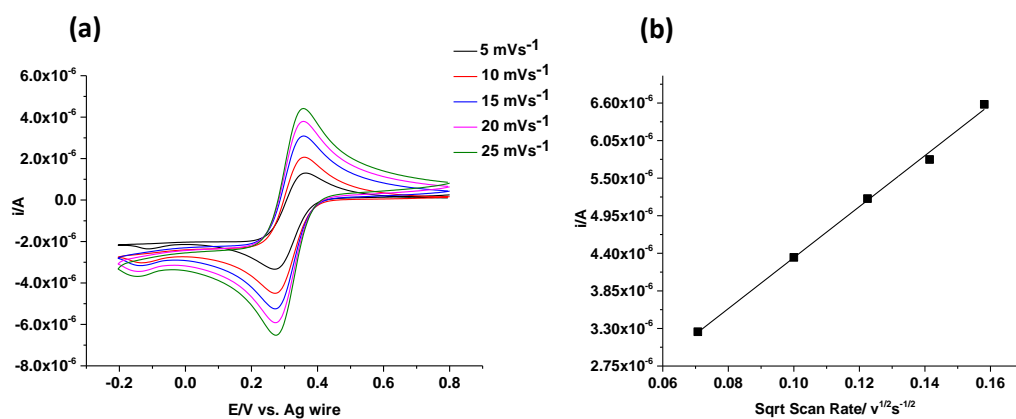


Figure 7.19: (a) Cyclic voltammograms of 0.02 mol dm⁻³ FeCl₃ in 50 wt% water: 50 wt% Reline and (b) plot of oxidation peak currents versus the square root of sweep rate.

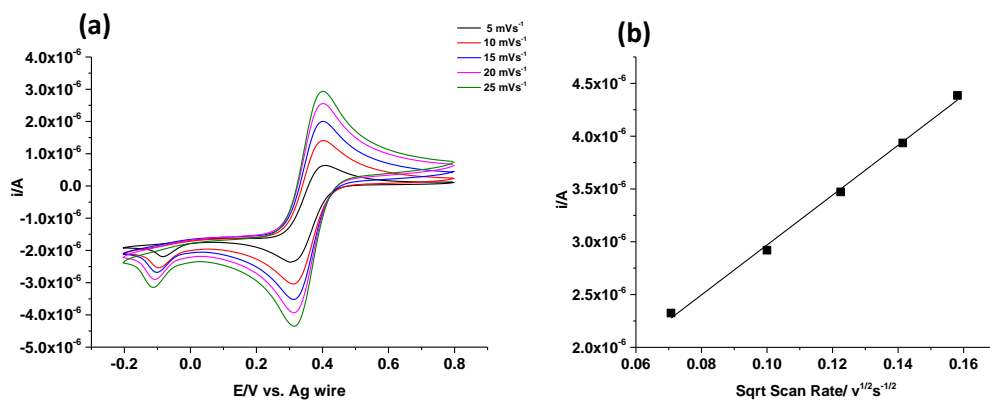


Figure 7.20: (a) Cyclic voltammograms of 0.02 mol dm⁻³ FeCl₃ in 70 wt% water: 30 wt% Reline and (b) plot of oxidation peak currents versus the square root of sweep rate.

The following published articles have been removed from the electronic version of this thesis due to copyright restrictions:

C. D'Agostino, L. F. Gladden, et al. Molecular and ionic diffusion in aqueous – deep eutectic solvent mixtures: probing inter-molecular interactions using PFG NMR, *Phys. Chem. Chem. Phys.*, 2015, 17, 15297-15304. DOI [10.1039/C5CP01493J](https://doi.org/10.1039/C5CP01493J)

A. P. Abbott, A. Y.M. Al-Murshedi, et al. Thermodynamics of phase transfer for polar molecules from alkanes to deep eutectic solvents, *Fluid Phase Equilibria*, 2017, 448, 99-104. DOI [10.1016/j.fluid.2017.05.008](https://doi.org/10.1016/j.fluid.2017.05.008)

A. P. Abbott, S. S. M. Alabdullah, et al. Brønsted acidity in deep eutectic solvents and ionic liquids, *Faraday Discussions*, 2018, 206, 365-377. DOI [10.1039/C7FD00153C](https://doi.org/10.1039/C7FD00153C)

The unabridged version can be consulted at the University of Leicester Library.